

Том 4 № 2 (2018)

ISSN 2413-9203

ТРАНСПОРТНЫЕ СИСТЕМЫ И ТЕХНОЛОГИИ

рецензируемый научный журнал

**TRANSPORTATION
SYSTEMS AND
TECHNOLOGY**
peer-review journal

VOL. 4 ISSUE 2 (2018)

transsyst.ru

УЧРЕДИТЕЛЬ И ИЗДАТЕЛЬ

Федеральное государственное бюджетное образовательное учреждение высшего образования «Петербургский государственный университет путей сообщения Императора Александра I»

«ТРАНСПОРТНЫЕ СИСТЕМЫ И ТЕХНОЛОГИИ»

Электронный рецензируемый научный журнал
Выходит ежеквартально – 4 раза в год
Основан в 2013 году

ИНДЕКСАЦИЯ

РИНЦ (Российский индекс научного цитирования)
Google Scholar
WorldCat
Ulrich's Periodical Directory

КОНТАКТЫ

Адрес: 190031, Санкт-Петербург, наб. реки Фонтаны, 115, ауд. 9/11-5
E-mail: info@transstyst.ru
WEB: www.transstyst.ru
Телефон: +7 (812) 6198152; +7 (911) 2384445

Научный редактор Ю. Ф. Антонов, доктор технических наук, профессор
Перевод на английский язык А. Ю. Гнатенко
Выпускающий редактор Т. С. Антонова
Редактор сайта А. В. Дитрих
Литературный редактор С. А. Зинченко
Верстка Л. А. Каратановой

СВИДЕТЕЛЬСТВО о регистрации средства массовой информации

Эл№ФС77-53673 от 17.04.2013 г. выдано Федеральной службой по надзору в сфере связи, информационных технологий и массовых коммуникаций

ОПИСАНИЕ ЖУРНАЛА

Сетевой электронный журнал "Транспортные системы и технологии" публикует статьи фундаментального характера и прикладного направления, а также обзорные статьи, относящиеся ко всем видам транспортной технологии

ПУБЛИКАЦИЯ В ЖУРНАЛЕ

Журнал отбирает материал для публикации из числа присланных для рассмотрения рукописей. В ходе отбора проводится независимое двойное слепое рецензирование членами редакционной коллегии и внешними экспертами. Для публикации рукопись, а также все сопроводительные и дополнительные файлы следует направить в редакцию через личный кабинет на сайте журнала по URL: <http://trassyst.ru/>
Рукопись и дополнительные материалы следует оформить в соответствии с правилами редакции, см. подробно по URL: <https://journals.eco-vector.com/transstyst/about/submissions>

ПОДПИСКА

Журнал распространяется через Интернет без ограничений и по адресно-целевой подписке через редакцию

© ФГБ ОУ «Петербургский государственный университет путей сообщения Императора Александра I», 2018

ТРАНСПОРТНЫЕ СИСТЕМЫ И ТЕХНОЛОГИИ

Том 4, № 2

2018

ЭЛЕКТРОННЫЙ РЕЦЕНЗИРУЕМЫЙ НАУЧНЫЙ ЖУРНАЛ

ГЛАВНЫЙ РЕДАКТОР

Зайцев Анатолий Александрович, доктор экономических наук, профессор

**ЗАМЕСТИТЕЛЬ ГЛАВНОГО РЕДАКТОРА,
НАУЧНЫЙ РЕДАКТОР**

Антонов Юрий Федорович, доктор технических наук, профессор

МЕЖДУНАРОДНАЯ РЕДАКЦИОННАЯ КОЛЛЕГИЯ

Колесников Владимир Иванович, академик Российской академии наук, доктор технических наук, профессор, Санкт-Петербург, Россия

Глухих Василий Андреевич, академик Российской академии наук, Научный руководитель НИИЭФА им. Д.В. Ефремова, доктор технических наук, профессор, Санкт-Петербург, Россия

Клюшпис Йоханнес, доктор наук 2-й степени, полный профессор Деггендорфской высшей технической школы, Мюнхен, Германия

Ли Вэйли, доктор технических наук, профессор, Пекинский транспортный университет, Пекин, КНР

Галкин Александр Геннадьевич, доктор технических наук, профессор, ректор Уральского государственного университета путей сообщения, Екатеринбург, Россия

Верескун Владимир Дмитриевич, доктор технических наук, профессор, ректор Ростовского государственного университета путей сообщения, Ростов-на-Дону, Россия

Паньчев Александр Юрьевич, кандидат экономических наук, доцент, ректор Петербургского государственного университета путей сообщения Императора Александра I, Санкт-Петербург, Россия

Хан Хьён-Сук, кандидат технических наук начальник Департамента Маглев и линейных двигателей, Старший научный сотрудник Корейского института машиностроения и материаловедения (KIMM), Тэджон, Республика Корея

Фэй Ни, кандидат технических наук, доцент, сотрудник Национального транспортно-инженерного центра Маглев, Университет Тондзи, Шанхай, КНР

Ма Чжисюн, кандидат технических наук, сотрудник Национального транспортно-инженерного центра Маглев, доцент Университета Тондзи, Шанхай, КНР

Сирирангси Пувадол, доктор технических наук, декан, Институт менеджмента «Паньяпиват», Паккред, Таиланд

FOUNDER AND PUBLISHER

Emperor Alexander I St. Petersburg State Transport University
St. Petersburg, Russia

"TRANSPORTATION SYSTEMS AND TECHNOLOGY"

Electronic peer-review journal
Issued 4 times a year (quarterly)
Established in 2013

INDEXING

eLibrary (Russian Science Citation Index)
Google Scholar
WorldCat
Ulrich's Periodical Directory

CONTACTS

Address: 190031, St. Petersburg, 115 Moskovskiy Ave., room 9/11-5
E-mail: info@transst.ru
Website: www.transst.ru
Phone: +7 (812) 6198152; +7 (911) 2384445

Science Editor Yu. F. Antonov, Doctor of Technical Science, Professor
Translation into English A.Yu. Gnatenko
The Executive Editor T.S. Antonova
WEB- Editor A.V. Dietrichs
Literary Editor S.A. Zinchenko
Layout Editor LA Karatanova

AIMS & SCOP

Network electronic journal "Transportation Systems and Technology" publishes articles of a fundamental nature and application areas, as well as review articles pertaining to all types of transport technology

JOURNAL CONTENT SELECTION

The journal selects based on the double-blind peer-review conducted by members of the editorial board and external experts.

To be published, the manuscript and all accompanying files should be sent to the editorial team through a personal account on the journal's website at: <http://transst.ru/>

The manuscript and additional materials should be prepared and arranged in accordance with the author guidelines (see in detail at: <https://journals.eco-vector.com/transst/about/submissions>)

SUBSCRIPTION

The Journal is distributed via Internet for free and by subscription via Editorial office

© Emperor Alexander I St. Petersburg State Transport University, 2018

TRANSPORTATION SYSTEMS AND TECHNOLOGY

Vol. 4, Issue 2

2018

ELECTRONIC PEER-REVIEWED RESEARCH JOURNAL

EDITOR-IN-CHIEF

Anatoly Zaitsev, Doctor of Economics, Professor

**DEPUTY EDITOR-IN-CHIEF,
THE SCIENCE EDITOR**

Yuri Antonov, Dr. Sc., Professor, St. Petersburg, Russia

INTERNATIONAL EDITORIAL BOARD

Vladimir Kolesnikov, Academician of the Russian Academy of Sciences, Doctor of Technical Science, Professor, St. Petersburg, Russia

Vasily Glukhikh, Academician of the Russian Academy of Sciences, Scientific Adviser at JSC «D.V. Efremov Institute of Electrophysical Apparatus», Doctor of Technical Science, Professor, St. Petersburg, Russia

Kluehspies Johannes, 2nd Dr.'s Degree, Full Professor at Deggendorf Institute of Technology, Munich, Germany

Weili Li, Ph.D., Professor, Beijing Jiaotong University, Beijing, China

Alexander Galkin, Dr. Sc., Professor, Rector of the Ural State Transport University, Yekaterinburg, Russia

Vladimir Vereskun, Dr. Sc., Professor, Rector of Rostov State Transport University, Rostov-on-Don, Russia

Alexander Panychev, Ph.D., Associate Professor, Rector of Emperor Alexander I St. Petersburg State Transport University, St. Petersburg, Russia

Han Hyung-Suk, PhD, Head of the Department of Maglev and Linear Drives, Principle Researcher, Korea Institute of Machinery & Material (KIMM), Daejeon, the Republic of Korea

Fei Ni, PhD, National Maglev Transportation Engineering Technology R&D Center (NMTC), Associate Professor at Tongji University, Shanghai, China

Ma Zhixun, PhD, National Maglev Transportation Engineering Technology R&D Center (NMTC), Associate Professor at Tongji University, Shanghai, China

Sirirangsi Poovadol, Doctor of Engineering, Deputy Dean at Panyapiwat Institute of Management, Pakkred, Thailand

СОДЕРЖАНИЕ		TABLE OF CONTENTS	
ОБЗОРЫ		REVIEWS	
Киреев А.А., Кожемяка Н.М., Кононов Г.Н. Высокоскоростная контейнерная транспортная система	5	Kireev A.V., Kozhemyaka N.M., Kononov G.N. High-Speed Container Transport System	
Д’Овидио Дж, Ланцара Дж. Инновации и эксплуатация итальянской магнитолевитационной системы «UAQ4» на основе сверхпроводимости	19	D’Ovidio G., Lanzara G. Innovations and Performance of Italian UAQ4 Superconducting Magnetic Levitated System	
Му С., Кан Цз., Ван С., Лю Й., Хэ Ц. Метод подавления тяговой пульсации для линейного синхронного двигателя с длинным статором	30	Mu S., Kang J., Wang S., Liu Y., He C. A Method of Thrust Ripple Suppression for Long Stator Linear Synchronous Motor	
ОРИГИНАЛЬНЫЕ СТАТЬИ		ORIGINAL STUDIES	
Жао Цз., Ван К., Ван Б., Гэ Ц., Ши Л., Ли Й. Специальная система возбуждения для анализа взаимосвязанных характеристик тяговой и левитационной сил магнитолевитационного поезда	45	Rao J., Wang K., Wang B., Ge Q., Shi L., Li Y. A Special Excitation System for Analysis of Coupling Characteristics of Thrust and Levitation Force of Maglev Train	
Богачев В.А., Терентьев Ю.А., Коледов В.В., Богачев Т.В. Джунгарский коридор для вакуумного магнитного левитационного транспорта: утраченные возможности или взвешенный оптимизм?	52	Bogachev V.A., Terentyev Y.A., Koledov V.V., Bogachev T.V. Dzungaria Corridor for Vacuum Magnetic Levitation Transport: Lost Opportunities or Weighted Optimism?	
Цинь Ф., Линь Й., Лу Д. Программно-аппартное моделирование пятисегментной тяговой системы высокоскоростного маглев-транспорта, используя DSPACE	62	Qin F., Lin Y., Lu D. Hardware-in-the-loop Simulation of High-Speed Maglev Transportation Five-Segment Propulsion System Based on DSPACE	
Ким К.К. Российский вариант транспортной системы «Hyperloop»	73	Kim K.K. The Russian Version of the Transport System “Hyperloop”	
Чжоу Д., Юй П., Ли Цз., Цуй П., Сон М. Адаптивный контроль вибраций путевой структуры на основе электромагнитов с высокочастотным резонансом для городской системы маглев	92	Zhou D., Yu P., Li J., Cui P., Song M. Adaptive Vibration Control of the Electromagnet-Track Coupled High Frequency Resonance for an Urban Maglev System	

Делле Сите В., Каваньяро М. Новая концепция модульного поезда маглев для городского транспорта	107	Delle Site V., Cavagnaro M. A New Concept of Modular Magnetic Levitation Train for Urban Transport
Хэ Й., Ван Й.С., Лу Ц., Чжан Л., Лян Ф. Проектирование линейного асинхронного двигателя для низкоскоростного маглев (160 км/ч) с вариативным контролем частоты скольжения	120	He Y., Wang Y.-S., Lu Q., Zhang L., liang F. Design of Single-Sided Linear Induction Motor for Low-Speed Maglev Vehicle in 160 km/h and Variable Slip Frequency Control
Хуан Цз., Чжоу С., Шан Л., У Цз., Сюй В., Ван Д. Анализ влияния неровности пути на плавность движения поезда маглев	129	Huang J., Zhou X., Shang L., Wu Z., Xu W., Wang D. Influence Analysis of Track Irregularity on Running Comfort of Maglev Train
Лай Ц., Лю Цз., Мэн Л., Чай С., Ван Ц., Сюй Й. Оптимизация планирования вспомогательной зоны остановки в средне-высокоскоростном маглев	141	Lai Q., Liu J., Meng L., Chai X., Wang Q., Xu Y. Optimization of the Auxiliary Stopping Area Planning in the Middle-to-High Speed Maglev
Кирхер Р., Ключпис Й., Палка Р., Фритц Э., Айлер К., Витт М. Электромагнитные поля в высокоскоростных транспортных системах	152	Kircher R., Klühspies J., Palka R., Fritz E., Eiler K., Witt M. Electromagnetic Fields Related to High Speed Transportation Systems
Соломин В.А., Соломин А.В., Коледов В.В., Трубицина Н.А. Многофункциональный линейный асинхронный двигатель с продольно-поперечным магнитным потоком для магнитолевитационного транспорта	167	Solomin V.A., Solomin A.V., Koledov V.V., Trubitsina N.A. Multifunctional Linear Induction Motor with Longitudinal-Transverse Magnetic Flux for Magnetic-Levitational Transport

UDC 629.027:621.318.3

DOI: 10.17816/transsyst2018425-18

© A. V. Kireev, N. M. Kozhemyaka, G. N. Kononov

Closed Joint-Stock Company “Scientific and Technical Center “PRIVOD-N”
(Novocherkassk, Russia)

HIGH-SPEED CONTAINER TRANSPORT SYSTEM

Background: The new scope of application for vehicles equipped with magnetic suspension is the freight container transportation. In order to realize the transit potential of the country, the increase in mean speed of the container trains is required.

Aim: The present work aims to explore the possibilities to develop the high-speed transport system equipped with magnetic suspension for container transportation along Euro-Asian land bridge.

Methods: As the research tools used methods of situational analysis, computer modeling, transport geography, technical and economic analysis.

Results: The market analysis results of the transit container transportation have shown that the major challenge for Russian transit development is the constrained traffic capacity of the existing transport corridors. The drastic solution to the problem can be the construction of a new high-speed transport system. The following factors determining the conditions for the creation of the new transport system have been identified: use of transport possibilities of the Azov-Black Sea basin; ensuring accessibility of the northern territories; development of technical solutions for the creation of a transport system with low-cost infrastructure. The combined traction levitation system has been developed based on the extremely simple design of the linear switched reluctance motor. The experimental researches of the full-functional physical model of the transport platform have been performed. The assessment of investment project efficiency has shown that despite the large start-up investment in the track infrastructure, the project has positive economic effect.

Practical importance: The computer model of the combined traction levitation system based on the linear switched reluctance motor has been designed. The concept of constructing a new transport system is proposed, taking into account the characteristics of the proposed operational region in poorly developed territories. The high-speed route has been proposed connecting the Azov-Black sea basin with the Pacific coastline and completely passing through the territories of Russia including some northern regions. The transit potential assessment has shown that due to the transit time reduction it is possible to attract the container freights with traffic volume of 1,52 million in twenty-foot equivalentunit.

Keywords: Container traffic, Conveyor container transport, Maglev freight train, Transport corridors, Linear switched reluctance motor.

The work has been carried out with the financial support of Russia’s Ministry of Education and Science. The unique identification code of studies RFMEFI57916X0132.

© А. В. Киреев, Н. М. Кожемяка, Г. Н. Кононов
ЗАО «Научно-технический центр «ПРИВОД-Н»
(Новочеркасск, Россия)

ВЫСОКОСКОРОСТНАЯ КОНТЕЙНЕРНАЯ ТРАНСПОРТНАЯ СИСТЕМА

Обоснование: Новой сферой применения транспортных систем на магнитном подвесе являются грузовые контейнерные перевозки. Для реализации транзитного потенциала страны требуется повышение маршрутной скорости контейнерных поездов.

Цель. Целью работы является исследование возможности создания скоростной транспортной системы с магнитным подвесом для контейнерных перевозок по Евро-Азиатскому сухопутному мосту.

Методика. В качестве исследовательского инструментария использованы методы ситуационного анализа, компьютерного моделирования, транспортной географии, технико-экономического анализа.

Результаты. Анализ ситуации на рынке транзитных контейнерных перевозок показал, что основным препятствием реализации транзитного потенциала России является ограниченная пропускная способность существующих транспортных коридоров. Кардинальным решением проблемы может стать строительство новой высокоскоростной транспортной системы. Выявлены факторы, определяющие условия создание новой транспортной системы. Среди них: использования транспортных возможностей Азово-Черноморского бассейна, обеспечение доступности северных территорий, разработка технических решений обеспечивающих создание транспортной системы с низко затратной инфраструктурой. Выполнена разработка комбинированной тягово-левитационной системы на основе предельно простого варианта линейного реактивного индукторного двигателя. Проведены экспериментальные исследования полнофункциональной физической модели транспортной платформы. Оценка эффективности инвестиционного проекта показала, что, несмотря на большие первоначальные капиталовложения в путевую инфраструктуру, проект имеет положительный экономический результат.

Научная новизна. Разработана компьютерная модель комбинированной тягово-левитационной системы на основе линейного реактивного индукторного двигателя.

Практическая значимость. Предложена концепция построения новой транспортной системы с учетом характеристик предполагаемого полигона эксплуатации на слабо освоенных территориях. Предложен маршрут высокоскоростной трассы, связывающий Азово-Черноморского бассейн с побережьем Тихого океана, полностью проходящий по территории России, затрагивая северные регионы. Оценка транзитного потенциала показала, что за счет сокращения времени транзита возможно привлечение на маршрут контейнерных грузов с объемом перевозок 1,52 млн. в двадцатифунтовом эквиваленте.

Ключевые слова: контейнерный трафик, контейнерный конвейерный транспорт, грузовой поезд маглев, транспортные коридоры, линейный реактивный индукторный двигатель.

Работа выполнена при финансовой поддержке Министерства образования и науки России. Уникальный идентификационный код исследований RFMEFI57916X0132.

INTRODUCTION

The general tendency for the development of the world transport system is the acceleration of the transport process, achieved by the formation of transport corridors, improvement of the transport and logistics structure of transportation, and the increase of speed transport modes [1].

The new scope of application for vehicles equipped with magnetic suspension is the freight container transportation. In order to realize the transit potential of the country, the increase in mean speed of the container trains is required.

New application of magnetic levitation transport systems (MLTS) in the sphere of freight transportation requires reconsideration of concept of its construction taking into account the properties of the area intended for operation.

The railway transport development strategy up to 2030 has special chapter for transit container transportation [2]. The territory of the Russian Federation is a natural bridge connecting Europe and Asia-Pacific Region states. For realization of transit potential of the country, the task is set to increase container trains speed. Now, the development of transport area is conducted at the expense of liquidation of gaps and “narrow sections” by virtue of reconstruction and construction of separate sections of transport network. The main project is considered to be construction of high-speed railway for accelerated delivery of containers from China, Central Asia and Eastern Europe to Europe – the Trans-Eurasia Container Mainline. This mainline will enable organization of container transportation with the speed of 140–160 km/h, ensure release of carrying capacity of Russia Far East railways.

Meanwhile, the idea of establishment of Eurasian Land Bridge deploying magnetic suspension technology [3]. However, until now no researches had been carried out to access capabilities of MLTS-based container transportation on the Eurasian Land Bridge.

The purpose of the work consists in studying the possibility of creating high-speed transport system with magnetic suspension for container transportation on Eurasian Land Bridge.

1. SETTING TASK

The basic tasks that were solved during the research are as follows:

- assessment of container transportation market situation;
- identification of factors that determine the conditions for the creation of a new transport system;
- forecasting the volumes of container transit traffic of a new high-speed transport system;

- identification of factors determining the route of the line;
- research of technical solutions ensuring realization of the project.

2. MATERIALS AND METHODS OF RESEARCH

As an instrument of research, the situation analysis methods were used, computer modelling, transport geography, technical and economic analysis.

3. RESULTS

3.1. Assessment of container transportation market situation

Today, most of the cargo transported from Asia to Europe and back is carried by sea, which is associated with a sharp increase in container freight turnover between the two continents. The second place in the cost volume of supplies is air transport. The list is closed by railway transport.

The biggest problem that exists in Euro-Asian maritime transport is related to very long shipment time. An alternative to maritime transport is land transportation, which can meet a significant part of the expected additional demand for transport services in the future. Distances by land between Europe and Asia are generally shorter than the distances by sea, especially if the points of departure and destination of the cargo lie deep in both continents.

Railway transport is becoming an optimal way of ensuring connections between ports and inland regions of a continent. Efficient operation of such railway routes as the Trans-Siberian Railway and the Trans-Asian Railway through China will enable creation of additional passage capacity, making it possible to form the niche demand for enhanced transportation [4].

Today, the journey speed of container trains along the Trans-Siberian Railway is 1550 km per day. This is achieved, mainly, by increasing the journey speed by reducing the number and duration of technological operations with train units, which undoubtedly increases the competitiveness of this type of transportation. At the same time, the desire to achieve the maximum possible technical speed is limited by the loss of the rest of the freight traffic along the Trans-Siberian Railway.

The assessment of transit potential of the Russian Federation in terms of goods traffic between Asia and the EU indicates that the at the expense of transit time by 25–30 % the sea way goods can be taken as well. The total share of land Eurasian transport can be increased from 1.9 to 18.5 %.

A cardinal solution to the problem might become the construction of new rapid transport system with containers carried at least 2500 km per day.

The new transport system can facilitate the release of the capacity of railways for freight traffic, direct uninterrupted communication between Europe

and Asia, and, if properly routed, can ensure the availability of transportation services for carrying goods in the Far North, Siberia, the Far East and remote regions of Russia.

3.2. Factors determining the conditions of creation of new transport system

Geopolitical factor. In the forming geopolitical realities, it is reasonable to consider the issue of Russia's using the transport strategic capacities of the Azov and Black Sea Basin in the long run [5]. Besides, to decrease political risk, it would be highly advisable to have the entire route laid on the territory of one country, for example with the starting points on Russia's Pacific coast and terminal points in logistical centers of the Azov and Black Sea Basin.

Northern territories' transport accessibility factor. There is a strategic need of priority construction of new extended lines in the poorly developed Northern regions of the country, for example north to the TSR and Baikal-Amur Mainline where the prospective natural resources can be found [6].

Technical and economic factor. Vast territory and high unit cost of MLTS flyover dictates demand in realization of minimum distance when choosing the route. Unlike conventional railways, a MLTS flyover does not require cleaning taiga territories, levelling the ground, bypassing natural obstacles. The flexible inclusion of the structure into landscape is ensured, creating prerequisite for straightening the track.

Taking into account the main factors determining the proposed route, we can outline the following route: the starting point is on the Pacific coast; the terminal point is one of the ports of the Azov and Black Sea basin. The southern ports of Russia are at the crossroads of the world trade routes, several transport corridors pass through them, in addition, it is the shortest way from the largest industrial centers from Russia to Europe, the countries of the Middle East, and Asia.

As the starting point of the route on the Pacific coast, we can choose the seaport of Vanino. It is a transport hub connecting railway, sea and road routes. Through Vanino shipments are delivered to the northeast regions of Russia, Japan, South Korea, China, Australia, the USA and other countries. The favorable geographical location of the port opens the way to the sea for cargoes travelling along the Baikal-Amur and Trans-Siberian railways.

The prospective route of the MLTS route is characterised by a very large length (approximately 7,000 km), potentially has a significant range of variation, the width of which can be several hundred kilometers, depending on the terrain features, geotechnical conditions, location of favourable crossings of broad rivers, and also from seismic and other unfavourable conditions on the sections of the direction of the mainline.

The route takes into account key factors: it connects the Azov and Black Sea basin with the Pacific coast, completely passes through the territory of the Russian Federation, including northern territories (up to 60° N), and its length is 25 % shorter than the length of existing routes.

3.3 Technical realization of the transport system

The critical need in creation of high-speed freight transportation systems, having a separate flyover route, generates the task to search for technical solutions, enabling us to decrease costs for construction and maintenance of MLTS.

The proposed route passes through remote low-accessible areas (water barriers, mountain ranges, wetlands, etc.) with a cold climate. In these conditions, transport systems with low-cost infrastructure and technical solutions are needed to ensure uninterrupted traffic on the mainline.

In Russia, Ltd. “PRIVOD-N” within the Federal Target Programme is developing transport system elements with magnetic suspension aimed at transporting goods through poorly developed northern territories.

The developers of the project have formulated a working hypothesis about construction of simple combined traction and levitation system on the basis of the switched reluctance motor, capable to simultaneously ensure levitation, traction and stabilization. This combined traction and levitation system enables using the passive discrete guideway with decreased materials consumption.

The functional scheme of the combined traction and levitation system, arranged on the basis of the switched reluctance motor, is shown in the Fig. 1.

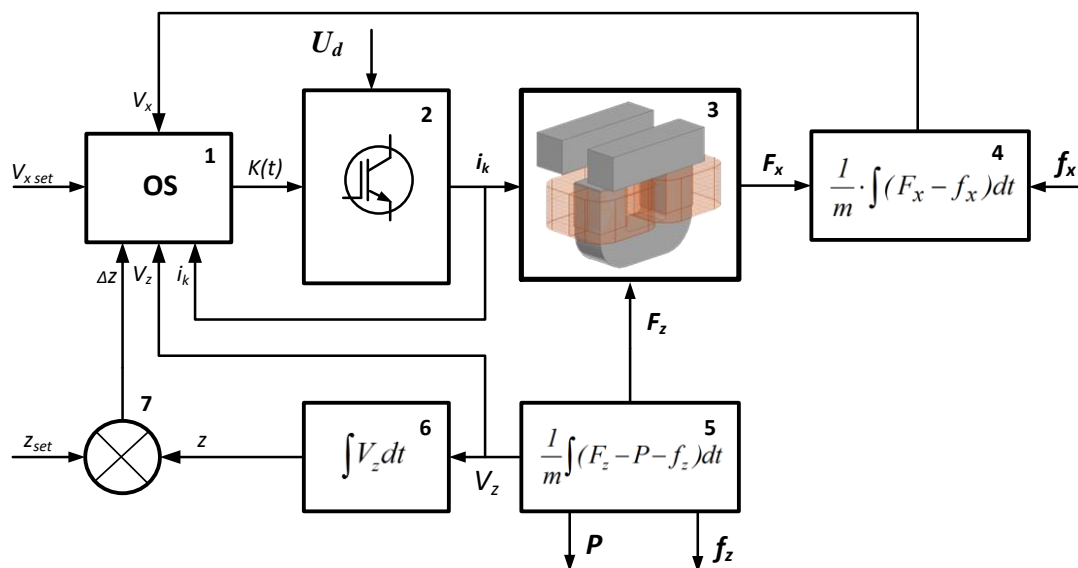


Fig. 1. Functional system of combined traction and levitation system

The system of operation 1 generates commutation function $K(t)$, operating switches of power keys of converter 2. Under the influence of the supply voltage U_d , the converter 2 generates phase currents i_k in the windings of the traction and levitation module 3. This generates the traction force F_x and the lifting force F_z . Under the action of the traction force F_x , the object moves at a speed V_x , overcoming the resistance to movement f_x (block 4). Lifting force F_z provides levitation of the object, compensating the weight of the object P and the action of the disturbing forces f_z (block 5). Under the action of these forces, the object moves in the vertical direction at a speed V_z . The gap signal z is formed at the output of the unit 6 by integrating the vertical travel speed V_z , is compared with the set value z_{set} in the block 7, and the error signal Δ_z is supplied to the input of the control system. In addition, when forming the switching function $K(t)$, the signals V_x , V_z , i_k and the speed reference signal $V_{x\ set}$ are used.

A peculiarity of the mathematical model of the combined traction and suspension system is the description of the linkage of the phase contour as a function of three variables:

$$\Psi_k = f(i_k, x, z), \quad (1)$$

where i_k – contour current;

x – horizontal motion coordinate;

z – vertical motion coordinate.

Generally, the mathematical model shows the system of equations describing:

- current balance in electromagnetic contours;
- electromechanical energy converters processes;
- object motion equations.

$$\left\{ \begin{array}{l} u_k = i_k \cdot R + \frac{\partial \Psi_k(i_k, x, z)}{\partial i_k} \cdot \frac{di_k}{dt} + \frac{\partial \Psi_k(i_k, x, z)}{\partial x} \cdot \frac{dx}{dt} + \frac{\partial \Psi_k(i_k, x, z)}{\partial z} \cdot \frac{dz}{dt}, \\ F_x = \sum_{k=1}^b \frac{\partial}{\partial x} \left(\int_0^i \Psi_k(i_k, x, z) di \right)_{\substack{i=const \\ z=const}}; \\ F_z = \sum_{k=1}^b \frac{\partial}{\partial z} \left(\int_0^i \Psi_k(i_k, x, z) di \right)_{\substack{i=const \\ z=const}}; \\ m \cdot \frac{d^2 x}{dt^2} = F_x - f_x; \\ m \cdot \frac{d^2 z}{dt^2} = F_z - m \cdot g - f_z, \end{array} \right. \quad (2)$$

where i_k – electromagnetic contour current;
 x – horizontal motion coordinate;
 z – vertical motion coordinate;
 Ψ_k – electromagnetic contour linkage;
 k – number of electromagnetic contour;
 b – number of electromagnetic contours;
 g – gravitational acceleration;
 m – weigh of levitated object;
 R – active resistance of contour;
 u_k – voltage applied to the electromagnetic contour;
 F_x – horizontal force generated by electromagnetic contour;
 F_z – vertical force generated by electromagnetic contour;
 f_x – force of resistance to motion;
 f_z – disturbing action.

On the basis of mathematical model of traction and levitation system, its computer realization in the graphical environment of imitation modelling Simulink has been developed. The computer model enables conducting modelling of dynamic regimes of the work.

The Fig. 2 shows results of modelling of electromechanical processes in traction and levitation system. The oscillograms of instant values of phase currents in traction and levitation module windings, instant force values on the coordinates x , y , z . Phase currents are formed in such a way that the total lifting force produced by the phase contours provides levitation of the object, and the total traction force – the predetermined speed.

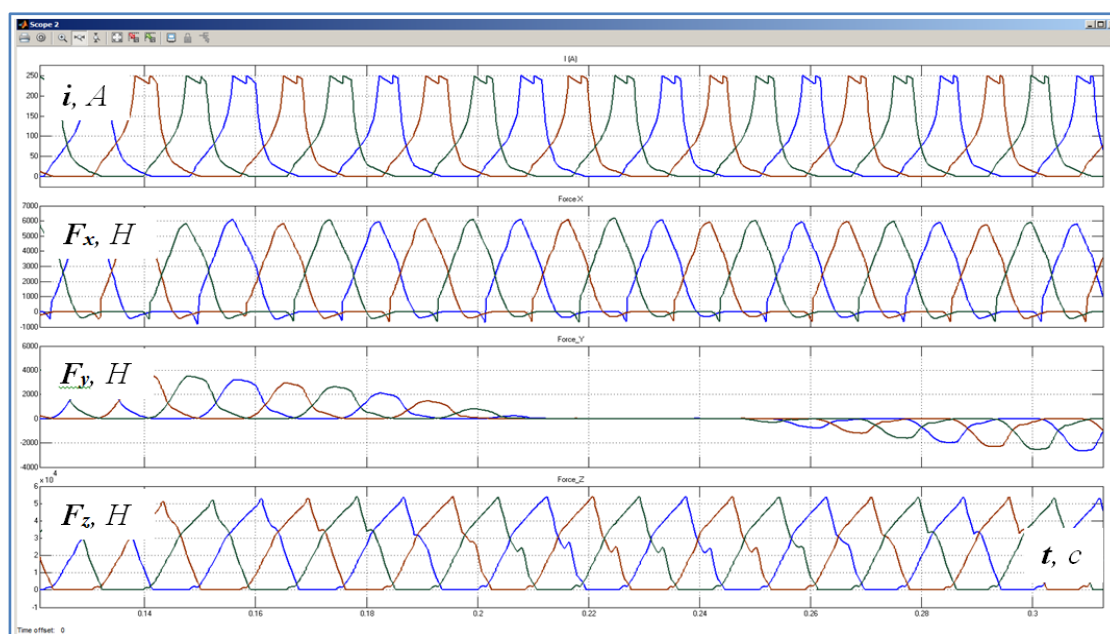


Fig. 2. Electromechanical processes oscillograms in traction and levitation system

The picture shows that when a disturbance on the coordinate y acts, a lateral displacement force F_y appears, which provides a course stabilization of the moving object.

Based on the results of computer simulation of processes in the combined traction and suspension system, the main technical solutions were developed. For experimental verification of the concept, a full-featured physical model of the transport platform was made and experimental studies of the system were carried out.

The main purpose of the experiment was to test the possibility of combining the functions of levitation and traction. The similarity of the processes taking place in the physical model is ensured by the similarity of the configuration of the magnetic system of the model of the traction and levitation module made on a scale of 1:7, the identity of the topology of the schemes of power converters of the model and the object, the identity of the control algorithms with the structure of the control system. The transport platform is equipped with four traction and levitation modules.

The Fig. 3 shows functional scheme of the module. Windings $L1$, $L2$, $L3$ of the module $A1$ are embedded into the power scheme of push-pull converter $UZ1-UZ3$, which are powered by accumulator battery $G1$. The control system forms algorithms of commutation of power keys $VT1$, $VT2$, converters $UZ1-UZ3$, ensuring levitation of the object and its linear motion along the guideway.

The input of the control system receives signals proportional to the currents in the windings I_{a1} , I_{b1} , I_{c1} from the current sensors $TA1-TA3$, the air gap δ_1 from the gap sensor BI , and also the logic signals fixing the position of the poles of the module magnetic system relative to the track elements from the block of position sensors $BL1-BL3$.

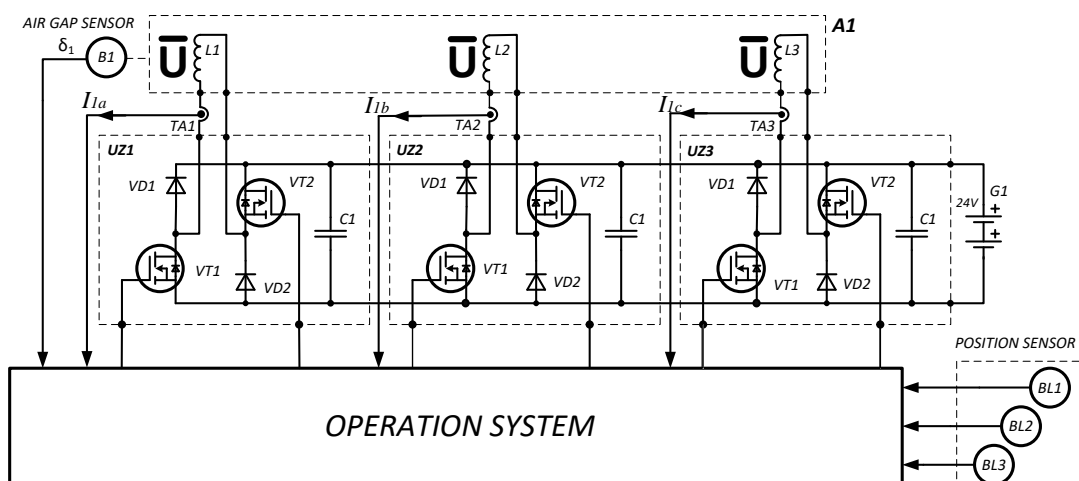


Fig. 3. Functional scheme of the module

In terms of construction, the traction and levitation module is fully autonomous and may be adapted to various construction forms of the transport platform.

The Fig. 4 shows the general view of the physical model of the transport platform.

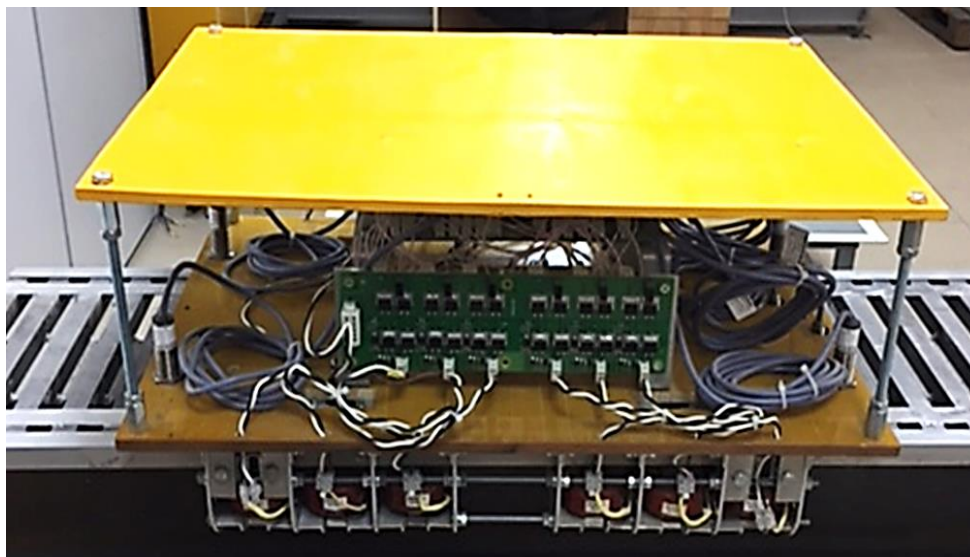


Fig. 4. General view of the physical model

The model has four traction and levitation modules, installed on the transport bogie; a platform on which electrical equipment is installed; additional technological platform on which cargo is installed during experiments.

During the experiments, the model was given a levitation regime. To achieve this, the windings of traction and levitation modules were supplied with DC, adjustable in magnitude as a function of the magnitude of the air gap between the module poles and the track elements. Further, the drive system was started, at which the currents in the phase windings were switched by the signals of the position sensors. The transport platform moved contactlessly along the track structure all this time.

The Fig. 5 shows oscillograms of electromechanical processes during transition of traction and levitation system from levitation regime to levitated motion regime. The oscillograms show the phase currents of the modules $I_{1a}-I_{4c}$, the signals of the gap sensors $\delta_1-\delta_4$, the signals of the position sensors D_a, D_b, D_c . The research of the physical model of the transport system has proved its working status [7].

After the research, the construction concept of freight magnetic levitation transport system was proposed for operation in poorly developed areas. The proposed MLTS should have passive guideway structure of flyover type and coupled stock consisting of autonomous platforms for carrying containers. Each

platform is equipped with easily-dismounted traction and levitation modules and electric and chemical energy accumulators. Power supply of the rolling stock may be carried out both from autonomous power plants and contact network.

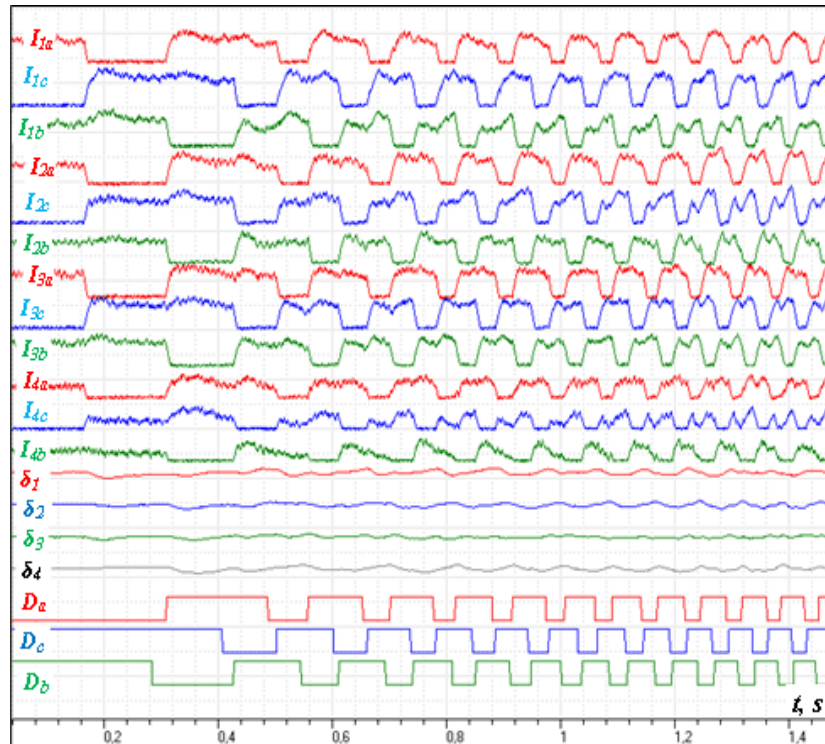


Fig. 5. Electromechanical processes oscillograms

The Fig. 6 shows cross-sectional view of the transport platform.

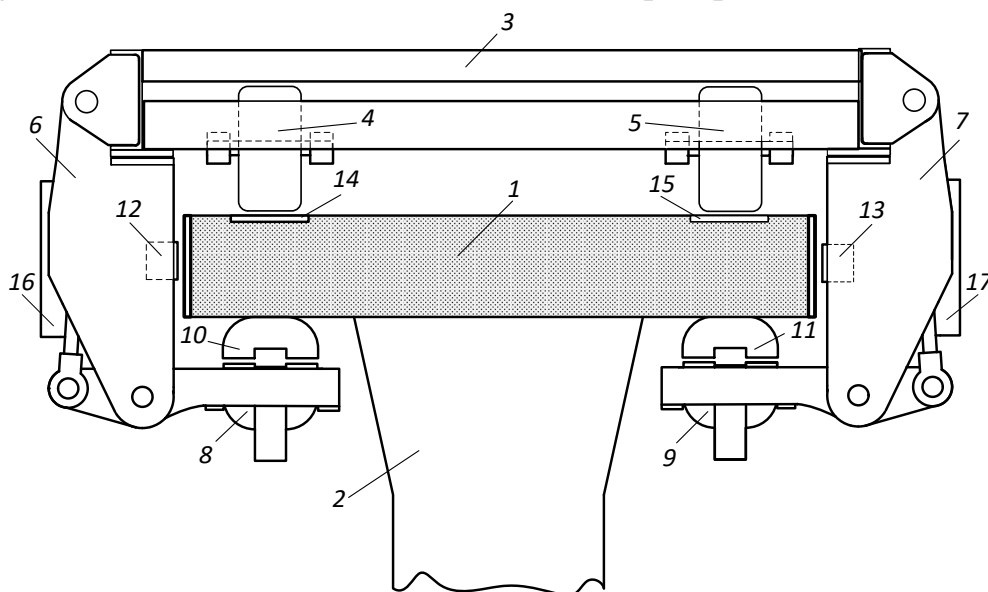


Fig. 6. Cross-sectional view of the transport platform

The Fig. 6 shows: guideway 1, resting on support 2; transport platform 3, equipped with wheel blocks 4 and 5 for moving platform along the guideway; transfer units 6 and 7, connecting stators of linear motors 8 and 9 and transport platform 3; rotor elements 10 and 11, installed in a row on the guideway 1 with the step equaling pole pitch of linear motor; rollers 12, 13 limiting lateral displacement of the platform. The surface of the guideway 1 has steel plates 14, 15 which serves as the groove for wheels 4 and 5 of the platform 3.

When current pulses are directed to the windings of the stators of linear motors from the converter devices 16, 17, a force interaction of the U-shaped magnetic circuits of the stator and the rotor occurs via an adjustable air gap. A traction, lifting and lateral stabilizing force is created, which is transmitted through the transfer units to the transport platform. This ensures a non-contact motion of the transport platform along the track structure.

A container train consisting of the 22 transport platforms described above with a total mass of 1.800 tonnes can transport 43 units of a 40-pound container at a speed of 180 km/h. The speed of motion of container cargo is not less than 3600 km/day. To realise the designed annual volume of transit container traffic of 1.52 million TEU, it is necessary that container trains follow with an interval of approximately 0.5 hours (49 container trains per day).

At the same time, 156 container trains must be simultaneously on the line in both directions. The park of transport platforms should be 3432 units (excluding reserve).

Thus, the proposed concept of constructing a high-speed container train is physically feasible and provides the forecasted annual volume of transit container traffic.

CONCLUSION

The development of the transport infrastructure of the Russian Federation is connected with the geographical location of the country as a natural transport corridor connecting the European and Asian-Pacific regions. The creation of a high-speed Euro-Asian transport system complies with the directive documents relating to the transport strategy of the Russian Federation for developing the potential of Euro-Asian transport links and transit freight.

The transport system can be implemented on the basis of modern magnetic levitation technology, which allows significant reducing operating costs, and, consequently, transport costs, due to contactless running of the transport platform along the track structure.

The new transport system will facilitate the release of the capacity of railways for freight transport, the direct transfer of cargo between Europe and Asia, and, if properly routed, will ensure the availability of transport services for

the transportation of goods in the Far North, Siberia, the Far East and remote regions of Russia.

References

1. Владимиров С.А. Мировая транспортная система и логистика: основные направления развития // Региональная экономика и управление: электронный научный журнал. – 2016. – №2(46). – С. 13–21. Режим доступа: <http://eee-region.ru/article/4602/> Дата обращения: 17.07.2018. [Vladimirov SA. The global transport and logistics system: main areas of development. *Regional economics and management: electronic scientific journal*. 2016;2(46):13-21. Available from: <http://eee-region.ru/article/4602/> (in Russ). Accessed July 17, 2018].
2. Мишарин А.С. Транспортная стратегия Российской Федерации: цели и приоритеты // Инновационный транспорт. – 2015. – № 1(15). – С. 3–7. [Misharin AS. Transport Strategy of the Russian Federation: goals and priorities. *Innotrans*. 2015;1(15):3-7. (In Russ.)].
3. Tennenbaum J. The New Eurasian Land-Bridge Infrastructure Takes Shape. *Executive Intelligence Reviev*. 2001;28(42):17-41. Available from: http://www.larouchepub.com/eiw/public/2001/eirv28n42-20011102/eirv28n42-20011102_016-the_new_eurasian_land_bridge_inf.pdf
4. Euro-Asian Transport Linkages. Expert Group Report. United Nations Economic Commission for Europe (UNECE). 2012. Available at: http://www.unece.org/fileadmin/DAM/trans/main/eatl/docs/EATL_Report_Phase_II.pdf Accessed July 17, 2018.
5. Раровский П.Е. Российский экспорт транспортных услуг в современных условиях // Российский внешнеэкономический Вестник. – 2016 – №5 – С.116–121. [Rarovskiy PE. Russia's exports of transportation services in contemporary conditions. *Russian Foreign Econ. Bull*. 2016;(5):116-131. (In Russ.)].
6. Копыленко В.А., Быков Ю.А., Турбин И.В., Космин В.В. Расширение сети железных дорог в малоосвоенных регионах России – одна из важных задач развития железнодорожного транспорта страны в XXI веке // Наука и транспорт. Модернизация железнодорожного транспорта. (Прил. к журн. Транспорт Российской Федерации). – 2008. – № 4. – С. 4–7. [Kopylenko VA, Bykov YA, Turbin IV, Kosmin VV. Expansion of the network of railways in the underdeveloped regions of Russia is one of the important tasks of the development of the country's railway transport in the 21st century. *Sci. and Transp. Modernization of Transport Russian Federation*. 2008;(4):4-7. (In Russ.)].
7. Kireev AV., Kononov GN, Lebedev AV. Starting operating mode of the combined traction levitation system of the vehicle equipped with magnetic suspension *Int. J. Power Electronics and Drive System (IJPEDS)*, 2017;8(1):176-183. doi: 10.11591/ijpeds.v8i1.pp176-183

Information about the authors:

Alexander V. Kireev, Cand. Sci. (Eng), Associate Prof.; address: 346428, Russian Federation, Rostov region, Novocherkassk, Krivoslykova St., 4a.
eLibrary SPIN: 9674-4388; ORCID: 0000-0003-1157-2402
E-mail: akireev@privod-n.ru

Nikolay M. Kozhemyaka, Cand. Sci. (Eng);
eLibrary SPIN: 7921-4510; ORCID: 0000-0002-3976-7546
E-mail: nkozhemyaka@privod-n.ru

Gennady N. Kononov;
eLibrary SPIN: 9565-6740; ORCID: 0000-0002-5511-9311
E-mail: gkononov@privod-n.ru

Сведения об авторах:

Киреев Александр Владимирович, к.т.н., доцент;
адрес: 346428 г. Новочеркасск, ул. Кривошлыкова 4а;
eLibrary SPIN: 9674-4388; ORCID: 0000-0003-1157-2402;
E-mail: akireev@privod-n.ru

Кожемяка Николай Михайлович, к.т.н.;
eLibrary SPIN: 7921-4510; ORCID: 0000-0002-3976-7546
E-mail: nkozhemyaka@privod-n.ru

Кононов Геннадий Николаевич;
eLibrary SPIN: 9565-6740; ORCID: 0000-0002-5511-9311
E-mail: gkononov@privod-n.ru

To cite this article:

Kireev AV, Kozhemyaka NM, Kononov GN. High-Speed Container Transport System. *Transportation Systems and Technology*. 2018;4(2):5-18. doi: 10.17816/transsyst2018425-18

Цитировать:

Киреев А.А., Кожемяка Н.М., Кононов Г.Н. Высокоскоростная контейнерная транспортная система // Транспортные системы и технологии. – 2018. – Т. 4. – № 2. – С. 5-18. doi: 10.17816/transsyst2018425-18

DOI: 10.17816/transsyst20184219-29

© G. D'Ovidio, G. Lanzara

University of L'Aquila

(L'Aquila, Italy)

INNOVATIONS AND PERFORMANCE OF ITALIAN UAQ4 SUPERCONDUCTING MAGNETIC LEVITATED SYSTEM

Abstract. This article concerned with technological innovations and performance of the UAQ4 Italian maglev train project which aims mainly to reduce energy consumption by eliminating any ordinary resistance to motion (magnetic drag included), except the aerodynamic drag if it operates in atmospheric environment.

The technological feasibility of the UAQ4 suspension and propulsion devices has been patented and successfully laboratory tested.

The train architecture and the work's principles of suspension and propulsion devices are all innovative, with concepts and technologies close to the aeronautical transport system.

Keywords: Superconducting magnetic levitated train, Low energy consumption, High temperature superconductors, Suspension system, Propulsion system.

INTRODUCTION

In the field of the ground passenger transportation systems, maglev system is unanimously considered the most technologically advanced and efficient in terms of speed, comfort and energy requirements.

Maglev trains technology was initially conceived with the aims to realize a vehicle able to float over the guideway using magnetic forces by replacing the mechanical contact between steel wheel/track.

Different levitation methods for practical application have been developed starting from the 70s.

The main current levitation approaches can be classified into the following three categories:

- a) Electromagnetic Suspension (EMS), based on the attractive force between actively controlled electromagnets on the vehicle undercarriage and the steel yoke of track.
- b) Electrodynamic Suspension (EDS), based on the repulsive force between low temperature superconductive electromagnets on board and short-circuited conductive coils on the track.
- c) Superconducting magnetic levitation (SML), with high temperature bulk superconducting (HTS) materials on board levitating in the static magnetic field of the track.

The first two systems (EMS and EDS) have reached a high level of technological maturity and operational reliability.



The EMS with the German Transrapid TR-07 train is fully operative in China [1].

The EDS with Japanese Yamanashi train were successfully tested for a long time and a top speed of 603 km/h has been reached; it is expected that this system will be ready for commercial applications [2].

Compared with the wheel-on-rail (WoR) train, EMS and EDS systems eliminate mechanical friction but introduce magnetic resistance to the motion that varying with the speed and technology.

The currently operating maglev systems don't achieve the full potential advantages of magnetic levitation, since suspension and propulsion are still affected by magnetic resistance to motion that imply significant power consumption.

When the levitated train travels along a guideway, eddy currents are induced in conductive sheets/coils by the magnetic fields.

The interaction between the magnetic fields produces both a lift/guidance forces and drag force, due to the resistive losses in the conducting sheets/coils.

This is a clear limitation of the use of such type of maglev systems in transport applications: the magnitude of the magnetic resistance plays a fundamental role not only on a technical standpoint but also for economic reasons, since the consumed energy increases substantially the operational costs.

The third levitation approach (SML) started thanks to the emergence, in the late 80s, of new sintered magnetic materials, such as $\text{YBa}_2\text{Cu}_3\text{O}_x$ (YBCO) bulk high temperature superconductors and $\text{Nd}_2\text{Fe}_{14}\text{B}$ (NdFeB) permanent magnets (PMs). This technology potentially allows to overcome the above cited operating limitations of the current maglev systems.

Even if SLM system is in the experimental stage for practical transportation applications yet, it seems to satisfy the expectation for a future generation maglev transportation systems.

Superconductors are the only type of material known today which has a perfect diamagnetic response and zero electrical resistance. The interaction between superconductor and static magnetic field generate a conservative force field.

German [3], Chinese [4], Brazilian [5] and Italian [6] research groups are working on this superconducting maglev technology by developing and testing practical applications in non-conventional guided transportation systems.

This paper illustrates the Italian UAQ4 project SML technology based that is under development at University of L'Aquila (Italy).

ITALIAN HIGH SPEED TRAIN RESEARCH EXPERIENCES

Italian research activities in the field of non-conventional transportation systems started in the early 70s at the University of Palermo, with the prototypal

construction of the IAP2 (Fig. 1) and IAP3 (Fig. 2) air cushion trains, that were operated on testing ground lines in the Trapani airport area (Sicily).

The IAP2 vehicle was propelled in a “U” shaped concrete guideway by an aeronautical propeller engine. Subsequently the IAP3 prototype was built. For the first time, this vehicle used an alternate current (AC), one-sided, linear induction motor for propulsion and active secondary suspensions [7, 8].

Despite the validation of several system innovations, air-cushions vehicle development was interrupted due to technological limitations (noise, energy consumption etc.) and other contingent factors of that historical period.



Fig. 1. IAP2 air-cushions vehicle

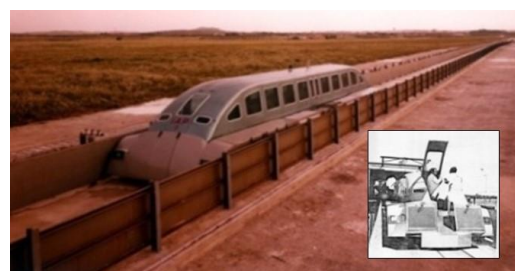


Fig. 2. IAP3 air-cushions vehicle

In the meantime, the research activities were focused on a magnetic levitation suspension with no resistance to motion, by studying an approach based on the interaction between superconducting mirror sheets and magnetic field. In 1990 the method based on the Meissner effect was proposed and patented to levitate, drive, and brake the vehicle by on-board sheets of superconductive material interacting with guideway magnetic fields [9].

Then, with the advent of the new sintered magnetic materials (YBCO and NeFeB), the research was renewed in the end 90s and the UAQ4 (short University of L’Aquila model 4) Italian maglev train project was carried out.

UAQ4 PROJECT AIMS AND ACHIEVEMENTS

The UAQ4 project is the outcome of abovementioned Italian research activities.

The suspension device produce passive, self-balancing interaction between on board superconducting skater devices and PMs distributed along the track. As consequence the train stably floats with a large air gap in all phases of motion, zero speed included, without control devices.

The UAQ4 project was started with the aim to study, define and test environment friendly technological solutions for mass transportation systems, in order to:

- a) Eliminate any ordinary resistance to motion (magnetic drag included), except the aerodynamic one.

- b) Realize a levitation system to lift and guide the vehicle in stable conditions in all phases of motion, zero speed included, and with negligible electric power consumption/requirements.
 - c) Use high efficiency propulsion/braking system, controlled from on board.
 - d) Realize lightweight vehicle and conceive a system architecture with concepts, technologies and level of comfort close to aeronautical systems.
- In order to achieve the project aims, the following four steps were planned:
- identify the most appropriate technologies by analysing their advantages/limitations and by elaborating algorithm a numerical model necessary for the design of main components;
 - build laboratory equipment for testing both levitation and propulsion phenomena;
 - validate the feasibility by building a fully working laboratory system, with all the components to lift, guide and propel the vehicle;
 - design a scaled system (Fig. 3);
 - full scale system preliminary design in immersive virtual reality (Fig. 4);
 - full scale system detailed design.

The first five steps were carried out while the sixth is under development. As per above, within the possible technological scenarios, the SML method and direct current linear propulsion device were considered the most suitable to meet the design constraints.



Fig. 3. UAQ4 mockup



Fig. 4. Immersive virtual reality design

TECHNOLOGICAL LABORATORY SYSTEM

The UAQ4 demonstrator system (Fig. 5) was designed and constructed to be quite simple: it consists of two main contact-less parts:

- A track (3.72 m long and 0.81 m wide) with three parallel permanent magnet guideways, of which the outer two are “V” shaped and the central one is “U” shaped. All guideways consist of iron beam with NdFeB permanent magnets arranged in the inner beams surfaces according to a proper polarity configuration.

- A bogie (0.72 m long, 0.81 m wide), with four “V” shaped superconducting “skaters” (each 0.185 m long) aboard, fixed to both sides of the body, and with the primary of a linear motor in the middle of the frame. The “skates” consists of “V” assembled close arrays of melt textured YBCO bulks cooled at low temperature (77 K at 1 atm.) by liquid nitrogen in a suitable cryogenic vessel.



Fig. 5. UAQ4 laboratory system

The interaction between superconducting “skates” and the magnetic field of the lateral guideways generates stable suspension and guidance of the vehicle.

Fig. 6 illustrates the finite element analysis results of the interaction between guideway magnetic field and superconductors of the “skate”. The resultant of the vertical (F_L) and lateral (F_G) components of the levitation forces (F_S) originates lift and guidance effects of the skate on the guideway.

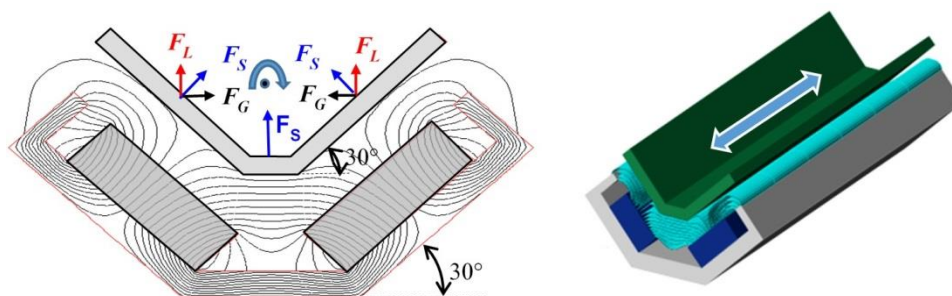


Fig. 6. Magnetic interaction schemes

Several tests have been performed to fully verify that the suspension modules of the bogie operate in a self-balanced condition [10–13] without magnetic resistance to the motion [14].

High values of guidance effect is obtained by summing the pin effect force to the lateral repulsive forces.

Suspension device doesn't require power consumption for levitation, except the negligible power needed for cooling the bulk superconductors. So, at ordinary motion condition, the traction energy depends only from aerodynamic resistance entity; and at constant and low speed it is almost zero.

Propulsion and braking are provided by an innovative direct current linear stepper motor, safely operating along the whole speed range [15–16]. The secondary of the linear motor that is installed in the middle of the vehicle frame separately provides propulsion by interacting with fixed primary component ("U" shaped central magnetic beam).

Suspension and propulsion devices have been patented [17–18] and laboratory successfully tested.

MAGNETIC RESISTANCE CONSIDERATIONS

The propulsion power $P(t)$ of a maglev train can be calculated, besides the running in tunnels and in curve whenever it is the case, as

$$P(t) = \sum R \cdot v(t) = [R_{ae}(v) \pm R_{gr} + R_{in}(\dot{v}) + R_{mag}(v)] \cdot v(t) \quad (1)$$

where $R_{ae}(v)$ is the aerodynamic resistance, R_{gr} is the gradient resistance, $R_{in}(\dot{v})$ is the inertial resistance and $R_{mag}(v)$ is the magnetic resistance that depends on technology, as well as better detailed below.

The motion resistances are evaluated by using the following relations:

$$R_{aero} = \frac{1}{2} \cdot \rho \cdot S \cdot v^2 \cdot (c_{af} + \frac{S}{S'} c_{at}) \quad (2)$$

$$R_{grad} = m \cdot g \cdot \sin \alpha \quad (3)$$

$$R_{iner} = m \cdot \frac{dv}{dt} \quad (4)$$

where m is the gross mass of the train, v is the train speed, g is the gravity acceleration, α is the angle of the guideway slope, ρ is the air density, c_{af} and c_{at} are the frontal and tangential aerodynamic coefficients, S and S' are the vehicle

frontal area and the train tangential area (depending on the number of cars in the train).

Considering regenerative electrical braking, the electric power $P_e(t)$ for propulsion is:

$$\begin{aligned} P_e(t) &= \frac{P(t)}{\mu} \quad @ \quad P(t) > 0 \\ P_e(t) &= \mu \cdot P(t) \quad @ \quad P(t) < 0 \end{aligned} \quad (5)$$

where μ is the efficiency of the propulsion system.

The integration in the time variable of $P_e(t)$ multiplied by the speed allows to obtain the train propulsion energy.

$$E_e(t) = \int P_e(t) \cdot dt \quad (6)$$

Compared with WoR system, EDS and EMS maglev technologies allow to avoid any mechanical contact between train and guideway and to eliminate rolling friction but, at same time, they generate an additional magnetic resistance that do not exist in WoR system.

Additional magnetic resistance (R_{mag}) depends on the kind of maglev technology: it is almost zero for UAQ4 technology while this takes on different values for the EMS and EDS technologies.

Stephan and Lascher [19] proposed a theoretical calculation method to determinate the additional magnetic resistances of the high speed EMS (Transrapid) and EDS (MLX01) systems. As reported by the Authors, the additional magnetic resistances depend on the considerations and parameters synthetically reported below.

EMS train's additional magnetic resistance (R_{mag}^{EMS}) is a function of two parameters as indicated by the relation (7):

$$R_{mag}^{EMS} = f(R_{LG}; R_{LM}) \quad (7)$$

where: R_{LG} is the linear generator resistance that is zero for speed up to 100 km/h and R_{LM} is eddy-current resistance (due to the eddy-currents in the guideway) [19].

EDS train's additional magnetic resistance (R_{mag}^{EDS}) is a function of four parameters as indicated by the following relation (8)

$$R_{mag}^{EDS} = f(K'_{coil}; K_{coil}; n; v_c) \quad (8)$$

where: K'_{coil} is specific coil coefficient that takes into account interference

among the solenoids consecutively set in a super-conducting magnet of the train; K_{coil} is the coil coefficient, n number of cars in the train and v_c is a specific speed coefficient [19].

According to Stephan and Lascher analysis results, Fig. 7 illustrates the additional magnetic resistance of EMS, EDS calculated for a fixed train configuration (five cars) at constant speed motion condition. In the same Fig. 7 we also report, for the same work conditions, the UAQ4 magnetic resistance graph. The different performances of the three selected systems in terms of magnetic resistance to motion are effectively highlighted in the same figure.

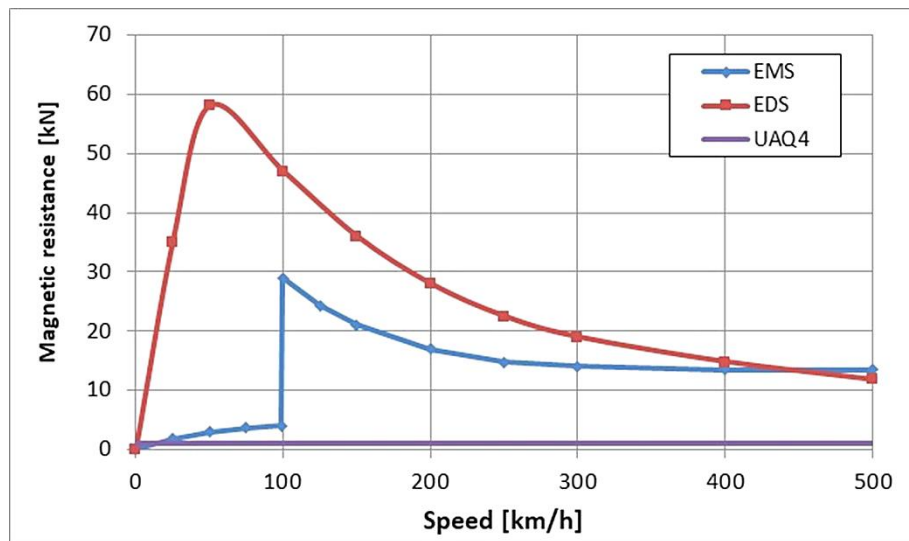


Fig. 7. Additional magnetic resistance for EMS, EDS and UAQ4

Moreover, a numerical comparison between the magnetic resistances of the three maglev systems (EMS, EDS and SML) and rolling resistance of a high speed wheel-on-rail system (WoR) has been performed.

Rolling resistance for WoR high speed train can be calculated by the following relation:

$$R_w = \left[0.7 + \frac{130}{m_{ax} \cdot g} + 0.009 \cdot v \right] \cdot m \cdot g \cdot \cos \alpha \quad (9)$$

where m_{ax} is the mass on axle, m is the train gross mass and α is the angle of the guideway slope. As relation (9) is empirical formulation, speed is in km/h, mass in ton and resistance in Newton.

Italian high speed WoR train (ETR500) [20] was taken into consideration.

Table 1 lists the convoy configurations and the carrying capacity of the different systems that were taken into account for resistance comparison analysis.

Fig. 8 illustrates the theoretical comparison between the specific

additional magnetic resistances (kN/passenger) for the three EMS, EDS and SML maglev systems (continuous lines) compared with the specific rolling resistance (kN/passenger) for WoR system (dotted line).

It can be noted that the specific magnetic resistance of UAQ system is almost zero. Moreover, EMS and EDS specific magnetic resistances are higher than the WoR specific rolling resistance up to a speed of around 180 km/h and 240 km/h, respectively. So, in term of motion resistance, WoR system is most efficiently than EMS and EDS at low/average speed values. On the contrary, for high speed motion EDM and EMS systems are more efficient.

Table 1. Guided systems carrying capacities

Technology	Train	N. of cars	Front car		Meaddle car		Train carrying capacity
			N.	Pass./car	N.	Pass./car	Pass./train
EDS	MLX1	5	2	24	3	70	258
EMS	Transrapid		2	62	3	84	376
SML	UAQ4		2	72	3	88	408
WOR	ETR 500		1	0	4	68	272

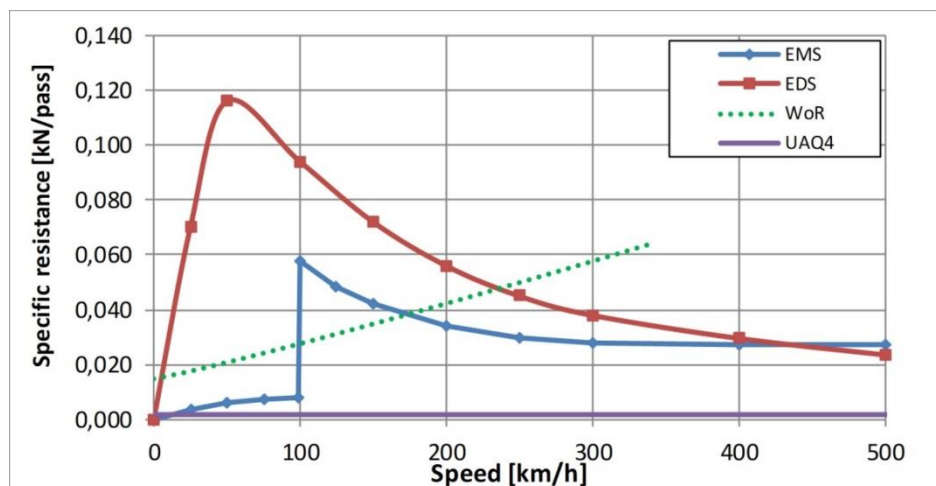


Fig. 8. Specific resistance for EMS, EDS, UAQ4 and WoR systems

INNOVATION AND ADVANTAGES

Compared with the international state of the art of maglev technologies, the UAQ4 system introduces the following significant innovations:

- three axes self-balancing magnetic suspension with large operative air gap;
- self-balancing and high guidance effect;
- no magnetic resistance to motion;
- high-efficiency propulsion system (direct current linear motor with a large air gap);
- near-zero energy consumption at low and constant speed;

- light-weight vehicle architecture close to aeronautical standard (light materials, big size, and high comfort level).

Even if the work criteria are valid for both low-speed and high-speed transportation applications, the UAQ4 system is particularly suitable for urban environment that involves short distances between stops, the ability to overcome longitudinal gradients, large accelerations, and low operating speed. In this context, the UAQ4 operates with negligible power consumption since the ordinary resistance to the motion is almost zero.

REMARKS AND OUTLOOK

The UAQ4 superconducting magnetically levitated system features were illustrated in this paper.

Compared to other magnetic levitation methods, UAQ4 system eliminates any magnetic resistance to the motion and its suspension device doesn't require power consumption for levitation, except the negligible power needed for cooling the bulk superconductors. Moreover, at ordinary motion condition, the UAQ4 traction energy depends only from aerodynamic resistance entity; at constant and low speed it is almost zero.

The basic research activities for defining and testing the UAQ4 superconducting magnetically levitated system technologies are mostly concluded. The system architecture has been defined and the full scale vehicle is under design.

The implementation outline asks for a consortium of interested industrial partners operating in the aeronautical and the traditional railway industries. The objective is to develop a full scale urban version system prototype with vehicles mainly powered by solar energy.

References

1. Magnetschwebbahn Transrapid in Shanghai. June 20, 2018. Available at: <https://www.hochgeschwindigkeitszuege.com/china/transrapid-china.php>
2. Maglev Systems Technology Division. June 20, 2018 Available at: <http://www.rtri.or.jp>
3. Schultz L, de Haas O, Verges P, Beyer C, et al. Superconductively levitated transport system: The SupraTrans project, *IEEE Trans. Appl. Supercond.*, 2005;15(2):2301-2305.
4. Wang J, Wang X, Wang Z, Ren Y, et al. The man-loading high-temperature superconducting MagLev test vehicle, *IEEE Trans. Appl. Supercond.* 2003;13(2):2134-2137. doi: 10.1109/tasc.2003.813017
5. Stephan RM, de Andre R, Ferreira AC. Superconducting Light Rail Vehicle" *IEEE Vehicular Technology Magazine*. 2012;7(4):122-127. doi: 10.1109/mvt.2012.2218437
6. Lanzara G, D'Ovidio G, Crisi F. UAQ4 Levitating Train: Italian Maglev Transportation System *IEEE Vehicular Technology Magazine*. 2014;9(4):71-77. doi: 10.1109/mvt.2014.2362859
7. Lanzara G. The IAP3 vehicle design and construction *High-speed surface transport Aeronautics Institute of Palermo University*; 2; 1973. (In Italian).

8. Lanzara G, Mattioli E. One-sided linear induction motor. *High-speed surface transport*. Aeronautics Institute of Palermo University; no. 2, 1973. (In Italian).
9. Lanzara G, inventor. Magnetically levitated vehicle with superconducting mirror sheets interacting with guideway magnetic field. *US Patent* no. 4979445, 1990.
10. D'Ovidio G, Crisi F, Navarra A, Lanzara G. Lift and guidance forces by using iron-magnetic track with side rims and passive HTC superconducting plate: experimental analyses *Materials Processing Technology*. 2007;181:18-24. doi: 10.1016/j.jmatprotec.2006.03.047
11. D'Ovidio G, Crisi F, Navarra A, Lanzara G. Comparison of maglev behavior of three inductors with static and dynamic field interacting with a HTC superconductor: test and evaluation *Physica C: Superconductivity and its applications*. 2006;449:15-20. doi: 10.1016/j.physc.2006.06.004
12. D'Ovidio G, Crisi F, Lanzara G. A “V” shaped superconducting levitation module for lift and guidance of a magnetic transportation system *Physica C: Superconductivity and its applications*. 2008;468:1036-1040. doi: 10.1016/j.physc.2008.05.154
13. D'Ovidio G, Crisi F, Lanzara G. Design and optimization of UAQ4 experimental maglev module. *Material Science Forum in Applied Electromagnetic Engineering*. 2011;1058:42-47. doi: 10.4028/www.scientific.net/msf.670.42
14. D'Ovidio G, Crisi F, Lanzara G. On the magnetic resistance of YBaCuO bulk superconductor dynamically interacting with troubled flux of iron-homopolar magnetic track. *Optoelectronics and Advanced Materials*. 2008;10:1011-1016.
15. D'Ovidio G, Crisi F. UAQ4 magnetic levitating train: propulsion system for urban transportation. *Energy and Power Engineering*. 2012;6:1952-1956.
16. D'Ovidio G, Crisi F. High speed propulsion system for UAQ4 magnetic levitating train. *Material Science Forum in Applied Electromagnetic Engineering*, vol.721, p. 9–14, Jun 2012. doi: 10.4028/www.scientific.net/msf.721.9
17. Lanzara G, D'Ovidio G, Crisi F, inventors. Magnetically levitated system for lifting and guiding constituted by bilateral iron magnetic guide-way with permanent magnets interacting with high critical temperature superconducting “runners”, with same shape of the guide-way one, set on board the vehicle (In Italian) *IT Patent* no.1386002, 2007.
18. D'Ovidio G, Lanzara G, Crisi F, inventors. Bipolar stepper linear motor for the propulsion of guided transportation systems, realized with d.c. supplied windings placed on board the vehicle, interacting with permanent magnets distributed on the bilateral iron magnetic guide-way of the track, (in Italian) *IT Patent* n. 1385998, 2007.
19. Stephan A, Lascher A. Comparison of Train of TRANSRAPID and MLXO1. *Proceedings of the 18th Magnetically Levitated System Linear Drives Conference*; 2008 Oct. 26–28; Shanghai, Japan. doi: 10.1109/MVT.2014.2362859
20. ETR.500 June 20, 2018. Available at: https://it.wikipedia.org/wiki/Treno_FS_ETR.500

Information about the authors:

D'Ovidio Gino, professor; address: Via G. Gronchi, 18, 67100 L'Aquila, Italy

ORCID: 0000-0003-3978-604X;

E-mail: gino.dovidio@univaq.it

Lanzara Giovanni, professor;

E-mail: giovanni.lanzara@gmail.com

To cite this article:

D'Ovidio G, Lanzara G. Innovations and Performance of Italian UAQ4 Superconducting Magnetic Levitated System. *Transportation Systems and Technology*. 2018;4(2):19-29. doi: 10.17816/transsyst20184219-29



DOI 10.17816/transsyst20184230-44

© S. Mu, J. Kang, S. Wang, Y. Liu, C. He

Tongji University
(Shanghai, China)

A METHOD OF THRUST RIPPLE SUPPRESSION FOR LONG STATOR LINEAR SYNCHRONOUS MOTOR

Abstract. With the advantages of high speed, low noise and high efficiency, the electromagnetic suspension (EMS) type maglev train has a good prospect in railway transportation. It is based on the long stator linear synchronous motor (LSLSM). However, due to cogging effect, end effect and the harmonics in the stator current and flux density distribution around the air-gap, the thrust generated by the LSLSM fluctuates. The thrust ripple brings noise, drop of control accuracy, even causes the resonance of train. In this paper, the thrust ripple produced by the cogging effect and flux linkage harmonics is analyzed. Then a method of harmonic current injection is proposed to compensate cogging force and reduce the thrust ripple, without influence the decoupling control of traction and suspension system. The injected current harmonics are controlled under multiple rotating reference frames independently. Finally, based on voltage equations of harmonics, the decoupled harmonic current controllers with harmonic voltage feedforward are designed, which improve the performance of current harmonics response and thrust ripple suppression. Simulation results on Simulink verify the effectiveness of proposed thrust ripple suppression method for LSLSM.

Keywords: Maglev, Long stator linear synchronous motor, Thrust ripple, Cogging force, Harmonic current injection, Multiple rotating reference frames, Voltage feedforward

INTRODUCTION

Without contact between vehicle and railway, maglev train is a one of the best options for future high-speed ground transportation system. The electromagnetic suspension (EMS) type maglev transportation system is one representative, and has been applied in the first commercial operation maglev line of world built in Shanghai. It shows advantages of high speed, low noise and high efficiency. The traction of vehicle is based on the long stator linear synchronous motor (LSLSM), where the railway is motor's long stator and the vehicle is the mover.

However, it suffers from the propulsion force fluctuation in operation, which brings noise, deteriorates control accuracy, even causes resonance of vehicle, makes passengers uncomfortable. Generally speaking, nonideal factors in practical LSLSM drive system are main reasons of thrust ripple, such as non-sinusoidal stator currents [1], cogging effect, end effect [2], harmonics of flux linkage, etc.

A lot of research works have been carried out to reduce the thrust ripple of LSM both from motor design and control algorithm. Many methods are

proposed on motor design and reduce thrust ripple by optimizing the structure, including magnet skewing or slot skewing, optimizing pole-arc coefficients [3], auxiliary pole [4] and unequal pole pitch of the stator and mover [5], etc. But the structure optimizing is not a universal method for all the LSM, and hard to eliminate all thrust harmonics.

Other researchers focus on the control strategies to suppress thrust ripple. Some methods to reduce the stator current harmonics by compensating the dead time effect of inverter are proposed [6, 7]. But it can't suppress the main thrust ripple caused by non-sinusoidal distributed magnetic field and cogging force. One way is to obtain the magnitude and phase of thrust ripple and compensate it on the control command. Adaptive algorithm [8], disturbance observer [9], repetitive control [10], iterative learning control [11] are studied since thrust ripple is periodical. Though stator current harmonics will cause electromagnetic force ripple, adequate electromagnetic force harmonics can counteract the reluctance force ripple of motor, which is the essence of suppressing thrust ripple. In [12], harmonic injection is proposed to reduce thrust ripple in linear flux-switching motor. But the harmonic current is controlled by current hysteresis controller, thus the switching frequency is variable. [13] introduces multiple reference frames to solve the bandwidth limits of traditional PI current controller in permanent magnet machines (PMSM). But the coupling of harmonic currents is not considered. In [14], harmonic voltage and current coupling model of PMSM is studied, improves the injection effect of harmonic current and torque ripple reduction performance.

This paper presents a thrust ripple suppression method by harmonic current injection with harmonic voltage feedforward for maglev LSLSM drives. The drive system is based on the rotor flux oriented control (RFOC), and only q -axis current is injected into current harmonics, which won't influence the decoupling of traction and suspension system [15]. Multiple reference frames, harmonic current decoupling and harmonic voltage feedforward are applied in the system, which overcome the bandwidth limits of conventional PI current controller and improve the effect of harmonic current injection and suppression of thrust ripple. The paper starts with introduction of the model of LSLSM, considering cogging force and exciting flux linkage harmonics. Then, thrust ripple suppression method is performed, including determination of proper injected harmonic current and control of reference harmonic current. In the following, simulation results on the LSLSM are presented. The conclusion is given in the end.

THRUST RIPPLE OF LONG STATOR SYNCHRONOUS MOTOR

A. Model of long stator synchronous motor

Assuming symmetry of three phase stator winding and ignoring magnetic saturation, hysteresis, and eddy current, the mathematical model of LMSM in

the rotor flux synchronous rotating coordinates can be written as:

$$\begin{cases} u_d = R_s i_d + L_d \frac{di_d}{dt} - \frac{\pi}{\tau_s} v \psi_q \\ u_q = R_s i_q + L_q \frac{di_q}{dt} + \frac{\pi}{\tau_s} v \psi_d \\ \frac{dv}{dt} = \frac{1}{m} (F_x - F_z) \end{cases} \quad (1)$$

where u_d , u_q , i_d and i_q are the stator voltages and currents on d, q axes, respectively; ψ_d and ψ_q are the stator flux on d, q axes respectively; R_s is total stator resistance; L_d, L_q are the total stator inductance on d, q axes respectively; τ_s is the pole pitch; v is the mover speed; m is the vehicle mass; F_x is the thrust force; F_z is the overall resistance force, consist of air resistance force, magnet resistance force and generator resistance force.

Unlike general rotary motor, the impedance of feed cable, stator section uncovered by vehicle pole and stator section covered by vehicle pole comprise the total stator resistance and inductance of LSLSM [16]. Since the length of stator section is much longer than vehicle length, the leak inductance of stator section uncovered by vehicle makes up the main part of total stator inductance, which leads to inductance L_d approximately equal to L_q .

The stator flux equation on d, q axes is expressed as:

$$\begin{cases} \psi_d = L_d i_d + \psi_{df} \\ \psi_q = L_q i_q + \psi_{qf} \end{cases} \quad (2)$$

where ψ_{df} and ψ_{qf} are the mover exciting flux linkage on d, q axes, produced by excitation winding of vehicle suspension electromagnetic.

The thrust force of LSLSM is composed of electromagnetic force F_e and cogging force F_{cog} , i.e.,

$$F_x = F_e + F_{cog} \quad (3)$$

where F_{cog} is the reluctance force due to slot effect; F_e is produced by the interaction between airgap flux and the stator currents, and equal to the mean value of thrust force. It can be expressed as:

$$F_e = \frac{3\pi}{2\tau_s} (\psi_d i_q - \psi_q i_d) = \frac{3\pi}{2\tau_s} [(\psi_{df} + L_d i_d) i_q - (\psi_{df} + L_d i_q) i_d] \quad (4)$$

Due to decoupling the armature field and excitation field, the rotor field-oriented control (RFOC) and $i_d = 0$ strategy are commonly applied for LSLSM control in practical [15]. In this case, (4) can be simplified as:

$$F_e = \frac{3\pi}{2\tau_s} \psi_{df} i_q \quad (5)$$

B. Flux harmonics

In an ideal LSLSM, where excitation flux is ideal sinusoidal distributed in the air gap, ψ_{qf} is equal to zero and ψ_{df} is constant under RFOC control.

However, because of manufacturing restrictions, there are $6k$ th spatial harmonics in practical in the mover flux linkage in practical, and can be expressed in Fourier series as:

$$\begin{cases} \Psi_{df} = \Psi_{d0} + \sum_{k=1}^{+\infty} \Psi_{d\pm 6k} e^{i\left(\pm 6k \frac{\pi x}{\tau_s}\right)} = \Psi_{d0} + \sum_{k=\pm 1, \pm 2, \pm 3, \dots} \Psi_{d6k} \cos\left(6k \frac{\pi x}{\tau_s}\right) \\ \Psi_{qf} = \Psi_{q0} + \sum_{k=1}^{+\infty} \Psi_{q\pm 6k} e^{i\left(\pm 6k \frac{\pi x}{\tau_s}\right)} = \sum_{k=1, 2, 3, \dots} \Psi_{q6k} \cos\left(6k \frac{\pi x}{\tau_s}\right) \end{cases} \quad (7)$$

where x is the mover position relative to phase A; Ψ_{d6k} and Ψ_{q6k} are the harmonic coefficients of $6k$ th flux harmonic on d, q axes respectively. The dc component of d -axis flux linkage Ψ_{d0} is non-zero, while Ψ_{q0} equals to zero.

According to the thrust equation, the spatial harmonics of flux linkage will result in the $6k$ th periodical thrust ripple of real LSLSM with sinusoidal fed stator currents. Moreover, it brings harmonics in back electromotive force (EMF), and deteriorate the control effect of current controller.

C. Cogging force

The stator windings are placed in the stator slots on LSLSM of maglev. When the mover poles approaching or leaving the stator teeth, the reluctance and magnetic field distribution vary. That leads to the fluctuation of magnetic energy of motor, generating additional reluctance force on mover. The cogging force is independent of the stator current while closely related to mover position. The period of cogging force is the distance between neighboring slots. Since there are six slots at each pole pair, the cogging force fluctuates 6 times within one pair of poles. Fourier expression of cogging force can be written as

$$F_{\text{cog}} = F_{c0} + \sum_{k=1}^{+\infty} F_{c\pm 6k} e^{i\left(\pm 6k \frac{\pi x}{\tau_s}\right)} \quad (8)$$

where F_{c6k} is the harmonic coefficients of $6k$ th component of Fourier series, and the dc component F_{c0} is equal to zero.

HARMONIC CURRENT INJECTION

A. Reference Harmonic Current

Taking Fourier expressions of flux linkage equation (7) and cogging force equation (8) into the thrust expression (3), it yields

$$F_x = \frac{3\pi}{2\tau_s} \left(\sum_{k=0}^{+\infty} \Psi_{d\pm 6k} e^{i\left(\pm 6k \frac{\pi x}{\tau_s}\right)} \right) \cdot i_q + \sum_{k=0}^{+\infty} F_{c\pm 6k} e^{i\left(\pm 6k \frac{\pi x}{\tau_s}\right)} \quad (9)$$

The formula shows that there will be $6k$ th periodical thrust ripple of LSLSM if i_q is kept constant when flux linkage harmonics and cogging force exist. One way to compensate the cogging force and suppress thrust ripple is to inject harmonic current into q -axis current. To generate $6k$ th periodical

electromagnetic force, 6 k th current harmonics are needed. The desired q -axis current can be assumed as

$$i_q^* = i_0 + \sum_{k=1}^{+\infty} i_{\pm 6k} e^{i\left(\pm 6k\pi\theta_e + \frac{\pi}{2}\right)} \quad (10)$$

where i_{6k} are the complex coefficients of 6 k th harmonics; θ_e is electrical angle of mover, and satisfies $\theta_e = \pi x / \tau_s$; $\pi/2$ is added since q -axis component is with a 90 degree phase lead.

Substituting (8) and (9) into (7), and Supposing the desired thrust is F_x^* , it yields the following formula

$$\frac{3\pi}{2\tau_s} \left(\sum_{k=0}^{+\infty} \Psi_{d\pm 6k} e^{i\left(\pm 6k\frac{\pi x}{\tau_s}\right)} \right) \cdot \left(i_0 + \sum_{k=1}^{+\infty} i_{\pm 6k} e^{i\left(\pm 6k\pi\theta_e + \frac{\pi}{2}\right)} \right) + \sum_{k=1}^{+\infty} F_{c\pm 6k} e^{i\left(\pm 6k\frac{\pi x}{\tau_s}\right)} = F_x^* \quad (11)$$

Numerous linear equations can be derived from above expression and thrust ripple of any order can be eliminated in theory if the number and amplitude of current harmonics are not limited. However, the bandwidth of controller is limited in reality, it will cause large error when tracking reference currents of high frequency. Meanwhile, too many currents harmonics also increase the burden of controller. Since the 6th harmonic thrust accounts for the biggest part of thrust ripple [5], only 6th current harmonics are needed to suppress the 6th harmonic thrust ripple. In this case, equation (11) can be expressed as

$$\frac{3\pi}{2\tau_s} \left(\Psi_{d0} + \Psi_{d-6} e^{-j6\frac{\pi x}{\tau_s}} + \Psi_{d6} e^{j6\frac{\pi x}{\tau_s}} \right) \cdot \left(i_{q0} + i_{-6} e^{-j6\frac{\pi x}{\tau_s}} + i_{6} e^{j6\frac{\pi x}{\tau_s}} \right) + F_{c-6} + F_{c6} = F_x^* \quad (12)$$

By combining the same order harmonic terms, it yields the following equation

$$\frac{3\pi}{2\tau_s} \begin{bmatrix} \Psi_{d0} & i_{-6}\Psi_{d6} & i_{6}\Psi_{d-6} \\ i_{-6}\Psi_{d-6} & \Psi_{d0} & 0 \\ i_{6}\Psi_{d6} & 0 & \Psi_{d0} \end{bmatrix} \begin{bmatrix} i_{q0} \\ i_{-6} \\ i_{6} \end{bmatrix} = \begin{bmatrix} F_x^* \\ -F_{c-6} \\ -F_{c6} \end{bmatrix} \quad (13)$$

From (13), the amplitude of desired q -axis current can be solved. Here the 12th electromagnetic force harmonic equations are neglected, since the force generated by harmonic current and flux harmonic is relatively small and will make the equation has no solution.

B. Multiple rotating Reference Frames

PI controllers are applied in traditional RFOC of LSLSM as d, q axes current controller. Restricted by bandwidth, it is difficult for PI controller to track ± 6 th harmonics reference current in d, q coordinate, especially at high speed. However, these harmonics in d, q coordinate can be converted to dc component in the coordinate rotating at the same frequency of harmonic. In this case, the synchronous reference frames rotating at multiple times the speed of

d, q coordinate are introduced and stator currents with different frequencies are controlled independently. The ± 6 th reference harmonic current in d, q coordinate corresponds to 7th and 5th harmonic in stationary reference frame, respectively. The multiple reference frames introduced in this paper are depicted as diagram below.

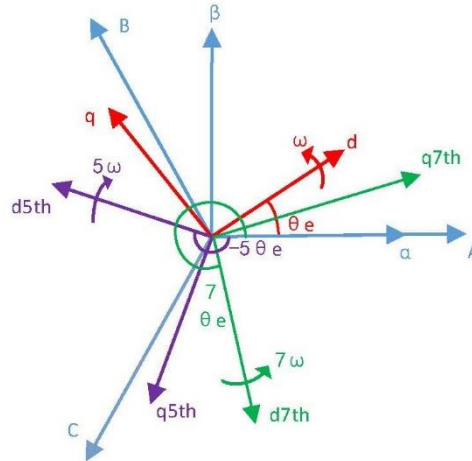


Fig. 1. The multiple reference frames of LSLSM, where A, B, C and α, β are the stationary reference frame; d, q coordinate rotate synchronously with mover, and $\omega = \pi \nu / \tau_s$ is the synchronous speed corresponding to electric angular speed of mover; $d5, q5th$ coordinate rotate at 5 times the speed of d, q coordinate reversely; $d7, q7th$ coordinate rotate at 7 times the speed of d, q coordinate in the same direction

The transformation matrix from α, β coordinate to multiple rotating reference frames can be expressed as

$$T(k\theta_e) = \begin{bmatrix} \cos(k\theta_e) & \sin(k\theta_e) \\ -\sin(k\theta_e) & \cos(k\theta_e) \end{bmatrix} \quad (14)$$

where $k = 1, -5, 7, \dots$

After coordinate transformation, current components with same angular speed with reference frame become constant, while others are alternating. Then the dc component can be abstracted after a low-pass filter, which is the magnitude of real current harmonic. Thus, the closed-loop feedback control of current harmonics can be established as shown below

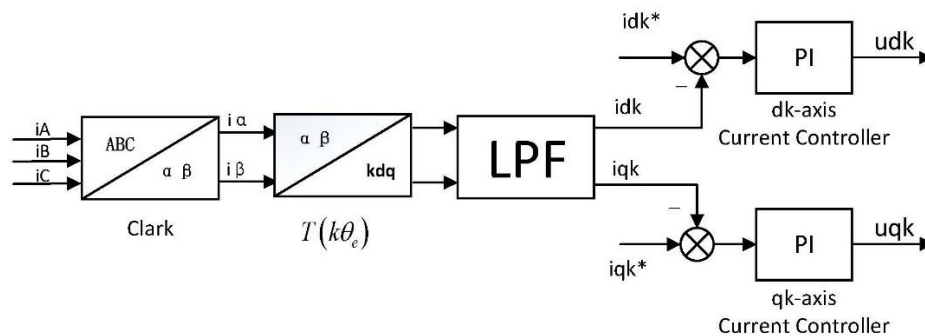


Fig. 2. The diagram of harmonic current closed-loop feedback control,

where idk^* and iqk^* are the reference values of k th harmonics current in k th reference frame,

and satisfy

$$\begin{cases} id5^* + i \cdot iq5^* = i_{-6} \\ id7^* + i \cdot iq7^* = i_6 \end{cases} \quad (15)$$

C. Harmonic Voltage Decouple and Feedforward Control

In conventional d, q axes current controller, the d, q axes currents are decoupled by compensation of EMF, the voltage equation in the d, q axes after compensation of EMF can be written as

$$\begin{cases} u_d^* = u_d + \frac{\pi}{\tau_s} v \Psi_q = R_s i_d + L_d \frac{di_d}{dt} \\ u_q^* = u_q - \frac{\pi}{\tau_s} v \Psi_d = R_s i_q + L_q \frac{di_q}{dt} \end{cases} \quad (16)$$

where u_d^* and u_q^* are d, q axes voltage generated by current PI controllers respectively.

Substitute (15) into (11), the desired current in d, q coordinate can be rewritten as

$$\begin{cases} i_{d5}^1 = i_{d5} \cos(-6\omega t) - i_{q5} \sin(-6\omega t) \\ i_{q5}^1 = i_{d5} \sin(-6\omega t) + i_{q5} \cos(-6\omega t) \\ i_{d7}^1 = i_{d7} \cos(6\omega t) - i_{q7} \sin(6\omega t) \\ i_{q7}^1 = i_{d7} \sin(6\omega t) + i_{q7} \cos(6\omega t) \end{cases} \quad (17)$$

where i_{d5}^1 and i_{q5}^1 are the voltage of 5th current harmonic in d, q coordinate; i_{d7}^1 and i_{q7}^1 are the voltage of 7th current harmonic in d, q coordinate.

Since the inductance L_d and L_q are approximately equal in LSLSM, $L = L_d = L_q$ is introduced to simplify the equation. By substituting (17) into (16), the harmonic voltage equations can be written as

$$\begin{cases} u_{d5}^1 = R_s i_{d5}^1 + 6\omega L i_{q5}^1 \\ u_{q5}^1 = R_s i_{q5}^1 - 6\omega L i_{d5}^1 \\ u_{d7}^1 = R_s i_{d7}^1 - 6\omega L i_{q7}^1 \\ u_{q7}^1 = R_s i_{q7}^1 + 6\omega L i_{d7}^1 \end{cases} \quad (18)$$

where u_{d5}^1 and u_{q5}^1 are the voltage of 5th current harmonic in d, q coordinate; u_{d7}^1 and u_{q7}^1 are the voltage of 7th current harmonic in d, q coordinate.

By rotating coordinate transformation of the voltage equations in d, q coordinate, the voltage equations of 5th current harmonic in $d5, q5$ coordinate can

be expressed as

$$\begin{cases} u_{d5}^5 = R_s i_{d5} + 6\omega L i_{q5} \\ u_{q5}^5 = R_s i_{q5} - 6\omega L i_{d5} \end{cases} \quad (19)$$

Similarly, the voltage equations of 7th current harmonic in $d7, q7$ coordinate can be expressed as

$$\begin{cases} u_{d7}^7 = R_s i_{d7} - 6\omega L i_{q7} \\ u_{q7}^7 = R_s i_{q7} + 6\omega L i_{d7} \end{cases} \quad (20)$$

To increase the response speed of harmonics, the voltage feedforward is introduced. The feedforward voltage can be calculated according to reference currents and voltage equations, that is

$$\begin{cases} u_{d5_com} = R_s i_{d5}^* + 6\omega L i_{q5}^* \\ u_{q5_com} = R_s i_{q5}^* - 6\omega L i_{d5}^* \\ u_{d7_com} = R_s i_{d7}^* - 6\omega L i_{q7}^* \\ u_{q7_com} = R_s i_{q7}^* + 6\omega L i_{d7}^* \end{cases} \quad (21)$$

where $u_{i_com}, i = d5, q5, d7, q7$ are the feedforward voltages on $d5, q5$ axes and $d7, q7$ axes, respectively.

From harmonic voltage equations in (19) and (20), it can be seen the currents in dk, qk axes are coupled. Thus, the decoupled harmonic current controllers with voltage feedforward are designed. The following diagram shows the structure of 5th current harmonic controller.

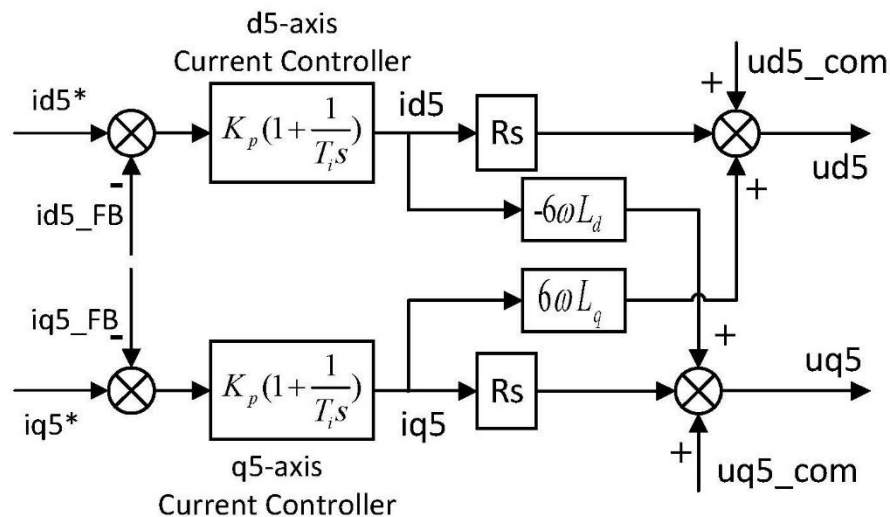


Fig. 3. The diagram of 5th harmonic current closed-loop feedback control,

where errors of harmonic current are sent to PI controller, whose output is also current. The final output of harmonic current controller is harmonic voltage, made up by feedback control voltage and feedforward steady state voltage.

The controller of 7th current harmonic can be designed in the same way according to (19) and (21).

SIMULATION AND RESULTS

The performance of the proposed thrust ripple suppression method for LSLSM has been tested through simulation experiments on MATLAB/Simulink. The LSLSM applied in simulation is one stator section of 960 m long with one maglev frame. The maglev frame of equal pole pitch is built in Maxwell software as shown in Fig. 4.

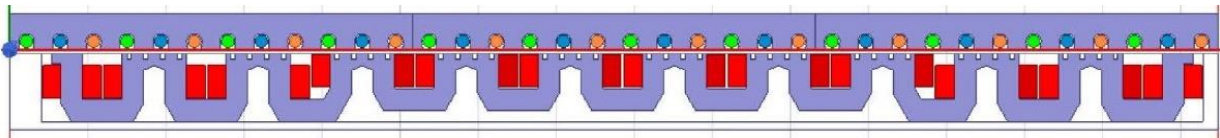


Fig. 4. Simulation model of LSLSM in Maxwell of equal pole pitch

Through finite element calculation, not only the parameters of maglev frame, but also the flux linkage with fluctuation and cogging force are obtained, considering non-linear properties of LSM. From that, the 6th harmonics of flux linkage and cogging force are obtained by Fourier transformation, and considered in the LSLSM simulation model. The main parameters of LSLSM are listed in Table 1, where the parameters of stator are based on the maglev test line.

Table 1. Parameters of LSLSM

Parameter	Value	Parameter	Value
Stator resistance (Ω)	0.2237	Excitation flux (wb)	0.1171
Stator inductance L_d (mH)	2.4817	Pole pitch (mm)	266.5
Stator inductance L_q (mH)	2.4764	Mass (kg)	3000

The block diagram of the thrust controlled LSLSM drive system is depicted in Fig. 5. Here only current closed loop control is included instead of position-speed-current control because it's enough to validate the effect of thrust ripple suppression. The LSLSM is fed by three level neutral point clamped voltage source inverter, whose rated voltage is 1900 V and rated current is 1200 A. The switching frequency of inverter and control frequency of current controller are 2 kHz. At first, the optimal reference current are determined by the current assignment block based on equation (13) and (15). The stator currents of different frequency are controlled independently in multiple reference frames. By coordinate transformations and low-pass filters, the feedback of current in multiple rotating reference frames are obtained from the measured stator current. The controller of current on d, q axes is a decoupled PI controller with voltage compensation for EMF. The 5th and 7th current harmonics are controlled by decoupled PI controllers with steady state voltage feedforward

on $d5, q5$ and $d7, q7$ coordinate, respectively. Finally, the control voltage of each current controller are transformed to α, β stationary reference frame, and together make up the voltage reference u_{α}^* and u_{β}^* of SVPWM, which generates gate signals of inverter.

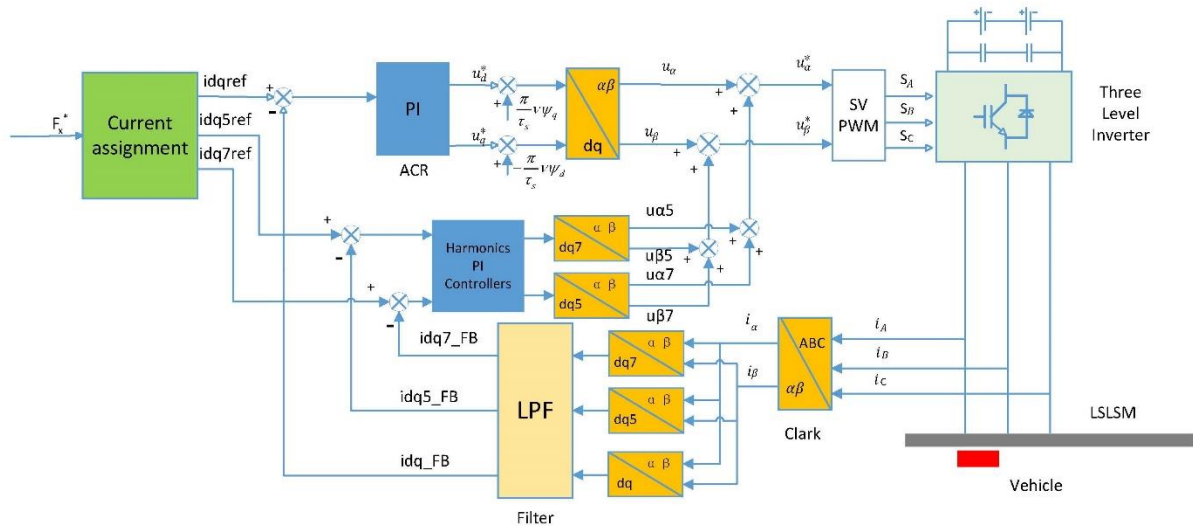


Fig. 5. The block diagram of thrust controlled drive system for LSLSM

In Fig. 6–8, results of one simulation test are shown. In this test, the thrust ripple of without harmonic current injection, harmonic current injection by proposed harmonic current controller and injection by conventional PI current controller are compared. From 0–1s, no harmonic current is injected into stator current. The proposed thrust ripple suppression strategy is applied at 1.0 s. From 2.0 s to the end, the injected harmonic current is controlled only by PI controllers on d, q axes. The load force is 1500 N and the maglev frame is propelled to 10.66 m/s and corresponding fundamental frequency of stator current is 20 Hz.

Fig. 6 shows the waveforms of thrust force. There are severe 6th thrust ripple before 1.0 s. The magnitude of thrust ripple is about 150 N, approximately to the cogging force. After applying the proposed harmonic current injection method, the thrust ripple is reduced significantly. But conventional PI controller can't control harmonic currents well, as the thrust ripple is nearly reduced after 2.0 s. The thrust waveforms during switching algorithm period are shown in Fig. 6 (b) and 6 (c). Fig. 6(b) shows the proposed algorithm can suppress thrust ripple very fast.

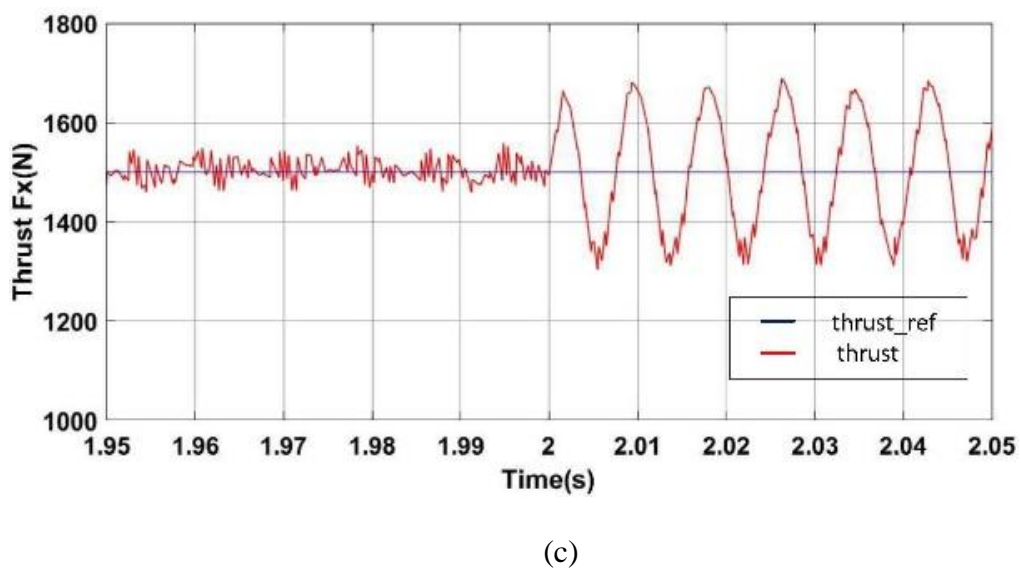
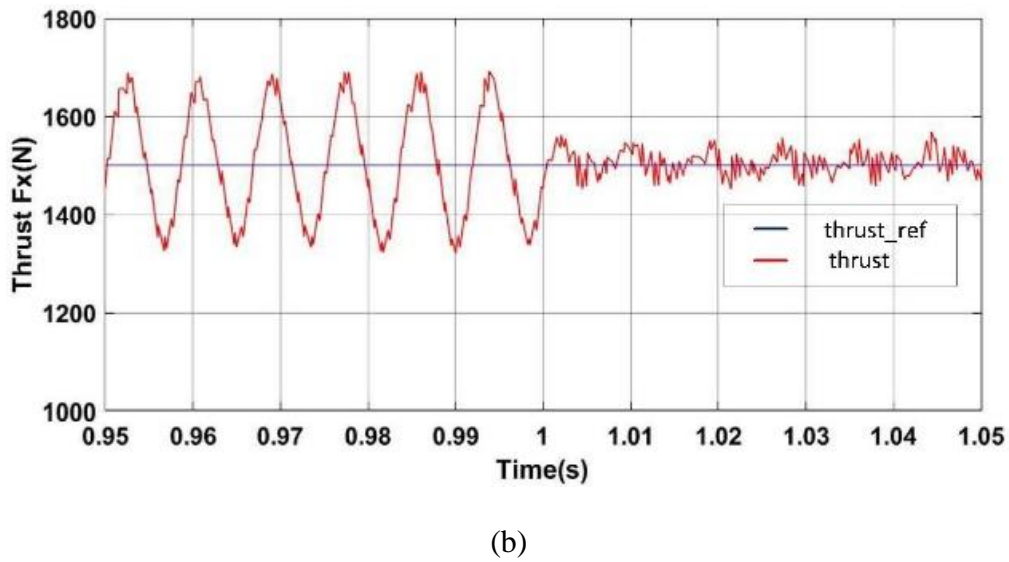
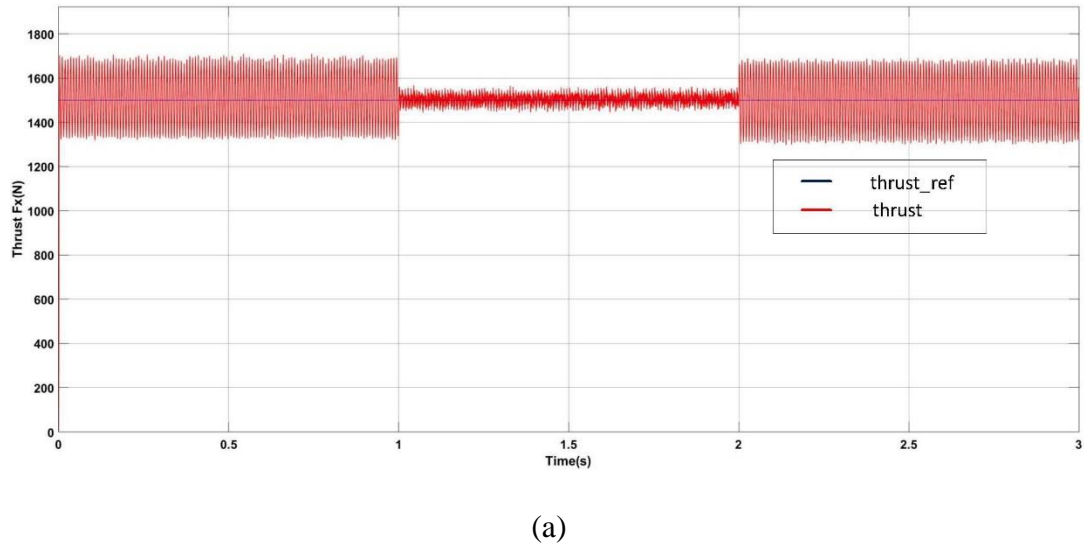


Fig. 6. The thrust waveforms of LSLSM

Spectrum analysis of thrust at 0.7 s, 1.7 s and 2.7 s are shown in Fig. 7 (a–c), respectively. The original magnitude of 6th thrust ripple is 10.38 % of the average thrust, about 155 N. After injection of harmonic current, the magnitude of 6th thrust ripple is reduced to 0.41 % of the average thrust, about 7 N. Meanwhile, the magnitude of 12th thrust ripple remains almost the same. It shows good effect of the proposed thrust ripple suspension method. It can be seen from Fig. 7(c) the harmonic current injection by current loop on d, q axes can't reduce thrust ripple but slightly increase it.

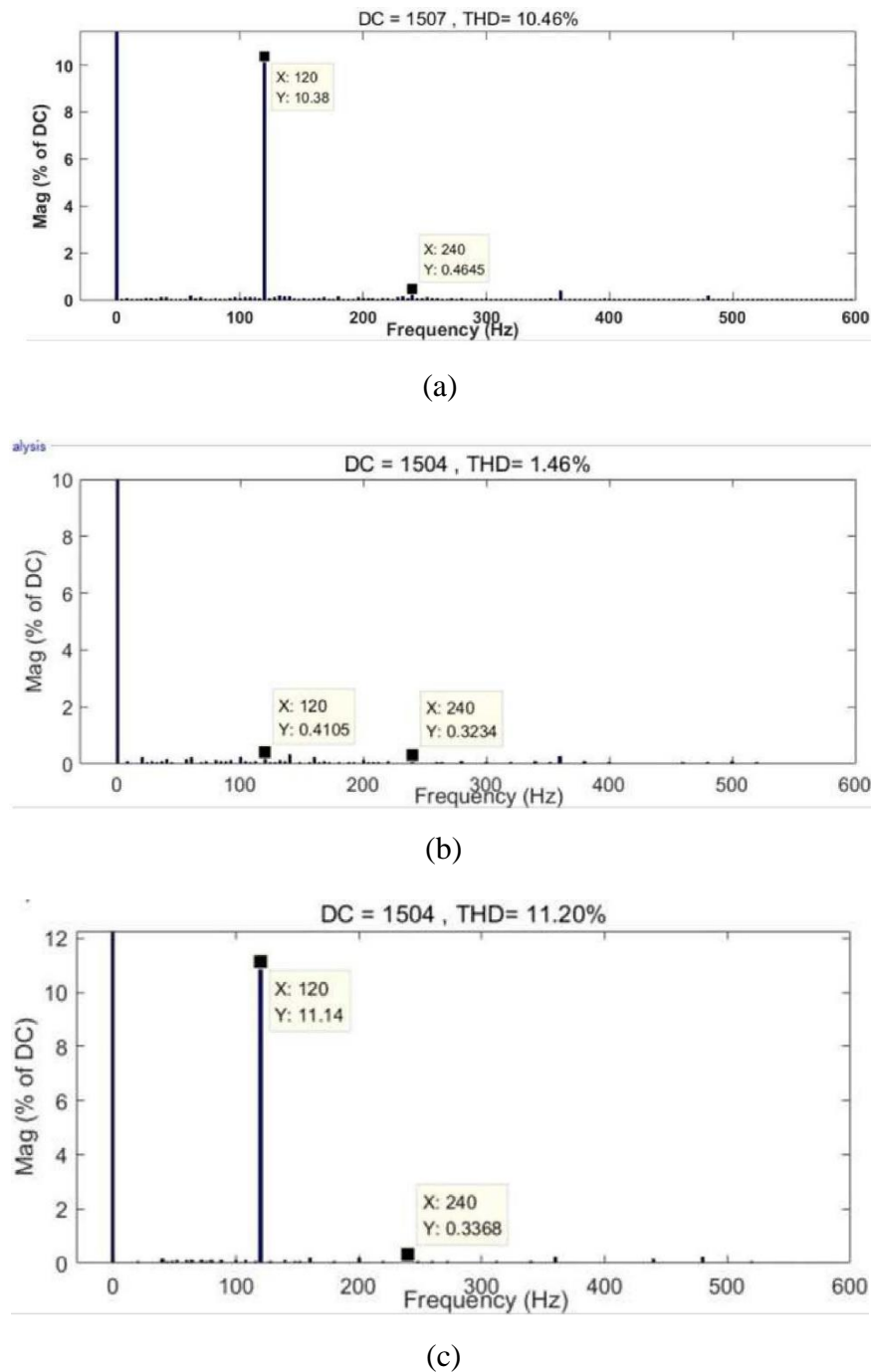


Fig. 7. The Spectrum diagram of thrust force at different times

The response of the currents on d, q axes are shown in Fig. 8. The current waveforms during switching algorithm are shown in Fig. 8(b) and 8(c). It can be seen current harmonics are injected into q -axis current after 1.0 s in Fig. 8(a). The waveform in Fig. 8(b) shows that the real currents can follow the reference values accurately and quickly, which validate the effectiveness of the proposed harmonic current controller. From Fig. 8(c), it can be seen there are large phase delay between reference harmonic current and feedback. That's why harmonic current injection by conventional PI current controller are not able to suppress thrust ripple well.

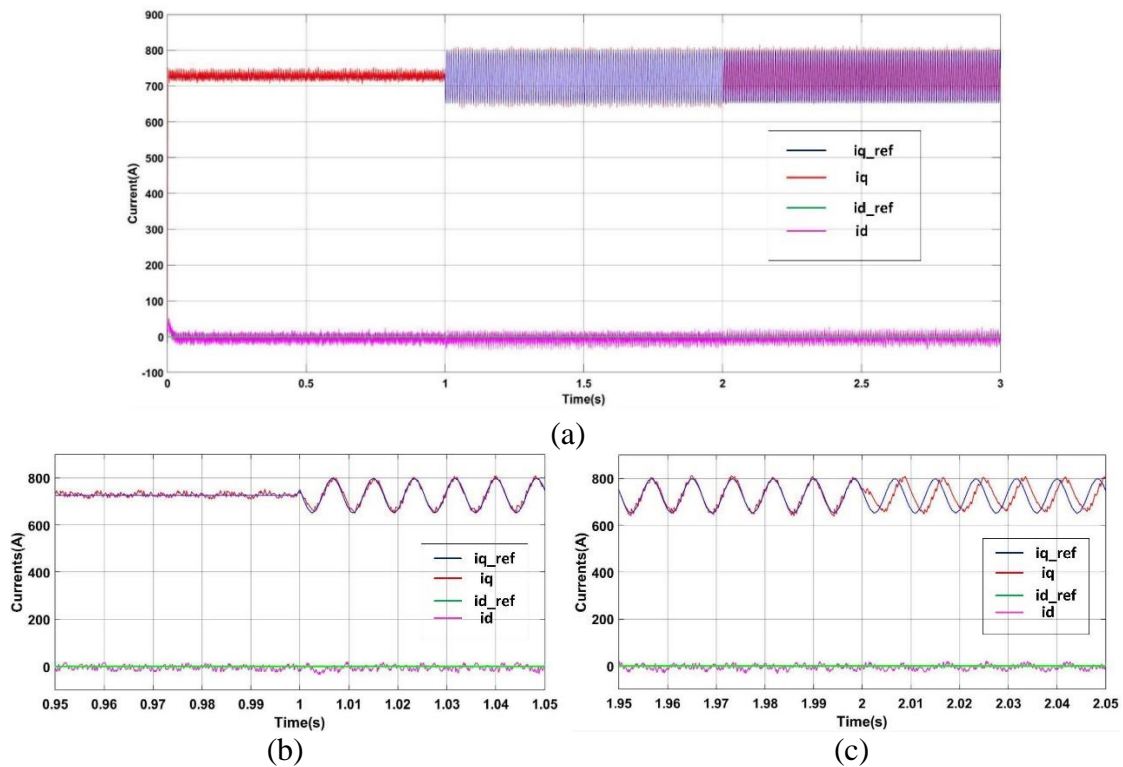


Fig. 8. The waveforms of stator current on d, q axes

CONCLUSION

A thrust ripple suppression method by harmonic current injection is presented in this paper. The LSLSM model considering flux linkage harmonics and cogging force is established, which are the main sources of thrust ripple. The flux linkage harmonics and cogging force are calculated by finite element method in Maxwell software. Harmonic current injection is proposed to generate harmonic electromagnetic force of opposite phase. The method to determine proper stator current is derived. The adequate stator current is made up by fundamental and 5th and 7th harmonics, which can suppress the main 6th thrust ripple of LSLSM effectively. Then, multiple rotating reference frames are introduced, since the alternating current and voltage become constant values in

the corresponding rotating coordinate. Harmonic currents are controlled independently in their synchronous rotating reference coordinate, which decoupled the control of fundamental and harmonic current, and overcome the bandwidth limitation of PI controller on d, q axes current. At last, the voltage model of harmonic current is studied. Based on the voltage equations, the decoupled harmonic current controllers are designed. The steady state voltage feedforward of harmonics current is applied, which increase response speed of harmonics current. Simulation test results validate the proposed scheme can suppress the 6th thrust ripple of LSLSM effectively and quickly.

ACKNOWLEDGEMENTS

This work was supported by the National Key Technology R&D Program of China (2016YFB1200602-02).

References

1. Lu G, Cheng H, He W, Zhang J, Pan G. Harmonic analysis of the PWM inverter fed LSM drive system. In the TRANSRAPID Shanghai. Proceedings of the 6th International Conference in Advances in Power System Control, Operation and Management, 2003. p. 547–557. doi: 10.1049/cp:20030646
2. Wang M, Li L, Yang R. Overview of thrust ripple suppression technique for linear motors. *Chinese Journal of Electrical Engineering*. 2017;2(1):77-84. Available at: <https://ieeexplore.ieee.org/document/7933117/>. doi: 10.23919/CJEE.2016.7933117
3. Ma M, Li L, Zhang J, Yu J, Zhang H, Jin Y. Analytical Methods for Minimizing Detent Force in Long-Stator PM Linear Motor Including Longitudinal End Effects. *IEEE Transactions on Magnetics*, 2015;51(11):1-4. doi: 10.1109/intmag.2015.7156725
4. Zhu YW, Lee SG, Chung KS, Cho YH. Investigation of Auxiliary Poles Design Criteria on Reduction of End Effect of Detent Force for PMLSM. *IEEE Transactions on Magnetics*. 2009;45(6):2863-2866. doi: 10.1109/tmag.2009.2018778
5. Yang G, Wang K, Zhang Z. Study on electromagnetic force ripple reduction of long stator linear synchronous motor based on unequal pole pitch. Proceedings of the International Conference on Electrical Machines and Systems. 2017. p. 1-4. doi: 10.1109/icems.2017.8055994
6. Hwang SH, Kim JM. Dead Time Compensation Method for Voltage-Fed PWM Inverter. *IEEE Transactions on Energy Conversion*, 2010;25(1):1-10. doi: 10.1109/tec.2009.2031811
7. Liao Y, Zhen S, LIU R, Yao J. Torque Ripple Suppression of Permanent Magnet Synchronous Motor by the Harmonic Injection. *Proceeding of the CSEE*, 2011;31(21):119-127. Available at: <http://www.pcsee.org/CN/Y2011/V31/I21/119#>.
8. Zhao S, Tan KK. Adaptive feedforward compensation of force ripples in linear motors. *Control Engineering Practice*, 2005;13(9):1081-1092. doi: 10.1016/j.conengprac.2004.11.004
9. Cho K, Kim J, Park H, Choi SB. Periodic adaptive disturbance observer for a Permanent Magnet Linear Synchronous Motor. Proceedings of the 51st IEEE Conference on Decision and Control (CDC), 2012. p. 4684–4689. doi: 10.1109/cdc.2012.6426591

10. Chen SL, Hsieh TH. Repetitive control design and implementation for linear motor machine tool. *International Journal of Machine Tools & Manufacture*, 2007;47(12):1807-1816. doi: 10.1016/j.ijmachtools.2007.04.009
11. Yan Y, Li W, Deng W, Zhang G, Xia C. Torque ripple minimization of PMSM using PI type iterative learning control. Proceedings of the IECON 2014 40th Annual Conference of the IEEE; 2014; IEEE; 2015. p. 925-931. doi: 10.1109/iecon.2014.7048612
12. Xu S, Zhao W, Ji J, Du Y, Zhang D, Liu G. Thrust ripple reduction of linear flux-switching PM motor using harmonic injected current. Proceedings of the International Conference on Electrical Machines and Systems; IEEE; 2014. p. 1886-1889. doi: 10.1109/icems.2013.6713220
13. Guan B, Zhao Y, Yi R. Torque Ripple Minimization in Interior PM Machines using FEM and Multiple Reference Frames. Proceedings of the Conference on Industrial Electronics and Applications; 2006; IEEE;2006. p. 1-6. doi: 10.1109/iciea.2006.257208
14. Shang KJ, Chen X, Zhou Y. A Harmonic Voltage and Current Coupling Permanent Magnet Synchronous Motor Model and Feedforward Control. *Transactions of China Electrotechnical Society*, 2017;32(18):131-142. Available at: <http://www.ces-transaction.com//CN/Y2017/V32/I18/131>. doi: 10.19595/j.cnki.1000-6753.tces.161956
15. Ge Q, Li Y, Kong L. A comparative study of FOC for long stator linear synchronous motor control. Proceedings of the International Conference on Electrical Machines and Systems (ICEMS); 2007; IEEE; 2007. p. 398-402. Available at: <https://ieeexplore.ieee.org/abstract/document/4411996/>.
16. Wang X, Liu H, Zhang S. High performance propulsion control of magnetic levitation vehicle long stator linear synchronous motor. Proceedings of the International Conference on Electrical Machines and Systems; 2011; IEEE, 2011. p. 1-6. doi: 10.1109/icems.2011.6073798.

Information about the authors:

Jinsong Kang, PhD, professor; Tongji University; No.4800, Cao An Road, Shanghai, China.
ORCID: 0000-0003-4875-1818;

E-mail: kjs@tongji.edu.cn

Siyuan Mu, Bachelor of science, PhD candidate;

ORCID: 0000-0002-3006-1301;

E-mail: siyuanmu@tongji.edu.cn

Shuo Wang, Master of science, PhD candidate;

ORCID: 0000-0003-3123-3942;

E-mail: 1988wangshuo@tongji.edu.cn

Yusong Liu, Bachelor of science, PhD candidate;

ORCID: 0000-0002-0520-389X;

E-mail: liuyusong@tongji.edu.cn

Cuiwei He, Master of science, Master;

E-mail: hcw1964@163.com

To cite this article:

Mu S, Kang J, Wang S, et al. A method of thrust ripple suppression for long stator linear synchronous motor. *Transportation Systems and Technology*. 2018;4(2):30-44. doi: 10.17816/transsyst20184230-44

DOI 10.17816/transsyst20184245-51

© J. Rao^{1,2}, K. Wang¹, B. Wang^{1,2}, Q. Ge¹, L. Shi¹, Y. Li¹

¹Key Laboratory of Power Electronics and Electric Drive,
Institute of Electrical Engineering Chinese Academy of Sciences

²University of Chinese Academy of Sciences
(Beijing, China)

A SPECIAL EXCITATION SYSTEM FOR ANALYSIS OF COUPLING CHARACTERISTICS OF THRUST AND LEVITATION FORCE OF MAGLEV TRAIN

Background: In the maglev train propelled by long stator linear synchronous motor (LSLSM), the thrust characteristics are one of important points to evaluate the performance of the system. However, coupling effect exists between the propulsion and levitation system. Therefore, the interference from the levitation system must be considered when the propulsion system is designed.

Aim: The article focus on the analysis of coupling characteristics of thrust and levitation force of maglev train, and a special excitation system is designed for the study.

Methods: In order to study the thrust performance under the fluctuating air gap field under laboratory conditions, a rotating synchronous motor has been designed to imitate the long stator linear synchronous motor applied in high speed maglev train. And a special excitation system is designed for the rotating synchronous motor, which can simulate the fluctuation of the exciting current during the actual operation of maglev train. The air gap of the rotating synchronous motor is kept as constant, and the fluctuating excitation current is added to the excitation winding of the rotating synchronous motor, thus the simulation of air gap magnetic field variation is achieved.

Results: The special excitation system of the experimental motor is introduced in detail.

Conclusion: The relationship between thrust and levitation force of long stator linear synchronous motor (LSLSM) in maglev train is strong coupling, non-linear, and dynamic. Complete decoupling of thrust and levitation force is not easy to be achieved. The experimental platform has been built to study the coupling characteristics of thrust and levitation force of maglev train.

Keywords: Excitation system, Coupling characteristics of thrust and levitation, Long stator linear synchronous motor (LSLSM), Performance of the propulsion, Maglev train.

INTRODUCTION

Maglev system utilizing long stator linear synchronous motor (LSLSM) propulsion and electromagnetic suspension has been applied in normal commercial operation [1–3]. The electromagnetic force that makes the train suspend upon the track is produced by the excitation magnetic field. The interaction between armature magnetic field and excitation magnetic field produces the thrust force. The thrust and levitation force are related to the

excitation magnetic field. This maglev system offers many advantages. However, it also has some disadvantages. Coupling characteristics are very complicated between thrust and levitation force. The characteristic of propulsion control system is one of the important points to evaluate the performance of the maglev train. However, the wide range field excitation fluctuations caused by external interference make the performance of the propulsion even worse [9–12]. The operation principle of a long stator linear synchronous motor and a rotating synchronous motor are the same. It is a convenient and feasible scheme to verify the propulsion control characteristics of maglev train on rotating synchronous motor. The structure of the LSLSM and test rotating synchronous motor are shown in Fig. 1 and Fig. 2. The air gap, distribution of air gap magnetic field, stator pole pitch and rotor pole pitch of the rotating synchronous motor are the same or equal proportion with the LSLSM applied in high speed maglev train.

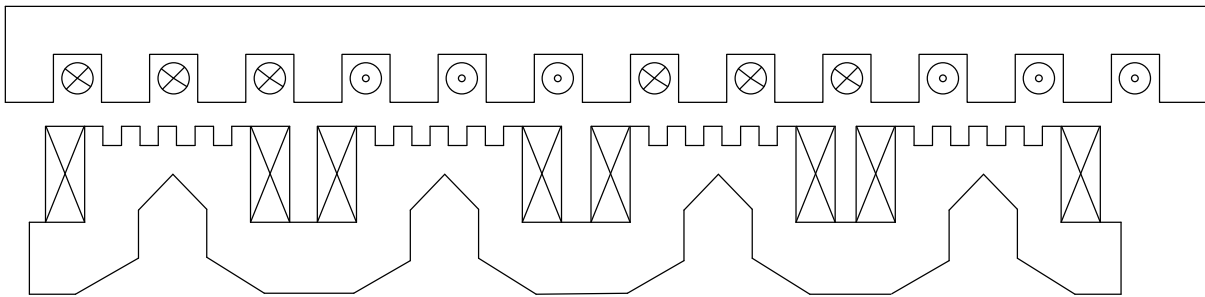


Fig.1. The structure of LSLSM

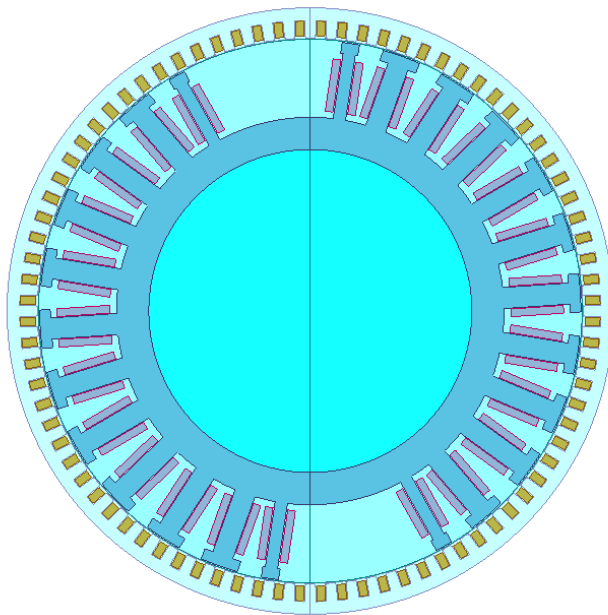


Fig. 2. The structure of the rotating synchronous motor

The air gap magnetic field variation of the synchronous motor can affect the thrust performance. The air gap of the LSLSM of the maglev train is variable, and the air gap magnetic field of the LSLSM is influenced by air gap and the excitation current. The suspension system of high speed maglev train must adjust the exciting current to keep the air gap as constant in actual operation. Therefore, no matter the fluctuating air gap or the change of levitation force can be reflected by the fluctuation of the excitation current. Considering the influence of excitation field fluctuation on propulsion control, a special excitation system of the rotating synchronous motor is introduced in this paper. The excitation system is designed to generate the constant DC current for the field excitation, and it also can generate the alternating current at different frequencies to simulate the fluctuation of the exciting current during the actual operation. By this way, the complex coupling relationship between thrust and levitation force can be simplified. Although the air gap length of the rotating synchronous motor is constant, the change of air gap magnetic field can be same with that in actual operation by this special excitation system.

SIMULATION AND EXPERIMENT

In order to simulated the excitation current of the maglev train, the reference value of the special excitation system is set according to the excitation current of the maglev train. The control system diagram is shown in Fig. 3.

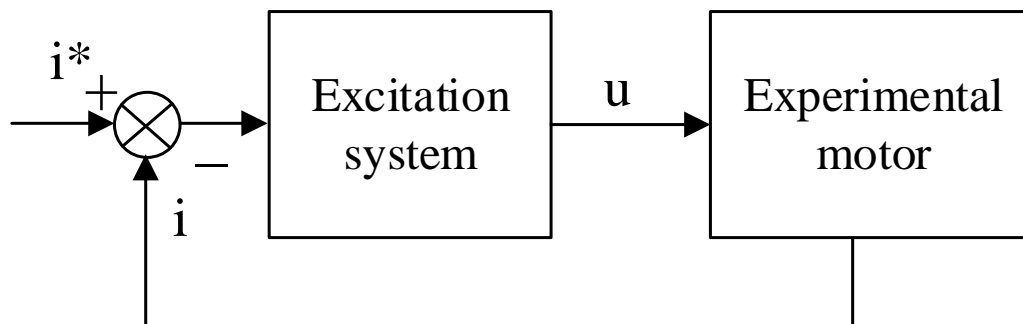


Fig. 3. The control diagram of the excitation

Current closed-loop feedback control is employed in the control the voltage source inverter for the special excitation system. The excitation winding of the motor is resistance-inductance load, thus high voltage is needed to produce the required wave current because of the large inductance of the excitation winding. Therefore, a boost circuit is designed in this excitation system. The topology structure of excitation source is shown in Fig. 4. L_2 and R is the excitation winding load.

In the simulation analysis of the excitation source, voltage closed loop control is used in the boost circuit unit, and current closed loop feedback control is used in the single phase full bridge inverter unit. When the reference of

excitation current is 12.5 A, the output current waveform of the excitation source is shown in Fig. 5. When the reference of excitation current is 12.5 A, besides, the sinusoidal fluctuation with amplitude 2.5 A and 3 Hz frequency is added. The output excitation current waveform of the excitation source is shown in Fig. 6.

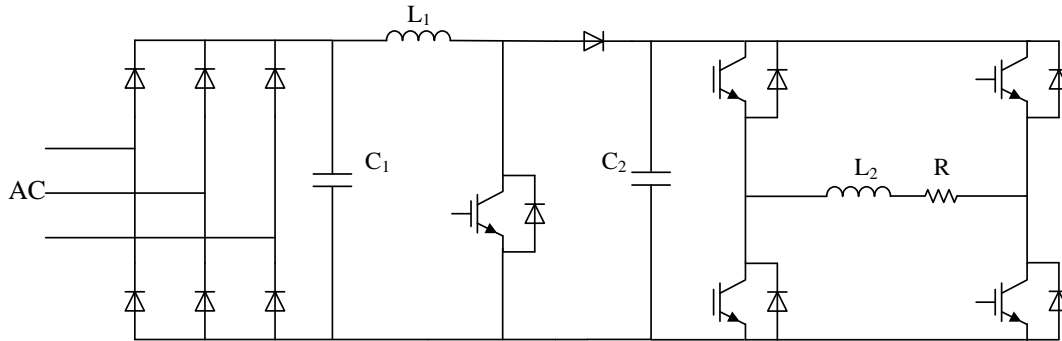


Fig. 4. Topology structure of excitation source

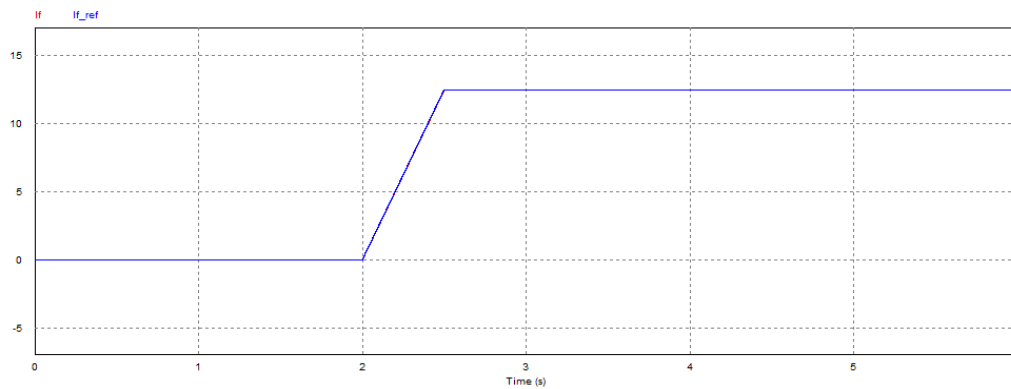


Fig. 5. Normal excitation current waveform

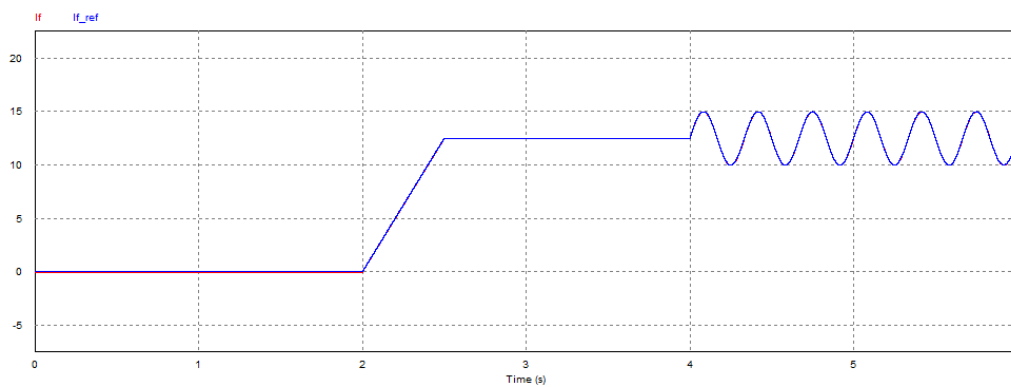


Fig. 6. Excitation current waveform with harmonic wave

In this experiment, the voltage reference value of voltage closed-loop of the boost circuit is 300 V. The output current reference is 12.5 A, the harmonic with frequency 3 Hz and amplitude 2.5 A is added to the output current reference at 5 seconds. At 10 seconds, the frequency and amplitude of the harmonic are changed. The output excitation current waveform is shown in

Fig. 7. Considering that the actual harmonics in the excitation current of maglev train are not sinusoidal, then random fluctuations are added to the excitation current reference in the experiment. Output voltage of the boost circuit and the excitation current waveform are shown in Fig. 8. The voltage reference value of voltage closed-loop of the boost circuit is still 300 V. The random fluctuations with frequency 3.33 Hz are added to the output current reference at 5 seconds.

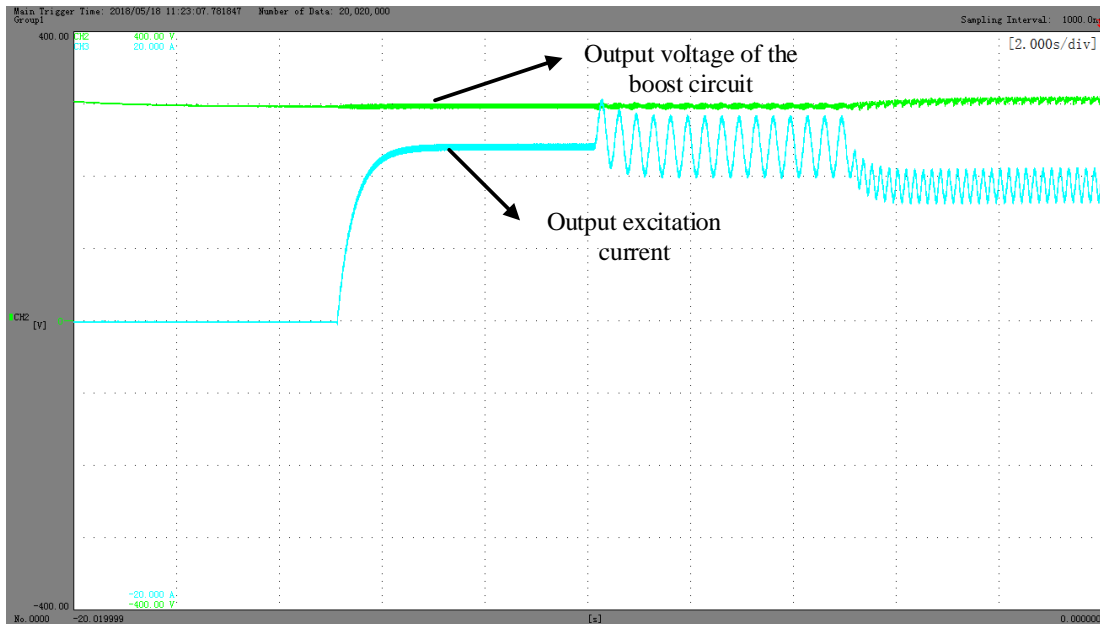


Fig. 7. Output voltage of the boost circuit and excitation current waveform

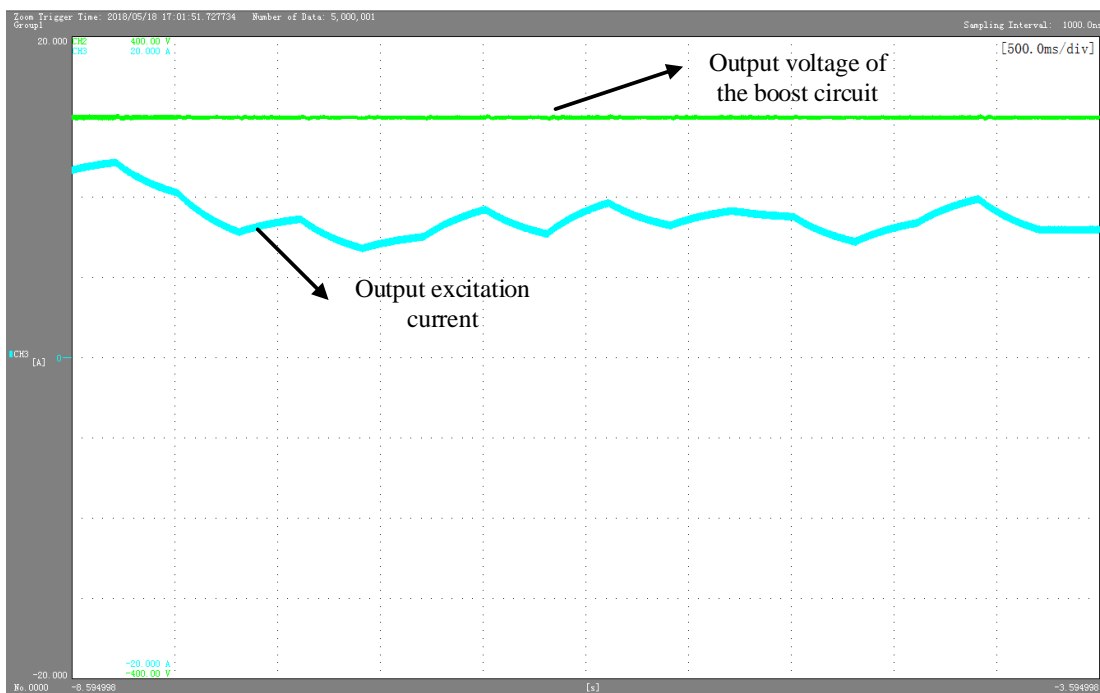


Fig. 8. Output voltage of the boost circuit and excitation current waveform

CONCLUSION

The excitation special device can not only provide normal excitation current, but also simulate the fluctuation of excitation current very well. The fluctuation of excitation current of maglev train can be got from the levitation system. And combined with the experimental motor and experimental platform, the traction characteristics of maglev train under fluctuating excitation current can be analyzed.

References

1. Weh H. Linear synchronous motor development for urban and rapid transit systems. *IEEE Transactions on Magnetics*. 1979;15(6):1422-1427. doi: 10.1109/TMAG.1979.1060438
2. Wang X, Liu H, Zhang S. High Performance Propulsion Control of Magnetic Levitation Vehicle Long Stator Linear Synchronous Motor. Proceedings of the International Conference on Electrical Machines and Systems. 2011; doi: 10.1109/ICEMS.2011.6073798
3. Rao J, Wang K. Study on Dynamic Coupling Characteristics of Thrust and Levitation Force of Long Stator Linear Synchronous Motor for Maglev Train. Proceedings of the 20th International Conference on Electrical Machines and Systems. 2017; doi: 10.1109/ICEMS.2017.8055995
4. Yang G, Wang K, Zhang Z. Study on electromagnetic force ripple reduction of long stator linear synchronous motor based on unequal pole pitch. Proceedings of the 20th International Conference on Electrical Machines and Systems. 2017; doi: 10.1109/ICEMS.2017.8055994
5. Perreault BM. Control Strategies for Linear Synchronous Motors. Proceedings of the International Electric Machines & Drives Conference. IEEE; 2007;2:969-971. doi: 10.1109/IEMDC.2007.382806
6. Jin J, Zheng L, Xu W, Guo Y, Zhu J. Experimental study on thrust and normal force of a permanent magnet linear synchronous motor. Proceedings of the International Conference on Electrical Machines and Systems. 2011; doi: 10.1109/ICEMS.2011.6073660
7. Lu B, Tan X, Li Q, Luo J. The Analysis of Excitation Current Changes in Long Stator Linear Synchronous Motor of Maglev. Proceedings of the Prognostics and System Health Management Conference (PHM-2014 Hunan). 2014; doi: 10.1109/PHM.2014.6988204
8. Ge QX, Li Y, Kong L. A Comparative Study of FOC for Long Stator Linear Synchronous Motor Control. Proceedings of the International Conference on Electrical Machines and Systems. 2007; p. 398–402.
9. Valluvan M, Ranganathan S. Modeling and control of magnetic levitation system. Proceedings of the International Conference on Emerging Trends in Science, Engineering and Technology (INCOSSET). 2012; p. 545–548. doi: 10.1109/INCOSSET.2012.6513963
10. Su K-H, Li C-Y. Supervisory Fuzzy Model Control for Magnetic Levitation System. Proceedings of the 13th International Conference on Networking, Sensing, and Control (ICNSC). IEEE 2016; doi: 10.1109/ICNSC.2016.7479025
11. Venghi LE, Gonzalez GN, Serra FM. Implementation and Control of a Magnetic Levitation System. *IEEE Latin America Transactions*. 2016;14(6):2651-2656. doi: 10.1109/TLA.2016.7555233

12. Kim C-H, Ahn C, Park G-W, Park DY. Levitation and Guidance Control of Passive Magnetic Levitation Tray System. *IEEE ISR 2013*. 2013; p. 1–2. doi: 10.1109/ISR.2013.6695692
13. Boldea I, Tutelea LN, Xu W, Pucci M. Linear Electric Machines, Drives, and MAGLEVs: An Overview. *IEEE Transactions on Industrial Electronics*. 2018; 65(9):7504-7515. doi: 10.1109/TIE.2017.2733492
14. Ho E, Sen PC. High-performance decoupling control techniques for various rotating field machines. *IEEE Transactions on Industrial Electronics*. 1995; 42(1):40-49. doi: 10.1109/41.345844
15. Chen Y, Jin JX, Zhao HB. Simulation and analysis the thrust force of a permanent magnet linear synchronous motor. Proceedings of the International Conference on Applied Superconductivity and Electromagnetic Devices. 2011; p. 235–238. doi: 10.1109/ASEMD.2011.6145109

Information about the authors:

Jian Rao, postgraduate student,
ORCID: 0000-0002-7585-9608;
E-mail: raojian@mail.iee.ac.cn

Ke Wang, Doctor of Electrical Engineering, Professor,
ORCID: 0000-0001-8561-5132;
E-mail: wangke@mail.iee.ac.cn

Boyu Wang, postgraduate student,
ORCID: 0000-0003-1505-1209;
E-mail: wangboyu@mail.iee.ac.cn

Qiongxuan Ge, Doctor of Electrical Engineering, Professor,
E-mail: gqx@mail.iee.ac.cn

Liming Shi, Doctor of Electrical Engineering, Professor,
ORCID: 0000-0002-7171-2422;
E-mail: limings@mail.iee.ac.cn

Yaohua Li, Doctor of Electrical Engineering, Professor,
E-mail: yhli@mail.iee.ac.cn

To cite this article:

Rao J, Wang K, Wang B, et al. A Special Excitation System for Analysis of Coupling Characteristics of Thrust and Levitation Force of Maglev Train. *Transportation Systems and Technology*. 2018;4(2):45-51. doi: 10.17816/transsyst20184245-51



UDC [УДК] 629.438.4

DOI 10.17816/transsyst20184252-61

© V. A. Bogachev¹, Y. A. Terentyev², V. V. Koledov³, T. V. Bogachev⁴

¹Rostov State Transport University (RSTU)

(Rostov-on-Don, Russia)

²Independent expert, official representative of ET3 in the Russian Federation

(Moscow, Russia)

³Institute of Radioengineering and Electronics of RAS (Kotelnikov IRE RAS)

(Moscow, Russia)

⁴Rostov State University of Economics

(Rostov-on-Don, Russia)

DZUNGARIA CORRIDOR FOR VACUUM MAGNETIC LEVITATION TRANSPORT: LOST OPPORTUNITIES OR WEIGHTED OPTIMISM?

Background: The complex of issues arising when considering possible options for the implementation of Eurasian transcontinental high-speed land transport corridors operating on the basis of vacuum magnetic-levitation technologies is analyzed. The exclusivity of Russia's geographical position in a substantial part lies in the fact that it is through its territory that China can be directly linked by these corridors to Western Europe and also to North America, the rationale is done.

Aim: Possible routes connecting Beijing and Shanghai with Moscow are analyzed. Transport highways of a truly innovative type will solve the urgent task of geopolitical level - to organize the states located on the Eurasian continent in a qualitatively new civilizational construction. The purpose of the research is as follows: to develop methods of solving the problems of finding optimal variants for the location of high-speed land transport corridors using computer mathematics systems. This should take into account the features of the territory, through which the transport route is planned to be carried out.

Methods: The economic, political, logistical, geographical, technical and technological aspects of these projects are discussed. Optimization methods are used, in particular, the calculus of variations.

Results: After the creation of a sufficiently informative and detailed informal picture, the basics of the corresponding mathematical models are constructed.

Conclusion: The historical area of Dzungaria is considered as the location of the main intermediate terminal for high speed vacuum magnetic levitation transport.

Keywords: High-speed land transport corridors, Magnetic-levitation technologies, Optimization methods, The problem of the calculus of variations.

The research is conducted with a support of the Russian Foundation for Basic Research (Grant No. 17-20-04236 офи_м_РЖД)

© В. А. Богачев¹, Ю. А. Терентьев², В. В. Колецов³, Т. В. Богачев⁴

¹Ростовский государственный университет путей сообщения (РГУПС)
(г. Ростов-на-Дону, Россия)

²Независимый научный эксперт, официальный представитель «ВТЗ» в
России (г. Москва, Россия)

³Институт радиотехники и электроники РАН
(г. Москва, Россия)

⁴Ростовский государственный экономический университет
(г. Ростов-на-Дону, Россия)

ДЖУНГАРСКИЙ КОРИДОР ДЛЯ ВАКУУМНОГО МАГНИТОЛЕВИТАЦИОННОГО ТРАНСПОРТА: УПУЩЕННЫЕ ВОЗМОЖНОСТИ ИЛИ РАЗУМНЫЙ ОПТИМИЗМ?

Обоснование: Анализируется комплекс вопросов, возникающих в процессе рассмотрения возможных вариантов реализации евразийских трансконтинентальных высокоскоростных наземных транспортных коридоров на основе технологий вакуумной магнитной левитации. В работе выполнено обоснование, согласно которому, исключительность географического положения России в значительной степени заключается в том, что именно через ее территорию Китай может быть напрямую связан подобными коридорами со странами Западной Европы, а также с Северной Америкой.

Цель: Анализируются возможные маршруты, соединяющие Пекин и Шанхай с Москвой. Транспортные магистрали действительно инновационного характера решают важную задачу геополитического масштаба, а именно: организовать государства Евразии согласно качественно новому цивилизационному укладу. Цель исследования заключается в следующем: разработать методы решения задач по поиску оптимальных вариантов местоположения высокоскоростных наземных транспортных коридоров с применением компьютерных математических систем. Следует учитывать и особенности территории, по которой планируется проложить данную транспортную линию.

Методы: Обсуждаются экономические, политические, логистические, географические, технико-технологические аспекты реализации данных проектов. Используются методы оптимизации, в частности, вариационное исчисление.

Результаты: После получения в достаточной степени информативной и подробной картины созданы соответствующие базовые математические модели.

Вывод: Историческая область Джунгария рассматривается в качестве основного промежуточного терминала для высокоскоростного вакуумного магнитолевитационного транспорта.

Ключевые слова: Высокоскоростные наземные транспортные коридоры, технологии магнитной левитации, методы оптимизации, проблема вариационного исчисления.

Исследование проведено при поддержке Российского фонда фундаментальных исследований (Грант №. 17-20-04236 офи_м_РЖД).



INTRODUCTION

In this paper, we analyze a number of issues that arise when considering possible options for the implementation of trans-Eurasian high-speed ground corridors operating on the basis of vacuum magnetic levitation transport (VMLT). A very extensive literature is devoted to a discussion of the comprehensive aspects of the application of magnetic levitation technologies in transport, including in vacuum tubes, from a wide variety of points of view [1–18]. Note that the conclusions made after a very versatile and detailed analysis of the expediency of using these technologies at the present time often turn out to be contradictory (it suffices to compare [2, 3, 4, 7, 10]).

The purpose of the present research is to develop mathematical methods of solving the problems of finding optimal variants for the location of high-speed land transport corridors using computer mathematics systems. This should take into account the characteristic features of the territory, through which the transport route is planned to be carried out.

SOME NATIONAL ASPECTS OF VMLT PROJECTS FOR THE RUSSIAN FEDERATION

Exclusiveness of the geographical position of Russia is expressed not only by the record area of the territory and by the fact that it is in two parts of the world. In modern geo-economic and geopolitical conditions, this exclusiveness is due to the fact that it is through Russia that China can be directly connected by high-speed land transport corridors with Western Europe and also with North America.

The relief of Central Asia that was rich in mountain systems served as a natural reason for the isolation of the Celestial Empire (which also provokes its artificial self-isolation) and, in general, the states of East Asia from Europe and even from Middle East until the end of the 19th century. The modern China, which is carrying out omnidirectional and all-pervasive expansion, not only makes up for the time-lost isolation from the Western world, supplemented by three decades of “classical” socialism. It is already clear to all that its goal is to become even more powerful in “multipolar” World.

By boosting its nomination for world leadership positions in economic, scientific, technical, technological and even to some extent social relations, China is building up the “muscular relief of the whole body” externally positioning itself at the same time not aggressively. It is clear that with such actively developing global market relations, further full-fledged progress is simply not possible without the transcontinental transport highways of a fundamentally new, real innovative type. As for such geographical neighbors of Russia and China as Kazakhstan, Uzbekistan, Turkmenistan, Kyrgyzstan and

Tajikistan, we note the following. It is known that from 1992 to 2012, China's aggregate trade with these five Central Asian countries increased 100-fold and increased to 46 billion dollars. Thus, one can't doubt their direct and even vital interest in the implementation of the projects of innovative high speed transportation under consideration.

DZUNGARIA CORRIDOR AS A PILOT PROJECT IN IMPLEMENTATION OF VMLT

When choosing trajectory for high speed overland route between Beijing and Moscow or Shanghai and Moscow operating on the basis of VMLT, the physical map of Central Asia immediately identifies Dzungaria, a historical region located in the Xinjiang Uygur Autonomous Region of China. As noted above, the geographic complexity of the situation is that across any of the possible routes connecting East China to Europe, one way or another, there is an extended chain of mountain systems passing one another. However, it is in Dzungaria that there are fairly wide and relatively flat passages in this chain. The most famous is called "Dzungarian Gate". We draw attention to another, less known passage located 150 km to the north of the "Dzungarian Gate".

So, let's consider from the geographical, political, economic and social point of view one of the possible nearly "rectilinear" routes connecting Beijing and Moscow. The movement from Beijing will take place all the time to the north-west-west. After crossing the Gobi Desert in a very insignificant extreme southern part of the territory of Mongolia, the Gobi Altai and the Mongolian Altai remain to the north of the route. The movement will again take place across the territory of China to its border with Kazakhstan. Here between the ridges of Dzungarian Alatau and Tarbagatai there is a flat passage, which we will call the "New Dzungar Gate". From the south of the route, there will be Lake Manas (Ike-Khan) and the city of Karamay. From the north – the city of Durbuljin (Emin) and Chuguchak (Tacheng). After crossing the border of China with Kazakhstan, the cities of Bakhta and Urjar will remain from the north. Further movement occurs practically along the plain. Leaving from the south of Lake Alakol and Balkhash and from the north – the top of 1565 m, and then from the south – Mount Ulytau (1133 m), located in the Kazakh, the route goes to the Southern Urals. The largest cities of Kazakhstan: Karaganda and Astana will remain located north of the route, respectively, at 150 km and 300 km. After crossing the border of Kazakhstan with Russia, the route enters the Orenburg region of Russia.

Let's sum up some results. The length of the entire route from Beijing to Moscow will be about 6150 km. The time of delivery of passengers and cargo will be close to the minimum in comparison with all other routes. From the point of view of the minimum material costs for surveying and construction

work, this route is also preferable to others. Indeed, the mountain ranges are left out, and the second half of the route passes almost across the flat terrain. In any case, for many well-understood reasons, somewhat north of the city of Urumqi, the center of the Xinjiang Uygur Autonomous Region, the main intermediate terminal should be located, which will serve as a powerful hotbed of economic and social development for the entire western part of China.

VARIATION APPROACH IN MATHEMATICAL MODELING OF TRANSPORT AND LOGISTIC CONSTRUCTINGS

When considering possible variants of the location of transport highways, immediately questions arise relating to their curvature. Even for traditional railroads constructed on the basis of the “wheel–rail” system, their curvature is the most important indicator determining the permissible speed of trains. For high-speed, and even more ultra-high-speed railroads, the value of this indicator becomes dominant.

For the transport-logistical constructions performed in this work, the general variation method for solving the corresponding optimization problems is proposed.

When considering possible options for the location of railways, questions immediately arise concerning their curvature. Even for traditional railway tracks built on the basis of the “wheel–rail” system, their curvature is the most important indicator determining the permissible speed of trains.

Consider a capsule levitating in an evacuated tube by means of electromagnetic field forces and performing the function of a passenger or freight vehicle. The trajectory of the movement of the capsule is a certain line located on the ellipsoid surface of the Earth. The retention of the capsule on the trajectory should be provided by the centripetal force, which is the resultant force of gravity and the forces of the electromagnetic field and equal

$$F(x, y, z) = \frac{mv^2}{R(x, y, z)}. \quad (1)$$

Here m – the weight of the capsule, $v = v(x, y, z)$ – the speed of its movement at the point of the line Γ with the coordinates x , y and z (in some selected rectangular Cartesian coordinate system), $R(x, y, z)$ – the radius of curvature of the line Γ at this point. As is known, the radius of curvature $k(x, y, z)$ of a line is expressed in terms of its curvature by equality

$$R(x, y, z) = \frac{1}{k(x, y, z)}.$$

In the “ideally-extreme” case for VMLT the line Γ represents the line of intersection of a common terrestrial ellipsoid with a plane passing through three points, two of which are the ends of the route and the third is the center of the Earth. If, at the same time, the velocity of the capsule turns out to be equal to the first space flight it will be held in the indicated “orbit” by gravity only being together with the cargo or passengers in weightlessness.

The formula (1) shows that in view of the planned supersonic and even “space” speeds of levitating capsules, one of the main initial criteria when considering the variants of the highways is their curvature.

Let us proceed to the presentation of the proposed variational method. We will consider an optimization problem of the form:

$$\min_{(x,y,z) \in \Gamma} R(x, y, z) \rightarrow \max$$

or equivalent

$$\max_{(x,y,z) \in \Gamma} k(x, y, z) \rightarrow \min$$

provided that the location of the lines are subject to some restrictions. In the situation considered in this paper these restrictions are dictated by the terrain on which it is planned to lay the transport backbone.

Before the method of solving the optimization problem, we make the following General geometric remark. It is known that among all lines connecting any two given points, the smallest length has a line segment. At the same time, the curvature of the straight line is zero at all points.

To the problem under consideration this simple observation is relevant for the following reason. The point is that finding a line having the smallest length among the points connecting two data points and satisfying certain given conditions is, from the computational point of view a simpler task (since it requires fewer resources) than finding among those lines the one with the greatest curvature function of points of a line) is the smallest. However, the above coincidence for a straight line does not allow far-reaching generalizations. The corresponding counterexample is shown in Fig.1.

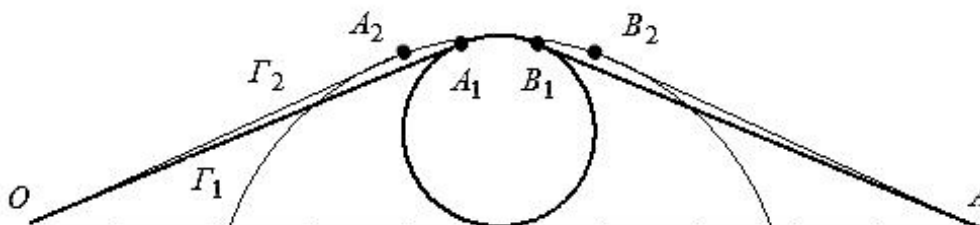


Fig.1. Lines Γ_1 and Γ_2

Let's give an explanation. The greatest value of a curvature of a line Γ_1 joining two fixed points O and A and not passing through the interior of a circle whose radius is assumed to be equal 1 is attained at each point of the arc

A_1B_1 of this circle and is equal to $k_1 = 1$. The greatest value of the curvature of the line Γ_2 , (also connecting points O and A and not passing through the interior of this circle) is reached at each point of the arc A_2B_2 of the circle of radius 2 and is equal to $k_2 = \frac{1}{2}$. However, the length of the curve Γ_1 is less than the length of the curve Γ_2 .

We also note that in the railway practice, for the coupling of the rectilinear part of the railway with the circular one, transitional curves are constructed to compensate for the resulting jump in the curvature of the path [19]. It is also not difficult to cite a counterexample taking this remark into account. In this case, for each of the more complex lines Γ_1 and Γ_2 the curvature will change continuously, but (as in the example above) the length Γ_1 is less than the length Γ_2 .

We now turn our attention to the fact that Lagrange or Newton polynomials are used in the interpolational constructions performed below in the process of optimization. Therefore, the curvature of the lines Γ received is a continuous (and even smooth) function.

Turn to the exposition of the algorithm for constructing a mathematical model in the environment of a computer mathematics system. For brevity and clarity, we confine ourselves to a two-dimensional case. Variation of the lines Γ whose ends are assumed to be at fixed points O and A of the abscissa axis (Fig. 2) will be performed in such a way that the appropriate terrain is taken into account. Namely, the lines Γ must bypass the soles of the mountains and the elevations located between the points O and A .

The segment OA is divided into n equal parts by points x_i . The corresponding ordinates y_i of the points of the plane can be found by a simple search, and using the randomization capabilities of the computer mathematics system. The main content of the constructions produced here is the choice of gaps in which the ordinates y_i can be changed. At the same time, the specificity of the terrain is taken into account (in Fig. 2 this relief is indicated by shaded parts of circles and ellipses).

The interpolation polynomial $y(x)$ (for example, of the above type) is built for the obtained points (x_i, y_i) of the plane. In principle, the use of splines is not excluded, although there are questions about the smoothness of

value is found, that is, the maximum of the function $|k(x)| = \frac{|y''_x|}{(1 + y'^2)^{\frac{3}{2}}}$.

The computational process ends with minimizing the indicated maxima and thereby finding the desired line.

In Fig. 2 shows a line Γ that is a graphical result of the computer mathematics solution of an optimization problem with a terrain relief depicted in the form of shaded parts of circles and ellipses. In this case, the random number generator and the interpolation polynomials of Lagrange and Newton were used.



Fig. 2. The line found by the computer mathematics system

CONCLUSION

We formulate the results of the paper.

1) A general variational method for solving optimization problems using analytical computing systems has been developed, which makes it possible to carry out transport and logistics studies to find the optimal options for the location of high-speed land transport corridors.

2) Based on the proposed method, calculations are performed through the system of analytical calculations, the result of which is the optimal route for the location of the transport corridor, given the restrictions on the terrain, characterized by the presence of mountain chains and elevations.

References

1. Магнитолевитационная транспортная технология / Под ред. В. А. Гапановича. – М.: Физматлит, 2014. 476 с. [Gapanovich VA, editor. Magnitolevitatsionnaya transportnaya tekhnologiya. Moscow: Fizmatlit; 2014. 476 p. (In Russ.)].
2. Магнитолевитационный транспорт: научные проблемы и технические решения / Под ред. Ю.Ф. Антонова, А.А. Зайцева. – М.: Физматлит, 2015. – 612 с. [Antonov YuF, Zaitsev AA, editors. Magnitolevitatsionnyi transport: nauchnye problemy i tekhnicheskie resheniya. Moscow: Fizmatlit; 2015. 612 p. (In Russ.)].
3. Зайцев А.А., Морозова Е.И., Талашкин Г.Н., Соколова Я.В. Магнитолевитационный транспорт в единой транспортной системе страны: Монография. – СПб: НП-Принт, 2015. – 140 с. [Zaitsev AA, Morozova EI, Talashkin GN, Sokolova YaV. Magnitolevitatsionnyi transport v edinoi transportnoi sisteme strany. St. Petersburg: NP-Print; 2015. 140 p. (In Russ.)].
4. Зайцев А.А. Отечественная транспортная система на основе магнитной левитации // Бюллетень Объединенного ученого совета ОАО «РЖД». – 2015. – № 6. – С. 22–27. [Zaitsev AA, Otechestvennaya transportnaya sistema na osnove magnitnoi levitatsii. *Byulleten' Ob"edinennogo uchenogo soveta OAO "RZhD"*. 2015;6:22-27 (In Russ.)].

5. Technical-economical comparison of Maglev and High Speed Systems. Available at: <http://archives-republicans-transportation.house.gov/Media/File/110th/Rail/3-20-07-roundtable-Brady-dornier.pdf>. Accessed September 15, 2016.
6. The website of the Evacuated Tube Transport Technology. Available at: <http://et3.com/>. Accessed October 25, 2016.
7. Терентьев Ю.А., Дроздов Б.В. Перспективы вакуумного магнитолевитационного транспорта // Мир транспорта. – 2017. – №1. – С. 90–95. [Terentiev YA, Drozdov BV. Prospects for Vacuum Magnetic-Levitation Transport. *World of Transport and Transportation*. 2017;1:90-95. (In Russ.)].
8. Островская Г. В. Магнитные дороги профессора Вейнберга (К 100-летию лекции «Движение без трения») // Вестник науки Сибири. – 2014. – № 2. – С. 6–16. [Ostrovskaya GV. Magnetic railways of professor Veinberg (Centennial of the lecture «Friction-free motion»). *Siberian Journal of Science*. 2014;2:6-14. (In Russ.)].
9. Дроздов Б.В. Геостратегические проекты дальневосточного развития России // Культура. Народ. Экофера: труды социокультурного семинара имени Бугровского. – Вып. 4. – М.: Спутник+, 2009. Режим доступа: <https://refdb.ru/look/1972048-pall.html>. Дата обращения: 15.09.2016. [Drozdov BV. Geostrategicheskie proekty dal'nevostochnogo razvitiya Rossii. *Kul'tura. Narod. Ekosfera: trudy sotsiokul'turnogo seminar imeni Bugrovskogo*. Available from: <https://refdb.ru/look/1972048-pall.html>. Accessed September 15, 2016 (In Russ.)].
10. Фиронов А.Н. Вакуумно-левитационный транспорт: перспектива или тупик? // Транспорт Российской Федерации. Журнал о науке, экономике, практике. – 2017. – № 3(70). – С. 44-47. [Fironov AN. Vacuum-levitation transport: any potential or standing no chance? *Transport of the Russian Federation. A magazine of science, economy and practice*. 2017;3(70):44-48. (In Russ.)].
11. Yamamura S. Magnetic levitation technology of tracked vehicles present status and prospects. *IEEE Transactions on Magnetics*. 1976;12(6):874–878. doi: 10.1109/tmag.1976.1059125
12. Cai Y., Chen SS. Dynamic characteristics of magnetically levitated vehicle systems. *Applied Mechanics Reviews, ASME*. 1997;50(11):647–670. doi: 10.1115/1.3101676
13. Meins J., Miller L., Mayer W.J. The high speed maglev transportation system transrapid. *IEEE Transactions on Magnetics*. 1998;24(2):808–811. doi: 10.1109/20.11347
14. Luguang Y. Progress of the maglev transportation in China. *IEEE Trans Applied Superconductivity*. 2006;16(2):1138–1141. doi: 10.1109/tasc.2006.871345
15. Lee KW, Kim KC, Lee J. Review of maglev train technologies. *IEEE Transactions on Magnetics*. 2006;42(7):1917–1925. doi: 10.1109/tmag.2006.875842
16. Zhang Y., Oster D., Kumada M., et al. Key vacuum technology issues to be solved in evacuated tube transportation. *Journal of Modern Transportation*. 2011;19(2):110–113. doi: 10.1007/bf03325748
17. Han H-S, Kim D-S. *Magnetic Levitation Maglev Technology and Applications*. Springer Science+Business Media, Dordrecht; 2016. 247 p. doi: 10.1007/978-94-017-7524-3_6
18. Винокуров В.А., Галенко А.А., Горелов А.Т. и др. Транспортные системы с магнитным подвешиванием и линейным электроприводом. Энциклопедия, в

40 т. – М.: Изд-во Машиностроение, 2008. – 656 с. [Vinokurov VA, Galenko AA, Gorelov AT et al. Transportnye sistemy s magnitnym podveshivaniem i lineinym elektropivodom. Moscow: Izdatel'stvo Mashinostroenie; 2008. 656 p. (In Russ.)].

19. Фихтенгольц Г.М. Курс дифференциального и интегрального исчисления. – М.: Изд-во Наука, 1969. – Т. 1. – 607 с. [Fikhtengol'ts GM. Kurs differentsial'nogo i integral'nogo ischisleniya. Moscow: Izdatel'stvo Nauka; 1969, vol. 1. 607 p. (In Russ.)].

Information about the authors:

Viktor A. Bogachev, PhD in Physico-mathematical sciences

Address: 344038, Rostov-on-Don, Russia, st. Lenina 44/2-4

eLibrary SPIN:2125-5198; ORCID: 0000-0003-1202-7318;

E-mail: bogachev-va@yandex.ru

Yuri A. Terentyev

ORCID: 0000-0002-0888-9057;

E-mail: teren_y@mail.ru

Victor V. Koledov, Doctor of Physico-mathematical sciences

eLibrary SPIN: 9291-1989; ORCID: 0000-0002-2439-6391;

E-mail: victor_koledov@mail.ru

Taras V. Bogachev, PhD in Physico-mathematical sciences

eLibrary SPIN:2262-0080; ORCID: 0000-0001-9641-0116;

E-mail: bogachev73@yandex.ru

Сведения об авторах:

Богачев Виктор Алексеевич, к.ф.-м. н., доцент

Адрес: 344038, Ростов-на-Дону, пр. Ленина 44/2-4.

eLibrary SPIN:2125-5198; ORCID: 0000-0003-1202-7318;

E-mail: bogachev-va@yandex.ru

Терентьев Юрий Алексеевич

ORCID: 0000-0002-0888-9057;

E-mail: teren_y@mail.ru

Коледов Виктор Викторович, д.ф.-м.н., с.н.с.

eLibrary SPIN: 9291-1989; ORCID: 0000-0002-2439-6391;

E-mail: victor_koledov@mail.ru

Богачев Тарас Викторович, к.ф.-м. н., доцент

eLibrary SPIN:2262-0080; ORCID: 0000-0001-9641-0116;

E-mail: bogachev73@yandex.ru

To cite this article:

Bogachev VA, Terentyev YA, Koledov VV, Bogachev TV. Dzungaria Corridor for Vacuum Magnetic Levitation Transport: Lost Opportunities or Weighted Optimism? *Transportation Systems and Technology*. 2018;4(2):52–61. doi: 10.17816/transsyst20184252-61

Цитировать:

Богачев В.А., Терентьев Ю.А., Коледов В.В., Богачев Т.В. Джунгарский коридор для вакуумного магнитного левитационного транспорта: утерянные возможности или взвешенный оптимизм? // Транспортные системы и технологии. – 2018. – Т. 4. – № 2. – С. 52–61. doi: 10.17816/transsyst20184252-61

DOI 10.17816/transsyst20184262-72

© F. Qin, Y. Lin, D. Lu

National Maglev Transportation Engineering R&D Center, Tongji University
(Shanghai, China)

HARDWARE-IN-THE-LOOP SIMULATION OF HIGH-SPEED MAGLEV TRANSPORTATION FIVE-SEGMENT PROPULSION SYSTEM BASED ON DSPACE

Aim: For exploring and testing the key technology of high-speed maglev transportation propulsion control system, this paper designs and establishes a hardware-in-the-loop (HIL) real-time simulation system of the high-speed maglev transportation five-segment propulsion system.

Materials and methods of the studies: According to the route conditions and propulsion segment division of Shanghai maglev demonstration and operation line, the real-time simulation platform based on dSPACE multiprocessor systems is implemented. The simulation system can achieve the functional simulation of all the high-power related equipment in the 5-segment area, including 8 sets of high-power converter units, 2 sets of medium-power converter units, 2 sets of low-power converter units, five-segment trackside switch stations and long-stator linear synchronous motors. The mathematical models of linear motors and converters are built in MATLAB/Simulink and System Generator, after compiling, they can be downloaded and executed in Field Programmable Logic Array (FPGA). All the interfaces connecting the simulation system to the propulsion control system physical equipment use real physical components as in the field, such as analog I/O, digital I/O, optical signals and Profibus.

Results: By using CPU+FPGA hardware configuration, the simulation steps are greatly shortened and the response speed and accuracy of real-time simulation system are improved. The simulation system can simulate multiple operating modes such as multi-segment, multi-vehicle, double-track, double-feeding, step-by-step stator section changeover, and so on. The simulation results show that the maximum speed of the simulation system can reach 500 km/h.

Conclusion: This HIL system can provide detailed real-time on-line test and verification of high speed maglev propulsion control system.

Keywords: Hardware-in-the-loop, real-time simulation, high-speed Maglev transportation, five-segment, propulsion system, dSPACE, FPGA.

INTRODUCTION

High-speed maglev transportation has the advantages of high speed, low energy consumption, low noise, no pollution and the strong ability to run over steep slopes and sharp curve and so on. So it is a suitable candidate for next-generation transport systems. Shanghai maglev demonstration and operation line is the first commercial operation line in the world, which utilizes long stator linear synchronous motor (LSLSM) propulsion and electromagnetic suspension [1].



The propulsion system is one of the core technology of high-speed maglev transportation system, which mainly includes propulsion control system, long stator linear synchronous motors, converters and trackside equipment. However, the development and testing of the propulsion control system face many difficulties. First of all, there is currently no long enough line for the propulsion control system to complete the high-speed test; secondly, the controller at the early stage of development inevitably suffers from various deficiencies, in which case high-speed test will bring a lot of danger and the cost will be relatively high [2]. Therefore, hardware-in-the-loop (HIL) real-time simulation is essential.

The purpose of HIL simulation is to simplify the difficulty of system development and accelerate the development and test of the system. The basic idea is to connect the real controller with the rest of the mathematical model in the system to form a semi-physical simulation system. Through the specially designed hardware interface circuit, the mathematical model running in the real-time simulation system receives the control instructions of the real controller and feeds back the operation results to the controller. Therefore, HIL simulation can complete software and hardware testing on the real controller, while reducing experimental costs [3].

In this paper, dSPACE is used to establish the HIL real-time simulation platform of the high-speed maglev transportation propulsion system. Taking Shanghai maglev train demonstration and operation line as a case of application, the simulation system enables the simulation of all converters, linear motors and trackside equipment in the 5-segment area. The simulation results show that the maximum speed of the simulation system can reach 500km/h.

SYSTEM OVERALL ARCHITECTURE

The propulsion HIL real-time simulation system includes the actual control system devices and the power simulation system devices. The configuration principles of the actual devices and the simulation devices are as follows:

- ✓ Power-related parts are implemented by simulation, such as converter units, linear motors, and trackside feed cables, etc.;
- ✓ Weak electricity and control related parts adopt actual devices, such as motor control units and converter control units inside the propulsion control system;
- ✓ The same devices are implemented with 1 to 2 sets of actual devices, and the rest is realized by simulation, such as trackside switch station control units;
- ✓ The interfaces between the simulation devices and the actual devices are configured as much as possible based on the actual interfaces (such as analog signal interfaces, digital signal interfaces, optical fiber

signal interfaces, Profibus interfaces, etc.), but for the convenience of debugging, some debugging interfaces (such as position signal interface) can be simplified and added.

The high-speed maglev propulsion HIL system uses Shanghai maglev demonstration and operation line as its application background. The total length of Shanghai line is approximately 30 kilometers, with two tracks A (downward) and B (upward). There are two propulsion substations on the whole line, respectively #1 propulsion substation and #2 propulsion substation, as shown in Fig. 1. Among them, #1 propulsion substation is equipped with two sets of high-power converter blocks, and #2 propulsion substation is equipped with two sets of high-power converter blocks, one sets of medium-power converter blocks and one sets of low-power converter blocks.

The whole line is divided into five propulsion segments (Fig. 1). Among them, the main line is divided into four propulsion segments: the main track PSE2A (red), PSE2B (blue), Longyang Road Station PSE1 (purple), Pudong Airport Station PSE3 (light green); the entire maintenance area is a propulsion segments PSE90 (rose red). Double-feeding is carried out in PSE2A and PSE2B propulsion segments. In the propulsion segments of PSE1, PSE3, and PSE90 operation takes place using single-feeding. The step-by-step method is adopted for the whole line, and each set of converter block is equipped with two sets of converter units, two sets of feeding cables and corresponding switching devices.

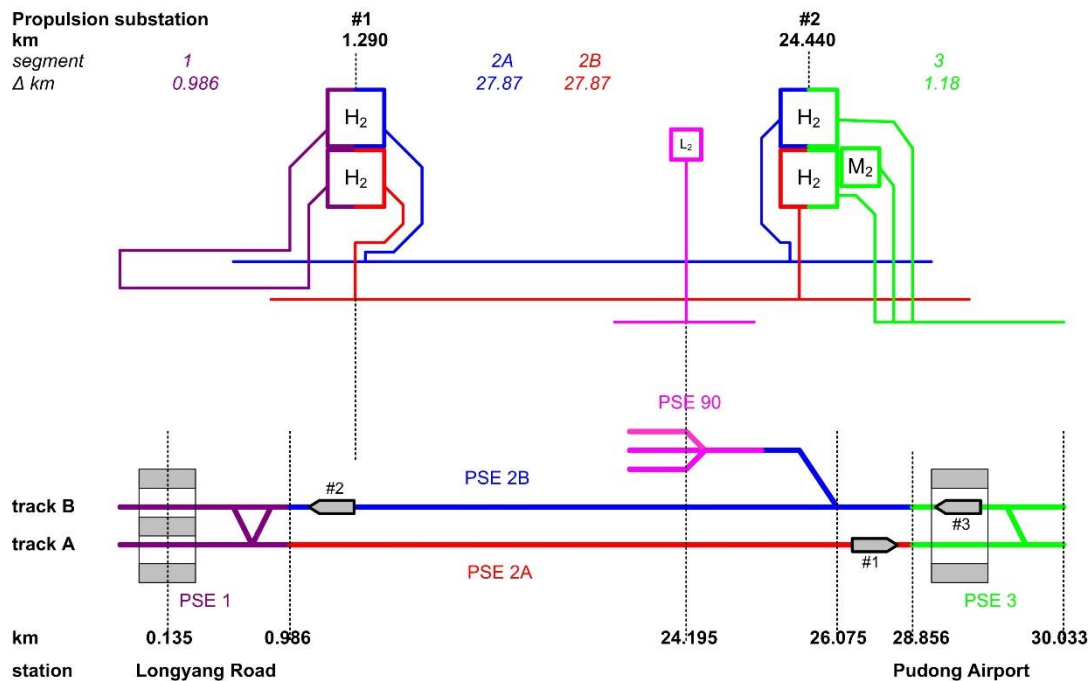


Fig. 1. Overall configuration of the propulsion system

According to the above requirements, the specific configuration of the propulsion HIL simulation system is shown in Fig. 2.

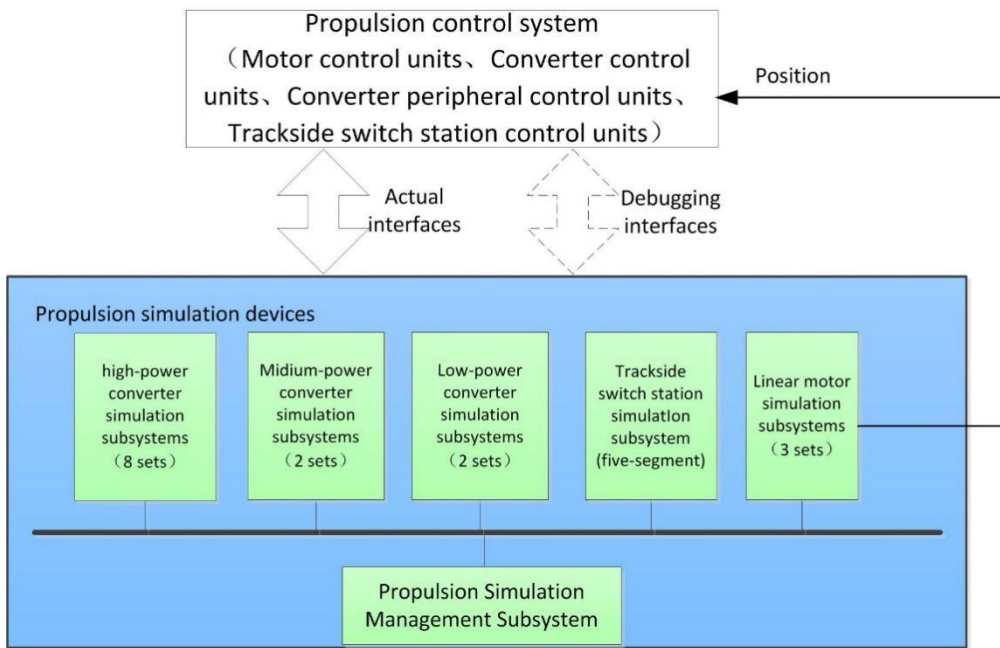


Fig. 2. The specific configuration of the propulsion HIL simulation system

1. Propulsion control system

In addition to trackside switch station control units, the rest of the propulsion control system uses physical devices, including motor control units (MCU), converter control units (CCU), converter peripheral control units, and the monitoring and diagnostic system. Since there are many trackside switch stations along the line (the average interval is 600 meters) and all trackside switch stations have the same working principle, only two sets of trackside switch station control units use actual devices, and the rest are implemented using simulation systems.

2. Propulsion simulation system

According to the function division, the propulsion simulation system mainly consists of 12 sets of converter simulation subsystems, trackside switch station simulation subsystem and 3 sets of linear motor simulation subsystems.

- 1) 12 sets of converter simulation subsystems include 8 sets of 15 MVA high-power converter simulation subsystems, 2 sets of 7.5 MVA medium-power converter simulation subsystems and 2 sets of 400kVA low-power converter simulation subsystems. Each set of converter simulation subsystem can achieve the functional simulation and interface simulation of a neutral point clamp (NPC) three-level back-to-back AC-DC-AC converter, input switchgears, input transform, output transform and output switchgears;
- 2) The trackside switch station simulation subsystem can implement functional simulation and interface simulation of all trackside switch stations and their control units within 5 propulsion segments. As the

trackside switch stations in each segment exchange information with the motor control units through redundant Profibus networks, so the trackside switch station simulation subsystem of five-segments needs to configure 10 Profibus communication interfaces;

- 3) The linear motor simulation subsystem is used to simulate the electromagnetic characteristics of the two long stator synchronous linear motors on the left and right sides of each column of the maglev vehicle and the vehicle's motion characteristics. 3 sets of linear motor simulation systems correspond to 3 maglev vehicles.

According to the requirements of the operation mode of the high-speed maglev propulsion system, the propulsion simulation system can realize the simulation of various working modes, such as single-feeding, double-feeding, and step-by-step stator section changeover mode, etc. For this reason, the converter simulation subsystems of different numbers and power levels can be co-simulated with different linear motor simulation subsystems and trackside switch station simulation subsystem. Therefore, the propulsion simulation system can implement different operating modes according to the operating mode of the high-speed maglev system.

In addition, the propulsion simulation system needs to configure the propulsion simulation management subsystem to realize the development and download of the simulation system models, online real-time monitoring and parameter modification. The propulsion simulation management subsystem can also inject faults and detect fault conditions in real-time simulation systems, set up various test cases, and complete the comprehensive testing and verification of the propulsion control systems. The propulsion simulation management subsystem can be made up of one or several host computers.

PROPULSION SIMULATION SYSTEM DESIGN

In the hardware configuration of the propulsion simulation system, five dSPACE real-time simulators are used to form a multi-processor system to implement the functional simulation and hardware interface simulation of the 5-segment propulsion power devices. The corresponding relationship between the subsystems of the 5-segment propulsion simulation subsystems and the dSPACE real-time simulators is shown in Fig. 3.

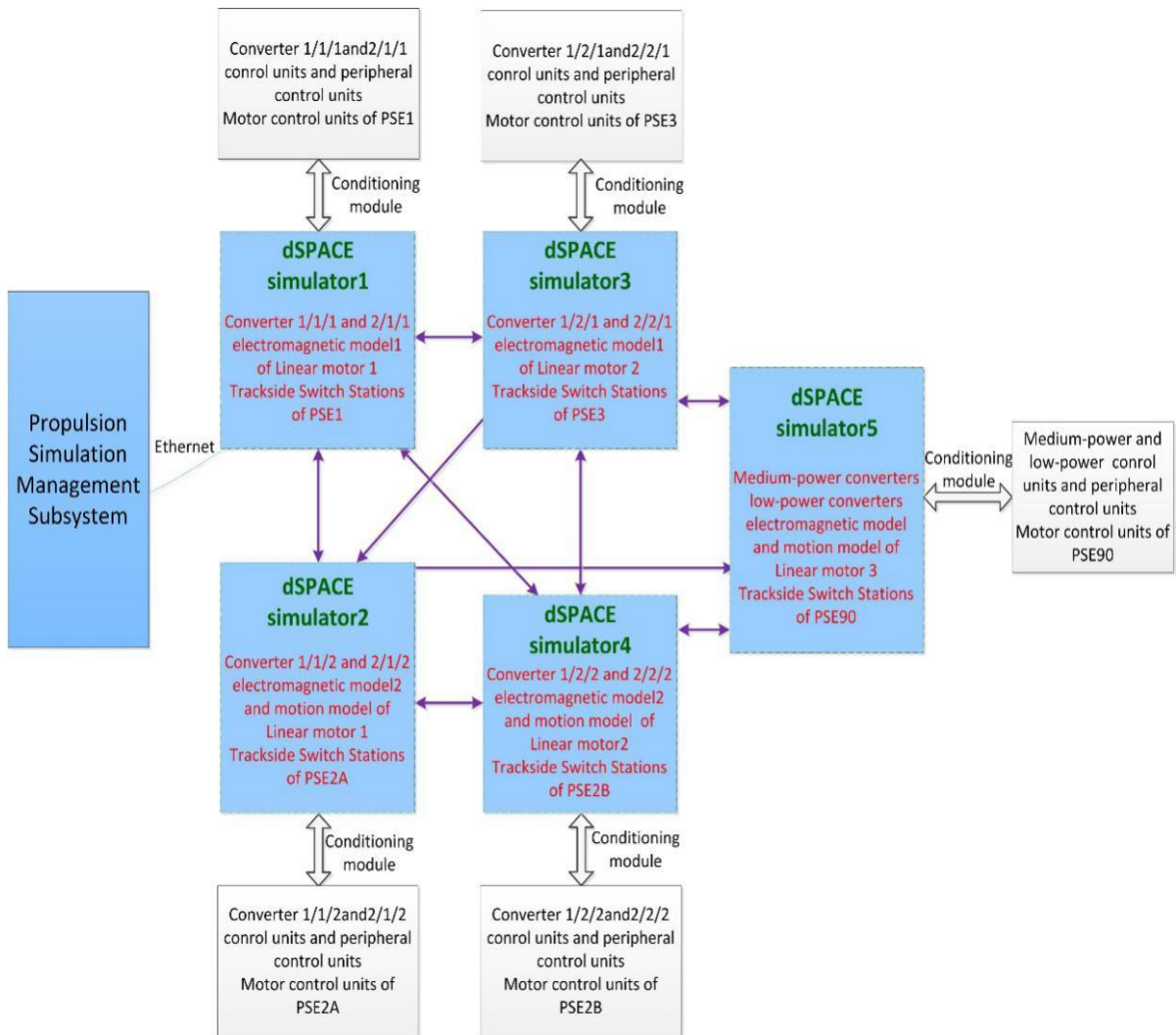


Fig. 3. Hardware configuration of 5-segment propulsion simulation system

Five dSPACE simulators communicate with each other through fiber optics to form a multi-processor system that enables real-time information exchange. The propulsion simulation management subsystem can be connected to any dSPACE simulator through an Ethernet network cable, enabling information exchange with 5 dSPACE simulators. The five dSPACE simulators receive instructions from the converter control units and converter peripheral control units through conditioning modules, and feedback voltage and current information. The conditioning modules are used to transform the actual interfaces of the propulsion control system into the signals that the dSPACE simulator can receive. The five dSPACE simulators receive the commands of trackside switch stations from the motor control units via the Profibus network and feed back the status information. The dSPACE simulator 2\4\5 feeds back the position information of the maglev vehicle to the corresponding motor control units through UDP interface respectively, in order to realize the position closed-loop control.

dSPACE real-time simulators use CPU + FPGA architecture, configured hardware boards includes DS1007 processor board, FPGA board and its piggyback module, Profibus board and D/A board. The DS1007 is connected to other boards via PHS bus and to the propulsion simulation management subsystem via Ethernet interface.

The processor board adopts a dual-core CPU. One of the CPUs is used to implement real-time simulation models with low real-time requirements and external interface models, such as trackside switch station simulation subsystems, trackside Profibus communication, UDP communication, etc. The other CPU mainly undertakes data exchange with the FPGA board, including parameter setting, on-line data observation, and interaction of simulation data, etc.

The FPGA board has 100 MHz clock period. It can be configured with 32 digital input/output channels and 12 analog input/output channels. The use of FPGA's high-speed computing capability can achieve the computational tasks of mathematical models with high real-time requirements, such as converters and long stator linear motor mathematical models. Because each FPGA board has a limited number of digital I/O channels and analog I/O channels, each dSPACE simulator requires the configuration of four FPGA boards to implement the mathematical models of two sets of converters and a set of long stator linear motor.

In view of the large number, large-scale and complex features of the propulsion system equipment, a decoupled modeling algorithm was used [4-5]. Firstly the independent model of each simulation subsystem was established using MATLAB/SIMULINK and System Generator software, such as the converter rectifier side mathematical model and inverter side mathematical model, single-feeding long stator synchronous linear motor mathematical model, double-feeding long stator synchronous linear motor mathematical model, etc. Secondly the energy storage element connected with the converter switching element is equivalent to a voltage source or a current source, then an equivalent decoupling circuit between subsystems is obtained. The independent equivalent circuits of all subsystems are cascaded into the equivalent circuit of the propulsion simulation system as a whole, which is also the overall mathematical model of the propulsion simulation system.

SIMULATION RESULTS

The propulsion simulation system and the propulsion control system make up the hardware-in-the-loop real time simulation system. The photos are shown in the Fig. 4, 5.



Fig. 4. Propulsion control system



Fig. 5. Propulsion simulation system

The HIL system can complete the simulation test of various operation modes, including multi-segment, multi-vehicle, double-track, single-feeding and double-feeding method. The propulsion control system uses rotor field oriented

control with constant excitation and stator current d axis component constant to zero, and realizes position, speed, and current three closed-loop control. The simulation step of the whole propulsion simulation system is 100 microseconds, but the operation time of the mathematical model of the converter and the linear motor in FPGA is only 400 ns. Thus, it can be seen that the hardware architecture of CPU+FPGA can guarantee the real time of the model operation to the maximum degree, so as to meet the real time requirement of the whole HIL system.

In the case of four sets of high power converters with double-feeding, the maximum operating speed of an unloaded maglev vehicle can reach 500 km/h. The Fig. 6 and Fig. 7 show the speed and acceleration curves.

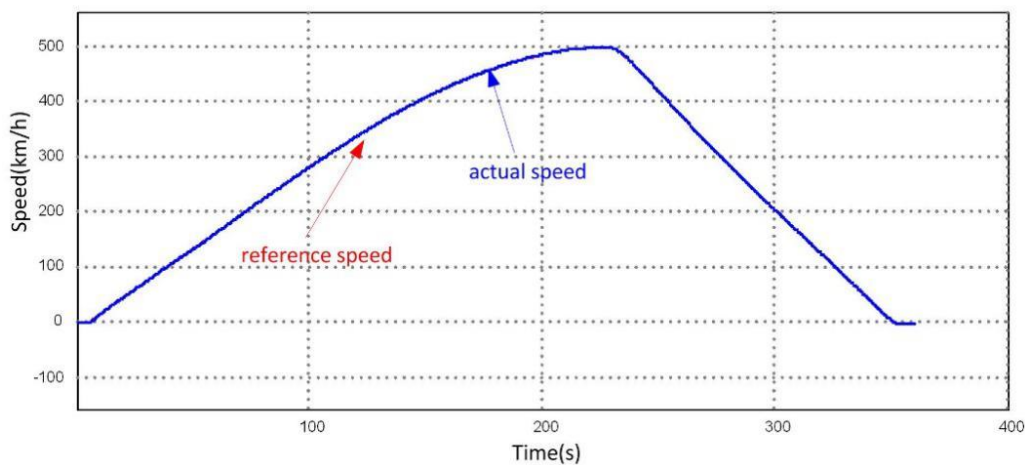


Fig. 6. Speed curve with a maximum velocity of 500 km/h

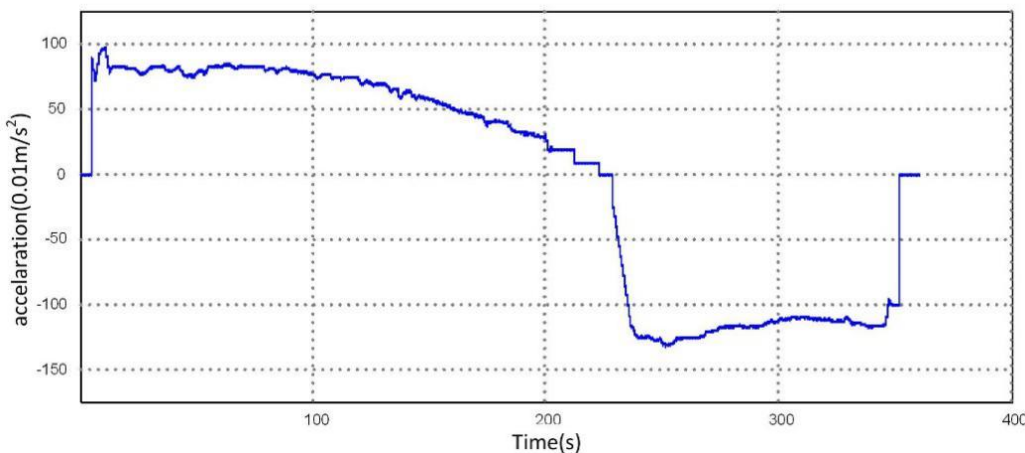


Fig. 7. Acceleration curve with a maximum velocity of 500 km/h

The velocity of the vehicle is accelerated from 0 to 500 km/h by maximum acceleration speed 1 m/s^2 and decelerated by maximum acceleration -1.2 m/s^2 . The total mileage is 27.5 km. As can be seen from the speed curve, the vehicle actual speed follows the given speed curve.

In the case of double-feeding, the speed and acceleration curves of the maglev vehicle with full load and a maximum operating speed of 430 km/h are shown in the figures below (Fig. 8, 9).

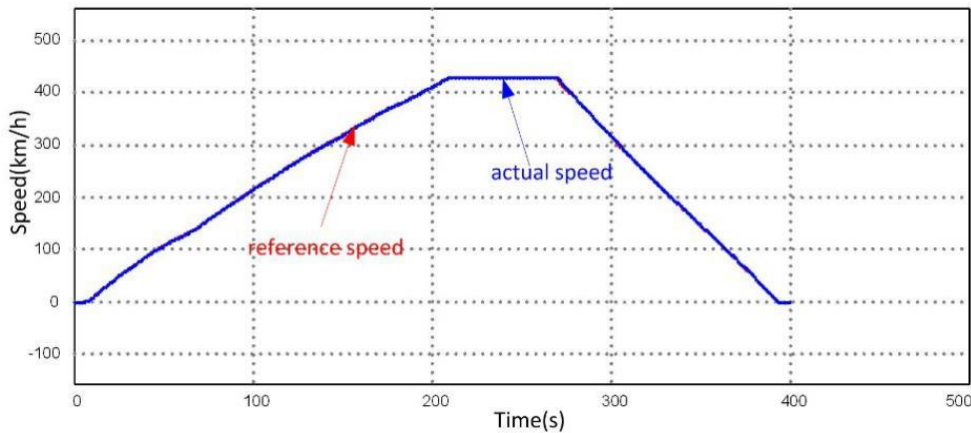


Fig. 8. Speed curve with a maximum velocity of 430 km/h

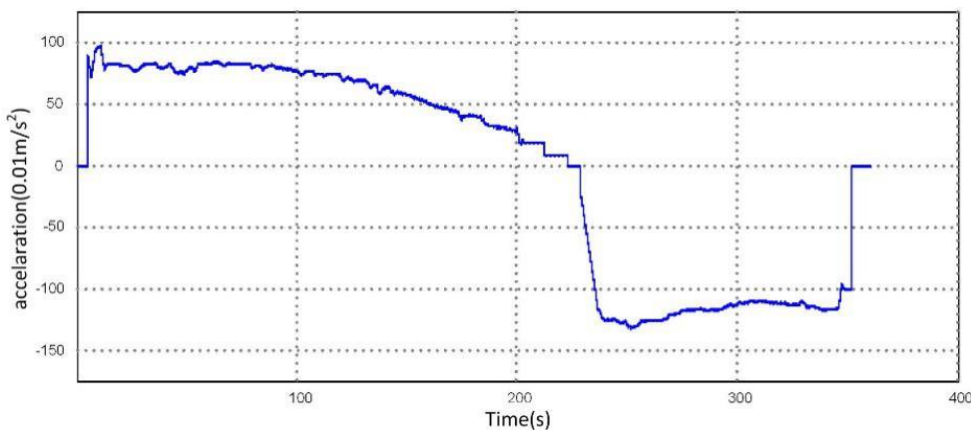


Fig. 9. Acceleration curve with a maximum velocity of 430 km/h

The vehicle runs at a constant maximum speed for 58 seconds. The total mileage is 27.496 km. Maximum acceleration at deceleration is -1.3 m/s^2 . The actual speed is basically consistent with the given speed curve.

CONCLUSION

This paper has established a HIL simulation system for high-speed maglev transportation propulsion system based on Shanghai maglev demonstration and operation line. dSPACE multiprocessor system is used to implement the functional simulation and hardware interface simulation of the 5-segment propulsion power-related devices. The simulation results verified that the real-time simulation is successful and the function of the propulsion control system has been verified. This system can provide detailed test and verification for the propulsion control system and can also be used for the planning and

design of high-speed maglev transportation, the hardware and software development in the propulsion control system, and system integration.

ACKNOWLEDGEMENT

This paper is supported by the National Key R&D Program of China, Research on Simulation Verification and Design Optimization of Key Technologies for High Speed Maglev Transportation System (No. 2016YFB1200602-02).

References

1. Wu X. *Maglev train*. 1st ed. Shanghai: Shanghai Sciences and Technology Press; 2003.
2. Terwiesch P, Keller T, Scheiben E. Rail vehicle control system integration testing using digital hardware-in-the-loop simulation. *IEEE Transactions on Control Systems Technology*, 1999;7(3):352–362. doi: 10.1109/87.761055
3. Li Y, Li Ming S, Hui Z, Du Y. Real-Time Simulation of Linear Synchronous Motor in Hardware-In-Loop Test System. Proceeding of The 13th International Conference on Electrical Machines and Systems (ICEMS2010); 2010 Oct.10–13; Incheon, South Korea. *IEEJ Transactions on Industry Applications*. 2010;131(2):1520–1523. doi: 10.1541/ieejias.131.nl2_5
4. Byoung-Kuk L, Ehsami M. A simplified functional simulation model for three-phase voltage-source inverter using switching function concept. *IEEE Transactions on Industrial Electronics*. 2001;48(4):309–321. doi: 10.1109/41.915410
5. Li Y, Li Ming S, Hui Z. Real-time simulation of linear synchronous motor drives with AC-DC-AC converters. Proceeding of the 6th IEEE Conference on Industrial Electronics and Applications; 2011 June 21–23; Beijing, China. IEEE 2011. p. 680–685. doi: 10.1109/iciea.2011.5975672

Information about the authors:

Feng Qin, PhD, assistant researcher; Caoan Highway 4800, Shanghai, China;
ORCID: 0000-0001-9945-1669;
E-mail: qinfeng@tongji.edu.cn

Ying Lin, master, assistant researcher;
ORCID: 0000-0002-2270-272X;
E-mail: carfieldlin@tongji.edu.cn

Diqiang Lu, PhD, assistant researcher;
ORCID: 0000-0003-2688-9023;
E-mail: ludiqiang@tongji.edu.cn

To cite this article:

Qin F, Lin Y, Lu D. Hardware-in-the-loop Simulation of High-Speed Maglev Transportation Five-Segment Propulsion System Based on DSPACE. *Transportation Systems and Technology*. 2018;4(2):62–72. doi: 10.17816/transsyst20184262-72

UDC 629.439

DOI 10.17816/transsyst20184273-91

© К. К. Kim

Emperor Alexander I St. Petersburg State Transport University
(Saint-Petersburg, Russia)

THE RUSSIAN VERSION OF THE TRANSPORT SYSTEM “HYPERLOOP”

Aim: development of the Russian version of the high-speed transport system “Hyperloop” characterized by improved technical and economic indicators.

Methods: We use the method of perforating the shell of the head part of the passenger capsule is used, the movement of which is carried out by a linear electric motor with a stator winding located on the pipe.

Results: As the research showed at a speed of about 500 km/h for the creation of vacuum we will spend more energy than overcoming the friction of the capsule on air. Therefore the density of air in the pipe can be lowered only by 1.5–2 times.

Conclusion: The construction of the vacuum-levitating transport in Russia is reasonable and justified economically but only among the densely populated centers, i.e. mainly in the European part of Russia.

Keywords: pipe, capsule, edge air flow, turbulent spots, perforated frontal part, suction.

© К. К. Ким

Петербургский государственный университет путей сообщения
Императора Александра I
(Санкт-Петербург, Россия)

РОССИЙСКИЙ ВАРИАНТ ТРАНСПОРТНОЙ СИСТЕМЫ HYPERLOOP

Цель: Разработка российского варианта высокоскоростной транспортной системы Hyperloop, характеризующейся улучшенными технико-экономическими свойствами.

Методы: Использовался метод перфорирования обшивки головной части пассажирской капсулы, движение которой осуществляется с помощью линейного электрического двигателя со статорной обмоткой, расположенной на трубе.

Результаты. Установлено, что при скорости около 500 км/ч для создания вакуума тратится больше энергии, чем на преодоление трения капсулы в разреженном воздухе. По этой причине давление воздуха в трубе может быть рекомендовано в 1,5–2 раза ниже атмосферного давления.

Заключение: Создание такого транспорта в России целесообразно и экономически обосновано только между мегаполисами с высокой плотностью населения, т. е. главным образом в Европейской части России.

Ключевые слова: труба, капсула, пограничный воздушный поток, пятна турбулентности, перфорированная головная часть, отсасывание.



INTRODUCTION

Nowadays we watch a revival of interest to the idea of the vacuum transport. It is supposed that the passenger capsules move with a speed of 500–1000 km/h in the pipe which has vacuum. The technical vacuum stipulates a very low aerodynamic resistance on the capsule movement. It affects the required power of the drive motors, in most cases, the linear induction motors. The large speeds of movement determine the transition from the mechanical pair of rail - wheel to the magnetic suspension of the capsule. The limitation caused with the minimizing of the pipe volume where you want to create vacuum and the desire to maximize the pipe cross section which determines the throughput of this system will necessarily lead to the minimum clearances between the outer surface of the capsule and the inner surface of the pipe. In this connection it is also reasonable the keeping of the capsule in the lateral coordinate to carry out by the forces of the electromagnetic field.

The objective of the research described in this paper was the developing of a compromise variant of the high-speed pipeline transport system without using the technical vacuum but with using the rarefied air in the pipe and the drive linear induction motor.

To achieve this objective we solved the following problems:

- to prove the suitability of using this transport system in Russia;
- to work out the method of lowering the head aerodynamic resistance of the moving capsule;
- to work out the engineering calculation method of the linear induction motor.

IMPLEMENTATION OF THE PROJECT OF THE VACUUM TRANSPORT IN RUSSIA

Let's analyze the profitability of this project based on the example of the building of the road between Moscow and St. Petersburg with the length of 634.14 km. This distance is 79.25 times more than the eight kilometer test track of the valley Quay, which costs 150 million \$. Therefore the cost of the road between Moscow and St. Petersburg is 11 billion and 185 million \$.

When 1 \$ is equal to 65 rubles, the cost of the road between Moscow and St. Petersburg will be 722 billion rubles. Taking the inflation into account this cost will reach 853 billion rubles.

As the ticket price between Los Angeles and San Francisco (the distance between them is 600 km) is planned 20 \$ that less than one-third of the ticket price of the Russian "Sapsan" at the same distance, therefore the ticket price in Russia will be 700 rubles.

We proceed from the fact that the safe passenger density during the test of the track "Transportation Technologies" (the project "Hyperloop") will be approximately 3400 passengers per hour, i.e. the annual volume will exceed 24

million people, it will amount to 16 billion rubles per year (24 million \times 700 rubles).

Therefore, the payback period of the road is equal to 53 years (853 billion rubles / 16 billion rubles) not taking into account the profits from the sale of surplus energy.

53 years is a very long time therefore it is advisable to increase the ticket price up to 1300 rubles that corresponds to the minimum ticket price of "Sapsan" then the price of the sold tickets is equal to 31 billion rubles per year (24 million people \times 1300 rubles).

In this case the road will payback for 27 years.

Let's note that formerly we didn't take into account the profit on the sale of surplus energy. As the senior Director of Hyperloop project says they plan to gain 25 million \$ annually from the sale of surplus energy. In rubles the receipts from the sale of energy will reach 1.5 billion per year, and it will be 40 billion rubles for 27 years. Because of this the payback period drops to 25 years. This aspect requires a further analysis due to the difference in the solar activity in California and Russia.

It should be noted that we don't consider the expenditure for the technical service of the road and capsules in this paper.

In order to compare it, let's consider the high-speed communication between Moscow and St. Petersburg.

The "Russian Railways" and "Siemens" signed the first contract in May 2006. The price of eight trains "Sapsan" was 276 million €, besides the "Russian Railways" also signed the 30-year contract for their technical service with the German concern (354,1 million €). Then the "Russian Railways" signed a firm contract with the German "Siemens" to deliver eight more high-speed trains "Sapsan". Their price and the expenditure of technical service amounted 600 million € which amounts 58 billion in the ruble equivalent.

Let's note that a separate high-speed line hasn't been built for "Sapsan" so the pass of more high-speed passenger trains demanded the removal of freight trains, it led either to the impossibility of their formation and the failure to remove the goods or to move them by a circuitous route. In this regard there is a need to build a separate high-speed line.

The cost of the planned road of the high speed railway "Nizhny Novgorod – Moscow" (its length is 400 km) will be 300 billion rubles by the preliminary calculations. We didn't take into consideration the costs of pulling down the buildings and payment of compensation for them, the rent of land, carry of infrastructure, etc. Approximately it may cost another 200 billion. As a result the cost of the building will be about 500 billion rubles. If we take the inflation and "misuse expenses" into consideration it will increase by 200 billion and it will be ~ 700 billion.

The distance between St. Petersburg and Moscow in a straight line is 650 km, it is by 1.62 times more than to Nizhny Novgorod. Therefore, at the linearly dependence of the building expenditures on the distance between Moscow and St. Petersburg the building of this road will cost 1.1 trillion rubles.

Let's take the expenditures of contracts with "Siemens" into account we will receive 1.158 trillion rubles.

The average ticket price on "Sapsan" is equal to 2000 rubles. If we suppose that the passenger traffic is 7 million people per year, in rubles it will give 14 billion rubles per year ($7 \text{ million} \times 2000 \text{ rubles}$) and the payback period is ~ 83 years (1.158 trillion rubles / 14 billion rubles).

It should be noted that the main economic factor of passenger transport is increasing the mobility of the population. If the "Sapsan" speed is 250 km/h, the capsule in the pipe is capable to speed up to 1200 km/h but we can suppose that its maximum speed will be limited by a more modest value of 500 - 700 km/h. But even in this case the building of the pipeline vacuum transport in Russia is also justified but only between densely populated centers, i.e. in the European part of Russia even if we don't to build separate roads for a high-speed movement as we see at this moment.

THE DEVELOPMENT OF THE UNIVERSITY

The question arises about the expediency of creating and maintaining a technical vacuum in the pipe. As the research showed: at a speed of about 500 km/h for the creation of vacuum we will spend more energy than overcoming the friction of the capsule on air. Therefore, the density of air in the pipe can be lowered only by 1.5–2. However, there are questions connected with the interaction of moving capsules with the oncoming air flow.

The pattern of flow around a two-piece capsule with the dimensions of the "Sapsan" by oncoming air flow at a speed of 600 km/h is shown in Fig. 1. At the movement of the capsule a boundary layer of air is formed on its surface. The causes of different kinds: the body surface roughness, the non-uniform of the flow of an air layer, the body vibration cause the appearance of small perturbations of the boundary layer. These perturbations lead to the appearance of turbulent spots which further convert the whole boundary layer practically into a turbulent condition that causes a sharp increasing of the aerodynamic drag of the capsule, the appearance of disturbing forces and moments acting on the capsule. If you do not struggle against this phenomenon you should increase the power of the drive motors and other devices which carry out the spatial magnetic keeping of the capsule, strengthen the capsule design, this aggravates their weight and dimension indicators.

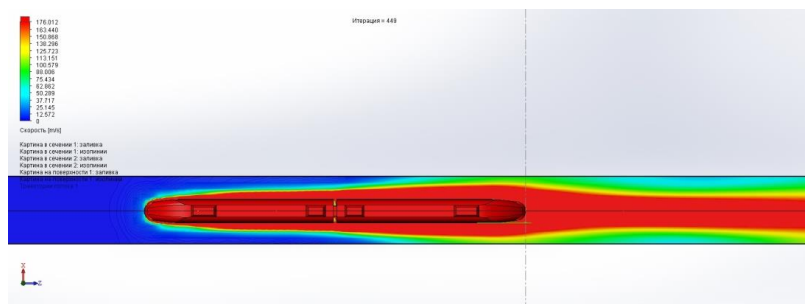


Fig. 1. The pattern of flow around a two-piece capsule with the dimensions of the “Sapsan” at a speed of 600 km/h

As we propose in [1, 2] it is possible to avoid partially the consequences of turbulences of the air boundary layer if we make the capsule front part perforated (Fig. 2). The suction of incipient turbulent spots of the air boundary layer is carried out through the holes (the hole diameter is ~ 100 microns, the distance between the adjacent holes is 0.7–1 mm) in the front part, owing to it the air boundary layer mainly keeps a laminar character. It can lead to reducing the aerodynamic drag up to 30 %. The air flow which passed through the perforated holes is used to condition and cool the current-carrying elements of the capsule. The suction can be also carried out forcibly by means of pumps [3–5].

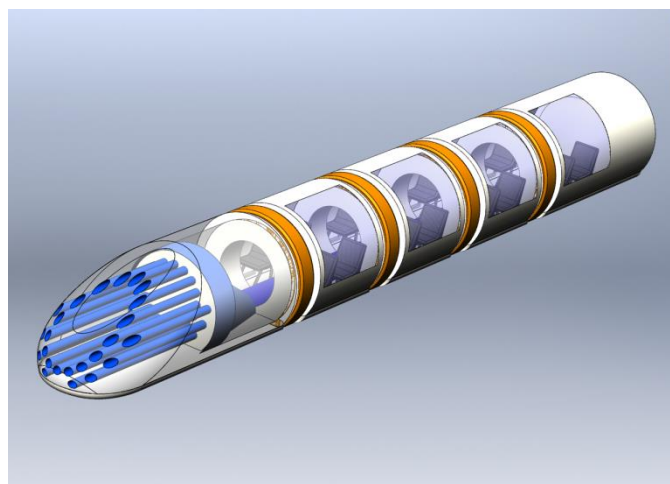


Fig. 2. The capsule with the perforated front part

One of the main units of the considered transport system is a traction linear induction motor with the one-sided stator. But where to place this stator? When we place it on the capsule the mass and dimensions are increased. Besides it is necessary to place a power source in it too as the traditional current collection is impossible at such speeds. We can avoid it if the stator is placed on the pipe along the whole length. However, in this case the cost of the pipe is

significantly increased. Nevertheless, this question was solved in favor of the location of the stator on the pipe.

In the proposed variant of the transport system the capsule mass is relatively small as it consists only of the mass of the body and the current-carrying elements placed on it (the mass of passengers is not taken into account).

One of the variants of the transport system with a stator located on the inner surface of pipe 1 made of ferromagnetic material. The stator has concentrated inductor winding 3 and distributed three-phase winding 4. There is a system of short-circuited turns 6 on capsule 5. Stator 2 of the linear motor consists of electrically unconnected separate sections (segments). The beginning and end of the segment are shown by the dashed lines. All the segments are made similarly: inductor winding 3 is in the beginning segment, then three-phase winding 4 starts. The pole pitch (τ) of three-phase winding 4 is equal to the distance (τ) between adjacent short-circuited turns 6.

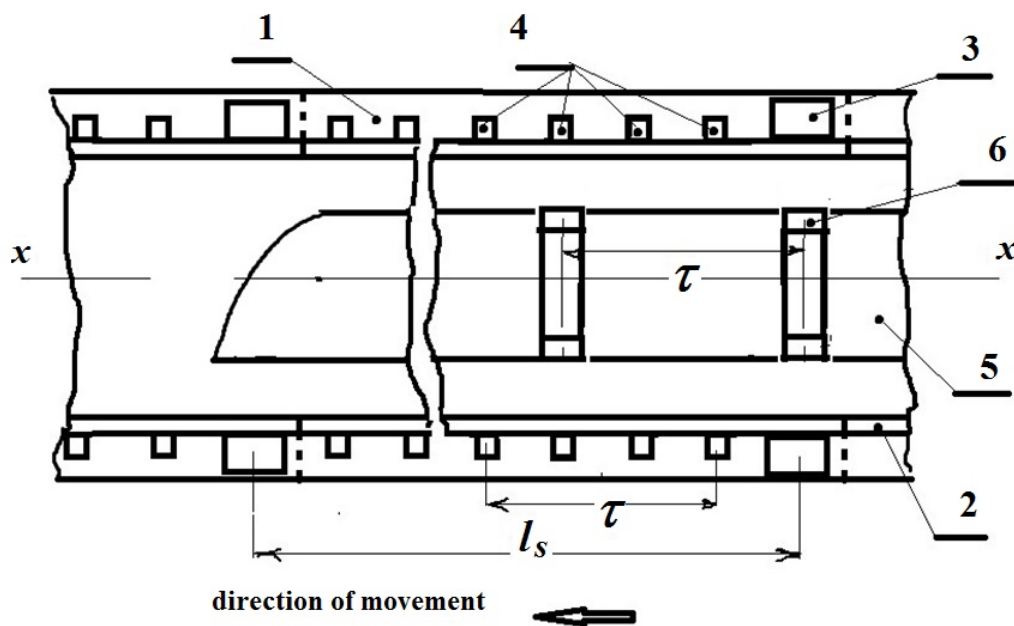


Fig. 3. The scheme of the transport system

The duration of the operation of any of the stator segment is equal to the period of time during which capsule 5 is within this segment. At this time period inductor winding 3 and three-phase winding 4 are fed by the power sources of the single-phase and three-phase sinusoidal current with the period $T=2\tau/v$, where v is the local speed of capsule 5. The power sources are not shown in Fig. 2. The current of inductor winding 3 is synchronized with the position of short-circuited turn 6 so that it reached the maximum value when the middle planes of inductor winding 3 and short-circuited turn 6 coincide. In this regard,

the directions of the currents induced in short-circuited turns 6 by the magnetic field of inductor winding 3 are alternated. It leads to the fact that the magnetic field of these currents is distributed along the x -axis periodically with the period 2τ . The main harmonic of this field can be considered as the field excitation. The length of the segment (l_s) should be such in order the decreasing of the field excitation on the length l_s was not too substantial, e.g., twice.

The frequency of current through three-phase winding 4 is strictly corresponded to the local speed of capsule 5. Therefore the speed of the running magnetic field of stator 2 with the spatial period equaled to 2τ and the speed of the field excitation are the same but these fields are shifted by the angle $\delta < \pi/2$ determined by the value of power consumed from the power source of the three-phase current [6–10].

The magnitude of the propulsive force is equal

$$F=3UE/(Xv) \sin\delta,$$

where U and E is the voltage and the EMF excitation of the segment of the three-phase winding, X is the phase inductive impedance of the segment of the three-phase winding taking into consideration the mutual induction with the other two phases.

In this variant of the transport system the capsule mass is relatively small because it is determined only by the mass of body and the mass of short-circuited turns placed on it.

As the scientific research are shown that the spindle-shaped form leads to the possibility of the capsule rotation relatively to the longitudinal axis. In order to avoid it we proposed a capsule design with the flat bottom. In addition to the stability of the movement this constructive solution allows to use a screen effect for the aerodynamic levitation of the capsule. The flat bottom leads to a more simple fabrication technology and operation of the transport system. Here we use the linear induction motor (LIM) with a one-sided stator as the drive motor. And the capsule bottom made of the electrical conductive material plays a role of the LIM runner. The stator is located opposite to the capsule bottom (on the pipe bottom). In spite of the low power characteristics LIM is one of the simplest constructive solutions for the transport systems of such type. We can carry out the levitation relatively simply using the well-known methods of magnetic suspension in the constructions with a one-sided stator. We can use the normal (perpendicular to the propulsive force) electromagnetic force arising in the LIM and it can reach a considerable value. That's why further we shall discuss some basic properties of the LIM with the one-sided stator. To increase the effectiveness of the LIM it is possible to use an additional bias winding, similar to that which was discussed earlier for the spindle-shaped variant.

Let's calculate the magnetic field of this motor (Fig. 4). Here area 0 simulates the ferromagnetic core of the inductor, area 1 is the capsule, area 2 is air. There is a three-phase winding on the border between areas 0 and 1. We assume that the dimensions of the inductor and the capsule in the x and y directions are infinitely large; the capsule acceleration occurs along the x direction.

Let's replace the three-phase winding by the current layer with the density equal to

$$j_{1y} = j_1 = J_m \cos(\omega_1 t - \alpha x), \quad \alpha = \frac{\pi}{\tau}, \quad J_m = \frac{m\sqrt{2}\omega k_{win}}{p\tau} I, \quad (1)$$

where τ is the pole pitch, m is the number of phases, w is the number of series-connected turns of the phase or the number of turns of one parallel branch, I is the effective value of the phase current, p is the number of pairs of poles, k_{win} is the winding factor.

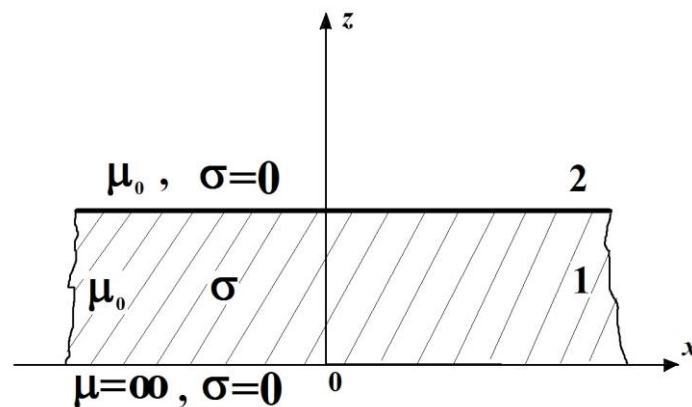


Fig. 4. The calculation scheme of LIM

The magnetic field in the capsule bottom is described by the equation

$$\Delta \mathbf{A}_1 - \mu_0 \sigma \frac{\partial \mathbf{A}_1}{\partial t} + \mu_0 \sigma (\mathbf{v} \times \text{rot} \mathbf{A}_1) = 0, \quad (2)$$

here Δ is the Laplace operator; \mathbf{A}_1 is the vector potential; σ is the conductivity of the material of the capsule bottom; $\mu_0 = 4\pi \times 10^{-7}$ H/m; \mathbf{v} is the speed of the capsule.

Since $\mathbf{A}_1 = \mathbf{j}A_1$, $\mathbf{v} = \mathbf{i}u$, equation (2) takes the form

$$\Delta A_1 - \mu_0 \sigma \frac{\partial A_1}{\partial t} - \mu_0 \sigma u \frac{\partial A_1}{\partial x} = 0. \quad (3)$$

In area 2 the field satisfies the Laplace equation

$$\Delta \mathbf{A}_2 = 0. \quad (4)$$

Let's move to the complex images and suppose that

$$A_1 = \dot{A}_{1m} e^{i(\omega_1 t - \alpha x)}, \quad A_2 = \dot{A}_{2m} e^{i(\omega_1 t - \alpha x)},$$

\dot{A}_{1m} , \dot{A}_{2m} are the complex amplitudes. Then (3) and (4) can be written as follows

$$\frac{d^2 \dot{A}_{1m}}{dz^2} - \lambda^2 \dot{A}_{1m} = 0, \quad (5)$$

$$\frac{d^2 \dot{A}_{2m}}{dz^2} - \alpha^2 \dot{A}_{2m} = 0, \quad (6)$$

The boundary conditions are: at $z = 0$ we have $H_x = J_m \cos(\omega_1 t - \alpha x)$,

$$\text{so } \left. \frac{\partial \dot{A}_{1m}}{\partial z} \right|_{z=0} = -\mu_0 J_m,$$

at $z = \delta$

$$\left[\dot{A}_m \right]_{S_{12}} = 0, \quad \left[\frac{\partial \dot{A}_m}{\partial z} \right]_{S_{12}} = 0, \quad (7)$$

at $z = \infty$

$$\dot{A}_{2m} \Big|_{z=\infty} = 0,$$

where $\lambda^2 = \alpha^2(1 + j\varepsilon)$, $s = \frac{\omega_1 - \omega_2}{\omega_1}$, $\varepsilon = \frac{\mu_0 \sigma s \omega_1}{\alpha^2}$, the parameter ε plays the role of the magnetic Reynolds number; ω_2 is the frequency corresponding to the capsule speed. From (5)–(7) it follows

$$\dot{A}_{1m} = \mu_0 J_m \dot{C} \left[(\lambda - \alpha) e^{\lambda(z-\delta)} + (\lambda + \alpha) e^{-\lambda(z-\delta)} \right], \quad \dot{A}_{2m} = 2\mu_0 J_m \lambda \dot{C} e^{(\delta-z)\alpha},$$

$$\dot{C} = C_a - iC_w = \frac{1}{\lambda \left[(\lambda + \alpha) e^{\lambda\delta} - (\lambda - \alpha) e^{-\lambda\delta} \right]}.$$

Hence we shall find out the formulas for the magnetic induction B_x , B_y , the density of eddy currents j_y in the capsule bottom

$$B_x = \dot{B}_{mx} e^{i(\omega_1 t - \alpha x)}, \quad \dot{B}_{mx} = 2\mu_0 J_m \lambda C [\alpha \operatorname{ch} \lambda(z - \delta) - \lambda \operatorname{sh} \lambda(z - \delta)], \quad (8)$$

$$B_z = \dot{B}_{mz} e^{i(\omega_1 t - \alpha x)}, \quad \dot{B}_{mz} = -i2\mu_0 J_m \alpha C [\lambda \operatorname{ch} \lambda(z - \delta) - \alpha \operatorname{sh} \lambda(z - \delta)], \quad (9)$$

$$j_y = j_m e^{i(\omega_1 t - \alpha x)}, \quad j_m = -i2J_m \alpha^2 \varepsilon C [\lambda \operatorname{ch} \lambda(z - \delta) - \alpha \operatorname{sh} \lambda(z - \delta)] \quad (10)$$

Let's find the stator magnetic field in area 1. Using (8), (9) and supposing $\sigma = 0$ in them we receive

$$B_x = \mu_0 J_m e^{-\alpha z + i(\omega_1 t - \alpha x)}, \quad B_z = -i\mu_0 J_m e^{-\alpha z + i(\omega_1 t - \alpha x)}. \quad (11)$$

Let's define the electromagnetic forces acting to the capsule with the volume $V = lbd$, where l is the length, b is the width, d is the thickness. The average values of these forces during the period of changing eddy currents are defined as follows:

for the propulsive force

$$F_x = \frac{k_l S}{2} \operatorname{Re} \int_0^\delta B_{mz}^* j_m dz = \frac{1}{2} \mu_0 J_m^2 \alpha^3 \varepsilon S C_m^2 k_l \left[\frac{\lambda_m^2 + \alpha^2}{\lambda_a} \operatorname{sh} 2\lambda_a \delta + \frac{\lambda_m^2 - \alpha^2}{\lambda_w} \sin 2\lambda_w \delta + 2\alpha(\operatorname{ch} 2\lambda_a \delta - \cos 2\lambda_w \delta) \right], \quad (12)$$

where k_l is the coefficient taking edge effects into account, $S = lb$, B_{mx}^* and B_{mz}^* are the conjugate complexes derived from (8) and (9); j_m is the complex amplitude of eddy currents (10);

for the normal (levitating) force

$$F_z = \frac{k_l S}{2} \operatorname{Re} \int_0^\delta B_{mx}^* j_m dz = \frac{1}{2} \mu_0 J_m^2 \alpha^2 \lambda_m \varepsilon S C_m^2 k_l \left[\alpha \lambda_m \sin 2\beta \left(\frac{\sin 2\lambda_w \delta}{\lambda_w} - \frac{\operatorname{sh} 2\lambda_a \delta}{\lambda_a} \right) + (\lambda_m^2 + \alpha^2) \sin \beta \cdot \frac{1 - \operatorname{ch} 2\lambda_a \delta}{\lambda_a} - (\lambda_m^2 - \alpha^2) \cos \beta \cdot \frac{1 - \cos 2\lambda_w \delta}{\lambda_w} \right].$$

Here $C_m^2 = C_a^2 + C_w^2$, $\lambda = \lambda_a + i\lambda_w = \lambda_m e^{i\beta}$.

If $\varepsilon \gg 1$ then $\lambda \approx \alpha \left(\frac{\varepsilon}{2} \right)^{0.5} \cdot (1 + i)$ so that $\lambda_m = \alpha \sqrt{\varepsilon}$, $\lambda_a = \lambda_w = \alpha \left(\frac{\varepsilon}{2} \right)^{0.5}$, $\sin \beta = \cos \beta = \frac{1}{\sqrt{2}}$. Therefore at a large magnetic Reynolds number we obtain the following approximate formulas for the electromagnetic forces

$$F_x = \mu_0 J_m^2 \alpha^4 \varepsilon S C_m^2 k_l \cdot \left[\left(\frac{\varepsilon}{2} \right)^{1/2} \left(\operatorname{sh} 2\alpha \left(\frac{\varepsilon}{2} \right)^{1/2} \delta + \sin 2\alpha \left(\frac{\varepsilon}{2} \right)^{1/2} \delta \right) + \operatorname{ch} 2\alpha \left(\frac{\varepsilon}{2} \right)^{1/2} \delta - \cos 2\alpha \left(\frac{\varepsilon}{2} \right)^{1/2} \delta \right], \quad (13)$$

$$F_z = \mu_0 J_m^2 \alpha^4 \varepsilon^{3/2} S C_m^2 k_l \cdot \left[\left(\frac{1}{2} \right)^{1/2} \sin(\alpha \varepsilon^{1/2} \delta) - \operatorname{sh}(\alpha \varepsilon^{1/2} \delta) + \frac{\varepsilon^{1/2}}{2} (\cos(\alpha \varepsilon^{1/2} \delta) - \operatorname{ch}(\alpha \varepsilon^{1/2} \delta)) \right].$$

Let's consider the induction motor as a symmetrical three-phase device. We write the Kirchhoff equations for one phase

$$\begin{aligned} \dot{U}_1 &= r_1 \dot{I}_1 + ix_{11} \dot{I}_1 + ix_{12} \dot{I}_2, \\ 0 &= r_2 \dot{I}_2 + ix_{22} \dot{I}_2 + ix_{12} \dot{I}_1, \end{aligned} \quad (14)$$

here r_1 and r_2 are the active resistances of the primary and secondary circuits; x_{11} and x_{22} are the total self-inductive reactances of these circuits; x_{12} is the mutual resistance. Eliminating the current \dot{I}_2 we receive

$$\dot{U}_1 = r_1 \dot{I}_1 + ix_{11} \dot{I}_1 + (r_{\text{ins}} + ix_{\text{ins}}) \dot{I}_1, \quad (15)$$

where r_{ins} and x_{ins} are the insertion resistances equal to

$$r_{\text{ins}} = \frac{x_{12}^2 r_2}{r_2^2 + x_{22}^2}, \quad x_{\text{ins}} = -\frac{x_{12}^2 x_{22}}{r_2^2 + x_{22}^2}. \quad (16)$$

Multiplying (15) by the conjugate complex current \dot{I}_1^* we shall obtain the equation of power balance for one phase. In this equation the terms $r_{\text{ins}} I_1^2$ and $x_{\text{ins}} I_1^2$ mean, respectively, the active and reactive powers of one phase of the primary circuit transmitted to the secondary circuit. If you introduce the concept of electromagnetic power \dot{S}_{EM} ($\dot{S}_{\text{EM}} = P_{\text{EMa}} + iQ_{\text{EMw}}$) into consideration then

$$r_{\text{ins}} = \frac{P_{\text{EMa}}}{m I_1^2}, \quad x_{\text{ins}} = \frac{Q_{\text{EMw}}}{m I_1^2}. \quad (17)$$

Thus the insertion resistances will be found if we know the electromagnetic power of the motor for some fixed value of stator current [11–16].

To calculate the LIM electromagnetic power let's multiply the first equation of (14) by I_1^* . Then we receive

$$\dot{S}_{EM} = -\dot{E}_{12}^* I_1, \quad (18)$$

where $\dot{E}_{12} = -ix_{12} \dot{I}_2$ is the effective value of the EMF induced in the primary circuit by the secondary field. This EMF is induced only by the z -component of the secondary field. Therefore, if we consider the electromagnetic processes in the capsule in the context of equations (14) we should take $B_x = 0$ in (8) and (9) and consider that B_z does not depend on z . In this regard as \dot{B}_{mz} we take its value at $z = 0$ multiplied by a coefficient k_B ($k_B < 1$), i.e.

$$\dot{B}_{mz} = -i2\mu_0 J_m \alpha k_B \dot{C}(\lambda \text{ch}\lambda\delta + \alpha \text{sh}\alpha\delta). \quad (19)$$

Further we write (18) like

$$\dot{S}_{EM} = -\frac{k_l}{2} \int_V \dot{E}_{m12} (k_B J_m)^2 dV, \quad (20)$$

where $\dot{E}_{m12} = \dot{B}_{mz} \cdot 2\tau f_1$ is the complex amplitude of the electric field strength which is corresponding to a magnetic field (19); J_m is the amplitude of the current density defined by the formula (1); k_l is the coefficient taking the edge effects into account. Then

$$\dot{S}_{EM} = P_{EMa} + iQ_{EMw} = i\mu_0 (k_B J_m)^2 k_l \alpha \dot{C}(\lambda \text{ch}\lambda\delta + \alpha \text{sh}\alpha\delta) V 2\tau f_1. \quad (21)$$

Thus the formulas (17) and (21) at the known stator current I_1 allow us to find the insertion resistances (r_{ins} and x_{ins}). In addition from (21) we can obtain the propulsive force

$$F_x = \frac{1}{2\tau f_1} \text{Re} \dot{S}_{EM} = \text{Re} [i\mu_0 (k_B J_m)^2 k_l \alpha \dot{C}(\lambda \text{ch}\lambda\delta + \alpha \text{sh}\alpha\delta)] \quad (22)$$

At the large magnetic Reynolds numbers as we have shown $\lambda = \alpha \left(\frac{\varepsilon}{2}\right)^{0,5} (1+i)$ and from (21) and (22) it follows

$$P_{EMa} = \mu_0 (k_B J_m)^2 k_l \alpha V 2\tau f_1 \cdot \{C_w [\lambda_0 (\cos\lambda_0\delta \text{ch}\lambda_0\delta - \sin\lambda_0\delta \text{sh}\lambda_0\delta) + \alpha \cos\lambda_0\delta \text{sh}\lambda_0\delta] - C_a [\lambda_0 (\sin\lambda_0\delta \text{sh}\lambda_0\delta + \cos\lambda_0\delta \text{ch}\lambda_0\delta) + \alpha \sin\lambda_0\delta \text{ch}\lambda_0\delta]\}, \quad (23)$$

$$Q_{EMw} = \mu_0 (k_b J_m)^2 k_l \alpha V 2\tau f_1 \cdot \{C_w [\lambda_0 (\cos \lambda_0 \delta \operatorname{ch} \lambda_0 \delta + \sin \lambda_0 \delta \operatorname{sh} \lambda_0 \delta) + \alpha \sin \lambda_0 \delta \operatorname{ch} \lambda_0 \delta] + C_a [\lambda_0 (\cos \lambda_0 \delta \operatorname{ch} \lambda_0 \delta - \sin \lambda_0 \delta \operatorname{sh} \lambda_0 \delta) + \alpha \cos \lambda_0 \delta \operatorname{sh} \lambda_0 \delta]\}, \quad (24)$$

$$F_x = \mu_0 (k_b J_m)^2 k_l \alpha V \cdot \{C_w [\lambda_0 (\cos \lambda_0 \delta \operatorname{ch} \lambda_0 \delta - \sin \lambda_0 \delta \operatorname{sh} \lambda_0 \delta) + \alpha \cos \lambda_0 \delta \operatorname{sh} \lambda_0 \delta] - C_a [\lambda_0 (\cos \lambda_0 \delta \operatorname{ch} \lambda_0 \delta + \sin \lambda_0 \delta \operatorname{sh} \lambda_0 \delta) + \alpha \sin \lambda_0 \delta \operatorname{ch} \lambda_0 \delta]\}. \quad (25)$$

The factor k_b is in the formulas for the electromagnetic power and propulsive forces (20)–(25). We can find it from the condition that the formulas (12) and (22) should give the same value of propulsive forces, though we used different approaches to receive them. Obviously it fully applies to the formulas (13) and (25). Thus the coefficient k_b is determined by one of the equations

$$k_b^2 = \frac{\varepsilon (\alpha C_m)^2}{2 \operatorname{Re} [i \delta \dot{C} (\lambda \operatorname{ch} \lambda \delta + \alpha \operatorname{sh} \lambda \delta)]} \cdot \left[\frac{\lambda_m^2 + \alpha^2}{\lambda_a} \operatorname{sh} 2\lambda_a \delta + \frac{\lambda_m^2 - \alpha^2}{\lambda_w} \sin 2\lambda_w \delta + 2\alpha (\operatorname{ch} 2\lambda_a \delta - \cos 2\lambda_w \delta) \right] \quad (26)$$

at the arbitrary magnetic Reynolds numbers and

$$k_b^2 = \frac{\varepsilon \alpha^3 C_m^2 \left[\left(\frac{\varepsilon}{2} \right)^{1/2} \left(\operatorname{sh} 2\alpha \left(\frac{\varepsilon}{2} \right)^{1/2} \delta + \sin 2\alpha \left(\frac{\varepsilon}{2} \right)^{1/2} \delta \right) + \operatorname{ch} 2\alpha \left(\frac{\varepsilon}{2} \right)^{1/2} \delta - \cos 2\alpha \left(\frac{\varepsilon}{2} \right)^{1/2} \delta \right]}{\delta \{C_w [\lambda_0 (\cos \lambda_0 \delta \operatorname{ch} \lambda_0 \delta - \sin \lambda_0 \delta \operatorname{sh} \lambda_0 \delta) + \alpha \cos \lambda_0 \delta \operatorname{sh} \lambda_0 \delta] - C_a [\lambda_0 (\cos \lambda_0 \delta \operatorname{ch} \lambda_0 \delta + \sin \lambda_0 \delta \operatorname{sh} \lambda_0 \delta) + \alpha \sin \lambda_0 \delta \operatorname{ch} \lambda_0 \delta]\}} \quad (27)$$

at the large magnetic Reynolds numbers.

Let's consider the electromagnetic motor parameters.

If we assume that the secondary magnitudes are reduced to the primary circuit in the equations (14) then the T-shaped equivalent circuit (Fig. 5) corresponds to them. In the scheme x_{M1} is the main inductive reactance of the primary circuit; $x_{\sigma 1}$ is the inductive leakage resistance of the primary circuit ($x_{\sigma 1} = x_{11} - x_{r1}$); $x_{\sigma 2}$ is the leakage inductive resistance of the secondary circuit ($x_{\sigma 2} = x_{22} - x_{r1}$); r_1 and r_2 are the resistances of the circuits. All these parameters can be calculated by the usual methods for the theory of electrical machines, except for $x_{\sigma 2}$, and r_2 .

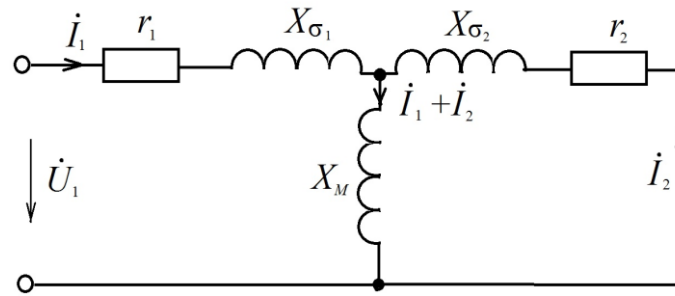


Fig. 5. The equivalent scheme

To calculate the main inductance x_{r1} we introduced the coefficient $k_l = \frac{l}{l_s}$ into the common equation for this parameter, where l is the capsule length, l_s is the stator length

$$x_{r1} = \frac{\pi\sqrt{2}f_1 w_1 k_{o\sigma} k_l \Phi_1}{I_1}.$$

Here f_1 is the frequency of the stator current; w_1 is the number of series-connected turns of the phase; Φ_1 is the magnetic flux per pole due to the stator current. In accordance with (11) we assume the peak of the magnetic induction of the primary field in the capsule equal to $B_1 = \mu_0 J_m k_B$, where J_m is given by the formula (1) and k_B is given by one of the formulas (26) or (27). Let's denote

$$k_B = \frac{\tau}{\pi\delta'}, \quad (28)$$

where δ' is some effective clearance. Then we can write

$$\Phi_1 = \frac{2}{\pi} \cdot \frac{\mu_0}{\delta'} \cdot 2\tau b \cdot \frac{m\sqrt{2}\varpi_1 k_{win} k_l}{\pi p} I_1,$$

where b is the capsule width. We have

$$x_{M1} = \frac{4\mu_0 f_1 2\tau b}{\pi\delta'} \cdot \frac{m(\varpi_1 k_{win})^2 k_l}{p}. \quad (29)$$

The calculation of the leakage field of a one-side stator is a separate task and needs some special consideration. Therefore let's limit by the approximate estimate of the corresponding parameter.

Let's define the total inductive reactance of the primary circuit x_{11} as the sum of two components: the inductive stator reactance x_{11}^0 due to the primary

field in the width of the inductor magnetic core and the inductive reactance x_{end} of the leakage field in the end parts

$$x_{11} = x_{11}^0 + x_{\pi}.$$

The component x_{11}^0 is the resistance of the whole stator winding calculated for the induction of the primary field on the stator surface. Therefore we receive the formula for x_{11}^0 from (29) supposing $\frac{\tau}{\pi\delta'} = 1$ and $k_l = 1$ in it

$$x_{11}^0 = 4\mu_0 f_1 \cdot 2b \cdot \frac{m(\varpi_1 k_{\text{win}})^2}{p}.$$

We shall find the inductive reactance x_{end} of the end part

$$x_{\pi} = 4\pi\mu_0 f_1 \varpi_1^2 \frac{0,175 - \frac{0,3\delta'}{\tau}}{p} (l_{\pi} - 0,64\tau),$$

where δ' is defined by the formula (29); l_{end} is the average length of the end part of one side of the stator.

Thus we can calculate the approximate value of the inductive leakage reactance of the primary circuit $x_{\sigma 1}$ by the formula

$$x_{\sigma 1} = 4\mu_0 f_1 \cdot 2b \cdot \frac{m(\varpi_1 k_{o\delta})^2}{p} \left(1 - \frac{\tau k_l}{\pi\delta'} \right) + x_{\pi}.$$

Here according to (28) $k_B = \frac{\tau}{\pi\delta'}$ but $k_B < 1$; in addition k_l is a small value as the capsule length is usually significantly less than the stator length. Therefore we should expect that the inductive leakage reactance of the primary circuit $x_{\sigma 1}$ will be considerably bigger than the main inductive reactance of the same circuit. It determines the low energy efficiency and the low power factor of the motor. To improve them it's necessary to divide the stator into separate electrically independent sections.

We obtained the calculation formulas (17), (21), (23) and (25) for the insertion resistances r_{ins} and x_{ins} . Knowing these parameters and having in mind that $x_{12} = x_{M1}$, we can find the secondary parameters using the equations (16)

$$r_2 = \frac{x_{\Gamma 1}^2 r_B}{r_B^2 + x_B^2}, \quad x_{22} = -\frac{x_{\Gamma 1}^2 x_B}{r_B^2 + x_B^2}$$

and after the inductive leakage reactance $x_{2\sigma}$ of the secondary circuit

$$x_{2\sigma} = x_{22} - x_{\Gamma 1}.$$

When we calculate the electromagnetic motor parameters it will be useful the information resulting from the ratio which establishes the connection between the magnetic induction B_m of the resulting field in the capsule (at the slip s_m) and MMF of the stator winding. The fact is that with the specified maximum of the propulsive force F_m we can consider that the value of B_m is known. Thus we speak about the definition of MMS of the stator by the known value of B_m . We can take

$$B_m = \left| \dot{B}_{mz} \Big|_{z=0} \right| \cdot k_B,$$

where \dot{B}_{mz} is given by the formula (9). Therefore

$$B_m = k_B \cdot \left| 2\mu_0 \alpha \dot{C} (\lambda \text{ch} \lambda \delta + \alpha \text{sh} \lambda \delta) \right| J_m. \quad (41)$$

Now we can find the amplitude J_m of the current density in the current sheet simulating the stator winding. But $J_m = \frac{\pi}{\tau} F$, where F is MMF of the stator winding

$$F = \frac{m\sqrt{2}}{\pi} \cdot \frac{\varpi_1 k_{o6}}{p} I_1.$$

In conclusion we give the equations characterizing the energy performance of LIM. The input power of LIM is equal

$$\dot{S}_1 = P_{1a} + iQ_{1p} = m\dot{U}_1 I_1^*,$$

where the connection between \dot{U}_1 and \dot{I}_1 is given by the equation (15); the efficiency is equal

$$\eta = \frac{P_{EMa}}{P_{1a}},$$

the power factor is

$$\cos \varphi = \frac{P_{\text{la}}}{(P_{\text{la}}^2 + Q_{\text{lp}}^2)^{1/2}}.$$

Thus we receive the main relations characterizing the electromechanical processes in the LIM in the form convenient for computational studies.

CONCLUSION

1. The creation of a pipeline transport with a rarefied medium in the pipe will require to solve the complex engineering problems. It will give a powerful incentive to the further development of the transport industry in Russia.

2. The construction of the vacuum-levitating transport in Russia is reasonable and justified economically but only among the densely populated centers, i.e. mainly in the European part of Russia.

3. It is reasonable to use the lower pressure in the pipe (1.5–2 times in comparison with atmospheric pressure), i.e. to refuse the use of the technical vacuum. We can partially compensate the increase of the aerodynamic resistance by using the perforated covering of the capsule head part.

4. It is perspective to use a linear induction motor with the stator located on the pipe wall.

БИБЛИОГРАФИЧЕСКИЙ СПИСОК / REFERENCES

1. Патент РФ на полезную модель № 24670/ 20.08.02. Бюл. № 23. Ким К.К. Кузов головного вагона высокоскоростного поезда. Режим доступа: http://www1.fips.ru/fips_serv1/fips_servlet. Дата обращения: 04.07.2018. [Patent RUS №24670/ 20.08.02. Byul. №23. Kim KK. *Body of the head car of the high-speed train*. Available from: http://www1.fips.ru/fips_serv1/fips_servlet (In Russ.)].
2. Патент РФ на полезную модель № 147076/ 27.10.14. Бюл. № 30. Ким К.К., Титова Т.С. Трубопроводный транспорт. Режим доступа: http://www1.fips.ru/fips_serv1/fips_servlet. Дата обращения: 04.07.2018. [Patent RUS №147076/ 27.10.14. Byul. № 30. Kim KK, Titova TS. *Pipeline transport*. Available from: http://www1.fips.ru/fips_serv1/fips_servlet (In Russ.)].
3. Кузнецов А.А., Мешкова О.Б. Модернизация спектрального оборудования для диагностирования и ремонта подвижного состава // Транспорт Урала. – 2009. – № 2. – С. 86–90. [Kuznecov AA, Meshkova OB. Modernizaciya spektral'nogo oborudovaniya dlya diagnostirovaniya i remonta podvizhnogo sostava. *Transport Urala*. 2009;2:86–90. (In Russ.)].
4. Кузнецов А.А., Глазырин А.В. Оценка структурных параметров стали методом атомно-эмиссионной спектроскопии // Омский научный вестник. – 2012. – №3 (112). – С. 240–245. [Kuznecov AA, Glazyrin AV. Ocenka strukturnykh parametrov stali metodom atomno-ehmissionnoj spektroskopii. *Omskij nauchnyj vestnik*. 2012;3(112):240–245. (In Russ.)].

5. Кузнецов А.А. Комплексные методы диагностирования промышленных изделий и узлов подвижного состава средствами атомно-эмиссионной спектроскопии – М.: Спутник, 2005. – 198 с. [Kuznecov AA. Kompleksnyye metody diagnostirovaniya promyshlennyh izdelij i uzlov podvizhnogo sostava sredstvami atomno-ehmissionnoj spektroskopii. Moscow: Sputnik; 2005. 198 p. (In Russ.)].
6. Иванов С.Н., Забоин В.Н., Кулаков В.В., Романов В.В. Электродинамические характеристики твердощеточных систем для сверхпроводящих униполярных машин // Известия вузов. Электромеханика. – 1984. – № 4. – С. 54–57. [Ivanov SN, Zaboin VN, Kulakov VA, Romanov VV. Elektrodinamicheskie kharakteristiki tverdoshchetochnykh sistem dlya sverkhprovodyashchikh unipolyarnykh mashin. *Izvestia vuzov. Electromechanika*. 1984;4:54–57. (In Russ.)].
7. Иванов С.Н. Использование электромеханических преобразователей в качестве устройств электронагрева // Научно-технические ведомости СПбГТУ. Основной выпуск. – 2008. – № 3. – С. 246–252. [Ivanov SN. Using the heat-generating electromechanical converters as a heater. *The scientific and technical files of SPbGTU*. 2008;3:246–252. (In Russ.)].
8. Иванов С.Н., Пащенко Ф.Ф., Амосов О.С. Синтез системы управления электромеханического преобразователя // Датчики и системы. – 2006. – № 8. – С. 18–24. [Ivanov SN, Pashenko FF, Amosov OS. The synthesis of the control system of electromechanical converters. *Sensors & Systems*. 2006;8:18-24. (In Russ.)]
9. Иванов С.Н. Проектирование элементов электротехнических комплексов для систем отопления транспортного назначения // Известия Петербургского университета путей сообщения. – 2010. – Вып. 3. – С. 105–114. [Ivanov SN. The design of components of electrotechnical complexes for heating systems of the transport. *Proceeding of Petersburg Transport University*. 2010;3:105–114. (In Russ.)].
10. Иванов С.Н. Системы управления электротехническими устройствами для генерации тепловой энергии и транспортирования теплоносителя // Известия Петербургского университета путей сообщения. – 2010. – Вып. 3. – С. 249–257. [Ivanov S.N. The control systems of the electrotechnical devices for generating heat energy and transporting the heat-carrying agent. *Proceeding of Petersburg Transport University*. 2010;3:249–257. (In Russ.)].
11. Иванов С.Н., Еськова А.В., Уханов С.В. Информационное обеспечение доказательства адекватности математической модели электромеханического теплогенератора // Известия вузов. Северо-Кавказский регион. Технические науки. – 2008. – С. 77–79. [Ivanov SN, Eskova AV, Uhanov SV. Informacionnoe obespechenie dokazatelstva adekvatnosti matematicheskoy modeli ehlektromekhanicheskogo teplogeneratora. *Izvestiya VUZov. Severo-Kavkazskij region. Tekhnicheskie nauki*. 2008:77–79. (In Russ.)].
12. Амосов О.С., Амосова Л.Н., Иванов С.Н. Синтез оптимальных систем управления электромеханическим теплогенерирующим комплексом // Информатика и системы управления. – 2009. – №1 (19) – С. 73–83. [Amosov OS, Amosova LN, Ivanov SN. Sintez optimal'nyh sistem upravleniya ehlektromekhanicheskim teplogeneriruyushchim kompleksom. *Informatika i sistemy pravleniya*. 2009;1(19):73–83. (In Russ.)].
13. Иванов С.Н., Скрипилев А.А. Эффективность надежности электроэнергетических систем // Ученые записки КнАГТУ. – 2016. – № III-1 (27). – С. 20–26. [Ivanov SN, Skripilev AA. Ehffektivnost' nadezhnosti ehlektroehnergeticheskikh system. *Uchenye zapiski KnAGTU*. 2016;III-1(27):20–26. (In Russ.)].

14. Иванов С.Н. Эффективность электроэнергетического оборудования // XX Междунар. научно-техн. конф. «Приоритетные направления развития науки и технологии». – Тула, 2016. – С. 80–81. [Ivanov SN. Ehffektivnost ehnergeticheskogo oborudovaniya. XX Mezhdunar. nauchno-tekhn. konf. “Prioritetnye napravleniya razvitiya nauki i tekhnologij”. (Conference proceedings) Tula, 2016. p. 80–81. (In Russ.)].
15. Есин П.А., Иванов С.Н., Шестоपालко Д.К. Эффективность применения композитных материалов в электротехнических установках // Ученые записки КнАГТУ. – 2017. – № III-1 (31). – С. 14–18. [Esin PA, Ivanov SN, Shestopalko DK. Ehffektivnost primeneniya kompozitnyh materialov v ehlektrotekhnicheskikh ustanovkakh. *Uchenye zapiski KnAGTU*. 2017;III-1(31):14–18. (In Russ.)].
16. Амосов О.С., Голоколос Д.А., Иванов С.Н., Со Х. Особенности проектирования электромеханических преобразователей для комплексных систем безопасности // Известия вузов. Электромеханика. – 2017. – Вып. 60. – №. 5 (197). – С. 5–11. [Amosov OS, Golokolos DA, Ivanov SN, Со H. Features of design of Electromechanical converters for integrated security systems. *Izvestia vuzov. Electromechanika*. 2017;60(5/197):5–11 (In Russ.)].

Information about the author:

Konstantin K. Kim, Doctor of Technical Sciences, Professor; address: 190031, St. Petersburg, Moscow av., 9;
eLibrary SPIN: 3278-4938; ORCID: 0000-0001-7282-4429;
E-mail: kimkk@mail.ru

Сведения об авторе:

Ким Константин Константинович, доктор технических наук, профессор; адрес: 190031, Санкт-Петербург, Московский пр., 9;
eLibrary SPIN: 3278-4938; ORCID: 0000-0001-7282-4429;
E-mail: kimkk@mail.ru

Цитировать:

Ким К.К. Российский вариант транспортной системы «Hyperloop» // Транспортные системы и технологии. – 2018. – Т. 4. – № 2. – С. 73–91. doi: 10.17816/transsyst20184273-91

To cite this article:

Kim KK. The Russian Version of the Transport System “Hyperloop”. *Transportation Systems and Technology*. 2018;4(2):73–91. doi: 10.17816/transsyst20184273-91



DOI 10.17816/transsyst20184292-106

© D. Zhou^{1,2}, P. Yu¹, J. Li¹, P. Cui¹, M. Song¹

¹ National University of Defense Technology
(Changsha, China)

² State Key Laboratory of Functional Materials for Informatics
Shanghai Institute of Microsystem and Information Technology
Chinese Academy of Sciences
(Shanghai, China)

ADAPTIVE VIBRATION CONTROL OF THE ELECTROMAGNET- TRACK COUPLED HIGH FREQUENCY RESONANCE FOR AN URBAN MAGLEV SYSTEM

This paper is a study of the electromagnet-track coupled high frequency resonance that frequently occurs in the urban maglev systems, it includes the following points:

Aim: The purpose of this study is to investigate the principle underlying the high frequency resonance occurs between the maglev train and the track, and to develop an appropriate vibration control algorithm which can be applied in the levitation controller, such that the resonance can be eliminated when the maglev train travels along the track.

Methods: In this paper, the model of the electromagnet-track coupled system is firstly established, in which some special cases, which correspond to the situations when the screws that fasten the F-rail to the sleepers are fatigue, or the stiffness of the rubber plates beneath the sleepers weaken for temperature reasons, are studied; and the reason that leads to the coupled resonance are explained as well. Secondly, an adaptive vibration control algorithm, which consists of a vibration observer and a tunable adaptive filter, is designed to suppress the high frequency electromagnet-track coupled resonance.

Results: Using this algorithm, when the train arrives at the spots where the coupled resonance may occur, the vibration observer will detect the occurring of the vibration and estimates its frequency, and then activate the adaptive filter and tune it to absorb the vibration.

Conclusion: The test indicates that this algorithm is capable of tuning itself to handle the unpredictable coupled resonance that occurs along the track, and it is simple and can be easily integrated into the levitation control code in a digital levitation control system.

Keywords: Vibration, Resonance, Track, Control, Adaptive, Urban maglev.

INTRODUCTION

On December 30th, 2017, the Beijing S1 urban maglev line began its commercial operation after years of argument and construction ever since 2011. Earlier in May, 2016, the first low speed urban maglev line in China – the Changsha Maglev Express, began to operate. The successful operation of these two maglev lines in China, together with the commercial maglev lines in Japan and Korea, indicate that the low speed urban maglev technology is tending to be mature, and its spread around the world is predictable.

However, as the development of test lines and the construction of commercial lines around China, more and more problems that related to the levitation control system of the train have been discovered. For example, the stability of the levitation control system under special track conditions, the reliability of the maglev controller, and the sensors under severe circumstances during the operation, etc. Another common problem for the urban maglev system may have been encountered – the vehicle-guideway coupled resonance (or coupled self-excited vibration in some literature). The coupled resonance occurs between the levitation control system and the track (or girder) when the track conditions are poor or the levitation control system is not well tuned. It is reported that the coupled resonance problem might be a fatal problem if it occurs on some light-weighted girders and cannot be well solved [1].

The maglev vehicle-guideway coupled resonance problem can be further divided into two major categories: the vehicle-girder coupled self-excited vibration, and the electromagnet-track coupled resonance. The former generally occurs on an elevated girder when the train is suspending in a standstill. It appears that the girder begins to vibrate and it can be clearly felt inside the train. The frequency of the girder vibration is generally below 30 Hz, which is determined by the natural frequency of the girder, but the energy of the vibration is large enough to cause levitation failure or even damages to the system structures. These problem has been noticed and discussed by Zhou et al.[2] The electromagnet-track coupled resonance appears as the vibration of the steel rails when the electromagnet is suspending at some specified locations. It may appear not as severe as the vehicle-girder coupled self-excited vibration, but the frequency is generally above 50 Hz, thus it can be clearly heard by passengers onboard the train or people inside the rooms beneath the tracks. To meet the requirements of the commercial line, such as the Beijing S1 maglev line, the electromagnet-track coupled high frequency resonance must be solved, and it is also the major problem to be discussed in this paper.

The electromagnet-track coupled resonance problem has also been noticed by Zhou et al., as discussed in [3–5], in which several methods to eliminate the coupled resonance has been tried. For example, in [3], an LMS cancellation algorithm has been proposed to generate a signal which is negative to the vibratory component mixed in the closed loop of the levitation control system, and different method for producing reference signals for the LMS algorithm have been proposed in these literature. In [5], the amplitude and frequency of the high frequency resonance can even be precisely computed, which agrees quite well to experiments. More detailed and comprehensive discusses of the coupled vibration problems can be found in the dissertation of Zhou [6]. In this paper, considering that the track conditions may differ as the train travels at different segments of the commercial line, and the amplitude, as well as the frequency, may vary as the train travels; therefore, a more reliable and robust method to eliminate the track-induced high frequency resonance needs to be developed. In

this paper, the principle of the high frequency resonance is firstly introduced; and based on this theory, a new vibration control structure, which consists of a vibration observer and a tunable adaptive FIR (finite impulse response) filter, is designed to suppress the electromagnet-track coupled resonance. This adaptive structure can tune itself to cancel the vibration when the high frequency resonance tends to appear, and it is suitable to work while the train is traveling along the maglev lines.

MODELING OF THE ELECTROMAGNET-TRACK COUPLED SYSTEM

During the test runs of the maglev trains, it is discovered that the electromagnet-track coupled high frequency resonance always occurs at the locations where the screws which fasten the F-rail to the sleepers are fatigue or slack; another case occurs when the stiffness of the rubber plates beneath the sleepers are weakened for some reasons like temperature. Here, a model with a not well supported track is discussed, as shown in Fig. 1. The latter case mentioned above may also be characterized as a weakly supported track.

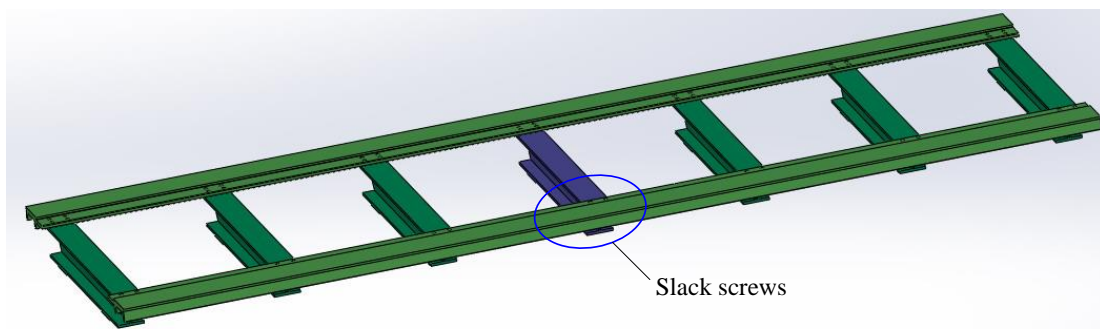


Fig. 1. A track model with slack screws connecting a sleeper and the rail

For the low speed maglev tracks, the rail is long and slim, thus it can be deemed as an Euler-Bernoulli beam with multiple supporters. A simplified model of the rail in each side of a track is shown in Fig. 2, in which each supporter is modeled as a combination of a linear spring and a torsal spring. The linear spring corresponds to the flexibility brought by the sleeper and the rubber plate beneath the sleeper; while the torsal spring characterizes the torsal rigidity of the sleeper since the rail are mounted to each sleeper by four hexagon socket screws. However, when the four screws are loose or fatigue, the stiffness of these springs will decrease or even disappear, leading to a weakly supported beam (say, the k -th support shown in Fig. 2). Fig. 2 also demonstrates the relative position of an electromagnet beneath the rail.

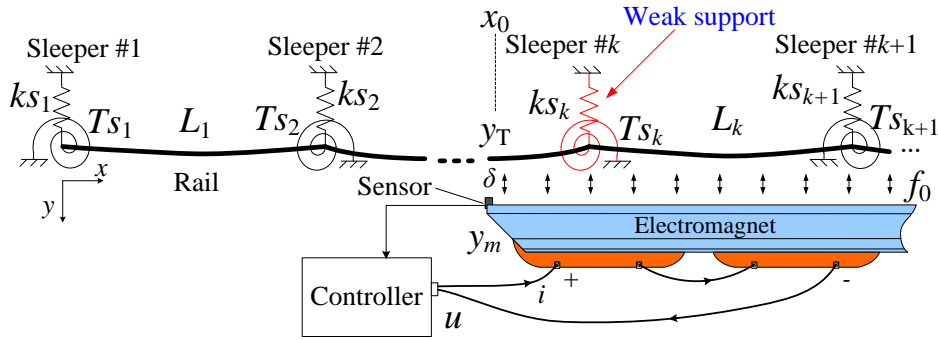


Fig. 2. Simplified model of the rail with multiple supporters

In Fig. 2, suppose that E , I , and ρ are the Young's modulus of the track material, the moment of inertia of the track cross section, and the mass per unit length of the track, respectively; ks_n and TS_n represent the equivalent stiffness of these two springs at the n -th sleeper, respectively; and L_n is the span length of the n -th span. Then, for the Euler-Bernoulli beam, the vertical displacement of the rail, $y(x,t)$, satisfies:

$$EI \frac{\partial^4 y(x,t)}{\partial x^4} + \rho \frac{\partial^2 y(x,t)}{\partial t^2} = f(x,t) \quad (1)$$

where $f(x,t)$ is the electromagnetic force distributed on the rail. Note that for the urban maglev system, $f(x,t)$ can be regarded as a evenly distributed force. Firstly consider the free vibration of the beam, and temporarily set $f(x,t) = 0$. Suppose that the free vibration of the beam can be expressed as $y(x,t) = \phi(x)\sin\omega t$, then according to Eq.(1), we have

$$\frac{EI}{\rho} \frac{\partial^4 \phi(x)}{\partial x^4} - \omega^2 \phi(x) = 0 \quad (2)$$

Eq. (2) indicates that the form of the solution for the mode shape, $\phi(x)$, can be described as a combination of trigonometric and exponential functions, thus for the n -th span of the beam, it can be written as:

$$\phi_{(n)}(x) = C_{n1} \sin(\lambda x) + C_{n2} \cos(\lambda x) + C_{n3} \text{sh}(\lambda x) + C_{n4} \text{ch}(\lambda x) \quad (3)$$

where λ is the spatial frequency. Substituting Eq. (3) into Eq. (2), yields:

$$\omega^2 = EI \lambda^4 / \rho \quad (4)$$

Referring to Fig. 2, it can be seen that for the N -th span beam, due to the effects of the springs, the bending moment and the shear force of the beam at the left terminal of the rail satisfy the following two equations, respectively:

$$EI \frac{\partial^2 \phi_{(1)}(0)}{\partial x^2} = TS_1 \frac{\partial \phi_{(1)}(0)}{\partial x} \quad (5)$$

$$EI \frac{\partial^3 \phi_{(1)}(0)}{\partial x^3} = -ks_1 \phi_{(1)}(0) \quad (6)$$

For the intermediate supports, the balance equations for the bending moment and the shear force of the beam can be expressed as follows:

$$EI \frac{\partial^3 \phi_{(n)}(x)}{\partial x^3} \Big|_{x=L_n} = ks_{n+1} \phi_{(n)}(x) \Big|_{x=L_n} + EI \frac{\partial^3 \phi_{(n+1)}(x)}{\partial x^3} \Big|_{x=0} \quad (7)$$

$$EI \frac{\partial^2 \phi_{(n)}(x)}{\partial x^2} \Big|_{x=L_n} = -Ts_{n+1} \frac{\partial \phi_{(n+1)}(x)}{\partial x} \Big|_{x=0} + EI \frac{\partial^2 \phi_{(n+1)}(x)}{\partial x^2} \Big|_{x=0} \quad (8)$$

At the right terminal, the bending moment and the shear force of the beam satisfy:

$$EI \frac{\partial^2 \phi_{(N)}(x)}{\partial x^2} \Big|_{x=L_N} = -Ts_{N+1} \frac{\partial \phi_{(N)}(x)}{\partial x} \Big|_{x=L_N} \quad (9)$$

$$EI \frac{\partial^3 \phi_{(N)}(x)}{\partial x^3} \Big|_{x=L_N} = ks_{N+1} \phi_{(N)}(x) \Big|_{x=L_N} \quad (10)$$

Note that the continuities of the displacement and slope of the beam at the intermediate supports require

$$\phi_{(n)}(L_n) = \phi_{(n+1)}(0) \quad (11)$$

$$\phi'_{(n)}(L_n) = \phi'_{(n+1)}(0). \quad (12)$$

Combing Eqs. (5)–(12) together, there will be totally $4 \times N$ equations, and they can be written in a matrix form:

$$\mathbf{A}_m \mathbf{C} = 0 \quad (13)$$

where \mathbf{A}_m is a $4N \times 4N$ matrix, and \mathbf{C} is the coefficients of the mode shapes described by Eq. (3), namely, $\mathbf{C} = [C_{11}, C_{12}, C_{13}, \dots, C_{N3}, C_{N4}]^T$. By solving Eq. (13), the unknown coefficients, as well as the spatial frequency of the beam, λ , can be obtained.

The solution of Eq. (1) can be described as a combination of all the modal shapes obtained above, namely:

$$y(x, t) = \sum_{k=1}^{\infty} q_k(t) \phi_k(x) \quad (14)$$

Here, $y_k(t)$ is the generalized displacement of the k -th order mode. Substituting Eq. (14) into Eq. (1), multiplying both sides of the resultant equation by $\phi_k(x)$, and integrating both sides along the beam, noticing the mode orthogonality condition for linear beams [7], one obtains

$$\ddot{q}_k(t) + \omega_k^2 q_k(t) = \frac{F_k(t)}{M_k} \quad (15)$$

where $M_k = \rho \int_0^L \phi_k^2(x) dx$, $F_k(t) = \int_0^L f(x, t) \phi_k(x) dx$, and $L = \sum_{k=1}^N L_k$.

Using the Laplace Transform, Eq. (15) can be rewritten as

$$q_k(s) = \frac{F_k(s)}{(s^2 + \omega_k^2)M_k} \quad (16)$$

Therefore, the vertical displacement of the beam at a specified location, x_0 , can be given by

$$y_k(x_0, s) = \frac{F_k(s)\phi_k(x_0)}{(s^2 + \omega_k^2)M_k} \quad (17)$$

For the electromagnetic force, $f(x, t) = F_m(t)/l_0$, where $F_m(t)$ is the total electromagnetic force produced by the coil pair, and l_0 is the length that the electromagnetic force covers. According to Fig. 2, it can be seen that

$$F_k(s) = \frac{F_m(s)}{l_0} \begin{cases} \int_{x_0}^{x_0+l_0} \phi_k(x) dx, & \text{if } x_0 + l_0 \leq L \\ \int_{x_0}^L \phi_k(x) dx, & \text{if } x_0 + l_0 > L \end{cases} \quad (18)$$

Therefore, Eq.(17) can be rewritten as another form:

$$y_k(x_0, s) = \frac{F_m(s)g_k(x_0)}{(s^2 + \omega_k^2)} \quad (19)$$

Here, $g_k(x_0)$ can be deemed as the k -th order mode gain of the beam, which is a coefficient that reflects the deformation response of the beam at x_0 when the beam is subjected to a unit force, F_m . The larger $g_k(x_0)$ is, the larger will be the displacement of the rail at x_0 . As a demonstration, for the Beijing S1 low speed urban maglev system, $l_0 = 1.32$ m, $L_n = 1.2$ m, $\rho = 130$ kg/m, $EI = 1.93 \times 10^6$ N m² (the last two parameters of are obtained by calculation); the stiffness of the linear and torsal springs are supposed to be: $ks_n = 1 \times 10^8$ N/m, and $Ts_n = 7 \times 10^{10}$ Nm/rad. For the strongly supported rail, all the sleepers are well fastened to the rail, thus the parameters for all the springs are identical with each other. Using the procedure presented above, the first three order mode shapes can be computed, as shown in Fig. 3, and their corresponding mode frequencies are 122.2 Hz, 129.3 Hz, and 141.5 Hz, respectively. This result is rather close to finite element analysis. Meanwhile, the mode gains for these three vibration modes can be obtained as well, which are shown in Fig. 4.

As a comparison, consider the case when the screws of one sleeper slack. Specifically, suppose that the weak support appears at the middle sleeper (see Fig. 1). In this case, the stiffness of the linear spring and the torsal spring will be prominently weakened, which are supposed to be 1/10 of the stiffness of other well fastened supports. The resultant vibration mode shapes as well as mode gains of the weakly supported rail can be computed, as shown in Fig. 5 and Fig. 6, respectively. Comparing Fig. 5 with Fig. 3, it can be seen that, due to the decrease of support stiffness in the middle of the rail, the shape of the first order mode shape changes dramatically – the displacement of the rail in the middle is more obvious than at other supports, which indicates that when the train moves

here, the rail displacement will significantly increase. Also, Fig. 6 shows a prominent increase of mode gain at the middle for the first order vibration mode. According to Eq. (19), this suggests that the vertical response of the rail at the middle will be larger than at other locations when the train passes the rail. This is a fundamental reason that leads to electromagnet-track coupled resonance when the track support weakens.

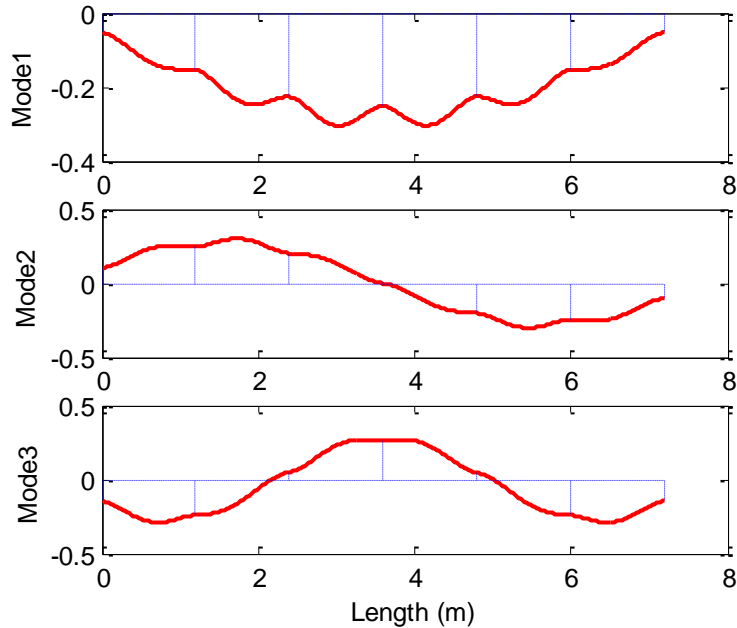


Fig. 3. The first three order mode shapes of the well-supported rail

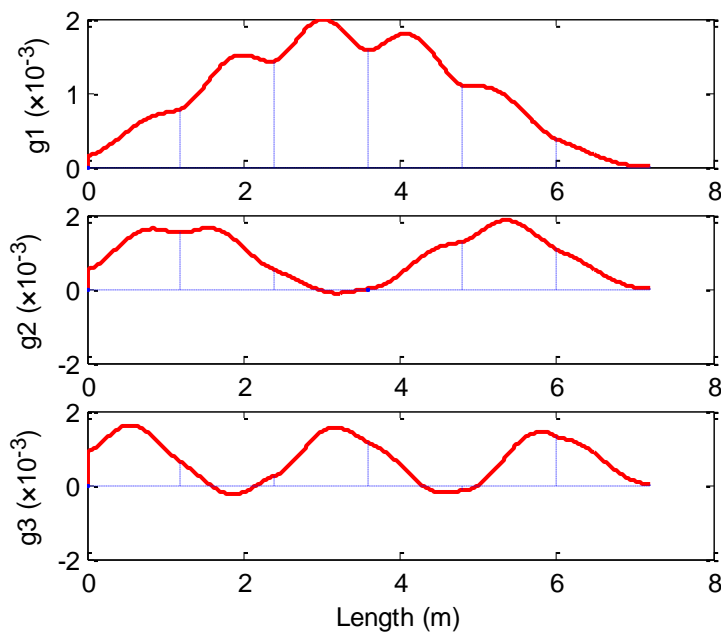


Fig. 4. Mode gains for the first three order vibration modes of the well-supported rail

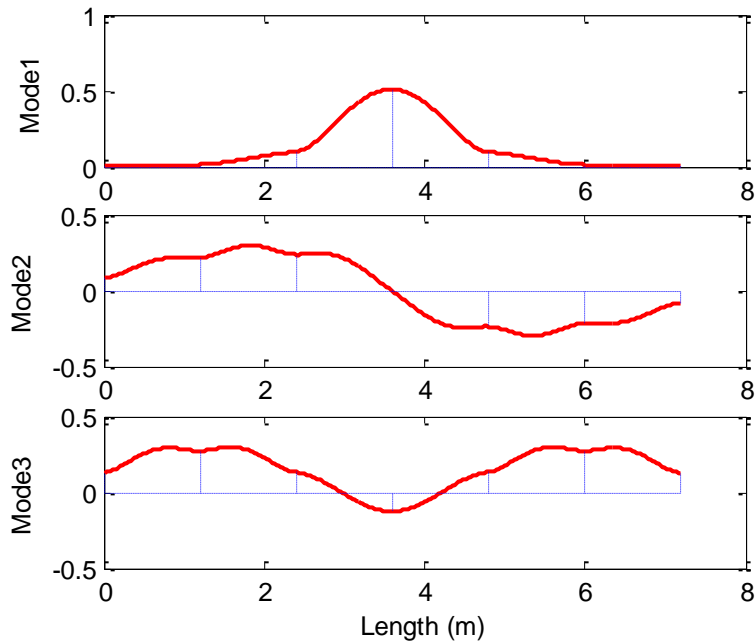


Fig. 5. The first three order mode shapes of the well-supported rail

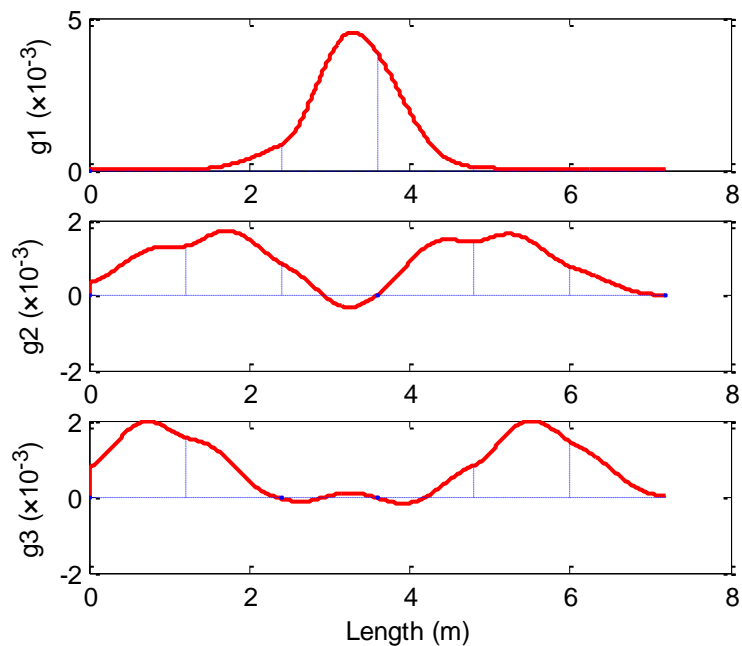


Fig. 6. The first three order mode shapes of the weakly-supported rail

Another significant change as a result of different rail support conditions is the mode frequency. For comparison, the mode frequencies, as well as mode gains when $x_0 = 3.3$ m, for these two cases are listed in Table 1. It can be seen that the fundamental mode frequency drops significantly as the middle support becomes weak, while the other two higher mode frequencies only decrease a bit. This is another reason why the coupled resonance tends to occur when the rail is

not well supported, since the lower the mode frequency is, the higher is the open loop gain, as is analyzed by Zhou et al. [2–6].

Table 1. Mode frequencies and mode gains for the normal and the weakly supported rail

Mode order	Mode frequency (Hz)		Mode gain ($\times 10^{-3}$)	
	Normal rail	Weak rail	Normal rail	Weak rail
1	122.2	76.4	1.82	4.53
2	129.3	126.1	-0.10	-0.31
3	141.5	133.2	1.51	0.10

For the levitation control system shown in Fig. 2, the levitation gap δ , which is the vertical distance between the electromagnet and the track measured by the gap sensor, can be described as

$$\delta(t) = y_m(t) - y_T(t) \quad (20)$$

where y_m is the vertical displacement of the electromagnet, y_T is the vertical deformation of the track at x_0 , which can be obtained by the superposition of all vibration modes using Eq. (14). To keep the levitation gap at a desired value, say, z_0 , a controller is needed to eliminate the levitation gap error. The PID cascade controller, which has been employed in [8], is also adopted here, which gives

$$i_e(t) = k_p [\delta(t) - z_0] + k_d \dot{y}_m(t) + k_i \int_0^t [\delta(\tau) - z_0] d\tau \quad (21)$$

where i_e is the desired current through the electromagnet coil. To achieve rapid response of the current, a current loop is utilized, and the control voltage is given by

$$u(t) = k_c [i_e(t) - i(t)] \quad (22)$$

Here, k_p , k_d , k_i , and k_c are constants which can be chosen to achieve desired dynamic performance of the control system. The current through the electromagnet coil satisfies [3]:

$$\frac{u(t)}{2} = i(t)R + \frac{\mu_0 AN_c^2}{2\delta(t)} \dot{i}(t) - \frac{\mu_0 AN_c^2 i(t)}{2\delta^2(t)} \dot{\delta}(t) \quad (23)$$

Here, A is the area of the electromagnetic pole, μ_0 is the space permeability, R is the resistance of the electromagnet coil, and N_c is the number of turns of the coil. The electro-magnetic force of a levitation unit is:

$$F_m(t) = \frac{\mu_0 AN_c^2}{2} \left(\frac{i(t)}{\delta(t)} \right)^2 \quad (24)$$

The vertical movement of the electromagnet can be described by:

$$m_1 \frac{d^2 y_m(t)}{dt^2} = -F_m(t) + m_1 g \quad (25)$$

in which m_1 is the equivalent mass of the levitation payload. Detailed discussion of the stability of the electromagnet-track coupled system has been presented in

previous published literature [3–5], which will not be repeated in this paper. Instead, as a demonstration, the stability of the coupled system discussed here will be investigated through numerical simulations. For example, if the parameters of the control system are chosen according to Table 2, and suppose that the track is well supported, the responses of the levitation gap and the displacement of the track can be obtained, which are shown in Fig. 7. It can be seen from Fig. 7(a) that, under the chosen parameters, the over-damped transient response of the levitation gap reflects a good performance of the levitation controller; more importantly, in this case, the vibratory response of the track tends to disappear, as shown in Fig. 7(b). This is a desired performance for a commercial maglev system.

Table 2. Parameters of the levitation control system

Parameter	Value	Parameter	Value
k_p	4000	m_1	820 kg
k_d	100	μ_0	$4\pi \times 10^{-7}$ H/m
k_i	0.01	A	0.01848 m^2
k_c	100	N_c	360
l_0	1.32 m	R	0.5 Ohm

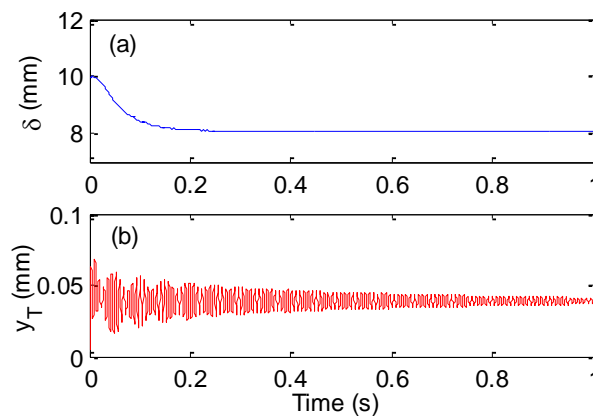


Fig. 7. Responses of the levitation gap and the displacement of the track under the well supported track

However, for the weakly supported track shown in Fig. 1, the fundamental frequency of the track drops dramatically, which greatly changes the stability of the electromagnet-track coupled system. Under the same parameters, the responses of the levitation gap and the track are shown in Fig. 8. Compared with Fig. 7, it is obvious that the electromagnet-track coupled system becomes unstable, and high frequency coupled resonance occurs. As the amplitude of the vibration grows, the noise arise which can be clearly heard by passengers aboard the train. This case has been encountered in the Tangshan low speed maglev test line, and it should be eliminated to prevent potential damage to track infrastructures.

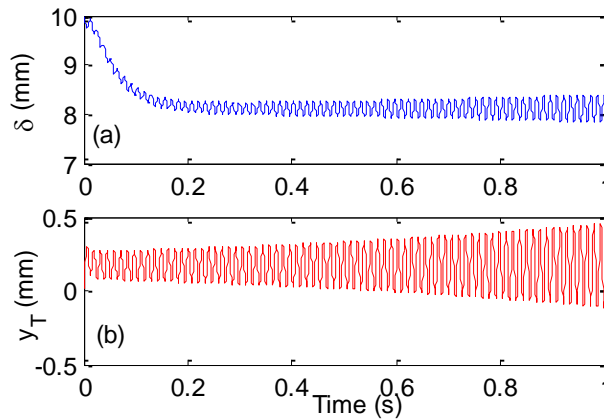


Fig. 8. Responses of the levitation gap and the displacement of the track under the weakly supported track

ADAPTIVE VIBRATION CONTROL SCHEME FOR THE ELECTROMAGNET-TRACK COUPLED SYSTEM

The self-excited vibration caused by weakly supported tracks seems inevitable for a practical maglev track since the fatigue or slack of screws may be unavoidable as a result of seasonal thermal expansions and contractions, as well as ground settlement. To eliminate the encountered self-excited vibration while the train is traveling, some special aspects should be taken into account: first, the frequency of the self-excited vibration is not a constant, but is variable due to the support conditions; second, the response of the vibration control scheme should be as rapid as possible; third, the vibration control scheme should not disturb the stability of the levitation controller, or at least it should not distinctly decrease the performance of the levitation control system.

Based on these considerations, an adaptive vibration control scheme, which is capable of tuning its parameters to cope with different track situations, is essential. Here, an adaptive vibration controller is proposed, as shown in Fig. 9. The block "CTL" represents the levitation controller which was described by Eqs. (20 – 22), "MAG" is the electromagnet whose output includes the current and the electromagnetic force; "H(s)" is the transfer function of the track. The mechanism inside the dashed box is the designed adaptive vibration controller which includes two major parts: the frequency estimator which was designated by a block "FE", and the adaptive FIR filter with an adaptive tuning mechanism, "ADJ". The basic idea of this scheme can be generalized as follows: as the self-excited vibration occurs, the vibratory component mixed in the expected current, i_{e0} , will exceed a certain value, and its frequency can then be estimated by the observer "FE"; a reference signal x , which is a sinusoid whose frequency equals the estimated frequency, ω_r , is generated for the FIR queue, \mathbf{X} . The output of the FIR filter, y_f , is then subtracted from i_{e0} , aiming to cancel the vibratory components in i_{e0} . To achieve precise cancellation, the weights of the

FIR filter, W , are adjusted by the adaptive mechanism ADJ, using the Least Mean Square (LMS) algorithm. If well tuned, the output of the cancellation, i_e , will not contain vibratory component, which indicates that the electromagnetic force, F_m , will not include vibratory excitation, either. Then, it can be inferred that the vibratory energy of the track will be dissipated as time elapses, and the self-excited vibration can thus be eliminated.

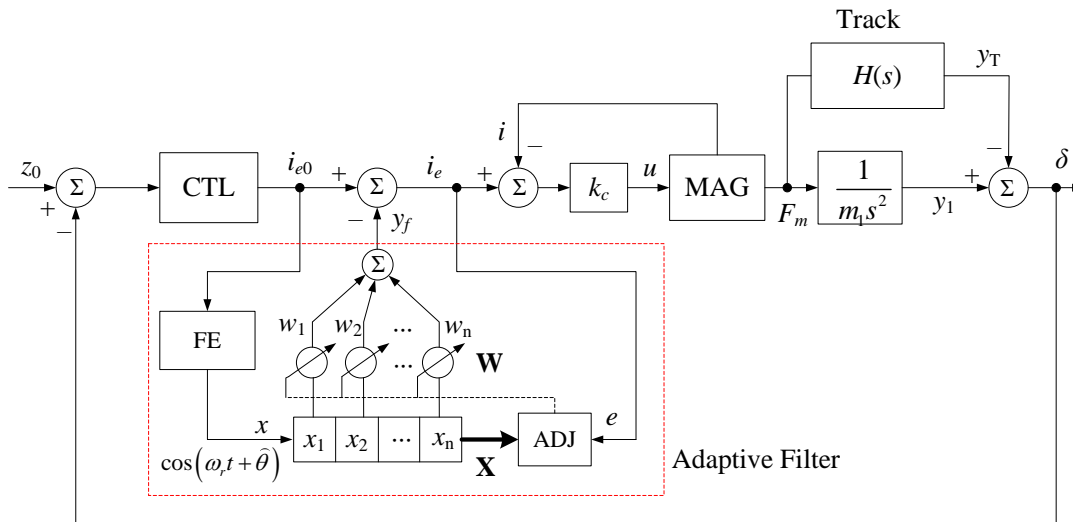


Fig. 9. Adaptive vibration control scheme combined with the maglev control system

From Fig. 9, it can be seen that

$$y_f = \mathbf{W}^T \mathbf{X} \quad (26)$$

$$i_e = i_{e0} - y_f \quad (27)$$

The purpose of the FIR filter is to produce a cancellation signal which is capable of eliminating the vibratory signal included in i_{e0} , thus its weights need to be tuned timely. The LMS algorithm is adopted here, and the weights of the FIR filter are updated according to the following rules:

$$w_n(k+1) = (1 - \alpha \mu_1) w_n(k) + 2\mu_1 e x_n(k) \quad (28)$$

where μ_1 is the convergence coefficient of the LMS algorithm, e is the cancellation error of the vibratory component in i_e , and α is a leakage coefficient that ameliorates the potential overflows of the weights caused by the accumulation of quantization errors.

To provide the FIR filter with a correct reference signal, a frequency estimator, FE, is utilized. Here, the frequency estimator developed by Regalia [9] is adopted here. This algorithm has been adopted by some other researchers, as in [10], which can be written as:

$$\begin{cases} \dot{x}_1 = x_2 \\ \dot{x}_2 = -2\zeta\omega_r x_2 - \omega_r^2 x_1 + k u_{hf} \\ \dot{\omega}_r = -g(k u_{hf} - 2\zeta\omega_r x_2) x_1 \end{cases} \quad (29)$$

where u_{hf} is the input of the estimator. However, Fig. 9 is only a demonstration of the basic principle of the adaptive vibration controller. In practice, more considerations are required to keep the adaptive FIR filter work properly. It can be noted that i_{e0} contains not only the vibratory component which is associated to the vibration of the track, but also the DC (direct current) component which produces a biased current to levitate the payload; the latter, however, would cause the error signal for the LMS algorithm, e , superimposed with a DC component, which would prevent the LMS algorithm from converging. To solve this problem, high pass filters, as well as a compensation method introduced in [4], may also be applied here. For simplicity, it is not repeated in this paper.

Fig. 10 shows the test result of this adaptive vibration control method. The simulation is undertaken when all the parameters of the levitation system are chosen following the example in the previous section. For comparison, the adaptive vibration controller (AVC) was disabled for the first two seconds. As discussed earlier, due to the weak support of the track, self-excited vibration occurs, and the amplitude of the vibration grows with time. Fig. 10(b) shows the result of the frequency estimation, from which it can be seen that as the amplitude of the vibration exceeds a small value (corresponding to 0.9s), the frequency estimator begin to work and the result converges to the actual vibration frequency, which is 77 Hz. Also, it can be seen from Fig. 10(c) that, the weights of the FIR filter are updated timely, and they are tuned in different manners as the reference frequency changes.

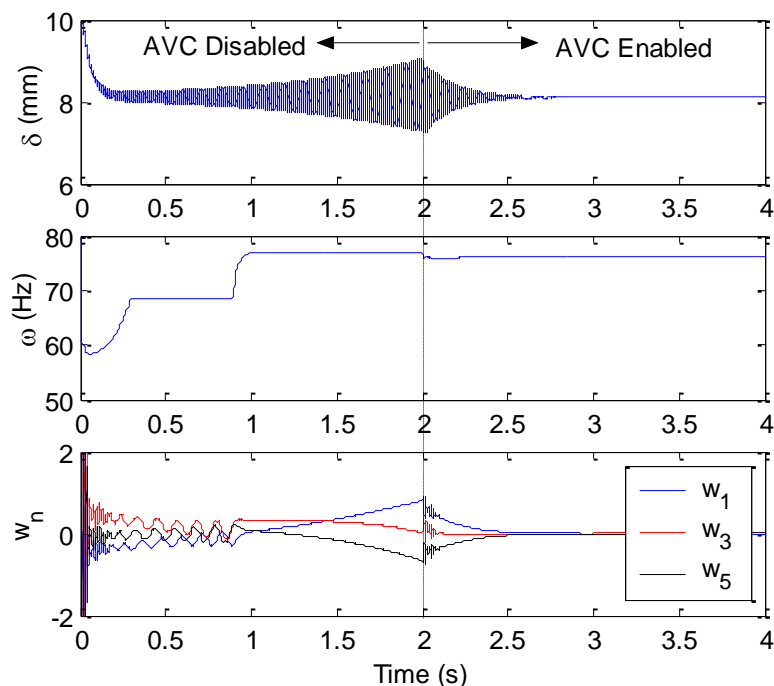


Fig. 10. Test result of the adaptive vibration control method. (a) the levitation gap; (b) estimated frequency; (c) selected weights of the adaptive FIR filter

Then, when time equals 2 s, the AVC is activated and the cancellation begins to take effect. It can be seen that the vibration begins to attenuate quickly afterwards. The weights of the adaptive filter also attenuate as the amplitude of the vibration decreases. The test result is satisfactory since the vibration of the result can be totally eliminated, and the electromagnet-track coupled system becomes stable.

CONCLUSION

In this paper, the principle of the track-induced coupled resonance problem in the urban maglev system is discussed. The major reason that leads to the electromagnet-track coupled vibration is analyzed, which reveals that the weak support of tracks may dramatically decrease the fundamental frequency of the track, whilst at the same time increase the mode gain of the fundamental vibration mode. These two factors destroy the conditions for the stability of the coupled system, leading to a self-excited vibration. Aiming to suppress the self-excited vibration when a maglev train travels, an adaptive vibration controller, which includes a frequency estimator used to observe the frequency, and an adaptive FIR filter which produces a cancellation signal to neutralize the vibratory component mixed in the control path, is presented. The LMS algorithm is employed to tune the weights of the FIR filter, which achieves a satisfactory performance of convergence. The test result indicates that the proposed adaptive vibration controller is capable of suppressing the electromagnet-track coupled resonance.

ACKNOWLEDGEMENT

This work was supported by the National Key Development Program of the 13th Five-year plan [grant number 2016YFB1200601-B12]; the Research Plan Program of National University of Defense Technology [grant number 2K16-02-02]; the Opening Foundation of the State Key Laboratory of Functional Materials for Informatics [grant number SKL-2017-07]; and National Nature and Science Foundation of China [grant number 11302252].

References

1. Zhou DF, Hansen CH, Li J, Chang WS. Review of coupled vibration problems in EMS maglev vehicles. *International Journal of Acoustics and Vibration*. 2010;15(1):10-23. doi: 10.20855/ijav.2010.15.1255
2. Zhou DF, Hansen CH, Li J. Suppression of maglev vehicle-girder self-excited vibration using a virtual tuned mass damper. *Journal of Sound and Vibration*. 2011;330:883-901. doi:10.1016/j.jsv.2010.09.018
3. Zhou DF, Li J, Hansen CH. Application of least mean square algorithm to suppression of maglev track-induced self-excited vibration. *Journal of Sound and*

- Vibration*. 2011;330:5791-5811. doi: 10.1016/j.jsv.2011.07.021
4. Zhou DF, Li J, Zhang K. An Adaptive Control Method to Suppress the Maglev Track-Induced Self-Excited Vibration. Proceedings of the 2011 International Conference on Consumer Electronics, Communications and Networks; 2011; Xian Ning, China. p. 4723–4727. doi: 10.1109/CECNET.2011.5768485
 5. Zhou DF, Li J, Zhang K. Amplitude control of the track-induced self-excited vibration for a maglev system. *ISA Transactions*. 2014; 53(5):1463–1469. doi: 10.1016/j.isatra.2013.12.016
 6. Zhou DF. *Research on Self-Excited Vibration Problems in EMS Maglev Vehicle-Guideway Coupled System* [dissertation]. Graduate School of National University of Defense Technology; 2011 (in Chinese).
 7. Svetlitsky VA. *Engineering Vibration Analysis (Worked Problems 2)*. Berlin: Springer-Verlag; 2004. doi: 10.1007/978-3-540-40970-0
 8. Zhou DF, Yu PC, Wang LC, Li J. An adaptive vibration control method to suppress the vibration of the maglev train caused by track irregularities. *Journal of Sound and Vibration*. 2017;408:331-350. doi: 10.1016/j.jsv.2017.07.037
 9. Regalia PA. An improved lattice-based adaptive IIR notch filter. *IEEE Trans. Signal Process.* 1991;39(9):2124-2128. doi: 10.1109/78.134453
 10. Bodson M, Douglas SC. Adaptive algorithms for the rejection of sinusoidal disturbances with unknown frequency. *Automatica*. 1997;33(12):2213-2221. doi: 10.1016/s0005-1098(97)00149-0

Information about the authors:

Danfeng Zhou, PhD, Lecturer; 109 Deya Road, National University of Defense Technology, Changsha, P.R. China.

ORCID: 0000-0001-5707-6530;

E-mail: zhoudanfeng@maglev.cn.

Peichang Yu, PhD, Lecturer;

E-mail: lofter@163.com.

Jie Li, PhD, Professor;

E-mail: lj@maglev.cn.

Peng Cui, PhD, Lecturer;

E-mail: cuipeng@maglev.cn.

Mengxiao Song, PhD, Student;

E-mail: songmengxiao14@nudt.edu.cn

To cite this article:

Zhou D, Yu P, Li J, et al. Adaptive Vibration Control of the Electromagnet-Track Coupled High Frequency Resonance for an Urban Maglev System. *Transportation Systems and Technology*. 2018;4(2):92-106. DOI: 10.17816/transsyst20184292-106

DOI 10.17816/transsyst201842107-119

© M. Cavagnaro¹, V. Delle Site²

¹Former Italian State Railway High Speed Direction Chief; currently, Rolling Stock and Railway System Consultant

²National Research Council of Italy
(Rome, Italy)

A NEW CONCEPT OF MODULAR MAGNETIC LEVITATION TRAIN FOR URBAN TRANSPORT

Aim: The aim of our project is to solve all technological and functional problems related to the development of the suspended urban Maglev, while maintaining the requirement of simplicity and low cost of construction, operation and maintenance. Both the infrastructure and the vehicle are designed to be industrially produced and assembled on site.

Methods: Our study is based on the theoretical and experimental results obtained during a project of the Italian National Research Council, concerning the performances of opposing permanent magnets, the design of the linear synchronous motor and the possible solutions for realizing the guidance system. On the basis of these results the study of the suspended system was carried out.

Results: The paper describes the suspended urban Maglev with PM/PM primary suspension (with opposing permanent magnets) and proposes a mechanical guidance system that uses for stabilization the same repulsive forces between permanent magnets. We also propose a new configuration with HTS/PM primary suspension (with high temperature superconductors opposed to permanent magnets), evaluating pros and cons of this solution. Finally we provide design data on the linear synchronous motor suitable for our system.

Conclusion: This paper describes our proposal for a suspended urban Maglev using permanent magnets; our interest focuses on the need to further develop industrially feasible solutions, easy to build and manage, in order to propose a system that is also commercially viable and competitive. The identified advantages justify further studies.

Keywords: Maglev, urban transport, suspended system, modular construction, cost saving.

INTRODUCTION

Despite promising prospects and many decades of research and development, all Maglev systems still face barriers to their success. However, Maglev technology has some very interesting features, especially for urban transport: the lack of contact between the vehicle and the track reduces maintenance costs; other important advantages are the distributed load, the reduced vehicle cross-section, the possibility of overcoming high slopes, the reduction of noise generated by train traffic. Therefore, the development of

Maglev systems must continue, but we need to focus on a new generation, custom-made solution for urban transport, characterized by simple construction, lightweight, low energy consumption, full automation, low cost of construction and operation.

Taking advantage of the improved performance of permanent magnets and building on the studies conducted over the past few years on the optimization of opposing magnets (including those conducted by the Italian National Research Council), an original solution of a suspended urban Maglev (where the vehicle is suspended under a fixed track) has been developed in order to meet these requirements of simplicity and low cost [1, 2, 3]. The first version of this system, already presented at the Maglev 2016 Conference in Berlin [4], adopted vehicle levitation and guidance systems based on repulsive forces between permanent magnets of specific shape and dimensions.

In this paper, we propose some solutions for realizing a reliable suspended Maglev system. We describe a mechanical driving control system for the low speed vehicles stabilization (for urban transport only) which levitate on opposing permanent magnets, and an updated version of the suspended Maglev layout, which adopts a primary suspension composed of high temperature superconductors and permanent magnets. Further technical measures are illustrated for ensuring the industrial feasibility and the competitiveness of this urban transport system.

THE SUSPENDED SYSTEM

Among all possible configurations of the system, we preferred to suspend the vehicle from above (Fig. 1), in order to concentrate the technological part (of the track and the vehicle) in a position that is not easily accessible. This solution allows the intrinsic protection of the magnets against tampering and makes the technological part very compact, also making switches design easier. Moreover, this choice leaves free space on the ground under the vehicle; no equipment is required on the ground along the path. In the case of an underground tunnel itinerary, the floor under the vehicle can be walked on and can be used as an escape route; consequently, free spaces at the sides of the route are not necessary. Vehicle end doors are emergency exits that can be used by passengers for escape.

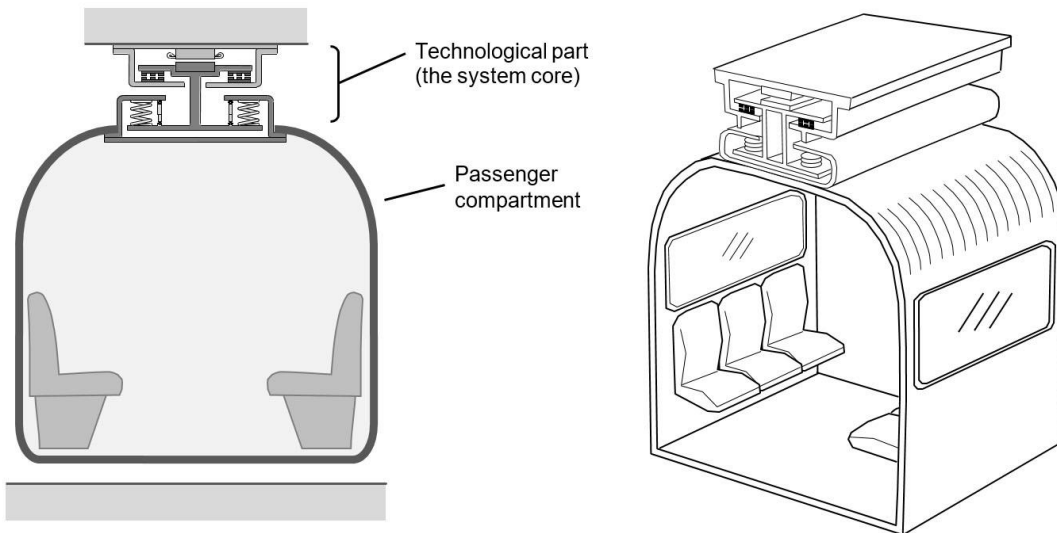
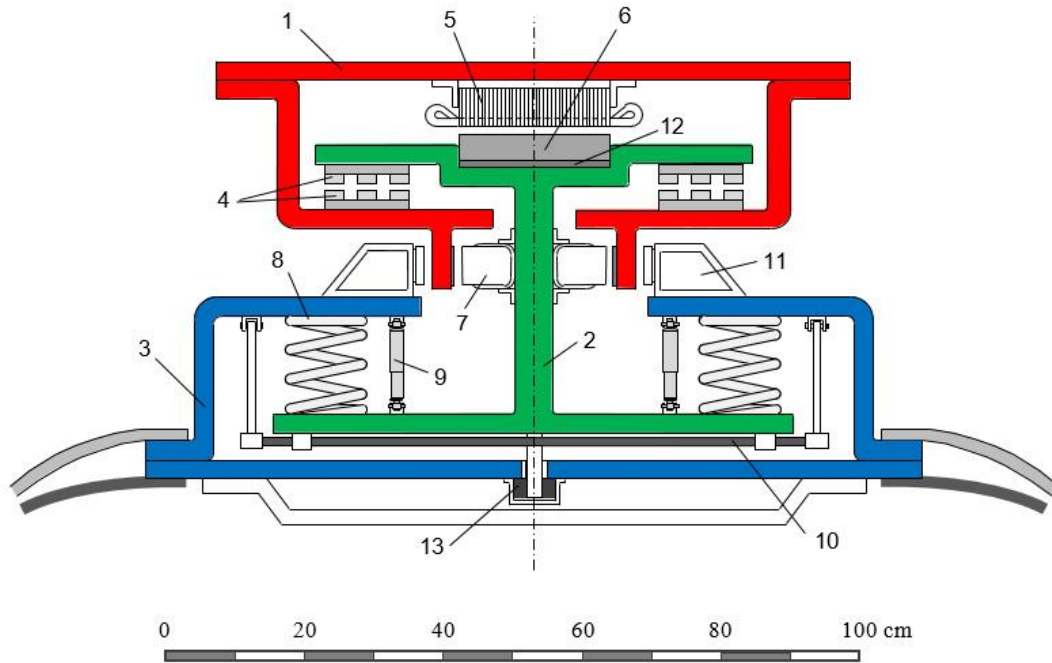


Fig. 1. The suspended Maglev configuration

Fig. 2 shows the solution chosen for the track (red) and the upper part of the vehicle: bogie (green), suspension and body frame (blue).

The track (red) consists of a metal box containing two beds of magnets laid on steel plates and the winding of the linear synchronous motor (LSM) for propulsion and braking. Outside the box, two iron guides ensure the reaction of the electromagnets (for stabilization) and the accidental contact of the anti-derailment skids. Track technology is very simple and feasible as an industrial product, divided into modules of lengths that best fit to production, transport and assembly on site.

The bogie (green) is an aluminum double-T beam (length 0.7 m). Each bogie rests on the track magnet beds through two opposing magnet plates (PM/PM primary suspension), fastened inside the upper wings of the double-T. The stabilization control device and the anti-derailment skids are placed on the vertical band of the double-T beam; they act on the track iron guide. The magnets of the LSM inductor are placed over the double-T. The elastic elements of the suspension, the bogie/vehicle connecting pin, two dampers and a torsion bar are fixed on the lower wings of the double-T beam.



1. Track box
2. Slipping bogie frame
3. Vehicle body frame
4. Primary suspension (permanent magnets)
5. LSM armature
6. LSM inductor
7. Stability control electromagnets
8. Secondary suspension springs
9. Shock absorbers
10. Torsion bar
11. Emergency brake and lateral end stop
12. Gap adjustment system
13. Bogie/vehicle connection

Fig. 2. The suspended Maglev system core - Solution A with PM/PM primary suspension

The body frame (blue) is an aluminum structure (length 1.6 m) that rests on two bogies by means of four springs (secondary suspensions). The body frames of the adjacent vehicle modules are coupled. Each body frame supports a traveler compartment (shell). The continuous support on the track facilitates not only the vehicle design (the bogie becomes almost continuous, each vehicle is a simple shell of very reduced length), but also that of the track supporting structures, because there is no concentrated load on them.

The passenger compartment. Each body frame supports a passenger compartment (shell). The shell dimensions are: length 1.6 m, width 2.2 m, height 2.2 m. The same 1.6 m long body frame can support three different shell types: the vehicle end module (with the escape doors), the module with access doors (door width 1.4 m) and the module with seats for passengers. Using these types of modules, different compositions of the convoy are possible.

The resulting train is similar to a flexible tube formed by the union of many modules. Fig. 3 shows a train suitable for low-capacity lines: total length of 26.4 m, composed of 15 modules (10 modules with seats + 5 modules with access doors). If the train can accommodate up to 4 travelers per square meter, the places offered are in total 205, of which 145 standing and 60 seated.

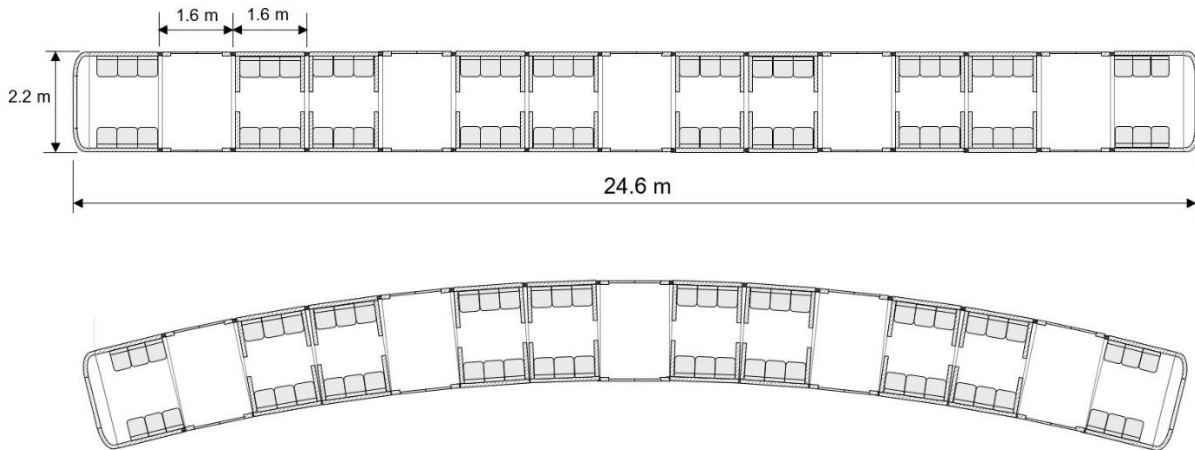


Fig. 3. Modular vehicle layout

With such short modules, even the relative displacements between the ends of the adjacent modules are very small; this facilitates the realization of the deformable coating to be applied along the entire perimeter of the shell. By adopting a minimum radius of 200 meters, the displacements between the ends of the adjacent shells are about 20 mm.

Compared to conventional systems, the vehicle has considerably lower weight and dimensions, as the load is distributed along its entire length. Therefore the vehicle does not have the great longitudinal bending moments operating on vehicles carried by bogies. Consequently, constructive simplification and a reduction in weight of both the infrastructure and the vehicle can be achieved.

In order to minimize maintenance costs and to guarantee the operating continuity, where possible, functions traditionally placed on board (such as the door opening/closing mechanism, the positioning braking system, etc.) can be installed on the ground. Therefore, the active technological part of the vehicle is restricted to the guidance systems, the emergency stop and the communication with the control center, besides lighting and speakers in the shell.

Lacking any contact between the vehicle and the track, vehicle braking must be guaranteed even in the event of a power failure. When the train is stopped at the station, the linear motor is not powered, but the train can be kept stationary by the automatic coupling between the train doors and the corresponding station fixed gates, thus avoiding longitudinal movements of the

train during entry and exit of travelers. Only an emergency brake remains boarded (the operating brake is the same synchronous machine). The remote control system actuates the emergency brake in case of speed excess, abnormal stopping in line, vehicle running back, etc.

As a whole, the proposed solution was strongly based on the simplicity and compactness of the primary suspension composed of permanent magnets in opposition. Two compositions of NdFeB permanent magnets on an iron plate, each 130 mm wide (with 54 m³ of magnetic material per linear meter), guarantee the levitation of a mass vehicle equal to 1,600 kg per linear meter, with a vertical gap of 12 mm (Fig. 4). That's all! Experimental tests confirmed these values.

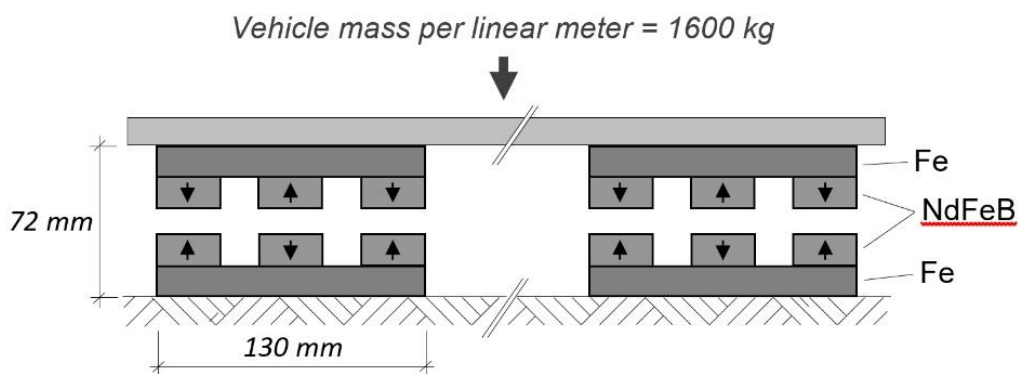


Fig. 4. Magnets' configuration to levitate a 1600 kg/m vehicle

The entire study presented in Berlin in 2016 was aimed at reducing operating costs by simplifying and, if possible, eliminating the active elements on the passenger compartment. The need for maintenance on the mobile part of the system had been reduced to the essential.

THE PRIMARY SUSPENSION

Many Maglev systems do not seem to be ready for commercial transport services, given the difficulties of industrializing systems with cheap, simple and reliable primary suspensions.

The primary suspension of our proposed system aims at these objectives, making use of the incalculable value of simplicity. The result (mass and volume occupied) is so substantial for the design of innovative urban transport systems, that we considered justified any effort aimed at perfecting an appropriate guidance device, capable of controlling the lateral instability inherent in the proposed system (magnets in opposition).

In a system with permanent magnets in opposition, in fact, a lateral displacement y of the upper magnets generates a horizontal force F_y directed in

the same direction as the displacement y . The moving part moves sideways (instability condition) until it stops on an obstacle (for example a fixed guide parallel to the path).

The load generated on the fixed guide depends on the lateral displacement performed. Fig. 5 shows the value of the horizontal force F_y as a function of the displacement y (experimental results referred to the system of Fig. 4 with 3 + 3 pairs of magnets). In order to keep the F_y force low, it is therefore necessary to limit the y offset as much as possible.

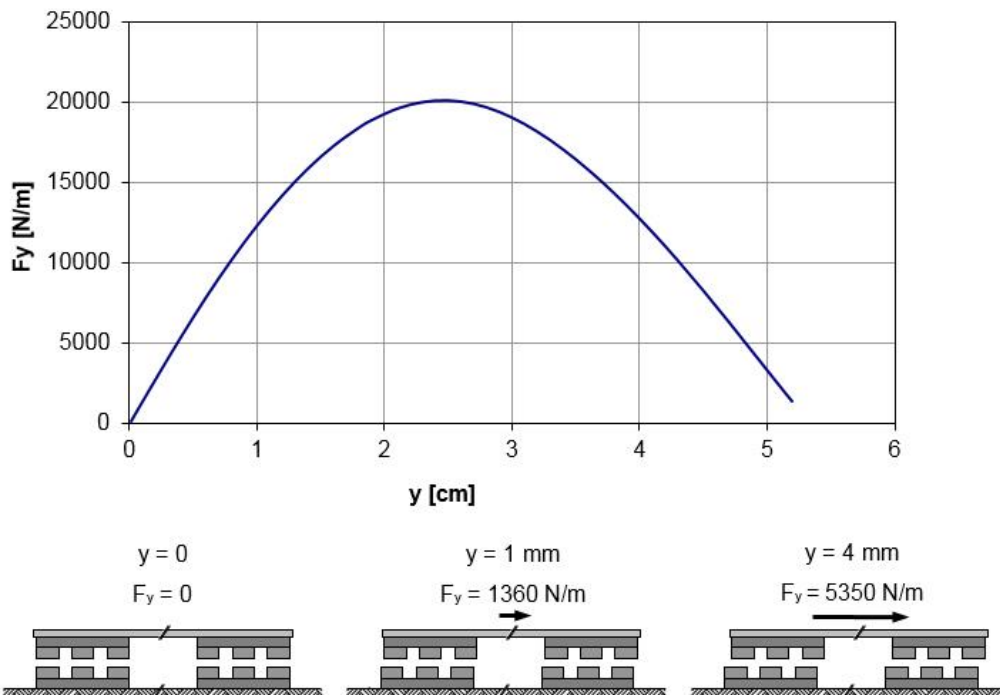


Fig. 5. Lateral force F_y as a function of displacement y , for magnets' composition of Fig. 3

At a lateral displacement y of a few millimeters there corresponds (for any number of pairs of magnets) an increase in force proportional to y and equal to about 8 % of the vertical load for each mm of displacement.

Therefore, in the case of small lateral displacements, a misalignment y corresponds to a horizontal force: $F_y \approx 0.08 \cdot P \cdot y$, where P is the vertical load (vehicle's own weight + transported load).

For example, with a vertical load equal to $P = 16000$ N per linear meter, a lateral force of about $F_y = 2050$ N acts on a 1.6 m long sliding frame, for each mm of lateral displacement.

To the lateral force $F_y \approx 0.08 \cdot P \cdot y$ (which is produced between fixed and movable magnets in the presence of a misalignment), an additional lateral force $P \cdot a/g$ is added, due to an uncompensated acceleration a [m/s^2] (positive or

negative). The total lateral force F_g that each sliding frame transmits to the fixed guide is therefore given by the sum (1):

$$F_g = 0.08 \cdot Py + P \frac{a}{g} \quad (1)$$

The principle on which the guidance system is based uses the same unstable force F_g . In fact, the lateral equilibrium is assured by an assisted regulation that moves the frame of the upper magnets in the opposite direction to that of the lateral load, until the latter is exactly balanced by the lateral repulsion force F_g acting between the upper magnets and the lower magnets.

Guidance devices (electromagnetic and/or mechanical), able to control the displacement y , have already been tested with encouraging results, even if their total reliability is not yet guaranteed (static tests carried out on prototype at the Polytechnic University of Turin [4, 5] have given satisfactory results, but these must be confirmed in dynamic conditions).

For urban Maglevs, which normally operate at a speed within 25 m/s, a simplified mechanical guidance system has been proposed, capable of keeping the force F_g on the fixed guide within very tight limits (no more than 1÷3% of the vehicle weight P).

A mechanical spacer adjusts the distance between the suspended material and the fixed guide parallel to the path (the spacer rests on the guide with a controlled F_g load). In this way it ensures that the load on the guide is contained within the tight limits indicated.

In case of a train with a weight of $P = 16,000$ N per linear meter and consisting of a succession of 1.6 long sliding frames, two spacers can be used for each sliding frame. For each spacer, the load F_g on the guide must always be between 130 and 390 N.

In this all-mechanical solution, the useful length of the spacer can be regulated by an electric motor (step-by-step type), that reduces the distance when the load (measured by a load cell inserted in the spacer itself) reaches an upper limit, and increases the distance when the load falls below a lower limit.

Other solutions (partly already tested) are certainly possible, both to overcome the all-mechanical servomechanism and to eliminate the mechanical contact on the fixed side guide.

AN ALTERNATIVE SOLUTION FOR THE PRIMARY SUSPENSION

The solution A in Fig. 2 shows a primary suspension consisting of opposing permanent magnets (PM/PM primary suspension) and guidance control by means of electromagnets.

As an alternative to this solution and partly giving up simplicity, our urban system can also use high critical temperature superconductors (HTS) in

cryogenics, kept at a temperature of about 77 K (liquid nitrogen). Fig. 6 shows the new arrangement (solution B) with primary suspension made by high temperature superconductors on the vehicle and permanent magnets on the track (HTS/PM primary suspension). This arrangement guarantees a stable levitation.

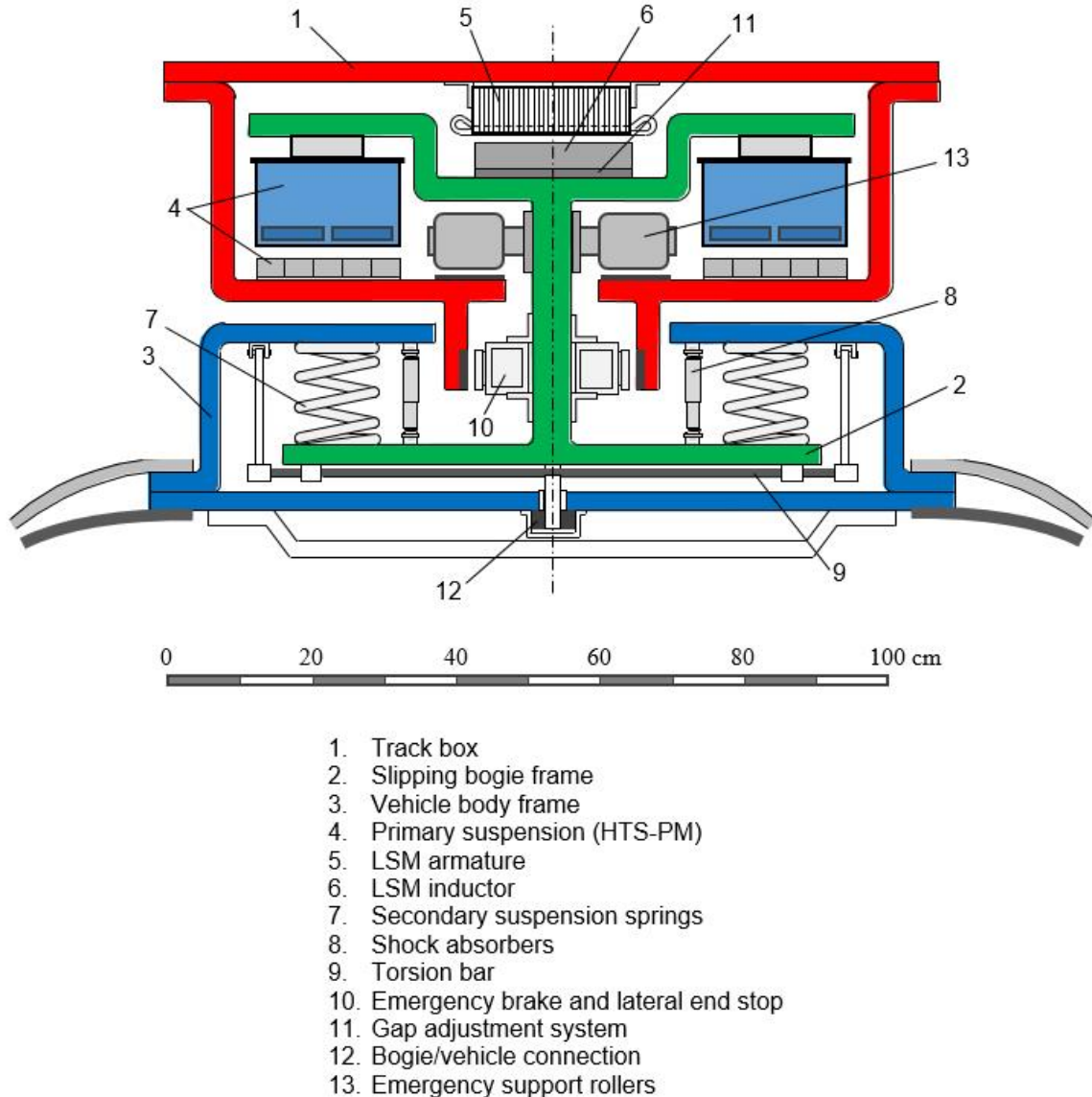


Fig. 6. The suspended Maglev system core – Solution B with HTS/PM primary suspension

This solution presents some unresolved problems:

- the high cost of YBCO superconductors;
- the operational cost for maintaining levitation capability (frequent recharge of the liquid nitrogen and restoration of superconducting conditions in the presence of a magnetic field – these activities require a dedicated plant);

- the risk of stopping the levitation due to the deterioration of the superconducting conditions, which obliges the provision of a safety support system on the vehicle (wheels or rollers).

SOME REMARKS ON PROPULSION SYSTEM DESIGN

The propulsion and braking forces in our system are generated by a Linear Synchronous Motor (LSM). The inductor, made up exclusively of permanent magnets, is carried by the sliding bogies and runs under the armature placed in the middle of the track (see Fig. 2 and Fig. 6). Therefore, the armature is as long as the railway line and the inductor as the vehicle.

A three-phase winding is arranged on the armature (with a pitch corresponding to the length of the excitation poles, Fig. 7), which is fed at a variable frequency by a generator located in the nearest station.

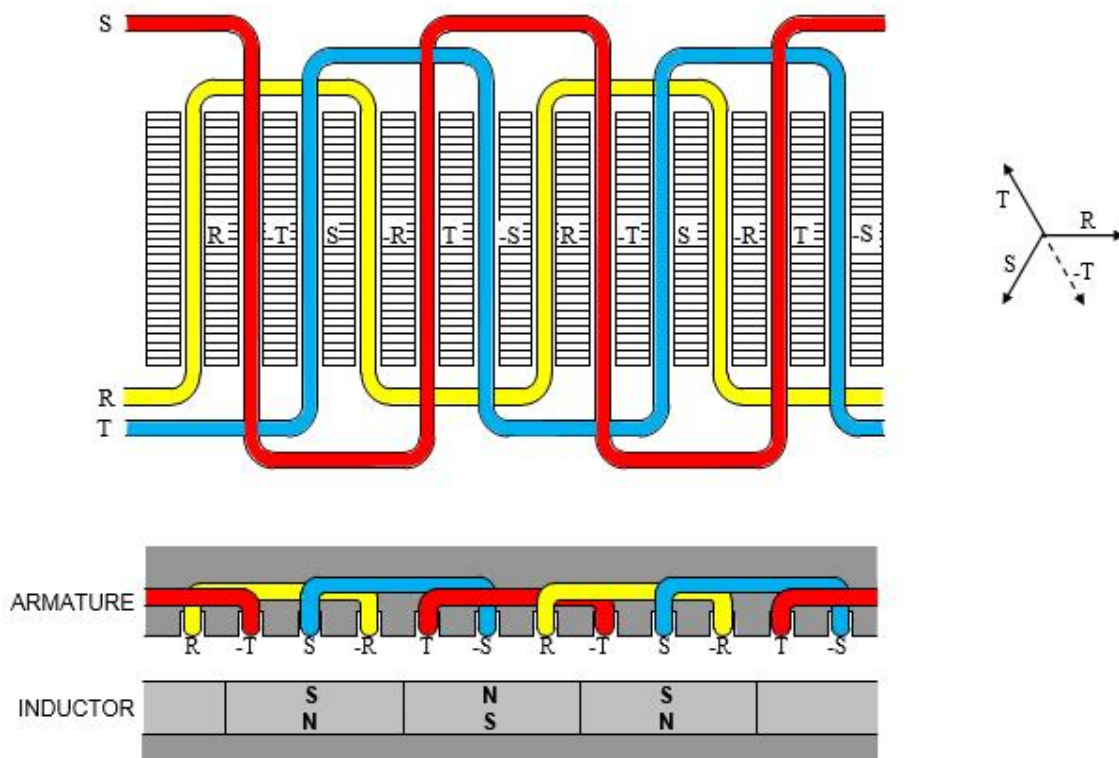


Fig. 7. The Linear Synchronous Motor (LSM)

The inductor poles (height h , semi-step p) are composed of NdFeB permanent magnets and have a sinusoidal profile (Fig. 8). Consequently, also the induction B inside the inductor poles is a sinusoidal function, which reaches the

maximum value B_m at the vertical median of the pole and is represented, along the axis, by the expression $B_\xi = B_m \sin \frac{\xi}{p} \pi$ (Fig. 9).

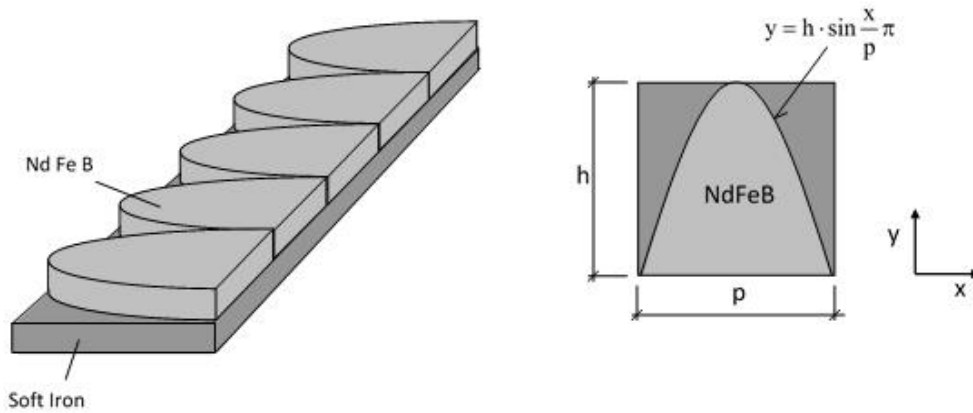


Fig. 8. Inductor shape

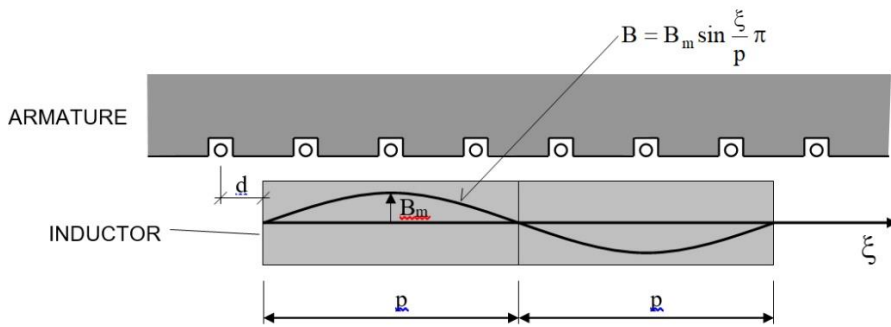


Fig. 9. Sinusoidal trend of induction within the inductor poles

The relationships between electrical, magnetic and mechanical quantities are:

$$E_{\text{eff}} = \frac{1}{\sqrt{2}} B_m \frac{h}{p} \nu l \quad (2)$$

$$I_{\text{eff}} \cdot \cos \delta = \frac{F_{ml}}{1.5\sqrt{2} B_m \frac{h}{p}} \quad (3)$$

where:

E_{eff} : effective electromotive force along the armature windings (V);

I_{eff} : effective current for each phase of the armature (A);

B_m : maximum induction (T);

$\delta = \pi d/p$, where d is the phase displacement of the inductor field with respect to the translating field generated by the armature (δ in degrees; d and p in meters)

F_{ml} : propulsion force per linear meter of inductor (N/m);

v : train speed (m/s);

l : train length (m)

Some considerations on formulas (2) and (3):

E_{eff} grows according to the train speed v , the train length l , the maximum induction B_m , the shape ratio h/p , while it is independent of the resistance acting on the train during its movement; the current I_{eff} referred to a phase is independent of the speed and the train length, and it varies inversely to the induction B_m , to the shape ratio h/p and to the $\cos\delta$; it grows proportionally to the resistance to motion referred to a linear meter of the train length.

Consequently, for high-speed trains, which run mainly under steady-state conditions with infrequent and not very high accelerations, low values of B_m (0.20÷0.25 T) and h/p ratio (0.4÷0.6) are chosen, not to exceed linked voltages of 2000÷2500 volts in the armature windings, even for trains of 200÷250 m in length.

On the contrary, for urban trains, characterized by very frequent and high accelerations, opposing criteria are adopted in order to limit Joule effect losses due to the high current density in the armature windings: high values of B_m (0.6÷0.8 T), of h/p ratio (1÷1.2) and of $\cos\delta$ (0.7÷0.9) (the angle δ must be between 0 and $\pi/2$ during propulsion and between 0 and $-\pi/2$ during braking).

CONCLUSIONS

Maglev systems will be competitive in the future against conventional systems only if researchers are able to develop simple solutions with low operational and maintenance costs. There are still important technical issues to be resolved and many different proposals are being developed.

This paper describes our proposal for a suspended urban Maglev. Our interest is focused on the need to find industrially feasible solutions, easy to build and manage, in order to propose a system that is also commercially competitive as an alternative to conventional railway. The benefits identified in the system encourage further studies and experiments.

References

1. Cavagnaro M, Delle Site V, Di Majo F, Goliani M. Repulsive magnetic levitation system with permanent magnets, Proceedings of the World Congress on Railway Research; 1999; Tokyo, Japan.
2. Di Majo F, Cavagnaro M, Delle Site V. Nuovi orizzonti per il trasporto guidato a levitazione magnetica. *Ingegneria Ferroviaria*. 2008;(2)105-121.

3. Cavagnaro M, Delle Site V. Saving Money with Maglev. An Urban Transport Revolution. Proceedings of the Maglev 2016 Conference; 2016; Berlin, Germany.
4. Carabelli S, Delprete C, Genta G, Zanolli S. Control of a Two Active Axes Suspension for Maglev Vehicles, Proceedings of the American Control Conference 97; 1997; Albuquerque, USA.
5. Carabelli S, Delprete C, Genta G, Muzzarelli M, Zanolli S. Passive Repulsive Maglev: Concept and Experimental Demonstration. *Vehicle System Dynamics*. 2000;34(5):333-356. doi: 10.1076/vesd.34.5.333.2056

Information about the authors:

Delle Site Vincenzo, mechanical engineer; National Research Council of Italy, Department of Engineering, Piazzale Aldo Moro, 7 – 00152 Rome, Italy;

ORCID: 0000-0002-1098-6745;

E-mail: vincenzo.dellesite@cnr.it

Cavagnaro Maurizio, electrical engineer; currently, rolling stock and railway system consultant;

E-mail: cavagnaro.maurizio@gmail.com

To cite this article:

Delle Site V, Cavagnaro M. A New Concept of Modular Magnetic Levitation Train for Urban Transport. *Transportation Systems and Technology*. 2018;4(2):107-119. doi: 10.17816/transsyst201842107-119

DOI 10.17816/transsyst201842120-128

Y. He^{1,2}, Y.-S. Wang¹, Q. Lu¹, L. Zhang², F. liang²

¹College of Electrical Engineering, Zhejiang University
(Hangzhou, China)

²CRRC Zhuzhou Electric CO., LTD.
(Zhuzhou, Hunan, China)

DESIGN OF SINGLE-SIDED LINEAR INDUCTION MOTOR FOR LOW-SPEED MAGLEV VEHICLE IN 160 km/h AND VARIABLE SLIP FREQUENCY CONTROL

Background: The mid-low speed Maglev train adopts the single-sided linear induction motors (SLIMs) as drive part, of which design and control method has become research hotspot when the velocity is elevated from 120 km/h to 160 km/h.

Aim: For SLIMs applied in 160 km/h low-speed maglev train, the design scheme is introduced and then a novel variable slip frequency control method is proposed.

Methods: This control method adopts low slip frequency at start-up to produce large starting traction force and high slip frequency during high velocity area to obtain great power. The influence to the normal force is also investigated.

Results: With this method, the weight of the system can be effectively reduced and the lightweight design of SLIM is realized.

Conclusion: The novel variable slip frequency control method meets the requirement of both high starting acceleration and enough residual acceleration for 160 km/h mid-low speed maglev train.

Keywords: Mid-low speed maglev train; linear induction motor; slip frequency; traction force; normal force

INTRODUCTION

The Changsha medium-low speed maglev line is the first commercial operation line in China and the longest one in the world. Its designed velocity is 120 km/h, and the running velocity is 100 km/h. During its two-year long commercial operation since May 6th, 2016, the longest mileage has reached 400,000 km and the punctuality rate has reached 99.8 %, which has set a good exemplary role. After the successful operation of the Changsha maglev line, the intercity transportation with higher speed class (160 km/h) by adopting the maglev train is put on the agenda. This paper presents the design of SLIMs for mid-low speed maglev train with velocity 160 km/h and optimizes the force performance from the aspect of control method.

1. BASIC PARAMETERS OF MAGLEV TRAINS IN CHANGSHA LINE

The mid-low maglev train in Changsha line consists of three coaches. Each coach covers five suspension frames, one converter and ten SLIMs. The

basic parameters of the train and the converter are listed in Table 1. Ten SLIMs are equally divided into two groups, which are connected in parallel. To five SLIMs in one group, the phase windings connected in series are transposed to reduce the end effect, as shown in Fig. 1. As it can be seen, three phase windings are Y connected.

Table 1. Basic parameters

Item	Parameters	Value
Vehicle	Voltage of power network /V	DC1000~1800
	Track gauge /mm	1860
	Running velocity/ km/h	100
	Design velocity / km/h	120
	Coach number	3
	Vehicle mass (AW2) /t	30
	Starting acceleration /m/s ²	1.0
	Average acceleration/m/s ²	0.4
	Residual acceleration/m/s ²	0.1
	Number of suspension frame	5
Converter	Input voltage /V	DC1000~1800
	Rated line voltage/ V	1100
	Rated maximum current /A	2×340
	Rated Continuous current /A	2×240

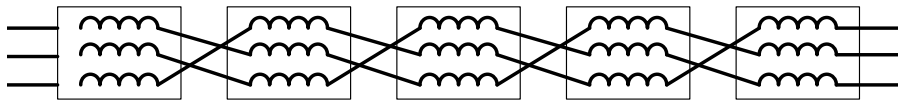


Fig. 1. The winding connection of five SLIMs in one group

2. DESIGN ANALYSIS OF SLIMS FOR 160KM/H MAGLEV TRAIN

2.1 Traction force requirement

The 160 km/h maglev train also adopts three coaches. Its resistance force can be calculated by adopting the resistance formula of the Changsha maglev line, which includes three components as follows.

1) Magnetic resistance force

The magnetic reluctance force D_m can be calculated by piecewise formula as follows:

$$D_m = \begin{cases} 3.354Wv & v < 5.6\text{m/s} \\ (18.22 + 0.074v)W & v > 5.6\text{m/s} \end{cases}, \quad (1)$$

where W is the vehicle mass (t), and v is the running velocity (m/s).

2) Relay resistance force

The relay resistance force D_c is almost constant, which value is 41.67 N.

3) Aerodynamic resistance force

The aerodynamic resistance force D_a mainly depends on the velocity and coach number.

$$D_a = (1.652 + 0.572N)v^2, \quad (2)$$

where N is the coach number.

The total resistance force D is the sum of three former components. The traction force F is obtained through the total resistance force and acceleration.

$$F = D_m + D_c + D_a + Wa = D + Wa, \quad (3)$$

where a is the acceleration.

When the running velocity is increased from 120 km/h to 160 km/h and the minimum residual acceleration is maintained at 0.1 m/s^2 , the power increases by 66.7 %, as shown in Table 2.

Table 2. Power requirement of the 160 km/h maglev train

Design velocity	120 km/h	160 km/h
Vehicle mass / t	30	32
Total resistance force / kN	5.65	8.76
Traction force/per motor / kg	50	62.5
Vehicle power / kW	490	816.7

2.2 Basic parameters of traction system

As the vehicle power increases, the number of converters or the capacity of single IGBT needs to be increased. Obviously, it is more economical to increase the IGBT capacity. The maximum current of available IGBT with matching voltage level is $2 \times 450 \text{ A}$. Therefore, the power can increase by 32 % in comparison with the Changsha lines with IGBT of $2 \times 340 \text{ A}$ maximum current.

Since the IGBT capacity does not increase by 66.7 %, it means the starting traction force should be reduced or the volume should be improved to reduce the starting current. According to the consultation with the OEM, the length of SLIM can be increased from 1,820 mm to 2,020 mm. In addition, the starting traction force is reduced since the starting acceleration is changed from 1.0 m/s^2 to 0.8 m/s^2 , which meets the start acceleration of the general intercity vehicle.

2.3 Vehicle configuration

The number of modules per train and the selection between available mode (five-string double-parallel) and new mode (two-string five-parallel mode) need to be determined. The most economical and reliable method is to keep the original vehicle structure.

2.4 Design requirements

Based on the foundation of the Changsha maglev line, the main design requirements of the 160 km/h maglev train are listed in Table 3.

Table 3. Power requirement of the 160km/h maglev train

Vehicle mass (AW2) / t	32
Mechanical air gap of SLIMs / mm	12
Length of the SLIM / mm	2020
Converter input current / A	2×450
Maximum vehicle velocity / (km/h)	160
Average starting acceleration(0~70 km/h) / (m/s ²)	≥0.8
Average acceleration (0-160 km/h) / (m/s ²)	≥ 0.4
Residual acceleration (160 km/h) / (m/s ²)	≥0.1

3. THE DESIGN OF SLIMS

3.1 Basic parameters

Based on the former analysis, the SLIMs, JX170, applied in the 160 km/h maglev train is designed, shown in Fig. 2. The train has the original five-module structure and SLIMs per coach with five strings two parallel connection mode. The motor basic parameters comparison with SLIM of the Changsha maglev line, JX130, are listed in Table 4.

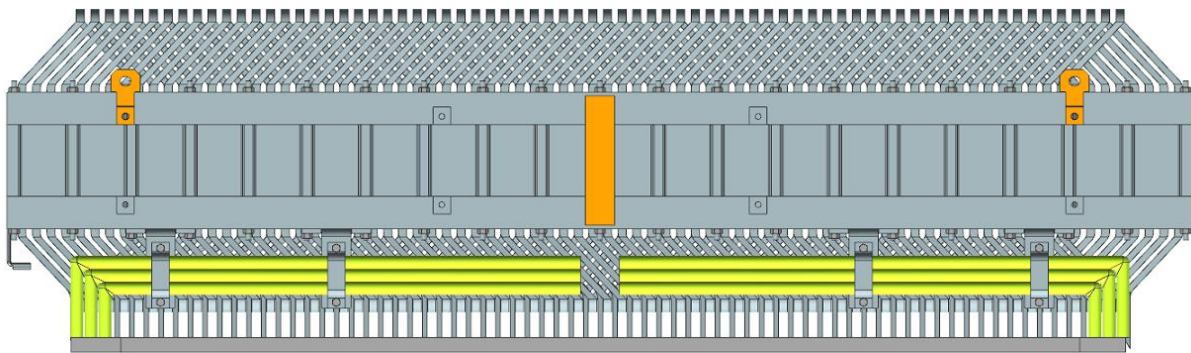


Fig. 2. JX170 SLIM

Table 4. Basic parameters comparison of two SLIMs

SLIM type	JX130	JX170
Rated voltage/V	220	
Pole number	8	
Thickness of the aluminum plate/mm	4	
Width of F-shaped rail/mm	220	
Starting current/A	340	450
Rated current/A	240	360
Starting force/N	3,234	2,764
Primary mass/kg	200	215
Pole pitch/mm	202.5	225
Primary length/mm	1,820	2,020
Air gap/mm	13	12

3.2 Control settings

The control method of the SLIMs for magnetic levitation trains is different from that of the induction traction motor for subways. First, for simple

control, the SLIMs for magnetic levitation trains generally use constant current and constant slip frequency control method. Second, SLIMs must consider the effect of the normal force. Therefore, the suitable slip frequency f_2 is important parameter for SLIMs.

With the equivalent circuit of an induction motor, the influence of slip frequency on SLIMs performance can be analyzed.

Normally, constant current control method is used during start-up. Their relationship is shown as follow. Apparently, the traction force is inversely proportional to the slip frequency, f_2 .

$$F_x = \frac{mR_2'(I_2')^2}{2\pi f_1 s} = \frac{mR_2'(I_2')^2}{2\pi f_2}, \quad (4)$$

when the starting acceleration of the train reaches 0.8 m/s^2 , the traction force per SLIM is 2567 N. Under this condition, the maximum slip frequency f_2 should be 15.7 Hz. If adopting the control method of constant slip frequency, the traction force at maximum velocity is 710N per SLIM and the residual acceleration of the train at 160 km/h is 0.13 m/s^2 .

At high velocity, the SLIM already adopts full voltage. The SLIM torque-slip curve is similar with induction-machine. As can be seen from Fig. 3, during the motor region, the higher the f_2 , the higher the slip, and the larger the traction force is.

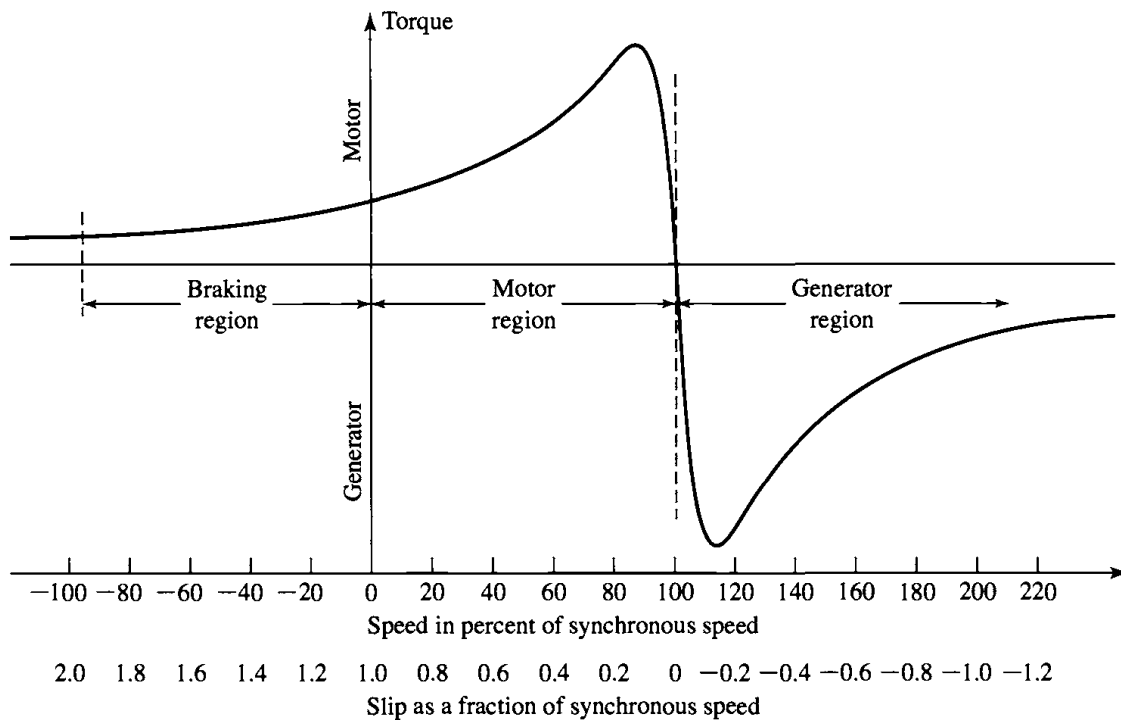


Fig. 3. Induction-machine torque-slip curve during whole operation area

When the required remaining acceleration is 0.1 m/s^2 , the traction force per SLIM is 612 N. To this required traction force, the minimum slip frequency f_2 is 13.7 Hz. If keeping this slip frequency as constant value, the starting traction force can be increased up to 2,764 kg.

In order to verify the former traction force at start-up and maximum velocity, the 3D model of JX170 is erected by 3D FEM. For slip frequency 13.7 Hz, the calculated thrust force at start-up is 2,720 N. For slip frequency 15.7 Hz, the calculated thrust force at maximum velocity is 753 N. Compared with the predicted results of equivalent circuit method, the errors are 44 N and 43 N under two conditions respectively. Apparently, the results of equivalent circuit method are reasonable.

Therefore, the slip frequency should be between 13.7 to 15.7 Hz. The traction characteristics are shown in Fig. 4 with the slip frequency values of 13.7 Hz and 15.7 Hz, respectively. And the normal force is considered acceptable.

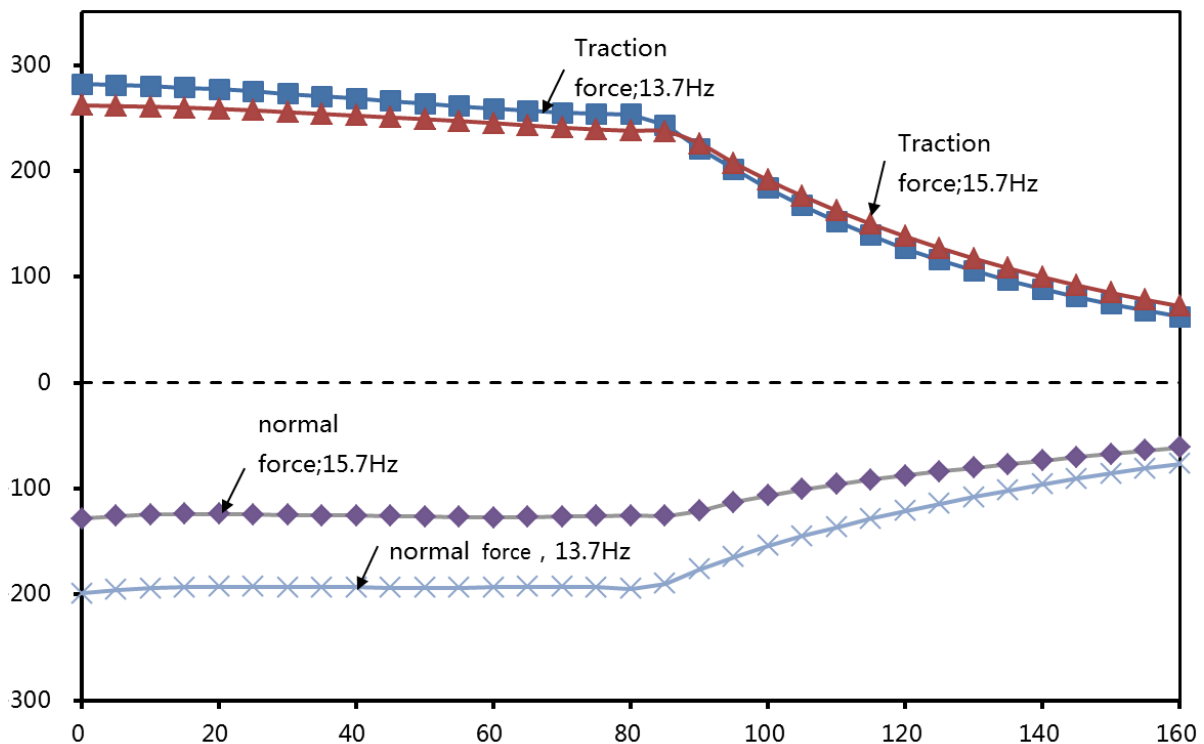


Fig.4. The traction characteristics with the constant current slip frequency 13.7 Hz and 15.7 Hz

4. VARIABLE SLIP FREQUENCY CONTROL METHOD

From former analysis, it can be deduced that the SLIM performance of high velocity or low velocity is inevitably sacrificed when a constant current and constant slip control method is applied. However, this can be avoided if variable

slip control method is adopted in SLIMs. Since they start with a lower starting frequency to produce larger starting traction force, and operate with higher slip frequency to obtain larger power at high velocity area, the capacity can be fully utilized.

To JX170 SLIMs, at the low velocity, the slip frequency 13.7 Hz is adopted to increase the starting traction force. At high velocity, the slip frequency is increased to 17.2 Hz, which increases the traction force. The traction characteristics are shown in Fig. 5. This method considers the starting acceleration and the residual acceleration of high velocity, which increases the starting capability and reduces the starting distance.

When the variable slip frequency control method is used, the traction characteristics of the train can only be within the envelope to meet a certain overload capacity. Moreover, it should not be far away from the envelope to make full use of motor capability as shown Fig. 5

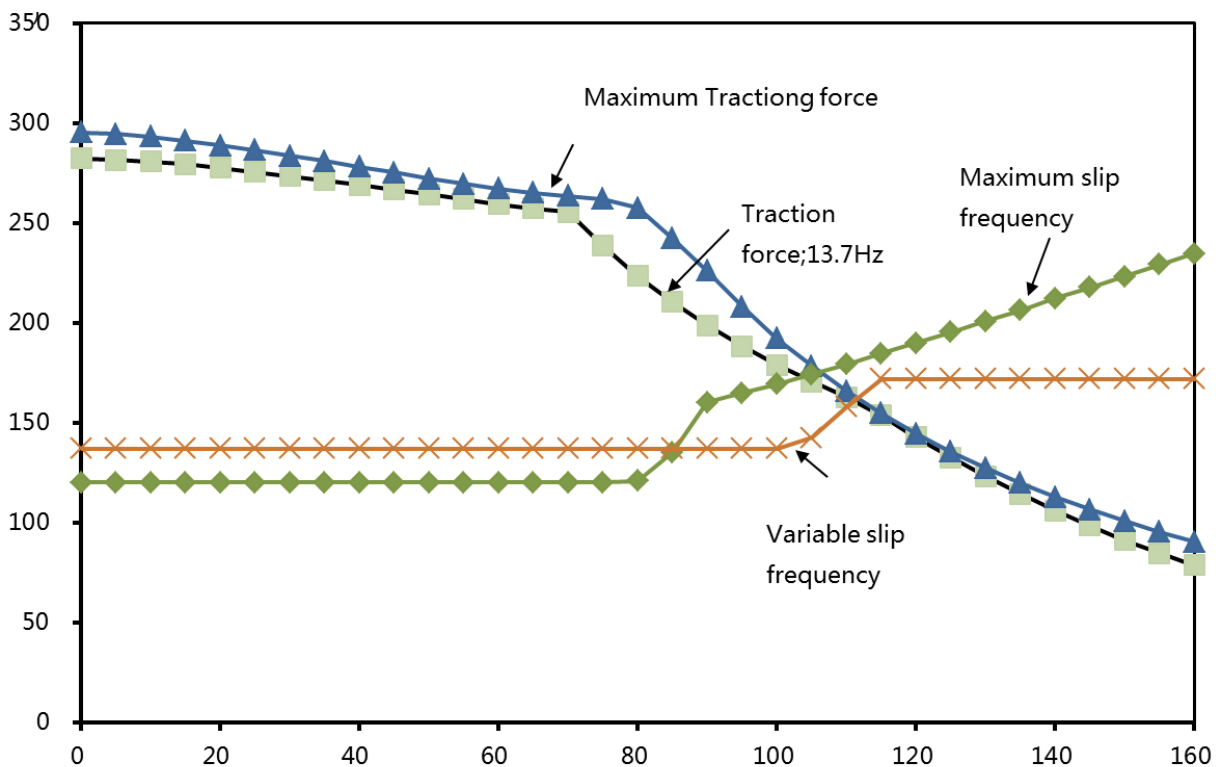


Fig. 5. Maximum traction force curve

With slip frequency change from 13.7 Hz to 17.2 Hz, the residual acceleration is increased by 70 % compared with the constant slip frequency control method, and then the acceleration time is reduced by 17 % and the acceleration distance is reduced by 22 %, as shown in Table 5.

Table 5. Starting performance of variable slip frequency control method

Control method	Constant slip frequency	Variable slip frequency	Change rate
Start-up frequency /Hz	13.70	13.7	
Start acceleration/(m/s ²)	0.86	0.86	
End-up slip frequency /Hz	13.7	17.2	
Residual acceleration/(m/s ²)	0.10	0.17	+ 70 %
Average acceleration/(m/s ²)	0.40	0.48	+ 20 %
Acceleration time /s	110.6	91.7	- 17 %
Acceleration distance/m	3,369	2,613	- 22 %

5. CONCLUSION

This paper presents the design of SLIMs for mid–low speed maglev train with velocity 160 km/h, which meets the performance requirement of the 160 km/h mid-low speed maglev train. It has the characteristics of derivative design and economical reliability.

It also proposes a variable slip frequency control method for the SLIM. With a lower slip frequency at start-up, the SLIM has a larger starting traction force. At high velocity, a higher slip frequency is used, and a larger motor power is realized. The train acceleration performance is optimized without additional space, mass and cost. This proposed control method can also be applied to other maglev trains driven by SLIMs.

References

1. Yan G L. The linear motor powered transportation development and application in China *Proc. IEEE*. 2009;97(11):1872-1880. doi: 10.1109/JPROC.2009.2030245
2. Gieras JF, Dawson GE, Eastham AR. Performance calculation for single-sided linear induction motors with a double-layer reaction rail under constant current excitation. *IEEE Trans. Magn.* 1986;IM-22(1):54-62.
3. Im DH, Park SC, Im JW. Design of single-sided linear induction motor using the finite element method and SUMT. *IEEE Trans. Magn.* 1993;29(2):1762-1766.
4. Dawson G, Eastham AR, Gieras JF, Ong R, Ananthasivam K. Design of linear induction drives by field analysis and finite-element techniques. *IEEE Trans. Ind. Appl.* 1986;IA-22(5):865-873.
5. Ye YY. The Theory and Application of Linear Motor. Beijing, China: Mech. Ind. Press, Jun. 2000.
6. Ham SH, Lee SG, Kim KS, Cho SY, Jin CS, Lee J. Study on reduction of transverse edge effect of single-sided linear induction motor for transportation system. Proc. Int. Conf. Electr. Mach. Syst., Tokyo, Japan, Nov. 2009, p. 1–4.
7. Lv G, Li Q, Liu ZM, Fan Y, Li GG. The analytical calculation of the thrust and normal force and force analyses for linear induction motor. Proc. 9th Int. Conf. Sig. Process., Beijing, China, Dec. 2008, p. 2795-2799.
8. Gieras JF, Dawson GE, Eastham AR. A new longitudinal end effect factor for linear induction motors. *IEEE Trans. Energy Convers.* 1987;EC-2(1):152-159.
9. Lu JY, Ma WM. Research on end effect of linear induction machine for high-speed

- industrial transportation. *IEEE Trans. Plasma Sci.* 2011;39(1):116-120. doi: 10.1109/TPS.2010.2085089
10. Kim D-K, Kwon B-I. A novel equivalent circuit model of linear induction motor based on finite element analysis and its coupling with external circuits. *IEEE Trans. Magn.* 2006;42(5):3407-3409. doi: 10.13334/j.0258-8013.pcsee.2015.15.026
 11. Yamaguchi T, Kawase Y, Yoshida M, Saito Y, Ohdachi Y. 3-D finite element analysis of a linear induction motor. *IEEE Trans. Magn.* 2001;l.37(5):3668-36741.
 12. Lv G, Zeng D, Zhou T, Liu Z. Investigation of forces and secondary losses in linear induction motor with the solid and laminated back iron secondary for metro. *IEEE Trans. Ind. Electron.* 2017;64(6):4382-4390. doi: 10.1109/TIE.2016.2565442
 13. Lu Q, Li Y, Ye Y, Zhu ZQ. Investigation of forces in linear induction motor under different slip frequency for low-speed maglev application. *IEEE Trans. Energy Convers.* 2013;28(1):45-153. doi: 10.13334/j.0258-8013.pcsee.2015.15.026

Information about the authors:

Yunfeng He, Ph.D, senior engineer;

ORCID: 0000-0002-9951-3919;

E-mail: heyunfeng@crrcelectric.com

You-Sheng Wang, bachelor, Professor;

ORCID: 0000-0002-8081-4957;

E-mail: eewangys@zju.edu.cn

Qinfen Lu, Ph.D, Professor;

ORCID0000-0002-3452-5564;

E-mail: luqinfen@zju.edu.cn

Lei Zhang, master, engineer;

ORCID: 0000-0003-0840-9401;

E-mail: zhanglei@crrcelectric.com

Fang Liang, master, engineer;

ORCID: 0000-0001-8874-9208;

E-mail: fangliang@crrcelectric.com

To cite this article:

He Y, Wang Y-S, Lu Q, et al. Design of Single-Sided Linear Induction Motor for Low-Speed Maglev Vehicle in 160km/h and Variable Slip Frequency Control. *Transportation Systems and Technology.* 2018;4(2):120-128. DOI: 10.17816/transsyst201842120-128.

DOI 10.17816/transsyst201842129-140

© J. Huang, X. Zhou, L. Shang, Z. Wu, W. Xu, D. Wang
Department of Civil Engineering, Tongji University
(Shanghai, China)

INFLUENCE ANALYSIS OF TRACK IRREGULARITY ON RUNNING COMFORT OF MAGLEV TRAIN

Background: In this article, the TR08 car of the Shanghai Magnetic Train Demonstration Line was prototyped and a multi-body dynamics simulation model was established. And based on the low-interference track irregularity power spectrum in Germany, track irregularity data was obtained. Used dynamic simulation software, completed the dynamic simulation analysis of the vehicle-rail model controlled by the proportion-integral-derivative control system PID parameters. It can be concluded that the vibration of trains passing through irregular tracks at different speeds, and evaluated its comfort. The optimal solution for the control of the PID parameters of the train also has been derived.

Aim: Evaluation of operational comfort and suspension gap control effect of Shanghai Maglev Train Demonstration Line by simulation analysis.

Methods: Simulation analysis.

Results: The vibration acceleration and suspension gap of Shanghai Maglev Train Demonstration Line has been obtained.

Conclusion: By adjusting the parameters of PID control system, the vibration acceleration of train can be reduced and the ride comfort can be improved.

Keywords: Track irregularity, PID, Comfort, Maglev train.

INTRODUCTION

High-speed maglev train system is a complex multi-body dynamics system, the train's running speed can reach 430 km/h, ride comfort and stability performance are two important problems in the process of the maglev train running. Ju [1] et al. have conducted relevant research on the influence of track irregularity on the stability of train operation, and proposed a proportional-integral (PI) control method. By establishing a single magnet-levitation system-orbital beam interaction model, Li [2] et al. researched the effect of track irregularity on the variation of the suspension state of a single magnet. FAN Qin-Hai [3] analyzed the variation characteristics of the suspension gap of the suspended electromagnet by analyzing the vibration of the maglev vehicle under the track irregularity excitation. By multi-body dynamic simulation of the train, the stability of passenger comfort and suspension guide system under the condition of track irregularity was researched.

Based on the Shanghai maglev demonstration line's TR08 car as the prototype of the model, a multi-body dynamic simulation model of the entire

maglev train system was built. In order to study the vibration of vehicle body and the stability of suspension guide system, the dynamic simulation analysis was carried out under the action of track irregularity. The main work includes the following:

Used the 3D modeling software to simplify the modeling of various parts of the TR08 model and conducted dynamic simulation of the model through an irregular road section. The track irregularity was based on the German's track irregularity power spectrum, by passing in different speeds to analyze the effect of track irregularity on the vehicle body's vibration response and the levitation gap stability at different vehicle speeds. Finally, summarized the dynamic performance of the model, included the ride comfort of the vehicle and the stability of the suspension system.

Vehicle Dynamics System Modeling

Used the three-dimensional modeling software and the dynamic simulation software to build a multi-body dynamics system model of a maglev train with a proportion- integral- derivative control system (PID).

The maglev train running mechanism was a complex multi-body movement mechanism. The levitation control system was also a unique system of maglev trains. A maglev train's car body consists of a carriage and four go-between mechanisms. The specific composition consists of a carriage, four suspension frames (eight suspension frames), 16 bolsters, 16 rocker levers, 4 traction devices, 14 Suspension electromagnet unit, 12 guide electromagnets, 2 brake electromagnets. There were also first and second suspension connection devices interconnected in Fig. 1.

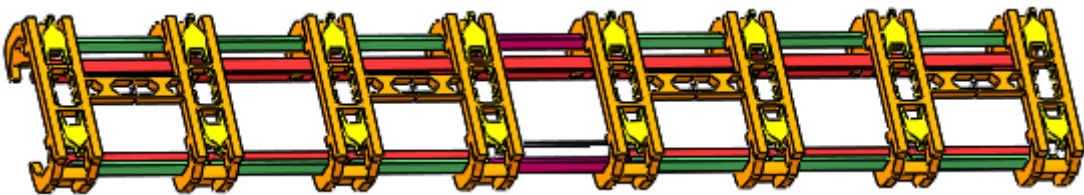


Fig. 1. Simplified model of the running mechanism

Taken each magnetic suspension, suspension electromagnets, guiding electromagnets, and compartment dynamics model as a substructure, and the overall model was a line moving platform. Then connected the suspension electromagnets and the guiding electromagnets between four suspension frames. Finally, the complete dynamic model of a maglev train was obtained by importing the substructure of the carriage. As shown in Fig. 2, there were 210 degrees of freedom for a maglev train model.

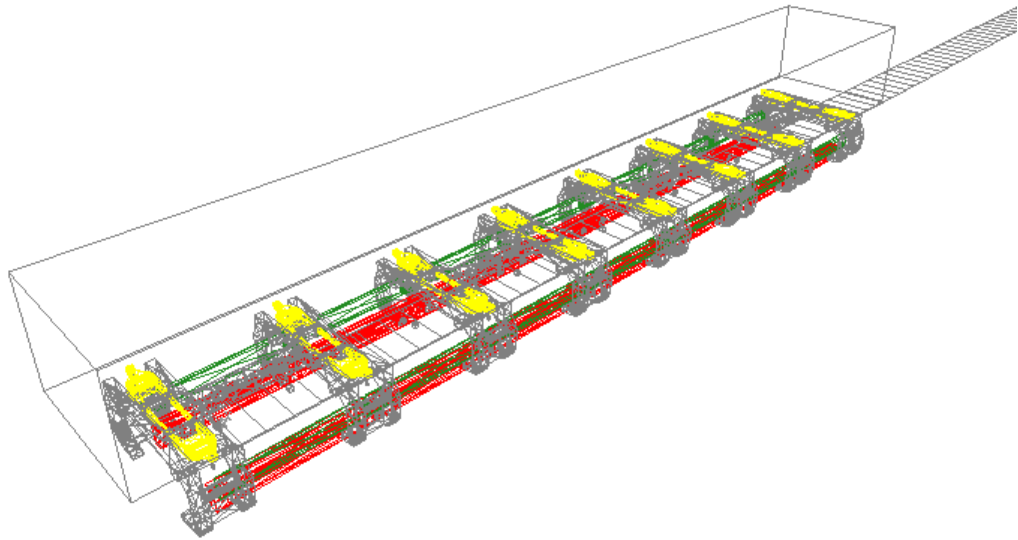


Fig. 2. Dynamic model of maglev train

COMFORT EVALUATION STANDARD

Through the study of Liu [4] et al. The International Organization for Standardization - Guidelines for the Impact of Vibration and Impact on People (ISO2631) [5] was selected as the comfort assessment standard. The comfort level was shown in table 1 [5].

Table 1. Classification of comfort levels

level	Effective acceleration (m/s^2)	Evaluation
1	<0.315	No discomfort
2	0.315~0.63	Slight discomfort
3	0.5~1.0	Moderately uncomfortable
4	0.8~1.6	Discomfort
5	1.25~2.5	Very uncomfortable
6	>2	Extremely uncomfortable

VIBRATION ANALYSIS UNDER TRACK IRREGULARITY

According to the merits of the country's railway track, each country divides unevenness into different levels. The construction standards for the rail beams of maglev trains in Shanghai are very strict. The random irregularity is far less than the best rail track in the world. Its irregularity is mainly caused by the random variation of the coils laid on the rails instead of the deformation of the rail beams. The construction of the Shanghai maglev train track was based on the German rail construction standards. Therefore, when analyzing the multi-body dynamics, the German orbital irregular power spectrum [6, 7] was used as

a benchmark. The German track grade is divided into two levels of high interference and low interference, to adapt to different speeds, in which the high interference level applies to speeds below 250 km/h, and the low interference level applies to speeds above 250 km/h. Due to the high standards of Shanghai's maglev train construction, one-tenth of the German low-interference spectrum can be used to express track irregularities. The vertical irregular power spectrum was shown in Equation 1 [7].

$$S_v = \frac{2.74162 \times 10^{-8}}{2.8855 \times 10^{-4} + 0.68039 \omega^2 + \omega^4} \quad (1)$$

In which S_v , ω are the vertical power spectral density (1/(rad/m)) and the spatial frequency of the track irregularity (rad/m).

According to the above power spectrum function, the vertical spatial irregularity sample was shown in Fig. 3. Add the spatial irregularity sample to the orbit separately to simulate the dynamic performance of the vehicle through the uneven track.

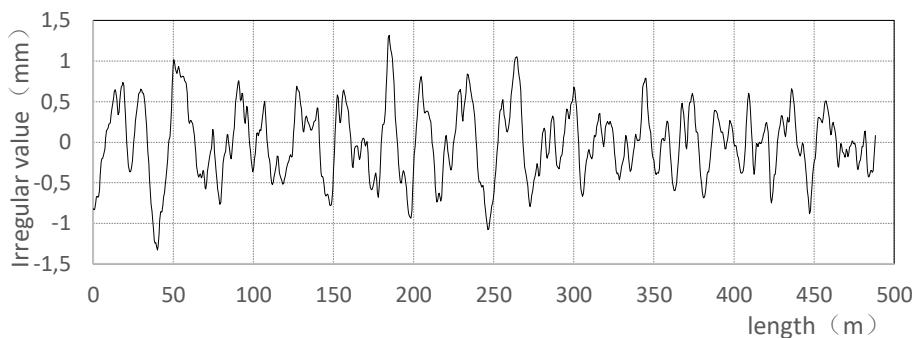


Fig. 3. Spatial Samples of Vertical Irregular

Input this vertical irregular track data to the established track model, and accelerate the speed to 100 km/h, 200 km/h, 300 km/h, 400 km/h, and 500 km/h with an acceleration of 1 m/s^2 , measure the vertical acceleration of the three observation points on the vehicle body and the suspension gap variation of the suspended electromagnets, and analyzed the comfort of the vehicle and the stability of the suspension system.

When the maglev train was loaded with a vertical random irregular track at a speed of 100 km/h, the vertical vibration accelerations of the three vibration measurement points on the vehicle body and levitation gaps were shown in Fig. 4.

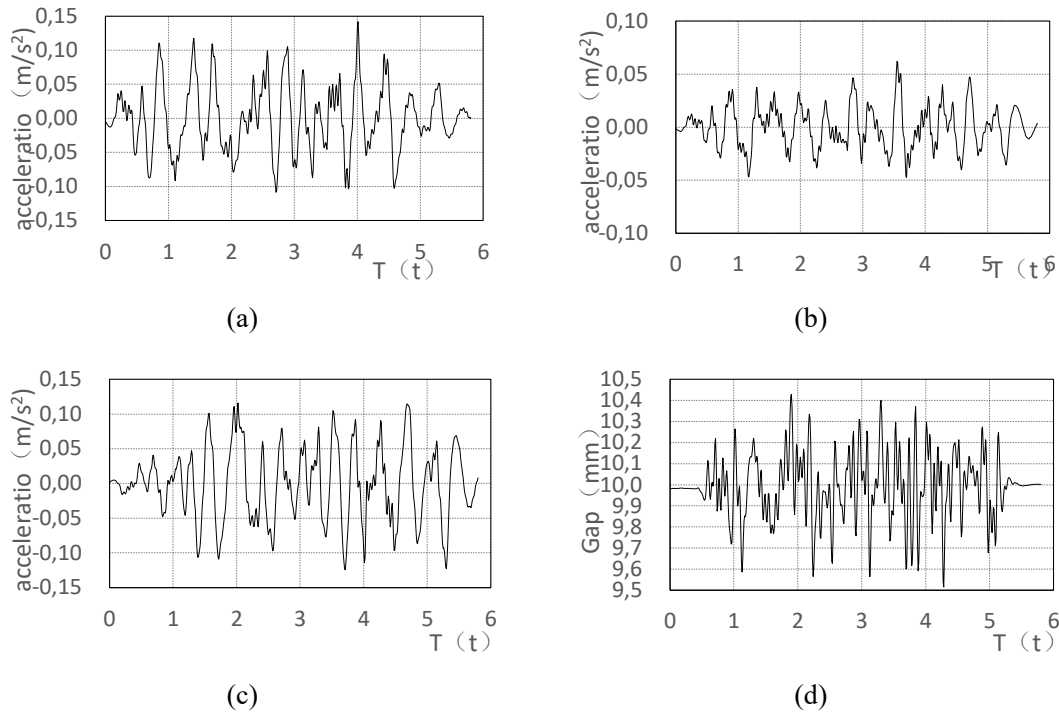


Fig. 4. Vertical Vibration Acceleration Curves of Front, Middle and Tail of 100 km/h (a), (b), (c), and the suspension gap variation curve (d)

It could be calculated that the vertical effective accelerations of the front, middle and rear marking points of the carriage during the integration period were $0.048 m/s^2$, $0.019 m/s^2$, $0.052 m/s^2$, the vertical effective vibration acceleration and the maximum vibration acceleration at the front, middle and rear of the carriage were all less than $0.315 m/s^2$. Passengers would not feel uncomfortable and comfort level 1. In general, the vertical acceleration of the front part of the carriage and the rear part of the carriage were obviously greater than that of the central part of the carriage. The RMS value was approximately 2.6 times that of the middle part of the carriage. The vibration of the vehicle body was dominated by the nodding vibration.

Suspension gap was stable at 10 mm before and after entering the irregular track. The maximum suspension clearance was 10.43 mm at the irregular track, the minimum suspension gap was 9.52 mm. The maximum fluctuation of suspension gap was 0.48 mm, which was much less than 2 mm. The suspension system was basically in a stable state.

When the maglev train was loaded with a vertical random irregular track at a speed of 200 km/h, the vertical vibration accelerations of the three vibration measurement points on the vehicle body and levitation gaps were shown in Fig. 5.

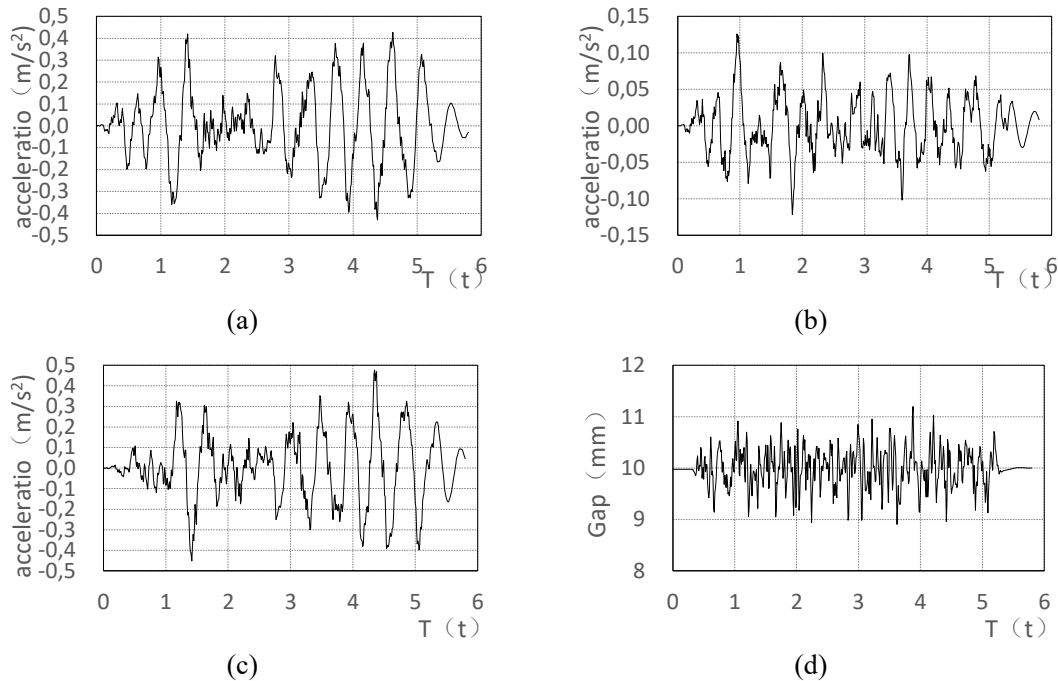


Fig. 5. Vertical Vibration Acceleration Curves of Front, Middle and Tail of 200 km/h (a),(b),(c), and the suspension gap variation curve (d)

It could be calculated that the vertical effective accelerations of the front, middle and rear marking points of the carriage during the integration period were 0.17 m/s^2 , 0.039 m/s^2 , 0.16 m/s^2 , the vertical effective vibration acceleration at the front, middle and rear of the carriage were all less than 0.315 m/s^2 . Passengers would not feel uncomfortable and comfort level 1. In the front and the tail part of the carriage, the acceleration value exceeds 0.315 m/s^2 in some periods, and the maximum acceleration value was 0.48 m/s^2 . Passengers will feel slightly uncomfortable as comfort level 2, duration was 1.1 s, about 18 % of the integration period. In general, the vertical acceleration of the front part of the carriage and the rear part of the carriage were obviously greater than that of the central part of the carriage. The RMS value was approximately 2.6 times that of the middle part of the carriage. The vibration of the vehicle body was dominated by the nodding vibration.

Suspension gap was stable at 10 mm before and after entering the irregular track. The maximum suspension clearance was 11.2 mm at the irregular track, the minimum suspension gap was 8.91 mm. The maximum fluctuation of suspension gap was 1.2 mm, which was much less than 2 mm. The suspension system was basically in a stable state.

When the maglev train was loaded with a vertical random irregular track at a speed of 300 km/h, the vertical vibration accelerations of the three vibration measurement points on the vehicle body and levitation gaps were shown in Fig. 6.

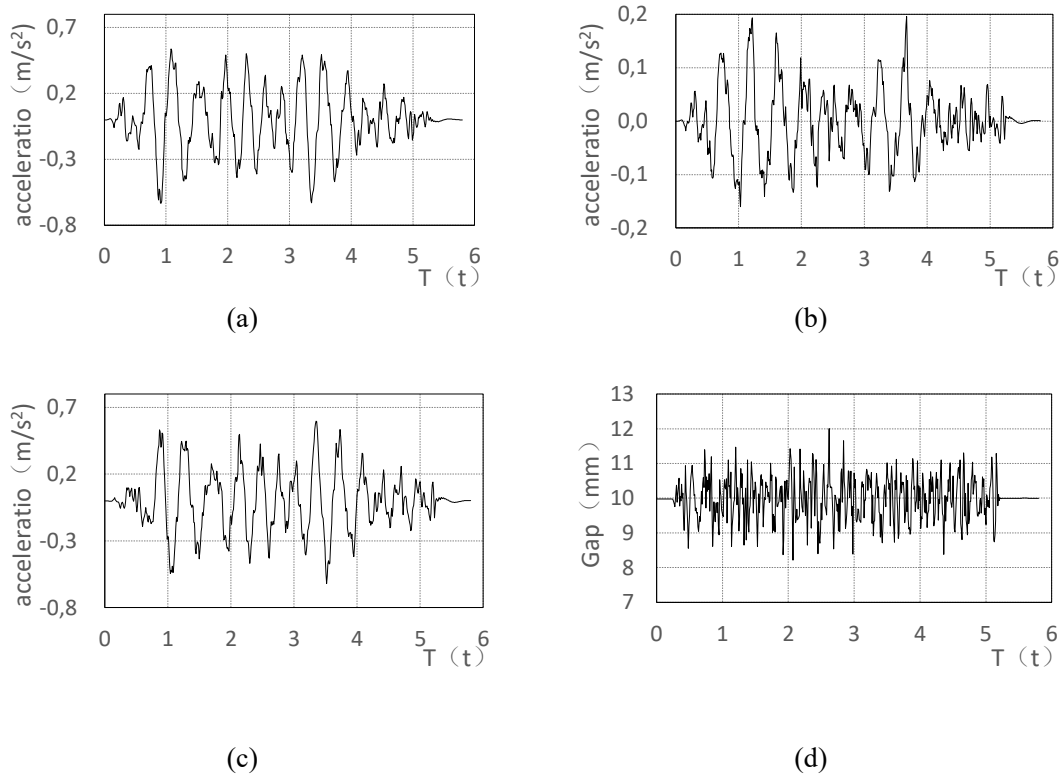


Fig. 6. Vertical Vibration Acceleration Curves of Front, Middle and Tail of 300 km/h (a), (b), (c), and the suspension gap variation curve (d)

It could be calculated that the vertical effective accelerations of the front, middle and rear marking points of the carriage during the integration period were $0.23 m/s^2$, $0.062 m/s^2$, $0.22 m/s^2$, the vertical effective vibration acceleration at the front, middle and rear of the carriage were all less than $0.315 m/s^2$. Passengers would not feel uncomfortable and comfort level 1. In the front and the tail part of the carriage, the acceleration value exceeds $0.315 m/s^2$ in some periods, and the maximum acceleration value was $0.63 m/s^2$. Passengers would feel slightly uncomfortable as comfort level 3. However, it only appeared for a moment. Most of the time, the comfort level was grade 1 or 2, which accounted for 53 % and 47 % of the integration time period. In general, the vertical acceleration of the front part of the carriage and the rear part of the carriage were obviously greater than that of the central part of the carriage. The RMS value was approximately 3.6 times that of the middle part of the carriage. The vibration of the vehicle body was dominated by the nodding vibration.

Suspension gap was stable at 10mm before and after entering the irregular track. The maximum suspension clearance was 12.01 mm at the irregular track, the minimum suspension gap was 8.21 mm. The maximum fluctuation of suspension gap was 2.01 mm, which exceeds 2 mm, but the overshoot was very small and the suspension system was stable.

When the maglev train was loaded with a vertical random irregular track at a speed of 400 km/h, the vertical vibration accelerations of the three vibration

measurement points on the vehicle body and levitation gaps were shown in Fig. 7.

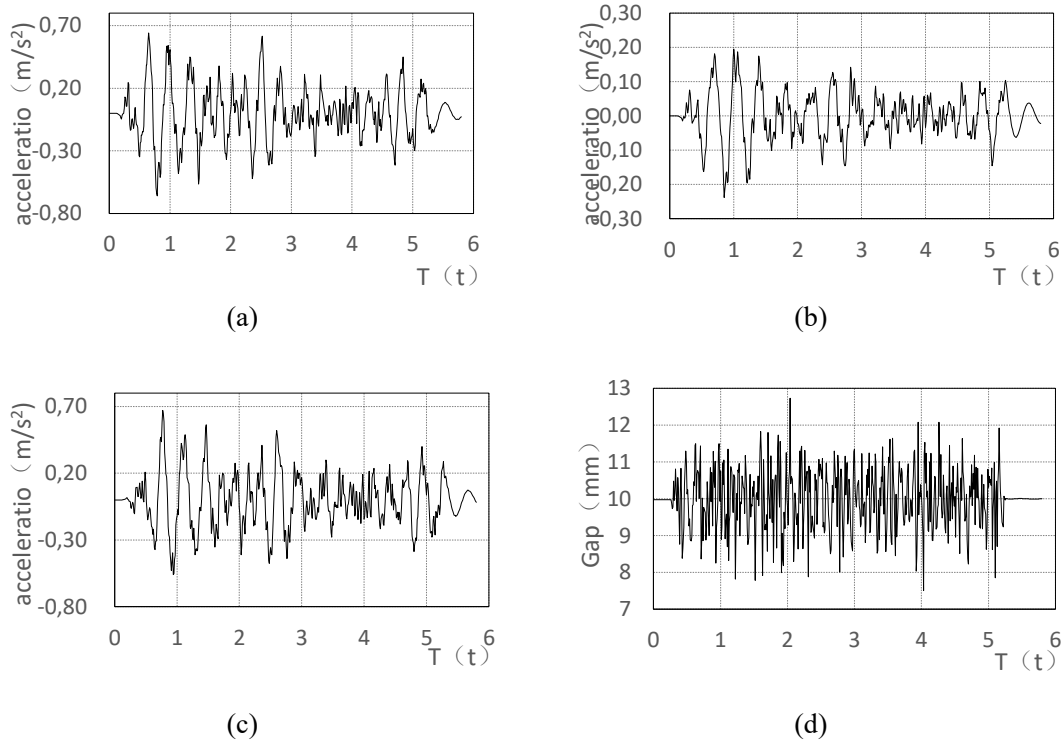


Fig. 7. Vertical Vibration Acceleration Curves of Front, Middle and Tail of 400 km/h (a), (b), (c), and the suspension gap variation curve (d)

It could be calculated that the vertical effective accelerations of the front, middle and rear marking points of the carriage during the integration period were 0.21 m/s^2 , 0.069 m/s^2 , 0.20 m/s^2 , the vertical effective vibration acceleration at the front, middle and rear of the carriage were all less than 0.315 m/s^2 . Passengers would not feel uncomfortable and comfort level 1. In the front and the tail part of the carriage, the acceleration value exceeds 0.63 m/s^2 in some periods, and the maximum acceleration value was 0.67 m/s^2 . Passengers would feel slightly uncomfortable as comfort level 3. However, it only appeared for a moment. Most of the time, the comfort level was grade 1 or 2, which accounted for 69 % and 31 % of the integration time period. In general, the vertical acceleration of the front part of the carriage and the rear part of the carriage were obviously greater than that of the central part of the carriage. The RMS value was approximately 2.9 times that of the middle part of the carriage. The vibration of the vehicle body was dominated by the nodding vibration.

Suspension gap was stable at 10mm before and after entering the irregular track. The maximum suspension clearance was 12.73 mm at the irregular track, the minimum suspension gap was 7.50 mm. The maximum fluctuation of suspension gap was 2.73 mm, which exceeds 2 mm, but the overshoot was very small and the suspension system was stable.

When the maglev train was loaded with a vertical random irregular track

at a speed of 500 km/h, the vertical vibration accelerations of the three vibration measurement points on the vehicle body and levitation gaps were shown in Fig. 8.

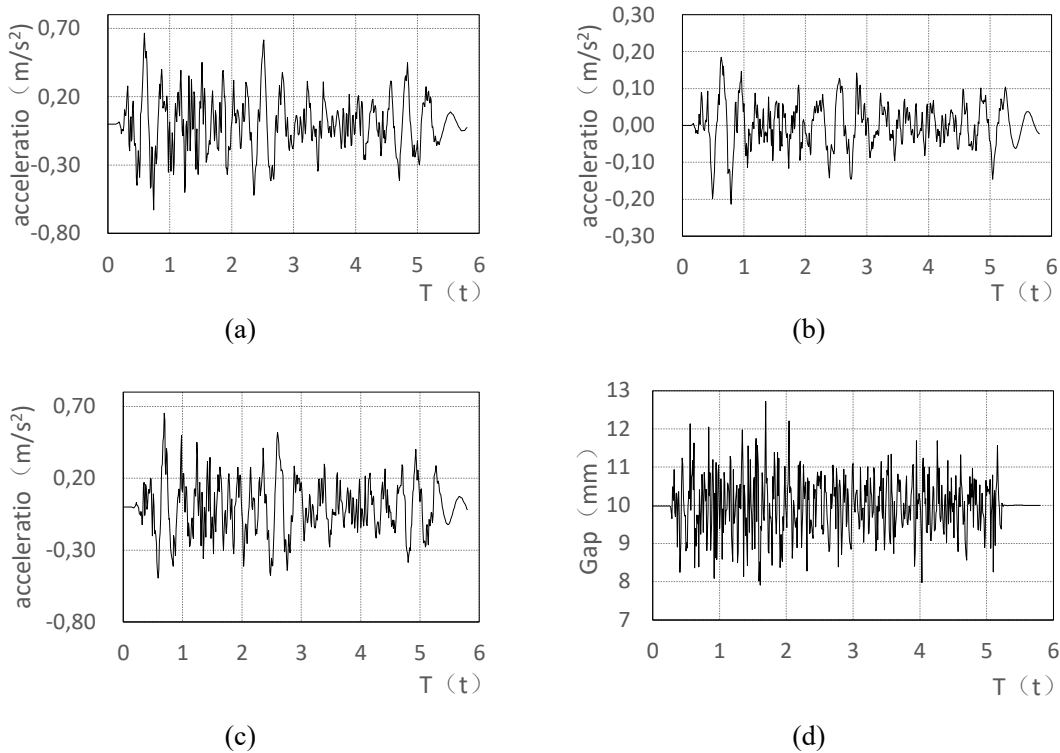


Fig. 8. Vertical Vibration Acceleration Curves of Front, Middle and Tail of 500 km/h (a),(b),(c), and the suspension gap variation curve (d)

It could be calculated that the vertical effective accelerations of the front, middle and rear marking points of the carriage during the integration period were 0.2 m/s^2 , 0.06 m/s^2 , 0.16 m/s^2 , the vertical effective vibration acceleration at the front, middle and rear of the carriage were all less than 0.315 m/s^2 . Passengers would not feel uncomfortable and comfort level 1. In the front and the tail part of the carriage, the acceleration value exceeds 0.63 m/s^2 in some periods, and the maximum acceleration value was 0.66 m/s^2 . Passengers would feel slightly uncomfortable as comfort level 3. However, it only appeared for a moment. Most of the time, the comfort level was grade 1 or 2, which accounted for 77 % and 23 % of the integration time period. In general, the vertical acceleration of the front part of the carriage and the rear part of the carriage was obviously greater than that of the central part of the carriage. The RMS value was approximately 3 times that of the middle part of the carriage. The vibration of the vehicle body was dominated by the nodding vibration.

Suspension gap was stable at 10mm before and after entering the irregular track. The maximum suspension clearance was 12.72 mm at the irregular track, the minimum suspension gap was 7.90 mm. The maximum fluctuation of suspension gap was 2.72 mm, which exceeds 2 mm, but the overshoot was very

small and the suspension system was stable.

Continue to increase the speed, it can be found that the frame vibration acceleration and suspension gap fluctuations have a tendency to decline. Fig. 9 was the curve of the maximum vibration acceleration and suspension gap fluctuation of the vehicle body at a vehicle speed of 100 km/h ~ 700 km/h. It could be seen from the figure that the maximum value of vibration acceleration and the variation trend of the fluctuation of the suspension gap were inverted U-shape, the maximum value appears near the speed of 400 km/h, and the vertical maximum vibration acceleration appears at the rear of the compartment with the maximum value of 0.67 m/s^2 , and the gap fluctuation was 2.73 mm.

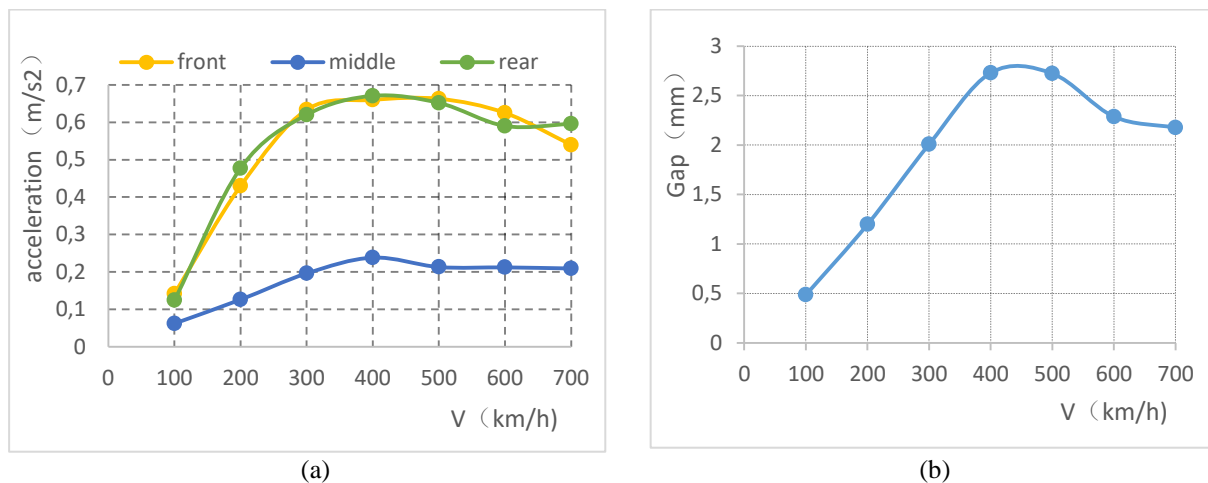


Fig. 9. The curve of the maximum vibration acceleration(a), and suspension gap fluctuation of the vehicle body (b) at a vehicle speed of 100 km/h ~ 700 km/h

The normal operating speed of Shanghai high-speed maglev train was generally 430 km/h. This control effect was not the most effective, the usual approach was to increase the suspension stiffness, and reduce the suspension stiffness, increase the suspension stiffness could make the vibration peak moves backward, reduce the suspension stiffness could move the vibration peak forward. Due to the large levitation control stiffness of the maglev train, if the stiffness was increased, the peak value may continue to appear when the vehicle speed increases. Therefore, we adopted a method to reduce the levitation stiffness. After trials, it was reasonable to choose K_p to be 5.8 E6N/m , and T_i and T_d remain unchanged. The peak of the vibration and guidance gap move forward to about 300 km/h. The curve of the maximum vibration acceleration and suspension gap fluctuation of the adjusted model was shown in Fig. 10. When the train was running at normal speed, the vibration and suspension stability were better.

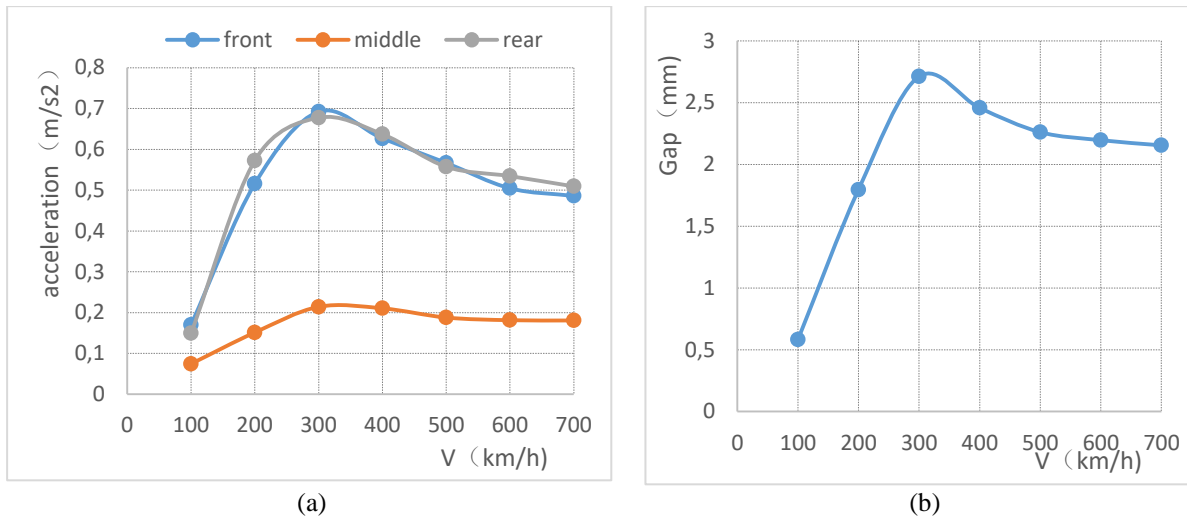


Fig. 10. the curve of the maximum vibration acceleration (a), and suspension gap fluctuation of the vehicle body (b) at a vehicle speed of 100 km/h ~ 700 km/h

CONCLUSION

Under the vertical irregular excitation of the track, the vertical acceleration of the vehicle body and the fluctuation of the suspension gap increased first and then decreased as the vehicle speed increased. Under the control of PID parameters, the vertical vibration acceleration of the car body and the peak value of the gap fluctuation of the suspension gap appeared at about 400 km/h. The passenger comfort level was class 1 in the compartment, 2 or 3 grades in some areas, and the fluctuation of the suspension gap was up to 2.73 mm. After adjusting the parameters of the PID, the peak value of the suspension gap appeared around 300 km/h, when the vehicle speed was 400 km/h, the maximum fluctuation of the suspension gap was 2.42 mm, which was reasonable.

ACKNOWLEDGMENTS

The research described in this paper was financially supported by the National 13th Five-Year Science and technology support program (Project No: 2016YFB1200602).

References

1. Ju SH, Leong CC, Ho YS. Control of Maglev trains moving on Bridges during foundation settlements. In: Chan K, Yeh J, editors. *Science and Engineering Research Center*. 2015: International Conference on Computer Information Systems and Industrial Applications; 2015 June 28–29; Bangkok, Thailand: Atlantis Press; 2015. p. 704–708. doi: 10.2991/cisia-15.2015.192
2. Li P, Hu W. Influence Analysis of Magnetic Track Beam Irregularity on the Suspended State. *Electric Drive for Locomotives*. 2016:65-68 (In China).
3. Fan Q. Discussion on the Demand of High-speed EMS Vehicle on Guideway

- Irregularity. *China Railway Science*. 2002;23:73-76 (In China).
4. Liu Z, Lin J. Evaluation and measurement for vehicle by ride comfort and ride index. *China Measurement Technology*. 2004;(2):39-40 (In China).
 5. Zhang X, Xie X, Yang S. Comparison of the Index Evaluating Railway Vehicle Comfort. *Journal of Jiamusi University (Natural Science Edition)*. 2011;29:661-666.
 6. Chen G, Zhai W, Zuo H. Comparing track irregularities PSD of Chinese main lines with foreign typical lines by numerical simulation computation. *Journal of the China Railway Society*. 2001;23:82-87 (In China).
 7. Department of Science and Technology of the Ministry of Railways, Southwest Jiaotong University. *ICE technical mission document for the German Federal Railways Intercity Express Train*. Chengdu: Southwest Jiaotong University Press; 1993. p. 301–309.

Information about the authors:

Jingyu Huang, Doctor of Civil Engineering, Professor; 021-69580183; National Maglev Transportation Engineering R&D Center, Tongji University, Shanghai, China.
ORCID: 0000-0001-6930-9354;
E-mail: huangjingyu@tongji.edu.cn

Xiong Zhou, Candidate of Master Degree
ORCID: 0000-0002-6341-4994;
E-mail: xiaoxiong@tongji.edu.cn

Liwei Shang, Master Degree
ORCID: 0000-0002-1516-3625;
E-mail: livesoph@qq.com

Zhewei Wu, Candidate of Master Degree
ORCID: 0000-0002-0454-2750;
E-mail: 1630355@tongji.edu.

Weinan Xu, Candidate of Master Degree
ORCID: 0000-0003-4083-423X;
E-mail: xu473933@163.com

Dongzhou Wang, Candidate of Master Degree
ORCID: 0000-0002-5296-3031;
E-mail: wangdongzhou@tongji.edu.cn

To cite this article:

Huang J, Zhou X, Shang L, Wu Z, et al. Influence Analysis of Track Irregularity on Running Comfort of Maglev Train. *Transportation Systems and Technology*. 2018;4(2):129-140. doi: 10.17816/transsyst201842129-140

DOI 10.17816/transsyst201841141-151

© Q. Lai¹, J. Liu¹, L. Meng¹, X. Chai¹, Q. Wang¹, Y. Xu²

¹State Key Laboratory of Rail Traffic Control Safety

Beijing Jiaotong University

(Beijing, China)

²CRRC Tangshan Co., Ltd

(Tangshan, China)

OPTIMIZATION OF THE AUXILIARY STOPPING AREA PLANNING IN THE MIDDLE-TO-HIGH SPEED MAGLEV

Background: The Auxiliary Stopping Area (ASA) is the special section that possesses power supply rail and personnel evacuation facilities, whose quantities and locations in a line are of great significance to reduce construction cost and improve transportation efficiency for the middle-to-high speed maglev.

Aim: This paper focuses on optimizing the length and location of the ASA for the middle-to-high speed maglev system to improve the robustness of maglev line.

Methods: Two evaluation indexes which reflect the ASA restricts on the train operation process was proposed. A model for optimizing the setting of the ASA is constructed, and solved by the genetic algorithm.

Results: The result of numerical examples shows that the proposed method can effectively improve the performances of the ASA.

Conclusion: This paper proposed two indexes to reflect the impact of station settings on train operations, which provides a method to optimize the ASA from qualitative optimization to quantitative optimization.

Keywords: the middle-to-high speed, maglev, line optimization, quantitative analysis, auxiliary stopping area, ASA, genetic algorithm

1. INTRODUCTION

As from January 1, 2018, there are four commercial operations of Maglev line in the world was built, and maglev has received more and more attention in China [1]. Compared with the wheel-rail system, the maglev has some excellent characteristics, such as smaller turning radius, lower noise, stronger climbing ability and lower maintenance cost [2]. The maglev system includes three-speed grades: low-to-middle speed maglev ≤ 100 km/h, middle-speed maglev ≤ 200 km/h and high-speed maglev ≤ 400 km/h. At present, except for the low-to-middle speed maglev uses short stator induction linear motor technology [3], the other two all take the long stator synchronous linear motor technology [4, 5]. Therefore, the middle-speed maglev and high-speed maglev are similar inline settings. In this paper, the middle-to-high speed maglev is used to represent the middle-speed maglev and high-speed maglev.

Generally, the safety operation of the middle-to-high maglev train needs to satisfy the following five-speed curve limits [5, 6]. The location and length of the ASA will affect the speed limit area in case the other line parameters were determined because only the ASA and station were installed with Power Rail (PR). The function of PR enables the maglev train to run again after it stops [7]. However, the ASA cannot cover all line because of the construction cost. Therefore, it is a dramatic significance to reasonably arrange the location and length of the ASA with the goal that guaranteed safe operation and low cost.

At present, some researchers mainly focus on optimizing the operating strategies of the maglev train which the location and length of the ASA were determined [8, 9]. However, when the bottlenecks of operation were considered during the design of the ASA, the implementation of operational strategies will be more feasible. A simulation optimization method was built by Bian [10], but no specific optimization goals were given by him, just optimize the ASA through qualitative judgment. So, in this paper, the restrictions of the ASA on the train operation process was analyzed in order to give a quantitative model.

The remainder of this article is organized as follow. **In Section 2**, the concept of the ASA was introduced, and the two evaluation indexes which reflect the ASA restricts on the trajectory planning was proposed. A model for optimizing the setting of the ASA is constructed, and the genetic algorithm is built to solve this model in **Section 3**. Numerical examples are given to validate the proposed methods in **Section 4**. Finally, **Section 5** gives the conclusion of this paper.

2. CONCEPTUAL ILLUSTRATION

In this section, the impact of the ASA was introduced, and two evaluation index was put forward to quantitatively describe the impact of the ASA on the train operation process.

2.1 The impact of the ASA

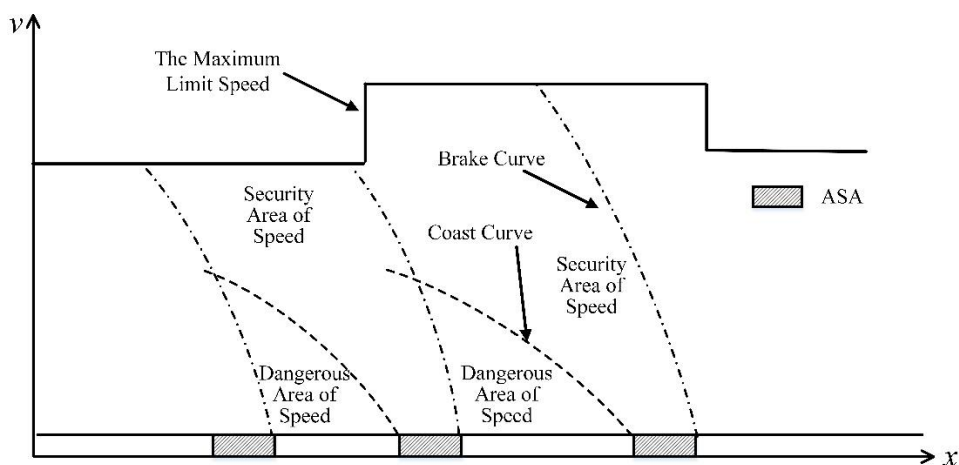


Fig 1. The impact of the ASA

Safe operation is a most important goal for every per transport system. Due to the operating mechanism of the MHSM (middle-to-high speed maglev), it has created a safety concept of “safe parking”. Safe parking means that the maglev can park in the designated area which calls ASA in any condition including run interference, malfunction or emergency situation.

The suspension and guiding of the MHSM are active control. The energy of the suspension device, guide device, and emergency braking system are root in the vehicle power supply system. The vehicle power supply system is composed of two part which including battery and linear generator of the vehicle. Then, the vehicle power supply system will choose one as a power supply approach according to the speed of maglev. When the speed of maglev is lower than the set speed (high-speed maglev is 80 km/h and middle-speed maglev is 100 km/h), the vehicle power supply system is the battery of the vehicle. When the speed of maglev is super than the set speed, the vehicle power supply system is the linear generator of the vehicle. In an unusual situation when the power of traction system is interrupted, the battery should guarantee the maglev continue to stay in suspension and braking. If the battery cannot be charged before the battery is exhausted, the maglev will not be able to levitate again. Therefore, to ensure the maglev have enough energy to levitate in a special situation, a couple of the ASA has been set in the interstation. Moreover, to ensure the passenger can evacuate the scene, the personnel evacuation facilities also be set in the ASA.

As shown in Fig. 1, the train should operate in the security area of speed to guarantee the safety.

2.2 Quantitatively describe the impact of the ASA

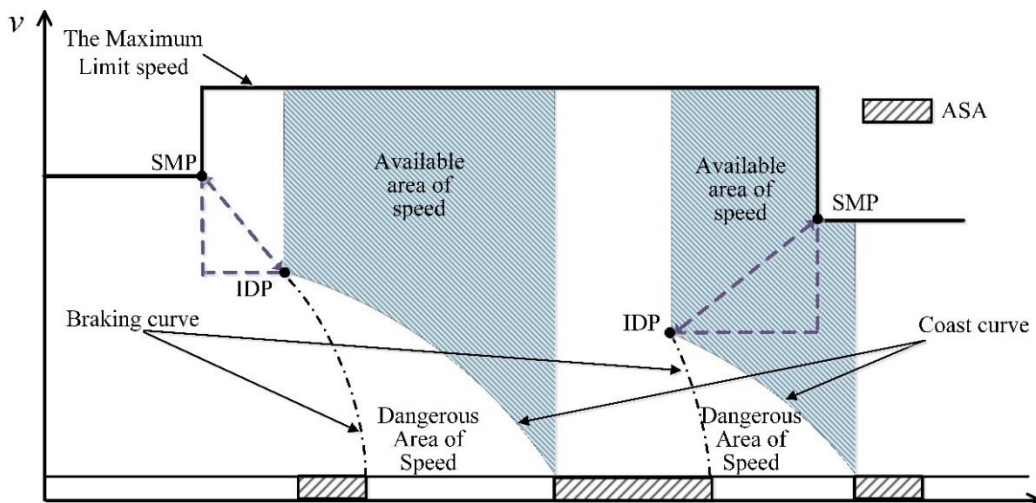


Fig. 2. Quantitatively describe the impact of the ASA

In this paper, the maximum limit speed is assumed to be known, which also indicated that the switching point of the maximum limit speed (SMP) was

determined. From the section 2.1, the maglev train should keep them operating in the security area of speed which was formed by the maximum limit speed, coast curve, and braking curve. The intersection of the braking curve and coasting curve was denoted as IDP.

Two quantification criteria which reflect the restrictions of the ASA on maglev train operation are discussed:

1. Available area of speed

As shown on the Fig. 2, the available area of speed is constructed by the maximum limit speed and coast curve. The smaller available area of speed is, the less selective speed can the train choose. Therefore, the available area of speed is taken accounted as an evaluation index for the impact of the ASA.

2. The Euclidean distance between the IDP and SMP

Relying solely on the index of the available area of speed is unable to meet the robustness of the operation because the train speed will also be fewer options when the IDP is closer to SMP. Thus, the Euclidean distance between the IDP and SMP is considered as the second evaluation index for the impact of the ASA.

3. METHODOLOGY

A model for optimizing the setting of the ASA was formulated considering the two evaluation index, and a genetic algorithm also was built to solve the model.

3.1 The optimization model of the ASA

Table 1. Basic variables

Symbol	Description
L	The length of the inner-station
L_A	The total length of the ASA
L_{\min}	The minimum length of the ASA
M	The number of the ASA
x	The point of the location
m	The index of the ASA, and $m \in [1, M]$.
x_m^{start}	The starting point of the m th ASA
x_m^{end}	The endpoint of the m th ASA
P	The number of the IDP
p	The index of the IDP, and $p \in [1, P]$
x_p	The location of the p th IDP
v_p	The speed of the p th IDP
C	The number of the SMP
c	The index of the SMP, and $c \in [1, C]$

Symbol	Description
x_c	The location of the c th SMP
v_c	The speed of the c th SMP
r	The cost of the ASA per meter

The minimum length of the ASA is determined, so the every ASA's length need to satisfy the Eq. (1.1):

$$x_m^{end} - x_m^{start} \geq L_{\min} \quad \forall m \in [1, M] \quad (0.1)$$

Due to reflect the relationship of different ASA on the line, we built the constraint as Eq. (1.2).

$$x_m^{end} \leq x_{m+1}^{start} \quad (0.2)$$

The total length of the ASA is limited by the length of inner-station, so:

$$\sum_{m=1}^M (x_m^{end} - x_m^{start}) = L_A \leq L \quad (0.3)$$

In here, we assume the coast curve and braking curve is determined. When we know the location of the ASA, we can calculate every IDP via the coast curve and braking curve.

From the Section 2, we know that the object goal function includes three aspects.

1. The available area of speed

We denote $p_m (p_m \in [1, P])$ is the index of the IDP which is the closest location among all the IDP to the m th ASA, and the location also is before the m th ASA.

$$p_m = \left\{ p : \min(x_m^{start} - x_p), \forall p \in [1, P] \right\} \quad (0.4)$$

The function of the maximum speed is $f^{\max}(x)$, and the $f_m^c(x)$ means the coast curve of the m th ASA. Owing to the coast curve is a non-linear function, so we reference the principle of calculus to divide the area into a small rectangle, and every length of a rectangle is Δx_m for the m th ASA's area. Δx_m can be calculated as Eq. (1.6), and Δx is the distance span which is determined.

So the available area of speed f^a can be calculated as Eq. (1.5).

$$f^a = \sum_{m=1}^M \left(\sum_{q_m=0}^{Q_m} 1 / \left(\left(f^{\max}(x_{p_m} + q_m \Delta x_m) - f_m^c(x_{p_m} + q_m \Delta x_m) \right) + \left(f^{\max}(x_{p_m} + (q_m + 1) \Delta x_m) - f_m^c(x_{p_m} + (q_m + 1) \Delta x_m) \right) \right) \right) \left(\Delta x / 2 \right) \quad (1.5)$$

The number of the rectangle indicated as Q_m , which can be calculated by Eq. (1.7).

$$\Delta x_m = \begin{cases} \Delta x & q_m < Q_m \\ (x_m^{start} - x_{p_m}) - (Q_m - 1) \Delta x & \end{cases} \quad (1.5)$$

$$Q_m = \left[(x_m^{start} - x_{p_m}) / \Delta x \right] \quad (1.6)$$

$[\bullet]$ is the symbol of down to the nearest integer.

2. The Euclidean distance between the IDP and SMP

We assume c_p ($c_p \in [1, C]$) is the index of the SMP which is the closest location among all SMP to the p th IDP, so:

$$c_p = \{c : \min |x_p - x_c|, \forall c \in [1, C]\} \quad (1.7)$$

Because the shorter of the distance between the SMP and IDP, the larger of the speed area for the maglev train. Thus, the concept of inverse function is considered in the model, so the Euclidean distance can be acquired by Eq. (1.9).

$$f^b = \sum_{p=1}^P \frac{1}{\sqrt{\left((x_{c_p} - x_p)^2 + (v_{c_p} - v_p)^2 \right)}} \quad (1.8)$$

From above, the objective function is Eq. (1.11), and α is the weights of f^b .

$$\min Z = f^a + \alpha f^b \quad (1.9)$$

3.2 The genetic algorithm to optimize the ASA

Owing to the variables x_m^{end} , x_m^{start} cannot be expressed directly in the f^a , f^b , which cause the object function is non-close-form. So, in this paper, we

built a genetic algorithm to solve the model.

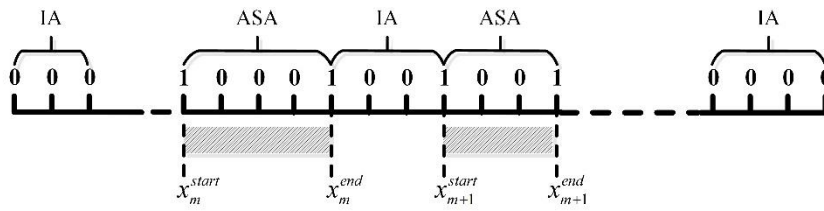


Fig 3. Chromosome representation of the setting of the ASA

We divide the inner-station into a small segment. As an illustration, Fig.3 shows that we mark up the split point as 1 or 0, and the span between a pair of 1 which does not contain 0 indicates that there exists an ASA, and the number of the segment for the m th ASA is c_m . Thus, by exchange, the values of the split point, a series of ASA which ranks in order will be acquired. There will exist interval area (IA) between two ASA, and the number of IA is $(M + 1)$, and $d (d \in [1, M + 1])$ is the index of IA. The number of the segment for the d th IA is denoted as c_d .

Subject to constraints Eq. (1.1)~Eq. (1.3), the method which transfers the binary variable to locations of the ASA was proposed.

(1) Calculate the length of the m th ASA.

$$x_m^{end} - x_m^{start} = L_{\min} + \left(\frac{c_m - 1}{c_{\min}} \right) (L_A - ML_{\min}) / \sum_{m'=1}^M \left(\frac{c_{m'} - 1}{c_{\min}} \right) \quad (0.10)$$

$$c_{\min} = \min \{ c_m : m \in [1, M] \} \quad (0.11)$$

c_{\min} is the minimum value among c_m .

(2) Calculate the length of the d th IA.

The length of d th IA is represented by l_d , so:

$$l_d = (L - L_A) c_d / \sum_{d'=1}^{M+1} c_{d'} \quad (0.12)$$

The process of the genetic algorithm to optimize the setting of the ASA is as follows, and K is a maximum number of iterations:

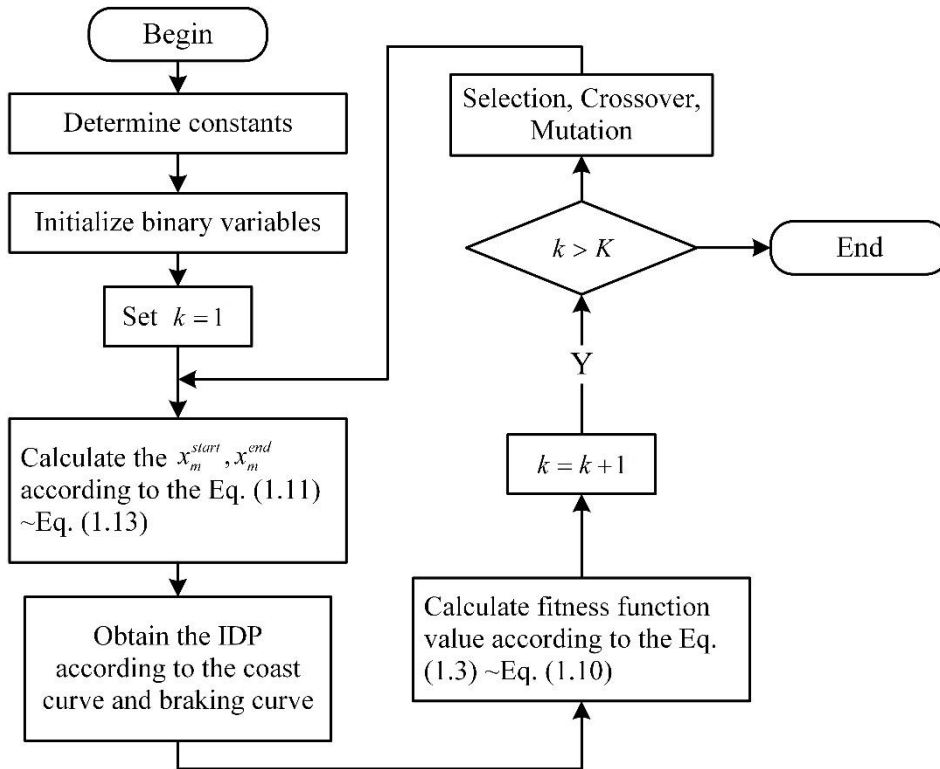


Fig. 4. The flow chart of the genetic algorithm to optimize the ASA

3. SIMULATION EVALUATION

A maglev line was constructed in order to validate the proposed model. The maximum limit speed was given as Table 2, and $L=9000\text{m}$, $L_A=4050\text{m}$. The braking curve and coast curve were obtained through the middle-speed maglev train which was under development by CRRC.

Table 2. The maximum limit speed

Speed limit section	speed
0~541.5	80
541.5~1431.2	200
1431.2~1534.7	80
1534.7~1849.7	180
1849.7~2107.5	100
2107.5~2660.8	200
2660.8~3263.8	120
3263.8~3906.2	150
3906.2~4556.9	200
4556.9~5329.6	180
5329.6~5621.9	100
5621.9~6058.3	200
6058.3~7018.6	80
7018.6~7190.5	200
7190.5~8328.4	100
8328.4~9000.0	80

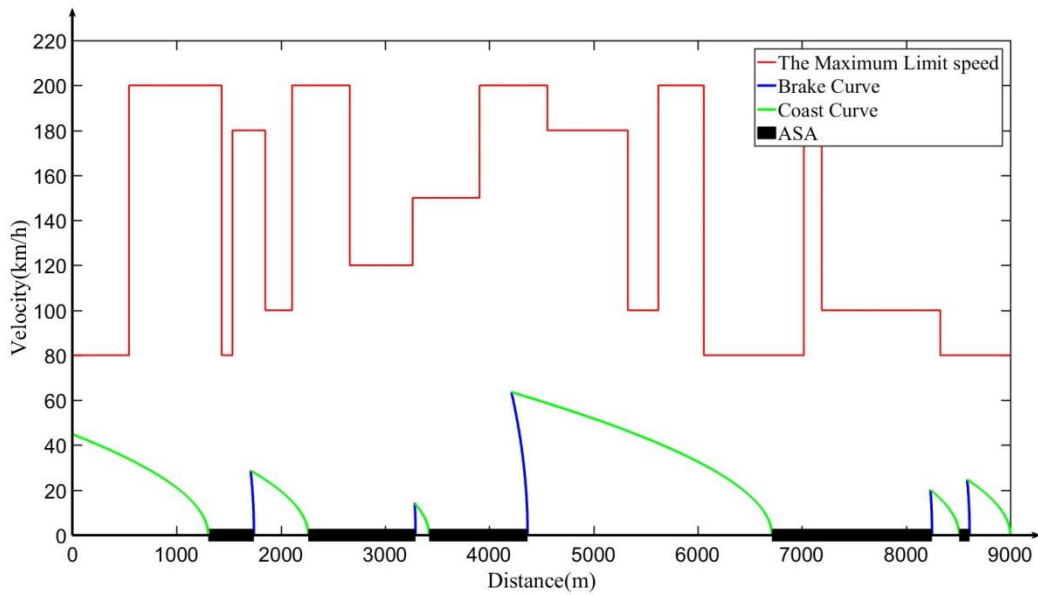


Fig. 5. The setting situation of the ASA before optimize

Fig. 5 shows the setting situation of the ASA which was produced by random initialization process. The number of the ASA is five, and maximum length of the ASA is 1536.9 m. The maximum length of the IA is 2344.7 m, which leads to the available area of speed too smaller.

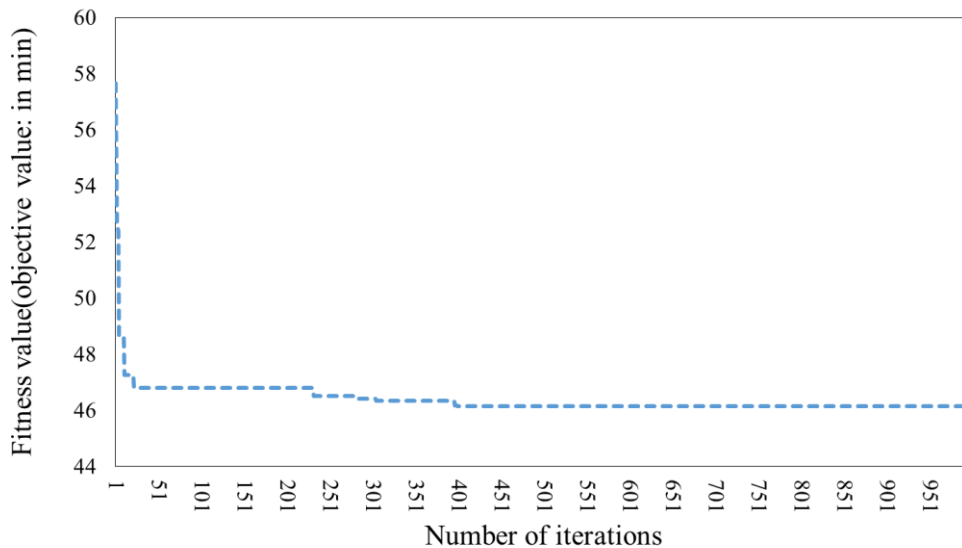


Fig. 6. The setting situation of the ASA after optimize

As illustrated in Fig.6, the iterative results of the genetic algorithm, and the minimum objective value decreases with increasing algebra until it is stationary. It is concluded that the genetic algorithm method can find better value for the model.

The result of 1000th generation was shown in Fig. 7. Compared with Fig. 5, it is can be found that the number of the ASA is greatly increased, and maximum length of IA is reduced. The changes of the ASA will guarantee the maglev train operate in safety, even the speed of the train is lower. Therefore, the result shows that the proposed model for optimizing the setting of the ASA was practical.

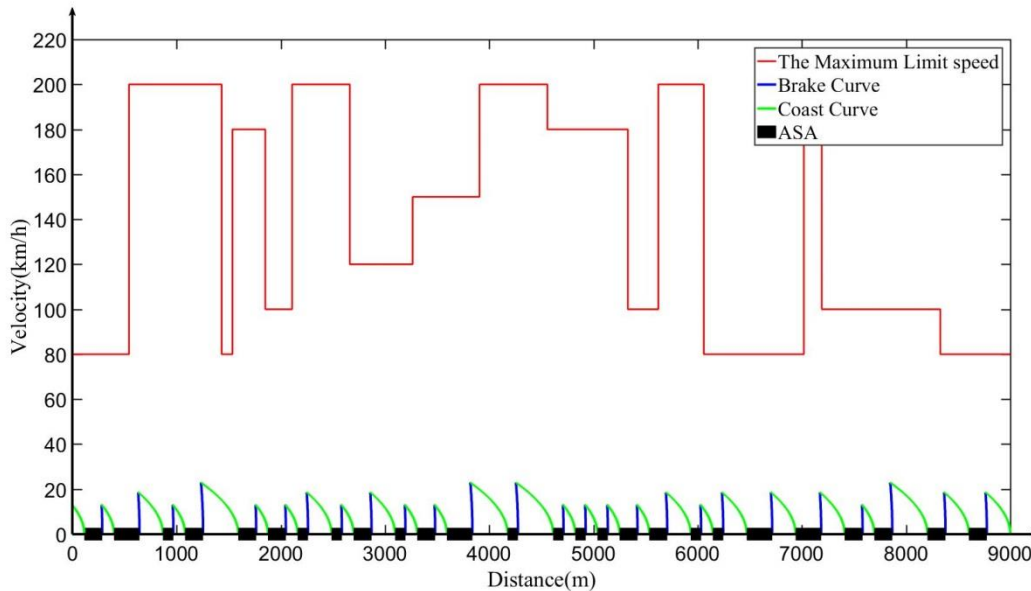


Fig.7. The iterative results of the genetic algorithm

5. CONCLUSION

A model to optimize the setting of the ASA on the middle-to-high speed maglev considering the operating robustness was built in this paper. This paper proposed two indexes to reflect the impact of station settings on train operations, which provides a method to optimize the ASA from qualitative optimization to quantitative optimization. The result of numerical examples shows that the proposed method can effectively improve the performances of the ASA.

In the future, we hope that the more line parameter is considered, which will make the model more practical. Furthermore, the impact of the ASA on multi-train also will be researched in the future.

ACKNOWLEDGMENT

The authors acknowledge the financial support of the National Key R&D Program of China (2016YFB1200600).

References

1. Yan L. Development and Application of the Maglev Transportation System [J]. *IEEE*

- Transactions on Applied Superconductivity*, 2008;18(2):92-99. doi: 10.1109/tasc.2008.922239
2. Lee HW, Kim KC, Ju L. Review of maglev train technologies [J]. *IEEE Transactions on Magnetics*, 2006;42(7):1917-1925. doi: 10.1109/tmag.2006.875842
 3. Xiao S, Zhang K, Liu G, et al. Optimal design of a for middle-low-speed maglev trains [J]. *Open Physics*, 2018;16:168-173. doi: 10.1515/phys-2018-0024
 4. Bing L, Tan X, Li Q, et al. The analysis of excitation current changes in long stator linear synchronous motor of maglev [C]. *Prognostics and System Health Management Conference. IEEE*, 2014:410-413. doi: 10.1109/phm.2014.6988204
 5. Zhang W, Wei W, Yang Y, et al. An Operation Control Strategy for the Connected Maglev Trains Based on Vehicle-Borne Battery Condition Monitoring [J]. *Wireless Communications & Mobile Computing*, 2018;(4):1-10. doi: 10.1155/2018/5698910
 6. Liu J, Wenqi WU. Research on 2-D Speed Protection Curve and Its Algorithm of High-speed Maglev Transportation [J]. *China Railway Science*, 2002;23(4):106-110.
 7. Chen D, Yin J, Chen L, et al. Parallel Control and Management for High-Speed Maglev Systems [J]. *IEEE Transactions on Intelligent Transportation Systems*, 2017;18(2):431-440. doi: 10.1109/tits.2016.2577037
 8. Jiang Y, Wu W, Liu J. Simulation of High-speed Maglev Train 2-D Speed Protection Curve [J]. *Journal of Tongji University (Natural Science)*, 2004;32(3):397-400.
 9. Liu Y. Basic Theory Research on New-type Maglev Train Operation Control System [D]. *Beijing Jiaotong University*, 2004.
 10. Bian J. Study on the Relevant Properties of the Maglev Train Operation Control System and the Characteristics of Auxiliary Stopping Area [D]. *Zhejiang University*, 2006.

Information about the authors:**Qingying Lai**, Ph.D. candidate;

ORCID: 0000-0001-8757-3183;

E-mail: yingzhikuangyu@163.com

Jun Liu Ph.D., Professor;

ORCID: 0000-0003-3242-3182

E-mail: jliu@bjtu.edu.cn

Lingyun Meng, Ph.D., Assistant Professor;

ORCID: 0000-0003-1999-1935;

E-mail: lym@bjtu.edu.cn

Xiaofeng Chai, Master graduate student,

ORCID: 0000-0002-4043-6672;

E-mail: 16120757@bjtu.edu.cn

Qunyan Wang, Master graduate student,

ORCID: 0000-0003-2448-4364;

E-mail: 16125780@bjtu.edu.cn

Yazhi Xu, Master, Assistant Engineer,

ORCID: 0000-0003-2224-5925;

E-mail: 16120757@bjtu.edu.cn

To cite this article:

Lai Q, Liu J, Meng L, et al. Optimization of the Auxiliary Stopping Area Planning in the Middle-to-High Speed Maglev. *Transportation Systems and Technology*. 2018;4(2):141-151 doi: 10.17816/transsyst201842141-151

DOI 10.17816/transsyst201842152-166

© R. Kircher¹, J. Klühspies¹, R. Palka², E. Fritz³, K. Eiler¹, M. Witt¹

¹The International Maglev Board

(Deggendorf, Germany)

²Department of Power Systems & Electrical Drives, West Pomeranian

University of Technology

(Szczecin, Poland)

³IfB - Institut für Bahntechnik

(Dresden, Germany)

ELECTROMAGNETIC FIELDS RELATED TO HIGH SPEED TRANSPORTATION SYSTEMS

Issue: The potential health risks on passengers and the environment related to electromagnetic fields caused by the operation of electrically driven high speed transportation systems has become a major issue. Especially the magnetic flux density or induction can generate physiological effects in body tissues.

Aim: In this paper, we compare calculated and experimental values of electromagnetic fields in rail-wheel systems such as ICE with the Maglev-systems Transrapid and the JR Maglev-system, based on available data.

Methods: To estimate the impact on passengers, the field contributions generated by the power supply system as well as by the drive and suspension systems are taken into account. For the comparison, the peak values of the electromagnetic fields have been considered.

Results: The results show, that there are no health risks from the electric fields. Regarding the magnetic induction, the calculated the peak values remain well below the limits given by national regulations. In the case of the Transrapid and the JR Maglev system, the measured peak values in the environment and inside the vehicle depend on the levitation and the guidance technology and the geometrical parameters. The JR Maglev system requires effective magnetic shielding measures which are connected with heavy materials. Since such materials may have a negative influence on the energy balance and the economics of operation, R&D efforts are focusing on the optimization of materials and the structure of shields.

Conclusion: In high speed transportation systems there are no potential risks from electrical fields. Regarding magnetic fields, the induction generated by the power supply and the drive system remain well below the frequency dependent limits. The situation is different for magnetic levitation systems, depending on the suspension and guidance technology. Especially the JR Maglev requires effective shielding measures. The shielding materials may have a negative impact on the energy balance.

Keywords: Electromagnetic fields, Physiological effects, Health risks, High speed transportation systems, Rail-wheel systems, ICE, Transrapid, Maglev

INTRODUCTION

Biological effects of electromagnetic fields are among the most serious environmental concerns in the public regarding health risks and quality of life.

The physiological effects of electrical, magnetic and electromagnetic fields on the human body are dependent on the frequency. The effects of static electric fields are limited to the surface of the human body and can cause motion of body hair and corona discharges.

Static magnetic fields exert forces on ferro- and diamagnetic materials as well as charged moving particles. This may lead to acceleration, torque effects and the induction of electric fields in the tissue.

In the low-frequency range up to some 100 kHz the main physiological effect is the electrical stimulation of excitable body tissues like muscles, nerves and sensory organs. Biological effects on nerves and other tissue of the body caused by induced currents are dominating. In the high frequency (HF) range thermal effects are increasingly important [1].

Because all electromagnetic fields (EMF) related biological effects in the low-frequency range are linked to peak values in the internal electrical field strength and magnetic flux density in body tissues all exposure limit values of the fields have to be taken into account. To reduce risks for health limits are imposed on the emission of electromagnetic fields (EMF). Table 1 shows the limits for the electric field strength and the magnetic induction for the different frequency ranges, as imposed by the German regulation BImSchV 26. In the case of high speed transportation systems, the low frequency range has to be considered, from static fields to frequencies up to about 1 kHz.

Table 1. Limits for the emission of electromagnetic fields, valid in Germany provided by the regulation BImSchV 26. The magnitude f is the frequency

Frequency (Hz)	Electric field strength (kV per meter)	Magnetic induction (μ Tesla)
0	-	500
1 – 8	5	40 000/ f
8 – 25	5	5 000/ f
25 – 50	5	200
50 – 400	250/ f	200
400 – 3 000	250/ f	80 000/ f
3 000 – 10 000 000	0.083	27

The article compares the electromagnetic fields generated by high speed transportation systems by a typical railway system and Maglev systems, based on available data. As examples for the comparison, the German high speed train ICE, the German magnetic levitation system Transrapid (TR), and the Japanese Maglev systems have been selected. The present comparison is focusing on the

electromagnetic field distribution and its influence to the passengers and on the environment outside. In the comparison, the maximum values of the electrical and magnetic fields are calculated.

In other European countries and Overseas similar upper limits exist, depending on the corresponding regulations.

In electrically powered high speed transportation systems, several contributions to the electromagnetic field distribution have to be considered:

- 1) Fields generated by the power supply system (external and internal);
- 2) Fields generated by the drive / motor system.

Other contributions from air condition and lighting are neglected in this comparison.

BASIC PHYSICAL RELATIONS

Electrical field

The maximum electrical field strength E_{max} is defined as

$$E_{max} = U_0/d \text{ [V/m]}, \quad (1)$$

where U_0 is the peak voltage and d the distance from the origin of the source of the field.

Magnetic field

The maximum magnetic field strength or magnetic induction B_{max} is given by

$$B_{max} = \mu_0 I_0 / (2\pi r) \text{ [T]}, \quad (2)$$

where μ_0 is the air permeability with a value of $4\pi \times 10^{-7}$ Vs/(Am), I_0 the peak current value, and r the distance from the wire or the current conductor.

The shielding of electrical fields can be realized in a simpler way than the shielding of magnetic fields since the metallic body of a train acts as a Faraday cage, shielding the internal space from low frequency electrical fields.

The efficient shielding of magnetic fields requires the application of special materials (ferromagnetic or superconducting). Therefore, much more attention has to be paid to emission of the magnetic fields generated by currents of the power supply and the drive system. These currents are determined by the power and the voltage level. The focus of the current investigation concerns the peak values of the power related magnetic fields.

RESULTS

Railway system

The power is supplied by substations feed by public or railway owned high voltage power grid to the transportation system via high voltage (HV) overhead wires. In general, the voltage level of AC systems is 15 kV or 25 kV with a frequency of 16.7 respectively 50 Hz. The maximum driving power is applied during acceleration of the train. The electrical peak power may achieve a value of several MW. The corresponding current value is in the range between several hundreds and a few kA along the pathway.

The drive system within the transportation equipment consists of inverters and three phase motors with a voltage level up to 2 kV. The frequency is in the range between 0 and 200 Hz [2]. The nominal operational speed considered for the ICE 3 is up to 330 km/h.

In general, two different situations for the exposure to electromagnetic fields have to be considered: 1. the emission of electromagnetic fields to the external environment, i.e. the impact to the neighbouring environment of the railway line, and 2. the exposure of passengers inside the train.

Calculation of the electrical field

1) The electrical field strength at a distance of 25 m from the overhead wire with a voltage of 25 kV is $E = 1000 \text{ V/m}$, which is well below the limit of 5000 V/m given in Table 1. Field strengths of 1 kV/m will cause in body tissue only a small electrical field of about 1 mV/m [1].

2) The estimation of the electrical field within the train is more complicated. The distance from the overhead wire is smaller but, on the other hand, the metallic roof of the wagon represents an electrical shielding. Therefore, the impact of the electrical fields from power supply of railway systems on the neighbouring environment and on passengers can be neglected.

Calculation of the magnetic field (induction)

To estimate the magnetic field or induction generated by the overhead power line, we have to consider the number of trains running within one section between 2 substations where the power is fed-in. At the newly, in Germany constructed ICE line between Nuremberg and Berlin, a typical distance between 2 substations is about 25 km. With 2–3 trains per hour in both directions, we can restrict to consider the power for 2 trains within the same section, only. In other words, the peak current in the overhead power line for at least 2 trains within this section could reach the value of $2 \times 850 \text{ A}$ in the case of 15 kV. At 25 kV the current is correspondingly lower. The magnetic induction generated by the peak current of 1700 A at a distance of 25 m from the overhead power line is $13.6 \mu\text{T}$, which lies well below the limit of $300 \mu\text{T}$ for the frequency of 16.7 Hz. Therefore, the impact of the magnetic field from the outside power supply to the

neighbouring environment along the railway line can be neglected.

The determination of the magnetic field or induction inside the train is more complicated. In the rail-wheel system and the example of the ICE 3, the power is supplied via the inverter stages to the motors. In case of the ICE, the mechanical power reaches 8000 kW at transition speed, respectively at the maximum speed of 330 km/h, delivered to 16 motors, each motor with a power of 500 kW. The driving concept consists of 16 motors, divided into 4 sections with 4 motors in each section [2]. We therefore focus on one section which supplies a power of 2000 kW. The power is delivered to the motors via a 3 stage transformation/conversion system: A single phase transformer transforms the voltage of 25 kV or 15 kV from the overhead line at the frequency of 50 Hz respectively 16.7 Hz to 2×1100 V. At the second stage, the AC voltage of 1100 V is converted into a DC voltage of 2800 V by 2 converters. At the third stage, the DC voltage is again converted to a 3-phase AC voltage ranging from 0 to 2000 V and a variable frequency in the range from 0 to 200 Hz which is applied to the 4 motors. As a result, a maximum efficient current value of 250 A is flowing to each motor at a constant speed of 330 km/h on a flat track.

For the calculation of the magnetic field inside the train, the current values at each stage have to be considered, in addition to the field induced by the external overhead wire. Since these values are taken from the efficient power, the maximum or peak values have to be used for the estimation of the peak magnetic field by

$$I_p = I_0 = I_{\text{eff}} \times \sqrt{2} \quad (3)$$

The effective current value at the secondary side of the transformer is about 900 A, the peak value 1273 A, at each of the 2 output lines with an output voltage of 1100 V. The maximum current value at the output of the two AC-DC converters is 1010 A, and the 3-phase DC-AC inverter delivers currents to the 4 motors up to 4 times 353 A (for the effective power of 250 kW of each motor. However, we have to consider that the 4 motors are distributed along the section.

The resulting magnetic induction generated by the components of the power supply system in one section, the transformer, the converter and the inverter feeding the motors is shown as a function of the distance from the system component in Fig. 1. However, we have to keep in mind, that there is some shielding of the stray fields by the material of the component containment. Especially for the stray field of the transformer much lower values than in Fig. 1 can be assumed due to the shielding of the containment.

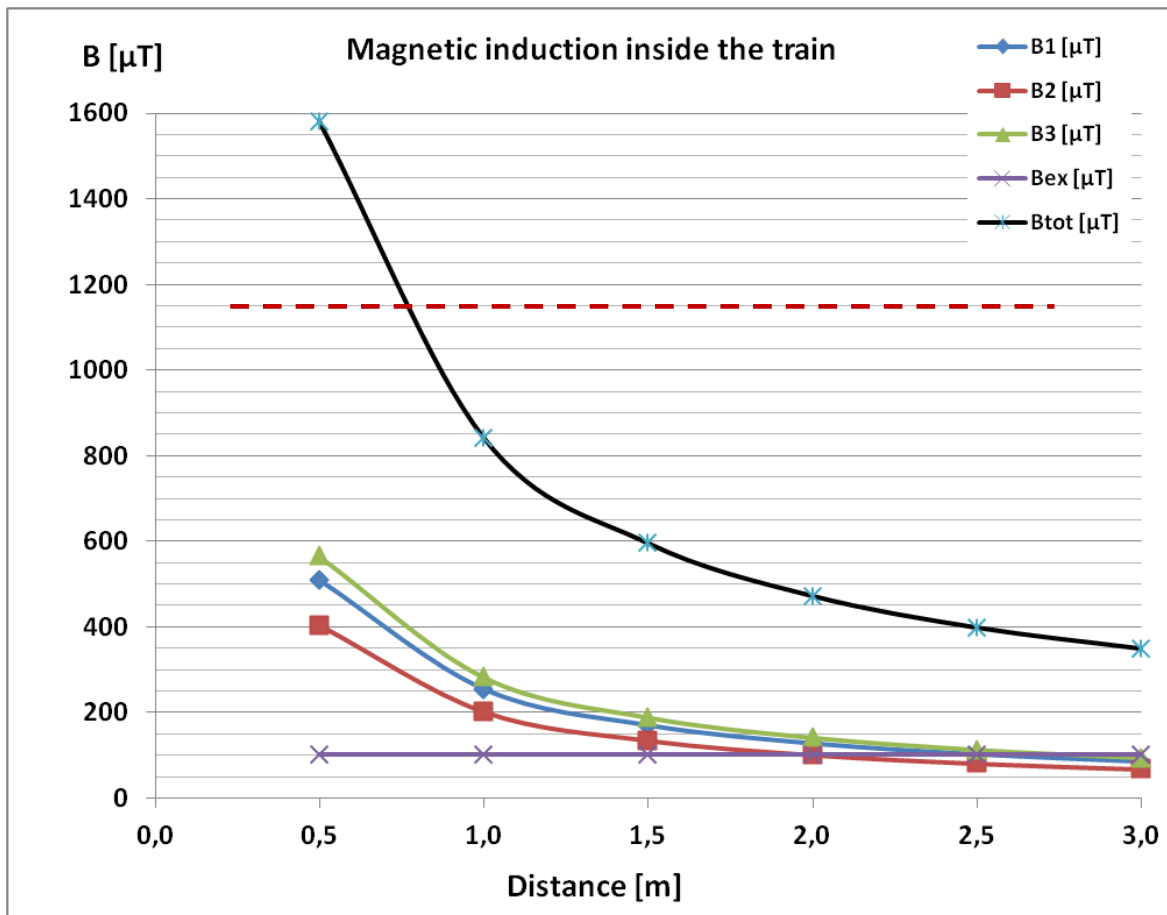


Fig. 1. The maximum magnetic induction generated by:

- the transformer (B_1),
- the converter (B_2),
- the inverter currents to the motors (B_3)

as function of the distance from the source of the magnetic field (system component)

B_{ex} is the field generated by the external overhead wires in both directions

B_{tot} is the sum of all magnetic field contributions

It is clearly seen that most of the contribution to the magnetic induction is caused by the large currents from the inverter to the motors (B_3). However, the four motors are distributed over the driven train section. The external field from the 2 overhead power lines is of minor influence, only. By adding the maximum values of all 4 contributions at a distance of 1 m, the total induction B_{tot} would peak around 800 μT . However, this is a theoretical and not a realistic value. Comparing with the frequency dependent limits of 300 μT (16.7 Hz), 500 μT (DC) and 200 μT (200 Hz) in Table 1, all field contributions remain well below the limits inside the train. In addition, the body of the wagon will further reduce the concentration of the magnetic field inside the train. The total magnetic induction inside the train depending on the distance from the location of the generated field is shown in Fig. 2.

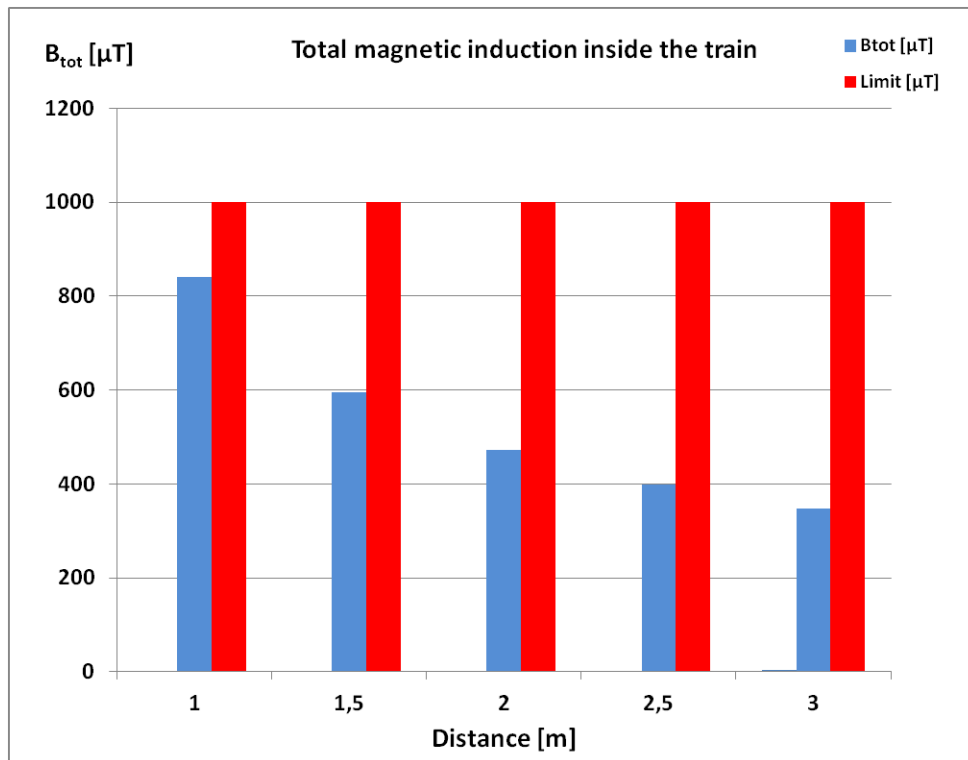


Fig. 2. The maximum total magnetic induction as a function of the distance from the location of the field generation.

Maglev systems

Maglev systems are propelled by linear motors. The power for the levitation system, the guidance and the propulsion is supplied via coils integrated into the guide way (track). As a consequence, electrical fields can be neglected, only magnetic fields have to be taken into account. In this article we compare the German system Transrapid and the Japanese system Linear Chuo Shinkansen. The Transrapid system is based on normal conductor magnet technology EMS, whereas the Japanese system is based on the superconducting Maglev technology EDS, using onboard superconducting magnets and normal conducting coils for levitation, guidance and propulsion integrated along the guide way [6].

1) Transrapid system

The Maglev system has no wheels, axles, transmissions, or pantographs. It does not roll; it hovers. Electronic systems guarantee that the clearance remains constant (nominally 10 mm). To hover, the Transrapid requires less power than its air conditioning equipment. The levitation system and all onboard electronics are supplied by the power recovered from harmonic oscillations of magnetic field of the track's linear stator (Those oscillations being parasitic cannot be used for propulsion anyway) at speeds above 100 km/h, while at lower speeds power is obtained through physical connections to the track. In case of power failure of the track's propulsion system Transrapid vehicle uses on-board backup batteries

that can supply power to the levitation system, which is therefore independent of the propulsion system.

Electronically controlled support magnets located on both sides along the entire length of the vehicle pull the vehicle up to the ferromagnetic stator packs mounted to the underside of the guide way. Guidance magnets located on both sides along the entire length of the vehicle keep the vehicle laterally on the track. Electronic systems guarantee that the clearance remains constant. To levitate the Transrapid requires less power than its air conditioning equipment. The vehicle is capable of hovering up to one hour without external energy. While travelling, the on-board batteries are recharged by linear generators integrated into the support magnets.

The Transrapid Maglev system uses a synchronous long-stator linear motor both for propulsion and braking. The linear motor is functioning like a rotating electric motor whose stator is cut open and stretched along under the guide way. The synchronous long-stator motor is divided in sections (typical stator length ranges between 500 and 2000 m) due to economic reasons (reduce losses) and reasons of propulsion.

Inside the motor windings, alternating current generates a magnetic traveling field which moves the vehicle without contact. The support magnets in the vehicle function as the excitation portion (rotor). The respective magnetic traveling field works in only one direction, and therefore makes moving train collisions less likely, as more than one train on the track section would travel in the same direction.

Recent developments suggest a reduction of the high voltage level in the propulsion system from previously 2–10 kV to a voltage level between 400–900 V along the line, with a frequency of 50 Hz [3]. The power is transmitted along propulsion sections of the guide way. Substations switch the power only in that section in which a vehicle is moving. Other sections are switched off and free of power. Fields are generated by the bearing system, the guidance and the linear drive system. The structure of the TR08 system is illustrated in Fig. 3.

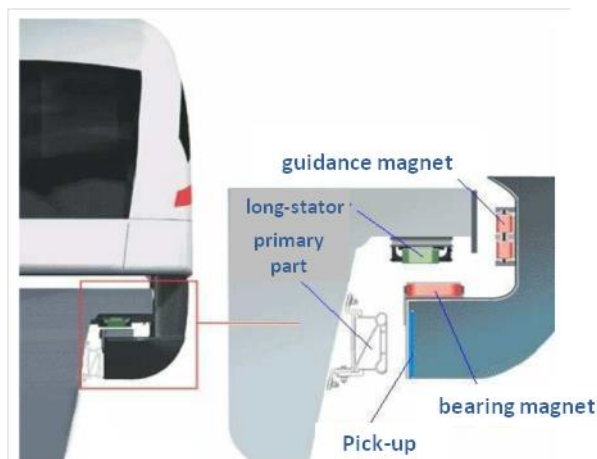


Fig. 3. Structure of the bearing and propulsion system of TR08 [4]

The nominal operational speed chosen for the comparison is 430 km/h. For the TR08 system of the Transrapid exist a wide basis of available information and experimental data by measurement.

We consider the magnetic field or induction in the neighbourhood of the guide way (track), as well as inside the vehicle.

The magnetic field or induction and its frequency dependence along the track is shown in Fig. 3a. The induction is lower than $10 \mu\text{T}$, even very close to the guideway. There is no impact to be expected for residential areas. The reason for the low induction values is the small gap between the bearing and the guidance magnets and the stator coils in the vehicle. This drastically reduces the stray fields outside the guideway.

The situation is different inside the vehicle. Since the linear motor coils are located in the vicinity of the floor of the vehicle, they generate higher induction values inside, as illustrated in Fig. 3b. The maximum value is, as expected, just on the floor with a maximum value up to more than $25 \mu\text{T}$, depending on the frequency. With increasing distance to the floor, the induction values decrease. All values are below the limits of the BImSchV 26, and even much lower than those of the rail-wheel system ICE3. For comparison, the earth magnetic field is in the range of $30\text{--}50 \mu\text{T}$, depending on geographical location.

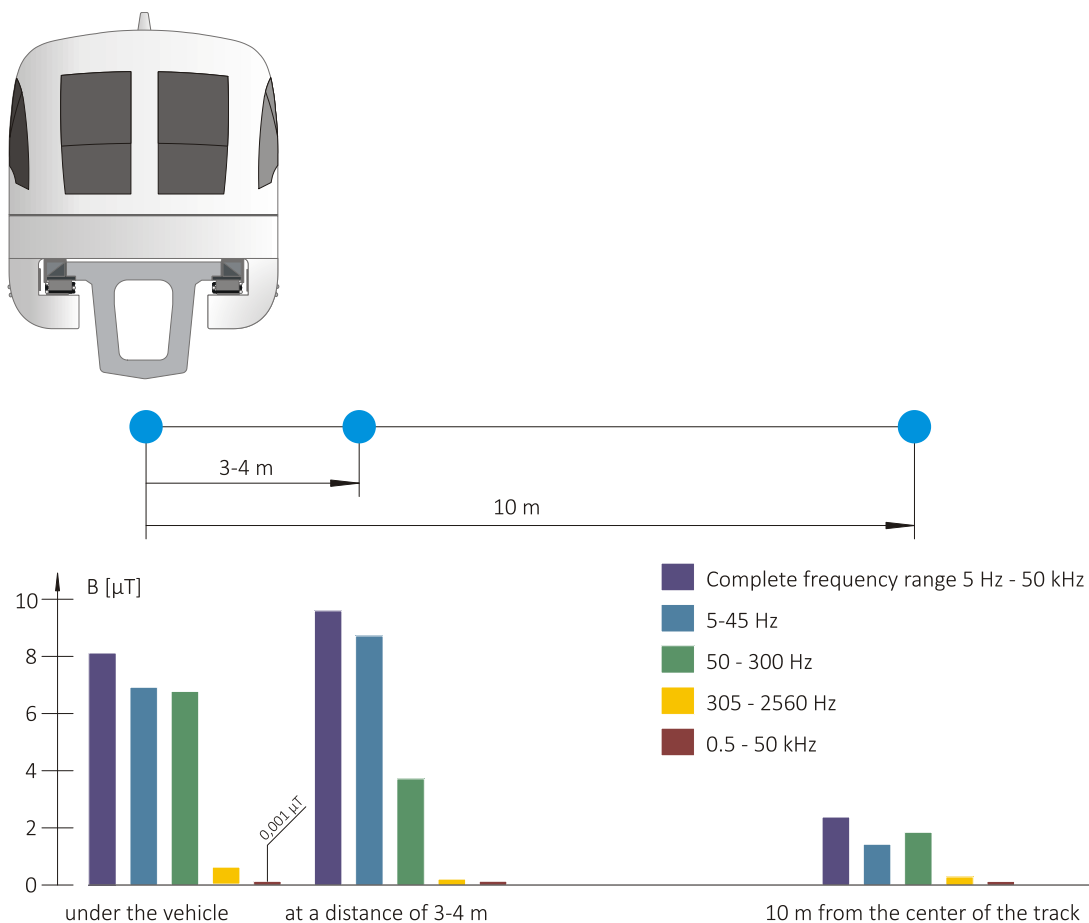


Fig. 4a. Magnetic induction along the track [5]

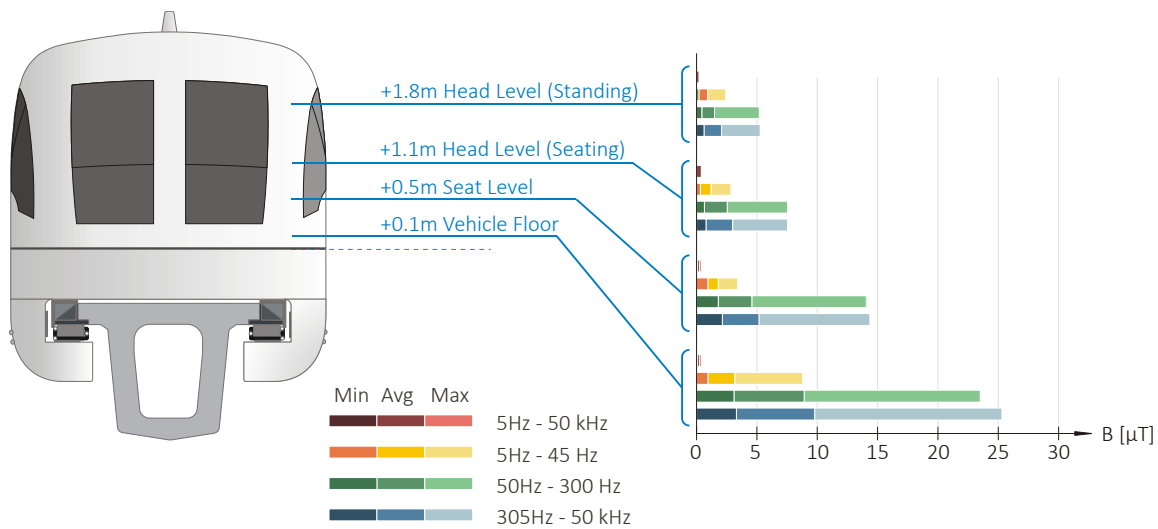


Fig. 4b. Magnetic induction inside the TR08 vehicle [5]

2) JR Maglev

Regarding the Japanese Maglev system only limited information and data are available. The data used in the present comparison are taken mainly from Japanese literature.

The Japanese Maglev system makes use of modern superconducting magnets which allow for a larger gap, and repulsive-type Electro-Dynamic Suspension (EDS). Moving magnetic fields create a reactive force in a conductor because of the magnetic field effect. This force holds up the train. The maglev-train has superconducting magnetic coils, and the guide ways contain the levitation coils. The Maglev concept of the SCMAGLEV is illustrated in Fig. 5a, 5b [6].

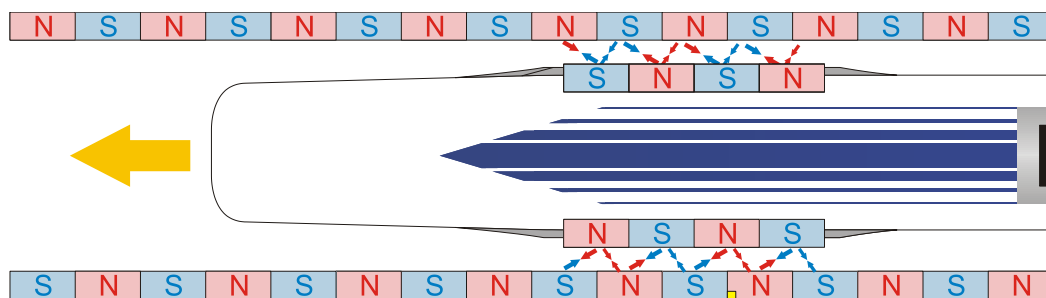


Fig. 5a. Propulsion concept of the superconducting MAGLEV [6]

The JR-Maglev train is driven by a Linear Synchronous Motor (LSM) System. This system is needed to supply power to the coils at the guide way.

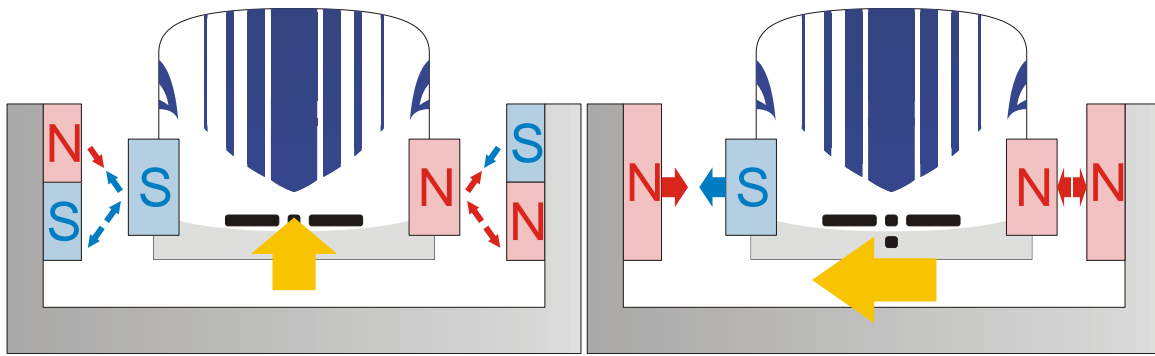


Fig. 5b. Levitation and guidance concept of the superconducting JR MAGLEV [6]

When the train is running at high speed, levitation coils on the guide way produce reactive forces in response to the approach of the superconducting magnetic coils onboard the trains. The EDS system has the advantage of larger gaps than the EMS system, but the EDS system needs support wheels which are required in low speed running, because the EDS system cannot produce a large levitation force at speeds below 150 km/h. However, once the train reaches a certain speed, the wheels will actually retract so that the train is floating. The Japanese MAGLEV system has a “self-stable” air gap of about 10 cm, whereas the Transrapid with EMS system has an air gap of 1 cm, which has constantly to be controlled. The levitation coils which are located along the guide way generate guiding and stabilizing forces. The following figure and tables are official data published in [7].

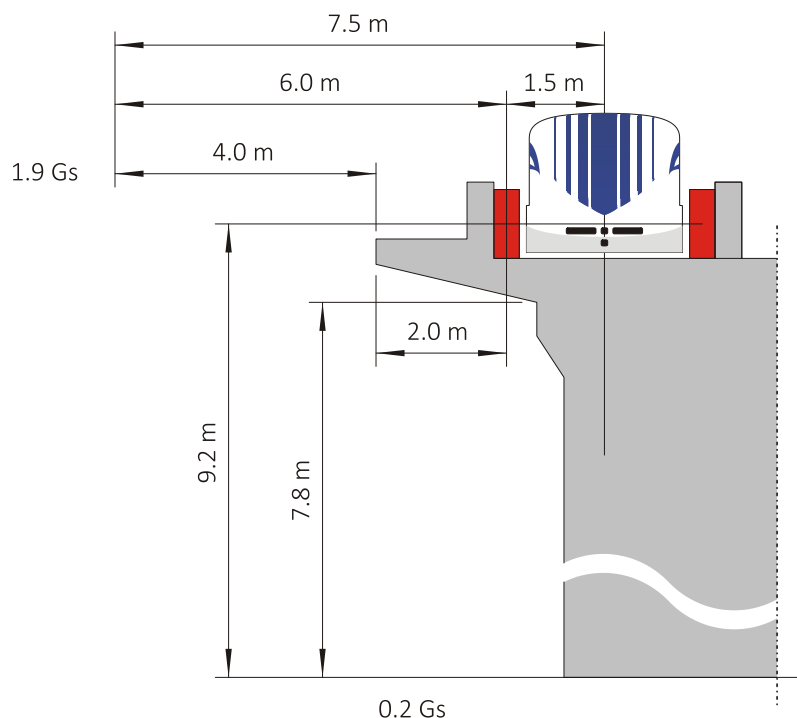


Fig. 6. Locations of the measurement points of the induction values.

Table 2. Maximum induction values inside the vehicle (at different locations).

Height	Position Condition	Inside of the vehicle			ICNIRP guideline
		Gangway	Passenger compartment. 1	Passenger compartment. 2	
1.5 m	Vehicle stop	440 μ T	X	310 μ T	400 mT
1.0 m	Static field	810 μ T	50 μ T	370 μ T	
0.3 m	Meas. equipm. 1	920 μ T	40 μ T	371 μ T	
	Vehicle running	900 μ T	X	430 μ T	
	Meas. equipm. 1				

Table 3. Induction values inside the vehicle (Data taken from Miyazaki line).

Measurement location		w/o shielding	w shielding
Center of seating row	1 m above floor	116 μ T	88 μ T
	seat level	96 μ T	64 μ T
	0.1 m above floor	112 μ T	58 μ T
Center of gangway	1.5 m above floor	90 μ T	89 μ T
	0.1 m above floor	105 μ T	83 μ T
Bogie position	1.0 m above floor	1.656 μ T	429 μ T
	seat level	2.697 μ T	382 μ T
	10 cm above floor	1.764 μ T	1.061 μ T
Gangway 1.4 m from connection	1.5 m above floor	134 μ T	206 μ T
	0.1 m above floor	1.841 μ T	366 μ T
	2.4 m from connection	1.5 m above floor	153 μ T
	0.1 m above floor	12.720 μ T	1.331 μ T

Table 4. Static and alternating induction values outside along the Linear Shinkansen line at various locations

	Measurement location	Magnetic induction
Static field	area 8 m ² under bridge	20 μ T
	area 4 m ² from guideway	190 μ T
	along the guideway	200 μ T
	Platform	800 μ T
	max. inside vehicle	1.330 μ T
Alternating field	along the guideway	200 μ T
	Propulsion generated max. by coil	200 μ T (at 100 km/h)
	Oncoming traffic max. inside vehicle	700 μ T (at 20 km/h)

Table 5. Regulations given by the National Environmental Research Center of Japan

Location	Max. Value of induction
Directly above motor	max. 600 μ T
Inside vehicle above reactor at floor	max. 4 000 μ T
0.05 m under the motor	max. 70 000 μ T
0.15 m under the motor	max. 20 000 μ T

A system has been proposed to reduce the magnetic field inside the vehicles of Superconducting Maglev Train by shielding measures [8]. Grain Oriented silicon steel (GO) has a high saturated magnetic flux density and also higher permeability than pure iron. So this is suitable as the material of magnetic shielding at the target level of less than 500 μT . The challenge consists in handling the magnetic anisotropy of this material. To avoid the problem of anisotropy a bi-lamellar shielding has been proposed to the coach. The outer shielding material is pure iron and the inner one is permalloy B, which has a relatively high saturated magnetic flux density in all categories of permalloy and has magnetic isotropy. The magnetic field in this double shielding system reaches a maximum value of 300 μT locally, but is less than 100 μT in almost all regions inside the vehicle. This maximum value corresponds to an open space without shielding, through which passengers can move from coach to corridor. The disadvantage of this bi-lamellar shielding is the increase in the weight of magnetic shield system. There still might be some room for further optimizing the shielding configuration in order to reduce the weight.

In order to evaluate the environmental concerns related to electromagnetic fields of high speed transportation systems we have to compare the maximum magnetic induction inside the vehicles at the location of passenger seats. Fig. 7 shows the maximum induction values to which passengers are exposed during the ride in the high speed transportation systems of this comparison, together with the corresponding limits.

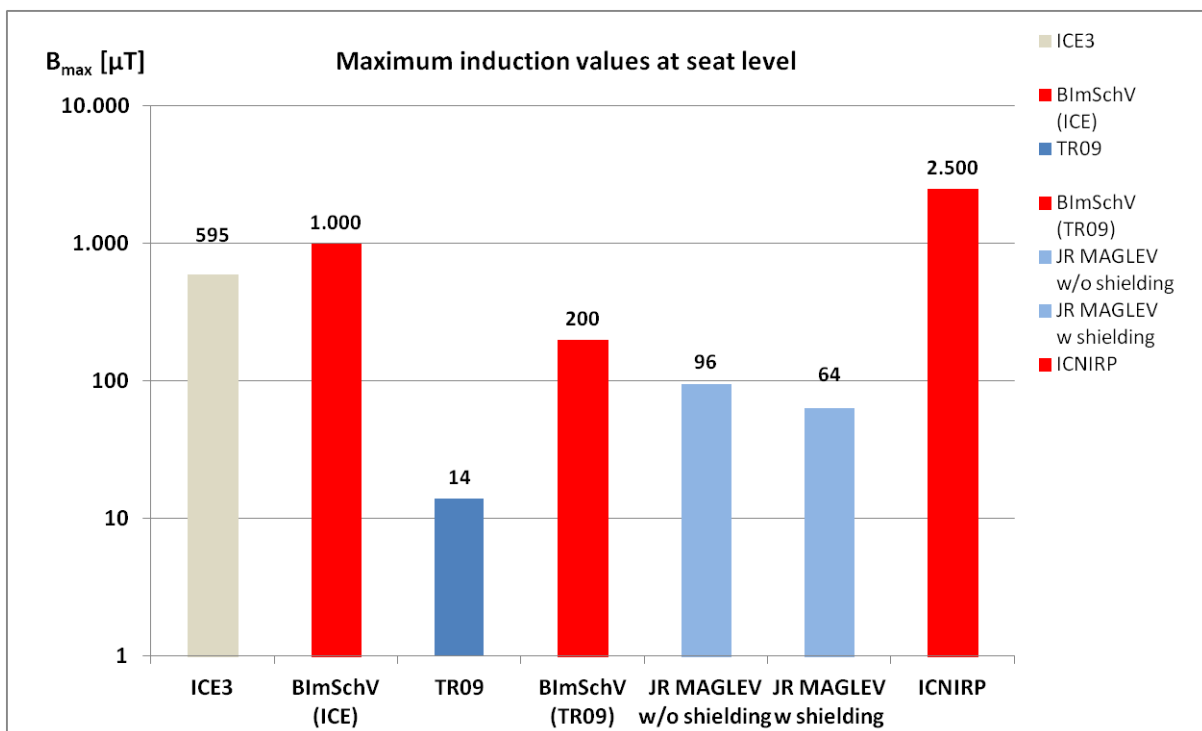


Fig. 7. Comparison of the maximum induction values inside the vehicle at passengers' position. The red columns are the corresponding limits given by BImSchV and ICNIRP, respectively

The values are represented on a logarithmic scale due to the high limit of ICNIRP. All induction values remain under the limits.

CONCLUSION

In the article, the electromagnetic fields generated by the power supply of high speed transportation systems have been calculated and compared. Since the biological effect of the peak electrical field strength of 1 kV/m is considered as negligible, the focus of the comparison was especially on the magnetic field which is more critical than the electrical field.

The worst case calculation for the railway system ICE results in induction values of about 600 μT , which is well below the limit given by BImSchV. Therefore, the power supply system of railway systems has no negative impact on passengers as well as on the environment.

In case of the high speed magnetic levitation transportation systems, the situation is different. The magnetic field strength strongly depends on the technology used for levitation, propulsion and guidance. In the case of Transrapid past investigations based on experimental measurements show that there is no negative impact of the magnetic induction on passengers and the environment to be expected. For comparison, the value of the magnetic field of earth at central Europe is 48 μT , which is more than 3 times the measured value in the Transrapid.

In case of the Japanese Maglev system, which uses superconducting magnets and a wide air-gap, considerable efforts are necessary to shield passengers from the high magnetic field strength. However, with present shielding measures the induction values inside the vehicle of the Maglev systems are 4 to 6 times higher than inside the Transrapid vehicle. In addition, the material for shielding high magnetic fields has the drawback of heavy weight, which has a negative influence on the energy balance. Research in Japan is focusing on new and innovative materials to reduce weight without loss of shielding properties.

References

1. Electromagnetic fields at workplaces, Final Report, FB400-E, Federal Ministry of Labour and Social Affairs, Nov. 2011, ISSN 0174-4992.
2. Binder A, Körner O. *Was treibt den ICE 3 und den Transrapid*. Darmstadt: Institut für Elektrische Energiewandlung; 2011.
3. August P. *Optimierungsstrategie für den Antrieb des Transrapid*, [Dissertation]. Dresden; 2010.
4. Bühler G, Czainski R. *CPS for the high-speed magnetic levitation system of Transrapid TR08*, 2005.
5. Rausch C. *Zevrail*, Glasers Annalen – Sonderheft Transrapid, 2003.
6. The Review “Superconducting Maglev (SCMAGLEV)”. *JR Central*, 2017.

7. Linear Shinkansen abunai, Linear Community Net, ISBN 978-4-8461-1315-5. 2014 May 30 (In Japanese).
8. Sasakawa T, Tagawa N. Reduction of Magnetic Field in Vehicle of Superconducting Maglev Train. *IEEE Transactions on Magnetics*. 2000;36(5):3676-3679. doi: 10.1109/20.908938

Information about the authors:

Kircher Roland, Dr., The International Maglev Board;
ORCID: 0000-0002-8807-8915;
E-mail: rk@maglevboard.net

Klühspies Johannes, Dr. habil. Dr. h.c., full professor;
ORCID: 0000-0001-6089-9853;
E-mail: jok@maglevboard.net

Palka Ryszard, Prof. Dr. Dr.;
ORCID: 0000-0003-3509-6500;
E-mail: rpalka@zut.edu.pl

Fritz Eckert, Dipl. Eng,
ORCID: 0000-0003-3422-227X;
E-mail: ef@bahntechnik.de

Eiler Kenji, Dipl. Eng. Dr. Eng.;
E-mail: kenji.eiler@maglevboard.net

Witt Michael, Dipl. Eng. Dr. Eng.;
E-mail: mikewitt@maglevboard.net

To cite this article:

Kircher R, Klühspies J, Palka R, et al. Electromagnetic Fields Related to High Speed Transportation Systems. *Transportation Systems and Technology*. 2018;4(2):152-166. doi: 10.17816/transsyst201842152-166

УДК [UDC] 621.313.333.2 + 06
DOI 10.17816/transsyst201842167-179

© V. Solomin¹, A. Solomin¹, V. Koledov², N. Trubitsina¹

¹Rostov State Transport University
(Rostov-on-Don, Russia)

²V. A. Kotelnikov Institute of Radio Engineering and Electronics
of the Russian Academy of Science
(Moscow, Russia)

MULTIFUNCTIONAL LINEAR INDUCTION MOTOR WITH LONGITUDINAL-TRANSVERSE MAGNETIC FLUX FOR MAGNETIC-LEVITATIONAL TRANSPORT

Background: Traction linear induction motors (LIM) at the current stage of human society development are the most promising for high-speed magnetic-levitation transport (MLT) and are already used in a number of commercial projects. Linear induction motors can be executed with longitudinal, transverse and longitudinal-transverse magnetic flux and have a large number of design options.

Aim: In addition to traction efforts, LIM develops the forces of magnetic-levitation and lateral stabilization (self-stabilization). The efforts of magnetic-levitation of linear induction motors with longitudinal and transverse magnetic flux are very significant in the zone of large slides (at low speeds) and decrease with increasing speed of the magnetic-levitation transport. To a lesser extent, the decrease in slip (at high speeds) affects the magnetic-levitation forces developed by a number of design variants of linear induction motors with a longitudinal-transverse magnetic flux, in which magnetic fields traveling in a transverse direction towards each other are additionally used. This is explained by the fact that at high and low velocities MLT, the LIM slip will be equal to unity relatively oppositely running in the transverse direction of the magnetic fields and the magnetic suspension forces will be maximum.

Methods: Running towards each other in the transverse direction of the MLT movement, magnetic fields cross the electrically conductive secondary element (playing the role of the track structure of the high-speed transport system) and induce electromotive forces in it, under the influence of which currents will flow.

Results: As a result, cross counter-directional mechanical forces are created which, in the symmetrical arrangement of the MLT crew relative to the track structure, are mutually balanced and do not have any effect on the motion of the magnetic-levitation transport. At lateral (transverse) displacement of the high-speed transport on the magnetic suspension relative to the track structure, the equilibrium of the transverse mechanical forces is disrupted and, under the effect of the effort difference, the MLT crew will be automatically returned to the original symmetrical position.

Conclusion: The distribution of magnetomotive forces (MMF) of a linear induction motor with a longitudinal-transverse magnetic flux, whose magnetic system is formed by the combination of longitudinally and transverse laminated cores, on the teeth of which the coils of a concentrated three-phase winding are located, is considered. The relations are represented

The article was written with the support of RFBR_RDF grant № 17-20-04236 «Magnetic cooling of perspective transport and energy systems».

in the form of a double Fourier series for calculating the resultant MMF value in the air gap of a linear induction motor with a longitudinal-transverse magnetic flux.

Keywords: Linear induction motor, Longitudinal-transverse magnetic flux, Magnetic levitation, Lateral stabilization, Magnetomotive force.

© В. А. Соломин¹, А. В. Соломин¹, В. В. Коледов², Н. А. Трубицина¹

¹ Ростовский государственный университет путей сообщения

(Ростов-на-Дону, Россия)

² Институт радиотехники и электроники им. В.А. Котельникова РАН

(Москва, Россия)

МНОГОФУНКЦИОНАЛЬНЫЙ ЛИНЕЙНЫЙ АСИНХРОННЫЙ ДВИГАТЕЛЬ С ПРОДОЛЬНО- ПОПЕРЕЧНЫМ МАГНИТНЫМ ПОТОКОМ ДЛЯ МАГНИТОЛЕВИТАЦИОННОГО ТРАНСПОРТА

Обоснование: Тяговые линейные асинхронные двигатели (ЛАД) на современном этапе развития человеческого общества являются наиболее перспективными для высокоскоростного магнитолевитационного транспорта (МЛТ) и уже используются в ряде коммерческих проектов. Линейные асинхронные двигатели могут выполняться с продольным, поперечным и продольно-поперечным магнитным потоком и иметь большое количество вариантов конструкций.

Цель: Помимо тяговых усилий ЛАД развивают усилия магнитной левитации и боковой стабилизации (самостабилизации). Усилия магнитной левитации линейных асинхронных двигателей с продольным и поперечным магнитным потоком весьма значительны в зоне больших скольжений (при низких скоростях движения) и уменьшаются с ростом скорости движения магнитолевитационного транспорта. В меньшей мере уменьшение скольжения (при высоких скоростях движения) влияет на усилия магнитной левитации, развиваемые рядом конструктивных вариантов линейных асинхронных двигателей с продольно-поперечным магнитным потоком, в которых дополнительно использованы бегущие в поперечном направлении навстречу друг другу магнитные поля. Это объясняется тем, что и при высоких и при низких скоростях движения МЛТ скольжения ЛАД относительно встречно бегущих в поперечном направлении магнитных полей будут равны единице и усилия магнитного подвеса будут максимальными.

Методы: Бегущие навстречу друг другу в поперечном направлении движения МЛТ магнитные поля пересекают электропроводящий вторичный элемент (играющий роль путевой структуры высокоскоростной транспортной системы) и индуцируют в нем электродвижущие силы, под действием которых потекут токи.

Результаты: В результате создаются поперечные встречно направленные механические усилия, которые при симметричном расположении экипажа МЛТ относительно путевой структуры взаимно уравниваются и не оказывают никакого влияния на движение магнитолевитационного транспорта. При боковом (поперечном) смещении высокоскоростного транспорта на магнитном подвесе относительно путевой

структуры равновесие поперечных механических усилий нарушится и под действием разности усилий экипаж МЛТ будет автоматически возвращен в исходное симметричное положение.

Выводы: Рассмотрено распределение магнитодвижущих сил (МДС) линейного асинхронного двигателя с продольно-поперечным магнитным потоком, магнитная система которого образована сочетанием продольно и поперечно шихтованных сердечников, на зубцах которых расположены катушки сосредоточенной трехфазной обмотки. Представлены соотношения в виде двойного ряда Фурье для расчета результирующего значения МДС в воздушном зазоре линейного асинхронного двигателя с продольно-поперечным магнитным потоком.

Ключевые слова: линейный асинхронный двигатель, продольно-поперечный магнитный поток, магнитная левитация, боковая стабилизация, магнитодвижущая сила.

INTRODUCTION

Magnetic levitation systems of high-speed transport, including vacuum ones, can occupy a worthy place in the world transport communications in the foreseeable future. Studies in the field of MLT and new technologies, using the phenomenon of magnetic levitation, in Russia have intensified in recent decades. The work on the creation and study of MLT and the use of magnetic suspension in industrial installations is carried out by Russian enterprises and organizations in Russia. The most significant results in this area of research have been achieved in St. Petersburg [1–7], where various systems of magnetic suspension are being developed and studied, scientific conferences and seminars are being held where the aspects of the functioning of high-speed magnetic-levitation transport are discussed, and an engineering cluster «Russian Maglev» was created. In addition to magnetic levitation systems, it is necessary to carry out work in the field of traction drive to create new types of MLT, where the main element is a linear motor. Linear motors for high-speed MLT can be induction and synchronous. At the present stage of development of high-speed transport systems, in our opinion, the most promising are linear traction induction motors. Traction LIM has been successfully operated in China for many years on a magnetic-levitation train connecting Shanghai with the airport. Linear induction motors can have various designs of magnetic cores (solid, discrete) and windings (distributed, concentrated, three- and two-phase). In our opinion, LIM with longitudinal-transverse magnetic flux is very promising for magnetic-levitation and vacuum transport, since these linear motors not only create traction and levitation forces, but also are capable of providing lateral stabilization of high-speed crew.

LINEAR INDUCTION MOTORS WITH A LONGITUDINAL- TRANSVERSE MAGNETIC FLUX

In linear induction motors with a longitudinal-transverse magnetic flux, magnetic systems allow magnetic lines of force to be closed in both longitudinal and transverse directions, which expands their functional capabilities. In a high-speed MLT, linear induction motors with a longitudinal-transverse magnetic flux, in which the same magnetic fields «run» towards each other in each cross-section of the LIM, can realize not only traction and levitation forces, but lateral stabilization, which increases the safety of traffic. Note, that lateral stabilization efforts when the crew is shifted are created automatically without any sensors and additional devices, due to changes in the magnetic fields counter-running in the transverse direction. Linear induction motors with a longitudinal-transverse magnetic flux have different design versions, but for high-speed magnetic-levitation transport, in our opinion, LIM is better suited, the multi-phase windings of which have connection circuits forming the same order of phases in the direction of vehicle movement, and in the transverse direction – to the middle of the series one, and after the middle – the opposite order of the phases [8–15]. The operating principle of the LIM data with a longitudinal-transverse magnetic field will be the same. When a multiphase winding of the LIM inductor is connected to a voltage source running magnetic fields are excited that cross the electrically conductive track structure, which plays the role of an anchor, and induce electromotive forces in it, under the influence of which currents will flow in the track structure. When the magnetic fluxes, running in the longitudinal direction, interact with the currents, inducted by them in the electrically conductive track structure MLT, traction and levitation forces are created. We note, that when the slip is equal to unity, the force of the magnetic suspension will be maximum. Under the influence of tractive force, the crew of the MLT will begin its movement. When magnetic fluxes running in the transverse direction interact with the currents, inducted by them, counter-directed lateral mechanical forces and magnetic suspension forces are created. If the transport crew is symmetrically located relative to the track structure, the lateral forces are the same, they balance each other and have no effect on the motion of the magnetic-levitation transport. If the movement of the MLT crew is displaced to the right or to the left (for example, under the influence of a strong side wind), then the equilibrium of lateral mechanical forces is violated and under the influence of the difference of these efforts the transport crew automatically returns to the former, symmetrical position. As for the magnetic suspension forces, created by the interaction of transversely running magnetic fields with currents in the track structure, they will not depend on the speed of the MLT. This is explained by the fact that the slip of the LIM inductor relative



to the transversely running magnetic fields will always be equal to unity. The design of a linear induction motor with a longitudinal-transverse magnetic flux [16] is capable of developing large efforts of a lateral stabilization of magnetic-levitation transport, by increasing the efficiency of the use of counter-current running magnetic fields. LIM with a longitudinal-transverse magnetic flux can be used in combination with an electrodynamic levitation system to accelerate the transport crew to the required speed, after which induction motors will be used in the lateral stabilization system of magnetic-levitation transport.

MATHEMATICAL MODELING OF THE DISTRIBUTION OF THE MAGNETOMOTIVE FORCE LIM WITH A LONGITUDINAL-TRANSVERSE MAGNETIC FLUX

For the electromagnetic calculation of LIM and determination of its integral characteristics, it is necessary to develop mathematical models of the machine taking into account the distribution of the magnetomotive force in the air gap and in the electrically conductive part of the secondary element (track structure MLT). Linear induction motors with longitudinal-transverse closure of magnetic flux have an open magnetic system and in their operation longitudinal and transverse end effects are manifested, which have a great influence on the traction properties of LIM. Therefore, when calculating, it is necessary to take into account the influence of end effects. In order to take into account the influence of longitudinal and transverse end effects, a linear induction motor is represented in the form of two computational models, which depict the distribution of magnetomotive forces in two mutually perpendicular directions. This approach to analyzing the properties of LIM will create a three-dimensional theory of linear electric motors with longitudinal closure of the magnetic flux. Later, an attempt was made to extend this theory to linear induction motors with a transverse magnetic flux, which made it possible to obtain good results that coincided with the experimental data. We use this approach to determine the magnetomotive force of linear induction motors with a longitudinal-transverse magnetic flux, the designs of which are intended for use on a promising high-speed magnetic-levitation and vacuum transport.

We use for analysis a number of assumptions that make it possible to obtain an analytical solution of the problem.

We assume, that the magnetic permeability of the magnetic circuit is equal to infinity; the electric conductivity of the magnetic circuit is zero; the inductor current is concentrated in an infinitely thin layer on the surface of the teeth facing the secondary element (electrically conductive path structure MLT); the current of the inductor generates in the direction of the «x» axis a

sinusoidally traveling MMF wave; the components of the current density along the «y» axis in the inductor and the secondary element are zero.

Let us consider a linear induction motor with a longitudinal-transverse magnetic flux, intended for magnetic-levitation transport, whose magnetic system is formed by transversely laminated Π -shaped cores, between each pair of which a longitudinal magnetic circuit is located. The coils of the concentrated three-phase winding cover the teeth of longitudinally and transversely laminated cores. The design model of this linear induction motor is shown in Fig. 1. The adopted coordinate system contains the “x” axis, oriented in the direction of motion, the «y» axis, located at the center of the rail section (secondary element), and the «z» axis, directed transversely to the displacement of the inductor. In the longitudinal direction, the MMF is distributed sinusoidally, and in the transverse direction the inductor of the traction LIM with the longitudinal-transverse magnetic flux is divided into 23 zones, for which the MMF distribution is shown (Fig. 2). This representation of the MMF allows one to take into account the influence of the transverse end effect. Magnetomotive forces for each of the zones of this LIM in accordance with the calculation models are presented as:

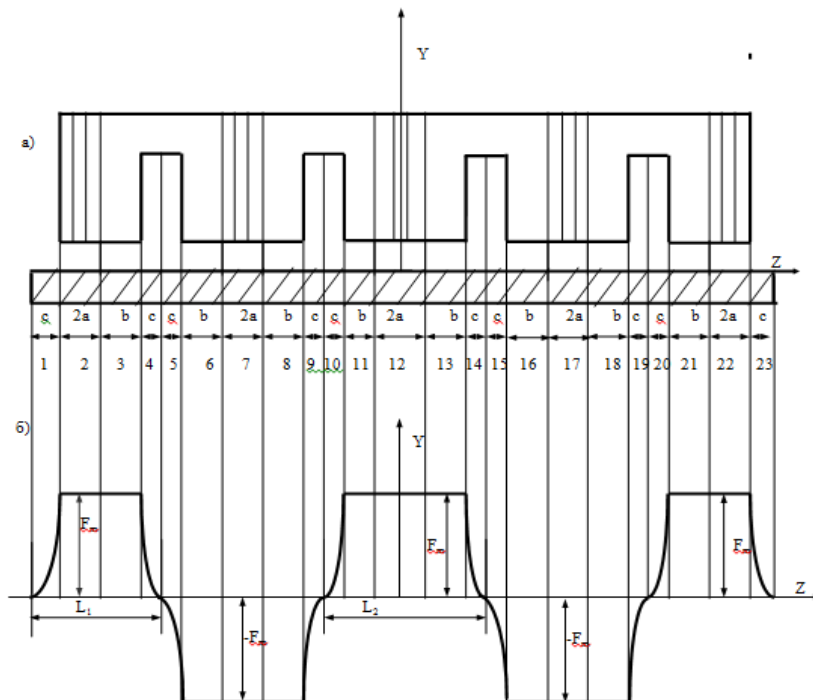


Fig 1. The design model of the LIM in the transverse direction:
a) the cross section of the LIM;
b) the distribution of the MMF in the transverse direction

$$F_1 = F_m \left[1 + \sin \frac{\pi(z + 5a + 4b + 4c)}{2c} \right] e^{j(\omega t - \frac{\pi}{\tau} x)}; \quad (1)$$

$$F_2 = F_3 = F_m e^{j(\omega t - \frac{\pi}{\tau} x)}; \quad (2)$$

$$F_4 = F_m \left[1 - \sin \frac{\pi(z - 3a - 3b - 3c)}{2c} \right] e^{j(\omega t - \frac{\pi}{\tau} x)}; \quad (3)$$

$$F_5 = -F_m \left[1 + \sin \frac{\pi(z + 3a + 3b + 2c)}{2c} \right] e^{j(\omega t - \frac{\pi}{\tau} x)}; \quad (4)$$

$$F_6 = F_7 = F_8 = -F_m e^{j(\omega t - \frac{\pi}{\tau} x)}; \quad (5)$$

$$F_9 = -F_m \left[1 - \sin \frac{\pi(z - a - b - c)}{2c} \right] e^{j(\omega t - \frac{\pi}{\tau} x)}; \quad (6)$$

$$F_{10} = F_m \left[1 + \sin \frac{\pi(z + a + b)}{2c} \right] e^{j(\omega t - \frac{\pi}{\tau} x)}; \quad (7)$$

$$F_{11} = F_{12} = F_{13} = F_m e^{j(\omega t - \frac{\pi}{\tau} x)}; \quad (8)$$

$$F_{14} = F_m \left[1 - \sin \frac{\pi(z - a - b)}{2c} \right] e^{j(\omega t - \frac{\pi}{\tau} x)}; \quad (9)$$

$$F_{15} = -F_m \left[1 + \sin \frac{\pi(z + a + b + c)}{2c} \right] e^{j(\omega t - \frac{\pi}{\tau} x)}; \quad (10)$$

$$F_{16} = F_{17} = F_{18} = -F_m e^{j(\omega t - \frac{\pi}{\tau} x)}; \quad (11)$$

$$F_{19} = -F_m \left[1 - \sin \frac{\pi(z - 3a - 3b - 2c)}{2c} \right] e^{j(\omega t - \frac{\pi}{\tau} x)}; \quad (12)$$

$$F_{20} = F_m \left[1 + \sin \frac{\pi(z + 3a + 3b + 3c)}{2c} \right] e^{j(\omega t - \frac{\pi}{\tau} x)}; \quad (13)$$

$$F_{21} = F_{22} = F_m e^{j(\omega t - \frac{\pi}{\tau} x)}; \quad (14)$$

$$F_{23} = F_m \left[1 - \sin \frac{\pi(z - 5a - 4b - 4c)}{2c} \right] e^{j(\omega t - \frac{\pi}{\tau} x)}. \quad (15)$$

$$\text{Where } F_m = \frac{2\sqrt{2}}{\pi} qm\omega c I_K k_{o\delta 1} \quad (16)$$

LIM with a longitudinal-transverse magnetic flux, the cross-section of which is shown in Fig. 1, can be represented as the sum of five linear motors, operating according to: three median, whose MMF change in the transverse

direction with a period of $T_2 = 2L_2$, and two extreme, whose magnetomotive force has a period of $T_1 = 2L_1$ along the «z» axis.

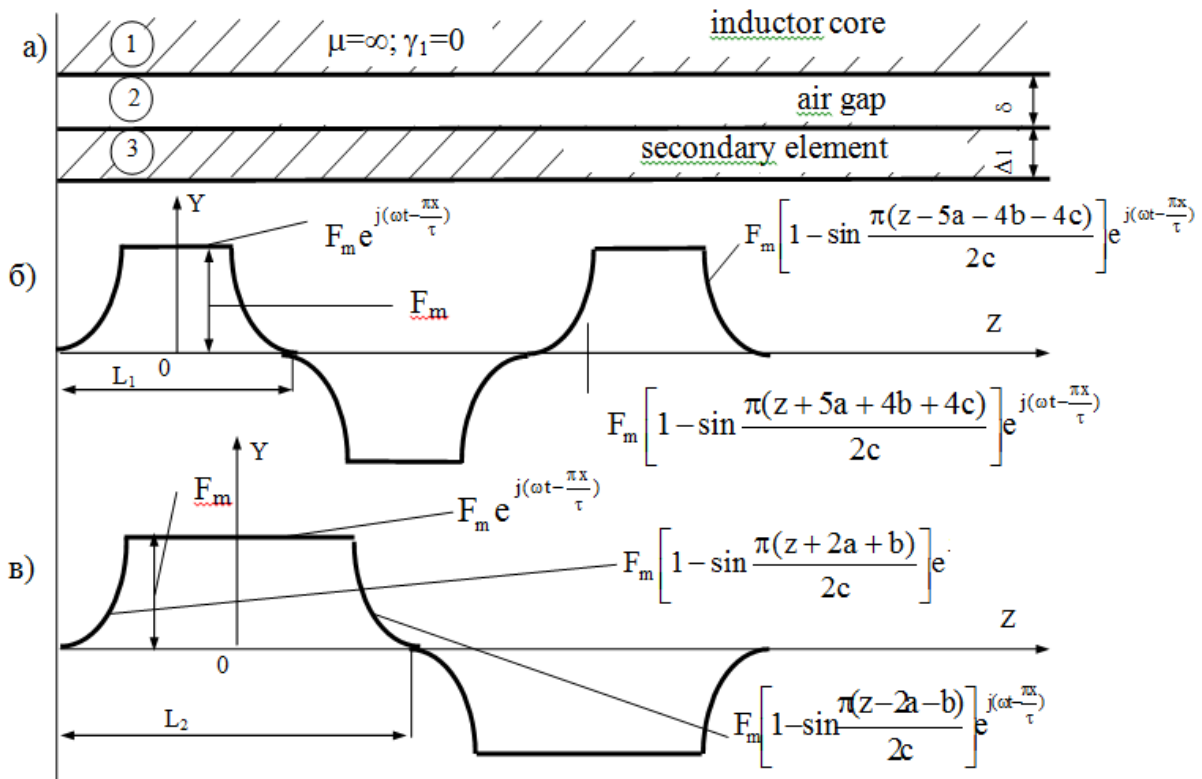


Fig 2. Design model and MMF of linear motor in the transverse direction:
a) the design model; b) distribution of MMF of median LIM; c) distribution of MMF of extreme LIM

In this case, the calculation can be performed separately for LIM 1, and the calculation results are doubled, and for LIM 2 (the results of the calculation are tripled). Summing the results of the calculation of LIM 1 and LIM 2, we obtain integral values of the parameters and characteristics of the LIM with a longitudinal-transverse magnetic flux.

A more detailed design model of the LIM (Fig. 2) denotes three zones:

- 1 – magnetic inductor system;
- 2 – air gap;
- 3 – conductive secondary element (track structure MLT).

When analyzing design models, we use the assumptions made earlier.

Design models and assumptions made earlier (Fig. 1 and Fig. 2) make it possible to represent the MMF of the extreme LIM 1 in the form of a periodic function with the period $T_x = 1$ along the «x» axis and with the $T_z = 2L_1$ period along the «z» axis in the form:

$$F_1(x, z, t) = \begin{cases} F_m e^{j(\omega t - \frac{\pi}{\tau} x)}; \\ \text{on condition } -p\tau \leq x \leq p\tau; \quad -(5a + 4b + 4c) \leq z \leq -(3a + 3b + 3c); \\ F_m \left[1 - \sin \frac{\pi(z - 5a - 4b - 4c)}{2c} \right] e^{j(\omega t - \frac{\pi}{\tau} x)}; \\ \text{on condition } -p\tau \leq x \leq p\tau; \quad -(3a + 3b + 3c) \leq z \leq -(3a + 3b + 2c); \\ F_m \left[1 + \sin \frac{\pi(z + 5a + 4b + 4c)}{2c} \right] e^{j(\omega t - \frac{\pi}{\tau} x)}; \\ \text{on condition } -p\tau \leq x \leq p\tau; \quad -(5a + 4b + 4c) \leq z \leq -(5a + 4b + 3c); \end{cases} \quad (17)$$

$$\text{where } F_m = \frac{2\sqrt{2}}{\pi} qm\omega_c I_c \kappa_{o\delta 1}; \quad (18)$$

Magnetomotive force of the median LIM-2 can be represented as periodic functions with a period of $T_x=1$ along the «x» axis and with a period $T_z=2L_2$ along the «z» axis, given as follows:

$$F_2(x, z, t) = \begin{cases} F_m e^{j(\omega t - \frac{\pi}{\tau} x)}; \\ \text{on condition } -p\tau \leq x \leq p\tau; \quad -(2a + b + c) \leq z \leq (2a + b + c); \\ F_m \left[1 - \sin \frac{\pi(z - 2a - b)}{2c} \right] e^{j(\omega t - \frac{\pi}{\tau} x)}; \\ \text{on condition } -p\tau \leq x \leq p\tau; \quad -(2a + b) \leq z \leq (2a + b + c); \\ F_m \left[1 + \sin \frac{\pi(z + 2a + b)}{2c} \right] e^{j(\omega t - \frac{\pi}{\tau} x)}; \\ \text{on condition } -p\tau \leq x \leq p\tau; \quad -(2a + b + c) \leq z - (2a + b); \end{cases} \quad (19)$$

Having performed a number of transformations, we represent the MMF of the «extreme» and middle LIM in the form of double Fourier series

For the extreme LIM the magnetomotive force is obtained as:

$$F_1(x, z, t) = \frac{8\tau F_m}{\pi^2 l} \sum_n \sum_\nu n_1 \left(\pi n \frac{z}{L_1} \right) \nu_k e^{j(\omega t + 2\pi \nu \frac{x}{l})}, \quad (20)$$

$$n_{n1} = \frac{1}{n \left[1 - \left(2n \frac{c}{l} \right)^2 \right]} \left[\sin \frac{\pi n \left(a + \frac{b}{2} + c \right)}{L_1} - 2n \frac{c}{L_1} \cos \left(\pi n \frac{a + \frac{b}{2}}{L_1} \right) \right] \quad (21)$$

where n – an integer, positive, odd number – order harmonic component of the MMF in the «z» axis direction, with the period of the first harmonic being $2L_1=2(2a+b+c)$;

v – harmonic order of the MMF along the «x» axis;

$n_{\pi 1}$ – a coefficient, that takes into account the MMF distribution in the zone of the frontal parts of the LIM 1 winding;

v_k – a coefficient, that takes into account the number of poles.

The magnetomotive force of the median LIM 2 is defined as follows:

$$F_2(x, z, t) = \frac{8\tau F_m}{\pi^2 l} \sum_n \sum_v n_{\pi 2} \left(\pi n \frac{z}{L_2}\right) v_k e^{j(\omega t + 2\pi v \frac{x}{l})}, \quad (22)$$

$$n_{\pi 2} = \frac{1}{n \left[1 - \left(2n \frac{c}{L_1}\right)^2\right]} \left[\sin \frac{\pi n(a+b+c)}{L_2} - 2n \frac{c}{L_2} \cos \left(\pi n \frac{a+b}{L_2} \right) \right], \quad (23)$$

where $L_2=2(2a+2b+2c)$.

CONCLUSIONS

1. The proposed method for modeling the distribution of the magnetomotive force LIM with a longitudinal-transverse magnetic flux makes it possible to reduce the real models of linear induction motors with a longitudinal-transverse magnetic flux with the complex structure of the magnetic inductor systems to the calculated mathematical ones. This can serve as a basis for creating a methodology for calculating the parameters and characteristics of traction LIM with a longitudinal-transverse magnetic flux, intended for use in high-speed magnetic-levitation and vacuum transport.

2. Linear induction motors with a longitudinal-transverse magnetic flux in high-speed MLT systems are capable, along with traction and levitation efforts, to realize automatic lateral self-stabilization of the transport crew relative to the track structure and are multi-functional devices.

3. Linear induction motors with a longitudinal-transverse magnetic flux in combination with an electrodynamic system of magnetic levitation are promising for magnetic-levitation transport.

БИБЛИОГРАФИЧЕСКИЙ СПИСОК / References

1. Антонов Ю.Ф., Зайцев А.А. Магнитолевитационная транспортная технология. – Москва: Издательство физико-математической литературы, 2014. – 476 с. [Antonov YuF, Zaitsev AA. Magnitolevitatsionnaya transportnaya tekhnologiya. Moscow: Izdatel'stvo fiziko-matematicheskoy literatury; 2014. 476 p. (In Russ.)].
2. Зайцев А.А., Талашкин Г.Н., Соколова Я.В. Транспорт на магнитном подвесе. – СПб: Издательство Петербургского государственного университета путей сообщения, 2010. – 160 с. [Zaitsev AA, Talashin GN, Sokolova YaV. Transport na

- magnitnom podvese. St. Petersburg: Izdatel'stvo Peterburgskogo universiteta pytei soobkheniya; 2010. 160 p. (In Russ.).
3. Антонов Ю.Ф., Зайцев А.А. Магнитолевитационный транспорт: научные проблемы и технические решения. – Москва: Издательство физико-математической литературы, 2015. – 612 с. [Antonov YuF, Zaitsev AA. Magnitolevitatsionnyy transport: nauchnyye problem i tekhnicheskiye resheniya. Moscow: Izdatel'stvo fiziko-matematicheskoy literatury; 2015. 612 p. (In Russ.).]
 4. Зайцев А.А., Морозова Е.Н., Талашкин Г.Н. и др. Магнитолевитационный транспорт в единой транспортной системе страны. – Санкт-Петербург: ООО «Типография «НП-ПРИНТ», 2015. – 140 с. [Zaitsev AA, Morozova EN, Talashin GN., et al. Magnitolevitatsionnyy transport v edinoi transportnoi sisteme strany. St. Petersburg: ООО 'Tipografiya 'NP-PRINT'; 2015. 140 p. (In Russ.).]
 5. Зайцев А.А. О современной стадии развития магнитолевитационного транспорта // Железнодорожный транспорт. – 2016. – № 12. – С. 62-65. [Zaitsev AA. O sovremennoy stadii razvitiya magnitolevitatsionnogo transporta. *Zheleznodorozhnyy transport*. 2016;(12):62-65. (In Russ)].
 6. Зайцев А.А. Магнитолевитационные системы и технологии // Железнодорожный транспорт. – 2014. – № 5. – С. 69-73. [Zaitsev AA. Magnitolevitatsionnyye sistemy i tehnologii. *Zheleznodorozhnyy transport*. 2014;(5):69-73. (In Russ.).]
 7. Антонов Ю.Ф., Зайцев А.А., Морозова Е.И. Исследование магнитодинамической левитации и электродинамического торможения грузовой транспортной платформы // Известия ПГУПС. – 2014. – Т. 4. – № 41. – С. 5–15. [Antonov YuF, Zaitsev AA, Morozova EI. Issledovanie magnitodinamicheskoi levitatsii i elektrodinamicheskogo tormozeniya gruzovoi transportnoi platformy. *Izvestia PGUPS*. 2014;4(41):5-15. (In Russ.).]
 8. Авторское свидетельство СССР на изобретение № 696579/05.11.79. Бюл. № 41. Попов А.Д., Соломин В.А., Хантимиров С.С. и др. Линейный асинхронный двигатель. Режим доступа: <http://patents.su/2-696579-linejnyjj-asinkhronnyjj-dvigatel.html>. [Author's certificate the USSR № 696579/05.11.79. Byul. № 41. Popov AD, Solomin VA, Chantimirov SS et al. *Lineinyi asinkhronnyi dvigatel*. Available from: <http://patents.su/2-696579-linejnyjj-asinkhronnyjj-dvigatel.html>. (In Russ.).]
 9. Popov AD, Solomin VA, Khantimirov SS, et al, inventor. *Linear inductor motor*. United States patent US 4216397. 1980 Aug 5. Available from: <https://patents.google.com/patent/US4216397A/en>.
 10. Popov AD, Solomin VA, Chantimirov SS und. and, inventor. *Linearer Asynchron motor*. Bundesrepublik Deutschland patent 2851038. 1983 Aug 11. Available from: <https://patents.google.com/patent/DE2851038A1/en?q=Pat.+2851038+Bundesrepublik+Deutschland>.
 11. Popov AD, Solomin VA, Khantimirov SS, inventor. *Moteur electrique asynchrone a mouvement lineaire*. France patent 7836932. 1981 Oct. 23. Available from: <https://patents.google.com/patent/US7836932B2/en?q=Pat.+7836932+France>.
 12. Авторское свидетельство СССР на изобретение № 868942/30.09.81. Бюл. №. 36. Попов А.Д., Соломин В.А., Хантимиров С.С., Шириков А.А. Линейный асинхронный двигатель. Режим доступа: <http://patents.su/3-868942-linejnyjj-asinkhronnyjj-dvigatel.html>. [Author's certificate the USSR № 868942/30.09.81. Byul. № 36. Popov AD, Solomin VA, Chantimirov SS, Shirikov AA. *Lineinyi asinkhronnyi dvigatel*. Available from: <http://patents.su/3-868942-linejnyjj-asinkhronnyjj-dvigatel.html>. (In Russ)].



13. Popov AD, Solomin VA, Khantimirov SS, et al, inventor. *Linear inducton motor*. United States patent US 4271367. 1981 Jun. 2. Available from: <https://patents.google.com/patent/US4271367A/en?q=Pat.+4271367+United+States>.
14. Popov AD, Solomin VA, Chantimirov SS, et al, inventor. *Linearer Asynchron motor*. Bundesrepublik Deutschland patent 3012917. 1984 March 8. Available from: <https://patents.google.com/patent/DE3012917A1/en?q=Pat.+3012917+Bundesrepublik+Deutschland>.
15. Popov AD, Solomin VA, Khantimirov SS, et al, inventor. *Moteur electrique asynchrone a movement lineaire*. France patent 8008928. 1983 Feb. 25. Available from: <https://patents.google.com/patent/US8008928B2/en?q=Pat.+8008928+France>.
16. Патент РФ на изобретение № 2268543/20.01.06. Бюл. № 2. Соломин А.В. Линейный асинхронный двигатель. Режим доступа: <http://bd.patent.su/2268000-2268999/pat/servlet/servletb65f.html>. [Pat. RUS № 2268543/20.01.06. Byul. №.2. Solomin AV. *Lineinyi asinchronnyi dvigatel*. Available from: <http://bd.patent.su/2268000-2268999/pat/servlet/servletb65f.html>. (In Russ.)].

Information about the authors:

Vladimir A. Solomin, Doctor of Technological sciences, Professor; address: 2, Rostovskogo Strelkovogo Polka Narodnogo Opolcheniya sq., Rostov-on-Don, 344038, Russia; eLibrary SPIN: 6785-9031; ORCID: 0000-0002-0638-1436; E-mail: ema@rgups.ru.

Andrei V. Solomin, Candidate of Technological sciences, Associate Professor; eLibrary SPIN: 7805-9636; ORCID: 0000-0002-2549-4663; E-mail: vag@kaf.rgups.ru.

Victor V. Koledov, Doctor of physico-mathematical Sciences, Professor Russian Academy of Sciences; eLibrary SPIN: 9291-1989; ORCID: 0000-0002-2439-6391; E-mail: victor_koledov@mail.ru.

Nadezda A. Trubitsina, Candidate of Technological sciences, Associate Professor; eLibrary SPIN: 4192-0487; ORCID: 0000-0001-6640-8306; E-mail: ema@rgups.ru.

Сведения об авторах:

Соломин Владимир Александрович, доктор технических наук, профессор; 344038, Ростов-на-Дону, пл. Ростовского Стрелкового Полка Народного Ополчения, 2; eLibrary SPIN:6785-9031; ORCID: 0000-0002-0638-1436; E-mail: ema@rgups.ru

Соломин Андрей Владимирович, кандидат технических наук, доцент; eLibrary SPIN:7805-9636; ORCID: 0000-0002-2549-4663; E-mail: vag@kaf.rgups.ru

Коледов Виктор Викторович, доктор физико-математических наук, профессор РАН; eLibrary SPIN: 9291-1989; ORCID: 0000-0002-2439-6391; E-mail: victor_koledov@mail.ru

Трубицина Надежда Анатольевна, кандидат технических наук, доцент; телефон:
+7(863)2726212;
eLibrary SPIN: 4192-0487; ORCID: 0000-0001-6640-8306;
E-mail: ema@rgups.ru

To cite this article:

Solomin VA, Solomin AV, Koledov VV, Trubitsina NA. Multifunctional Linear Induction Motor with Longitudinal-Transverse Magnetic Flux for Magnetic-Levitational Transport. *Transportation Systems and Technology*. 2018;4(2):167-179. doi: 10.17816/transsyst201842167-179

Цитировать:

Соломин В.А., Соломин А.В., Коледов В.В., Трубицина Н.А. Многофункциональный линейный асинхронный двигатель с продольно-поперечным магнитным потоком для магнитолевитационного транспорта // *Транспортные системы и технологии*. – 2018. – Т. 4. – № 2. – С.167–179. doi: 10.17816/transsyst201842167-179

